Transcription factors, microRNAs and extracellular vesicles at the crossroad of right and left heart failure

Transcription Factors, microRNAs and Extracellular Vesicles at the crossroad of right and left heart failure.

Raquel Figuinha Videira

PhD Thesis Co-Supervision between the

University of Porto and the University of Maastricht

 ISBN: 978-94-6423-872-3

Transcription Factors, microRNAs and Extracellular Vesicles at the crossroad of right and left heart failure.

Dissertation

To obtain the degree of Doctor at the Maastricht University and Doutor em Ciências Cardiovasculares at the FMUP- University of Porto on the authority of the Rector Magnificus, Prof. dr. Pamela Habibović and Prof. Dr. António Sousa Pereira to be defended on

11th July at 16:00 hours.

by

Raquel Figuinha Videira

Approved after corrections
Prof. dr. Pamela Habibović
Rector Magnificus

Supervisors:

Prof. dr. Paula da Costa Martins

Prof. dr. Inês Falcão-Pires (Porto University)

Assessment Commitee:

Prof. dr. Judith Sluimer (Chair)

Prof dr. Marjo Donners

Prof. dr. Marie-Jose Goumanz (Leiden University, The Netherlands)

Dr. Perpétua Pinto-do-Ó (Porto University, Portugal)

Prof. dr. Lino da Silva Ferreira (Coimbra University, Portugal)

Prof. dr. Kevin Vernooy

This thesis was funded by Fundação para a Ciência e Tecnologia on an Individual Fellowship SFRH/BD/129507/2017 to R.F.V. And "Project Twinning “RESETageing” with the Ref: 952266.

TABLE OF CONTENTS

CHAPTER 1

“General Introduction”

Preamble

The 20th-century society believes that human beings are free; therefore, they are directly responsible for what they think and do. In free-will, your conscience has an intention responsible for practicing an action. In other words, first, we make a decision, and then we act.

However, Benjamin Libet has shown that our actions could precede our intention to act. That means an action can be done, and a justification supporting an intention will follow it. This raises the question of whether the human being has or not free-will. Determinism states that if we do not have free-will, all we have left is to accept our faith without any responsibility for our actions. In this way, every action is caused by a previous action.

It is tough to deny that our past experiences, current environment, the people surrounding us, and many other things do not affect our choices and actions.

Compatibilism combines free-will with determinism, since it believes that the universe works in a law-like order, as in determinism. However, it still has the power to choose and make changes if needed or wanted, as in free-will.

When it comes to heart failure, it is natural to apply a determinism philosophy. The heart responds to pathophysiologic stimuli in a complex and highly regulated manner. Initially, a single particle affects another particle that, in turn, will affect other. As a result, a pathway is triggered. However, the complexity of the heart does not allow a single particle perspective. Instead, multiple pathways are simultaneously activated and repressed. For that, cardiac cells are constantly influenced by transcription factors and microRNAs.Nevertheless, the compatibilism philosophy can also be applied since cells can influence each other's behavior by sending messages via extracellular vesicles.

As observed in this thesis, the right and left ventricle respond in distinct manners to the same pathophysiological stimulus, supporting a free-will philosophy also occurs. Usually, cell free-will vanishes when new mechanisms are discovered.

The laws that regulate society tell us that human beings have free-will. Therefore, considering the prevalence of heart failure, we can choose to reverse it. By finding new mechanisms and creating new tools may be possible to create an alternative path at the crossroad of heart failure.

Heart failure

The European Society of Cardiology defines heart failure (HF) as a "clinical syndrome in which individuals show signs and symptomology as consequences of an irregular cardiac structure and function". In other words, HF is the endpoint result of long-lasting cardiac conditions and cardiovascular diseases (CVDs), where the heart cannot pump blood efficiently, eventually leading to multiple organ dysfunction and death [1].

HF affects more than 26 million people worldwide and remains an increasing health and economic global problem [2]. The current knowledge about HF heterogeneity and its wide range of pathophysiologic mechanisms led to its clustering into different cohorts: left ventricle or right ventricle failure (LVF and RVF, respectively) according to which ventricle is dysfunctional. Some of the LVF and RVF differences can be explained by the specific left ventricle (LV) and right ventricle (RV) intrinsic features regarding their origin, molecular signature, structure, shape, hemodynamics, and lung-heart interaction.

In the adult heart, RV displays a crescent shape chamber where venous blood is pumped towards the lungs to be re-oxygenated [3]. The extremely trabeculated yet, thin walls of the RV support high blood volume rather than high pressure, probably due to its connection with low impedance pulmonary circulation [4]. Differences in pressure and volume between both ventricles are reflected in rectangular LV versus trapezoidal RV pressure-volume loops. Although the ejection fraction of LV and RV results in the same cardiac output, the LV requires five times more energy than the RV due to its increased wall stress [4]. While clearly distinct, the LV and the RV share a common septum that explains their interdependency at the morphological and physiological levels. It is estimated that RV function depends on LV free wall contraction since this generates more than half of the RV mechanical work needed for RV contraction [5].

Inline, the pathophysiology of both ventricles might allocate common processes, but responsible for different outcomes after treatment may be owed to ventricle-specific phenomena. For example, due to intrinsic features of ventricle physiology and anatomy, RV tolerates better volume overload than pressure overload, which is better well stood by the LV [4].

Shared features between the maladaptive remodeling of the right and left ventricle include reactivation of the fetal gene program, a metabolic switch, hypertrophy, and fibrotic events, namely extracellular matrix remodeling and collagen deposition [4]. However, the same events are triggered by different stimuli, and they can occur at separated stages and with different intensities. For example, fibrotic events are less extensive in RV during pressure-overload, while in volume overload conditions, the LV develops much less fibrosis than the RV [6].

Both ventricles develop hypertrophy in response to pressure overload conditions, but the pathways that trigger and sustain hypertrophy seem different. Initially, calcineurin (Cn) is activated in both ventricles; in the LV, Cn dephosphorylates the nuclear factor of activated T-cells (NFAT) leading to its nuclear translocation and subsequent activation of hypertrophic genes like regulator of calcineurin 1.4 (RCAN1.4) [7]. However, in RV, the transcription of hypertrophic genes is preferentially activated by the myocyte enhancer factor-2 (Mef2) [8], which was possibly triggered by calcineurin.

However, the first physiological divergences concerning left versus right ventricle start as early as embryonic development and continue throughout adult life. During cardiac embryogenesis, the primary heart field locally expresses the transcription factor (TF) T-box (Tbx) 5 and heart and neural crest derivate-expressed protein (Hand) 1 that gives rise to LV, the bullet-shaped ventricle responsible for pumping oxygenated blood to the rest of the body [9, 10]. Therefore, LV displays thick but smooth walls that show high resistance to pressure-overload conditions. In contrast, the RV embryonically derives from the second heart field which is enriched in TF heart and neural crest derivate-expressed protein 2 (Hand2, also known as *dHand*) and Tbx20. In fact, Hand2 has been associated with multiple cardiac pathologies and heart failure [7, 11, 12].

The transcription factor Hand2 in the heart

Hand2 is a basic helix-loop-helix (bHLH) TF described as a transcriptional activator. In the members of this superfamily of TFs, a bHLH structure consists of a short alpha-helix connected by a loop, a short extended chain of amino acids, to a second longer alpha-helix, that usually binds the major groove of DNA [13]. The Hand2 gene, composed of two exons encoding a 217-amino acid protein, is located on the human chromosome 4q33 [14]. Frequently, bHLH proteins can form homo- and heterodimers. Heterodimers are preferentially formed with E-proteins, namely Hand2/E-12, that bind to DNA through an E-box (CANNTG) sequence consensus at a DNA binding site carrying the CATCTG sequence [15].

The function of Hand2 was first described during mouse embryonic development, with its expression becoming detectable in the lateral mesoderm from day 7.75 *post coitum* (p.c.) and in the caudal region and throughout the developing heart at day 8.5 p.c.[16]. Posteriorly, *Olson et al.* showed that from embryonic day (E) 7.75 Hand2 expression becomes restricted to the future pulmonary ventricle (usually RV) segments, but after E10.5 and throughout the adult heart, Hand2 expression is drastically low [17]. Hand2 was revealed to be crucial for embryonic development considering that growth retardation and severe heart defects are observed by E9.5 in Hand2 null embryos, which die due to hypoplasia of the RV and vascular defects at E10.5 [17].

Hand2 expression is not defined by the left-right axis, but it is intrinsically associated with the pulmonary ventricle; in fact, mice with *situs inversus* condition (characterized by reversal of the left-right asymmetry) showed that the expression of Hand2 was restricted to the primordial pulmonary ventricle, that is located on the left side [3]. These results highlight that Hand2 is fundamentally intertwined with pulmonary circulation.

Upon cardiac injury, there is a reactivation of a fetal gene program. Similar to other genes, Hand2 is re-expressed in the failing adult heart and contributes to maladaptive remodeling in the pressure overloaded LV induced by transverse aortic constriction (TAC) [7]. While Hand2 upregulation leads to LV hypertrophy growth, LV and RV dilation, and consequently failure, cardiac depletion of Hand2 confers cardiac protection and inhibits maladaptive remodeling of the pressure-loaded LV [7].

However, mice exposed to phenylephrine hypertrophic stimulus demonstrated an increased Hand2 expression in LV and a decreased Hand2 expression in RV. In rats, the same study reported that pressure overload-induced by supra-renal aortic-banding led to an initial

increase in Hand2 levels followed by a drastic decrease in both LV and RV, 5 days after banding [18].

In contrast, in the adult healthy human heart, Hand2 is expressed in all four chambers, but predominantly in the RV and less notably in the right atria [14]. The role and expression of Hand2 in the human adult heart are still controversial, with studies reporting that Hand2 expression is stable in a set of CVDs such as hypertrophic, dilated, ischemic, or sarcoid cardiomyopathies [14, 19]. In turn, others reported that Hand2 is significantly upregulated in failing human hearts from etiologies such as ischemic cardiomyopathy and non-ischemic dilated cardiomyopathy [7]. Interestingly, patients with pulmonary stenosis and congenital heart disease present a Hand2 loss-of-function mutation [20, 21].

In summary, Hand2 regulates gene expression by affecting transcription efficiency. Alterations on Hand2 homeostasis might cause pathological events, including pathological cardiac remodeling. It is known that Hand2 is intrinsically connected with RV during embryonic development, although no association has been established regarding the role of Hand2 in adult RV. Therefore, studying Hand2 on RV failure might be crucial to understanding the mechanisms involved in the pathogenesis and finding new potential therapeutic targets for the disease.

However, transcription factors are not the only players involved in the regulation of gene expression, in fact, a major fraction of coding gene expression is regulated by microRNAs.

MicroRNAs

MicroRNAs (miRs) are a conserved class of small non-coding RNAs that control gene expression at a post-transcriptional level. In contrast to the TF Hand2, which mainly promotes gene expression by activating transcription, most miRs act by repressing gene expression, with a few exceptions [22]. Responsible for regulating up to 60% of the coding genes, mature miRs are composed of a single strand of RNA of 21 to 23 nucleotides [23]. Currently, 38589 miRs are annotated in the human genome but, more than 48 thousand mature miRs from 271 organisms have been reported (miRBase v22, 2019). The first findings were described in *Caenorhabditis elegans* studies in 1993 [24], where the lin-4 transcript, a non-coding gene product, was shown to prevent the translation of another gene, lin-14 [24]. Since then, miRs have been implicated in multiple biological events including development, differentiation, growth, and metabolism. Moreover, alterations in miR expression patterns were also associated with several pathologies including cancer [25], HIV [26], atherosclerosis [27], and HF [28], among others.

Most studies on the mechanisms by which miRs exert their functions report on post-transcriptional repression of gene expression where a miR seed sequence, corresponding to nucleotides 2-7 at the 5’ end of the miR, recognizes its target mRNAs through Watson-Crick base complementary usually at 3’ UTR that binds to the seed sequence [29]. It is the degree of complementarity that determines which mechanism is triggered. A high complementary degree is associated with mRNA destabilization following degradation while lower complementary levels are linked to translation repression [30]. A feature of miRs biology is that a single miR can have multiple mRNA targets and one single mRNA can be targeted by different miRs, which could be particularly attractive as a therapeutic target.

Finally, miRs might also be secreted to the extracellular space inside vesicles, bound to lipid particles or in a free form [31], and play a major role in intercellular communication,

particularly in cardiac pathological remodeling. In this regard, extracellular miRs, predominantly plasmatic miRs, are helpful as diagnosis and prognosis tools in cardiac disease as biomarkers.

Biomarkers

According to WHO, a biomarker "is any substance, structure, or process that can be measured in the body or its products and influence or predict the incidence of outcome or disease". It should be easy to access, stable with high sensitivity and specificity and, give fast and accurate results [32]. Indeed, human biomarkers can be found in tissues, urine, saliva, blood, and plasma, among others [33].

In the context of cardiac pathologies such as myocardial infarction, aortic stenosis (AS), and others, the most described plasma biomarkers include cardiac troponins, C-reactive protein, and natriuretic brain peptides A and B [34].

Cardiac troponins are involved in the contractile function of the cardiomyocytes by their binding capacity to tropomyosin. They are frequently associated with myocardial injury, namely with myocardial infarction, where cardiac troponins were found to be upregulated [35].

C-reactive protein is usually associated with inflammatory CVDs like atherosclerosis since their expression levels are elevated on activation of the classical complement pathway. However, circulating C-reactive protein upregulation is not an exclusive marker of CVDs [36].

B-type natriuretic peptide (BNP) is produced and secreted into extracellular space in response to cardiomyocyte stretch, as observed in AS. In AS patients, BNP is described to be elevated and correlates with the severity of the stenosis, aortic valve area, peak velocity, peak trans-valvular gradient, and it correlates inversely with aortic valve area [37]. Interestingly, circulating levels of BNP were also associated with patient outcomes after aortic valve replacement surgery [37].

Since their discovery in the 1980s, biomarkers have become crucial tools in cardiovascular clinical practice. Despite their routine use in CVDs' diagnosis and prognosis, the aforementioned biomarkers are considered "late-stage" biomarkers, since they only detect pathological events after their occurrence [34]. Therefore, biomarkers that can predict cardiac pathological events or detect them at an early disease stage are urgently needed but extremely challenging to achieve. Additionally, prognostic accuracy improvement will be unlikely achieved by using a single biomarker but rather a strategy based on a multi-marker approach [34].

Although the biomarker concept is frequently associated with proteins related to pathophysiological features of HF, miRs have recently emerged as potential biomarkers due to their ability to reflect stretch and stress, myocyte injury and necrosis, inflammation, fibrosis, and extracellular matrix turnover [32].

For example, AS patients showed higher levels of miR-21 (a miR associated with cardiac fibrosis) in both cardiac tissue and plasma samples compared with the controls individuals [38]. Furthermore, miR-21 levels also correlated with trans-valvular gradients and myocardial collagen [38].

An extensive review of the role of miRs as biomarkers for different CVDs has been made elsewhere [33, 39-41].

Extracellular vesicles

As aforementioned, miRs can be secreted into extracellular space after being incorporated into extracellular vesicles (EVs). EVs are double-layer vesicles secreted by cells to mediate cardiac intercellular communication, frequently altered under cardiac pathological events.

Besides miRs, it has been shown that EVs carry other non-coding RNAs as long non-coding RNAs, mRNAs, proteins, lipids, and even viral particles. Recently, multiple EVs types have been described including oncosomes, exomeres, vexosomes, apoptotic bodies, but EVs mediated cardiac communication is predominately carried by exosomes and microvesicles [42-46]. Size, surface markers, surface charge, lipid profile, and density are some of the properties that help differentiate exosomes from microvesicles. Exosomes (30–150 nm) derive from early endosomes that are then matured into multivesicular bodies (MVBs), and, depending on cholesterol composition, MVBs can follow two different pathways [45]. High cholesterol vesicles are usually fused with the plasma membrane and their content is released into extracellular space whereas vesicles with low cholesterol composition are sent to the lysosome pathway to be degraded along with their content [47]. In turn, microvesicles (100 nm up to 1 μm) are generated by direct outward budding of the plasma membrane of the cell [45]. Microvesicles share many features with exosomes, and therefore, in this thesis, no distinction will be made between both types, which will be collectively referred to as EVs.

EVs' membranes are composed of specific lipids and proteins which can be used to identify them. Such in the case of tetraspanins (CD9, CD63, CD81), integrins, growth factor receptors, and heterotrimeric G proteins, among others [45].

Upon release into extracellular space, EVs can enter the bloodstream or be internalized by surrounding cells to induce behavioral changes [48]. The majority of the studies report that EVs can either bind surface receptors present in the plasma membrane or fuse non-selectively with the plasma membrane. After that EVs are uptaken by endocytosis and internalized into the endolysosomal compartment of the recipient cell [49]. However, to deliver functional molecules and have a role in cardiac communication, EVs and their cargo should escape from lysosomal processing [50]. To date, it is still unknown whether some cells exhibit a higher capacity for internalizing EVs than others. The lack of technology that allows accurate tracking of EVs without external manipulation hinders new advances in EVs research and translation of basic science into clinical practice namely in CVDs [50]. Recent advances in 3D cardiac models have allowed the investigation of EVs' effect on a human-based *in vitro* model that closely resembles the micro-environment of a human heart [51].

In summary, different players such as TFs, EVs, and miRs are fundamental pieces for finding therapeutic targets in the multicellular road against heart failure.

Thesis Aim and Overview

Cardiovascular Diseases (CVDs) are the leading cause of mortality and morbidities worldwide. WHO predicts that by 2030 the number of deaths triggered by CVD will rise to 23 million, imposing a significant economic burden. To stop and even revert this trend, new therapeutic targets and monitoring tools must be found. Heart failure (HF), described as the inability of the heart to pump enough blood, makes up the end road of many CVDs. Hence, this

road is not a straightforward highway but consists of heterogeneous trails with different vehicles as important inter players. **This thesis explores the plurality of HF, embracing multiple perspective views of HF and their regulators to contribute to avoiding it and treating it.** Our research focus was not merely on HF in general but on distinguishing the molecular players underlying right and left ventricular failure. Additionally, we aimed to find new prognosis tools based on non-coding RNA technology for left ventricle reverse remodeling after aortic valve surgery, overlooking the conventional "diagnosis-only" feature of biomarkers. At last, our goal was to monitor the cardiac intercellular transfer of vesicles by color change in recipient cells using a 3D model, and assess how EV-based intercellular communication is changed during HF.

Chapter II investigates the contribution of the Hand2 transcription factor to RV remodeling in response to pressure overload injury and parallels Hand2 impact in RVF versus LVF. Hand2 revealed to be an important player to withstand RV pressure-overload conditions, as deletion of cardiac Hand2 is associated with severe cardiac dysfunction and RVF. These results contrast to what was observed in LV pressure overload, where inhibiting *Hand2* expression could prevent cardiac dysfunction.

Chapter III reviews the state of the art regarding circulating non-coding RNAs, including miRs, lncRNAs, and circRNAs, as potential plasma biomarkers of cardiac remodeling and reverse remodeling and associated CVDs. The discussion shares our perception of the current role of these molecules as diagnostic and prognostic tools and their path toward clinical use.

Chapter IV focuses on both novel and reported miRs as potential blood-based biomarkers for cardiac reverse remodeling, specifically after aortic valve surgery in aortic stenosis patients. Our data suggest that miR-133a and let-7b can help predict the type of RR after AVR surgery in AS patients, which could potentially become new biomarkers to be further used in clinical practice.

Chapter V resumes the current literature on cell-cell communication via exosomal non-coding RNAs during cardiac pathological remodeling. We focused on how non-coding RNAs, namely miRs and lncRNAs, can be transferred through exosomes and act on recipient cells contributing to pathological remodeling of the heart. Additionally, we also addressed how inter-organ communication could affect cardiac remodeling based on non-coding RNAs and exosomal transfer.

Chapter VI addresses intercellular communication on a new 3D *in vitro* model-engineered heart myocardium, by using the Cre-loxP recombination system. Our preliminary data demonstrate that EV transfer can be traced at 2D and 3D levels, particularly between cardiomyocytes and stromal cells. Simultaneously, we investigated whether EV content is active in recipient cells, and showed that the donor cell can transfer mRNAs through EVs that may contribute to host cell behavior changes. Also, we assessed whether miR content in EVs is altered in HF conditions. Further studies on EV transfer using this method will elucidate on timing, biodistribution, and trafficking of cardiac EVs.

Chapter VII closes this thesis by providing a general discussion and summary of the included topics, followed by future perspectives.

References

1. Guha, K. and T. McDonagh, *Heart failure epidemiology: European perspective.* Curr Cardiol Rev, 2013. **9**(2): p. 123-7.
2. Ponikowski, P., et al., *Heart failure: preventing disease and death worldwide.* ESC Heart Fail, 2014. **1**(1): p. 4-25.
3. Thomas, T., et al., *The bHLH factors, dHAND and eHAND, specify pulmonary and systemic cardiac ventricles independent of left-right sidedness.* Dev Biol, 1998. **196**(2): p. 228-36.
4. Friedberg, M.K. and A.N. Redington, *Right versus left ventricular failure: differences, similarities, and interactions.* Circulation, 2014. **129**(9): p. 1033-44.
5. Santamore, W.P., et al., *Left ventricular effects on right ventricular developed pressure.* J Appl Physiol, 1976. **41**(6): p. 925-30.
6. Modesti, P.A., et al., *Different growth factor activation in the right and left ventricles in experimental volume overload.* Hypertension, 2004. **43**(1): p. 101-8.
7. Dirkx, E., et al., *Nfat and miR-25 cooperate to reactivate the transcription factor Hand2 in heart failure.* Nat Cell Biol, 2013. **15**(11): p. 1282-93.
8. Paulin, R., et al., *A miR-208-Mef2 axis drives the decompensation of right ventricular function in pulmonary hypertension.* Circ Res, 2015. **116**(1): p. 56-69.
9. Takeuchi, J.K., et al., *Tbx5 specifies the left/right ventricles and ventricular septum position during cardiogenesis.* Development, 2003. **130**(24): p. 5953-64.
10. McFadden, D.G., et al., *The Hand1 and Hand2 transcription factors regulate expansion of the embryonic cardiac ventricles in a gene dosage-dependent manner.* Development, 2005. **132**(1): p. 189-201.
11. Liu, H., et al., *HAND2 loss-of-function mutation causes familial dilated cardiomyopathy.* Eur J Med Genet, 2019. **62**(9): p. 103540.
12. Lu, C.X., et al., *A novel HAND2 loss-of-function mutation responsible for tetralogy of Fallot.* Int J Mol Med, 2016. **37**(2): p. 445-51.
13. Alberts, B., et al., *Molecular Biology of the Cell 5th edition New York.* NY: Garland Science, 2007.
14. Natarajan, A., et al., *Human eHAND, but not dHAND, is down-regulated in cardiomyopathies.* J Mol Cell Cardiol, 2001. **33**(9): p. 1607-14.
15. Dai, Y.S. and P. Cserjesi, *The basic helix-loop-helix factor, HAND2, functions as a transcriptional activator by binding to E-boxes as a heterodimer.* (0021-9258 (Print)).
16. Srivastava, D., P. Cserjesi, and E.N. Olson, *A subclass of bHLH proteins required for cardiac morphogenesis.* Science, 1995. **270**(5244): p. 1995-9.
17. Srivastava, D., et al., *Regulation of cardiac mesodermal and neural crest development by the bHLH transcription factor, dHAND.* Nat Genet, 1997. **16**(2): p. 154-60.
18. Thattaliyath, B.D., et al., *HAND1 and HAND2 are expressed in the adult-rodent heart and are modulated during cardiac hypertrophy.* Biochem Biophys Res Commun, 2002. **297**(4): p. 870-5.
19. Yu, C.W., et al., *Terminal deletion of the long arm of chromosome 4. Report of a case of 46, XY, del(4)(q31) and review of 4q- syndrome.* Ann Genet, 1981. **24**(3): p. 158-61.
20. Cohen, A.S.A., et al., *Haploinsufficiency of the basic helix-loop-helix transcription factor HAND2 causes congenital heart defects.* Am J Med Genet A, 2020. **182**(5): p. 1263-1267.
21. Sun, Y.M., et al., *A HAND2 Loss-of-Function Mutation Causes Familial Ventricular Septal Defect and Pulmonary Stenosis.* G3 (Bethesda), 2016. **6**(4): p. 987-92.

22. Vasudevan, S., Y. Tong, and J.A. Steitz, *Switching from repression to activation: microRNAs can up-regulate translation.* Science, 2007. **318**(5858): p. 1931-4.
23. Friedman, R.C., et al., *Most mammalian mRNAs are conserved targets of microRNAs.* Genome Res, 2009. **19**(1): p. 92-105.
24. Lee, R.C., R.L. Feinbaum, and V. Ambros, *The C. elegans heterochronic gene lin-4 encodes small RNAs with antisense complementarity to lin-14.* Cell, 1993. **75**(5): p. 843-54.
25. Esquela-Kerscher, A. and F.J. Slack, *Oncomirs - microRNAs with a role in cancer.* Nat Rev Cancer, 2006. **6**(4): p. 259-69.
26. Sun, B., R. Yang, and M. Mallardo, *Roles of microRNAs in HIV-1 Replication and Latency.* Microrna, 2016. **5**(2): p. 120-123.
27. Laffont, B. and K.J. Rayner, *MicroRNAs in the Pathobiology and Therapy of Atherosclerosis.* Can J Cardiol, 2017. **33**(3): p. 313-324.
28. Duygu, B., L.J. de Windt, and P.A. da Costa Martins, *Targeting microRNAs in heart failure.* Trends Cardiovasc Med, 2016. **26**(2): p. 99-110.
29. Brennecke, J., et al., *Principles of microRNA-target recognition.* PLoS Biol, 2005. **3**(3): p. e85.
30. Wu, L., J. Fan, and J.G. Belasco, *MicroRNAs direct rapid deadenylation of mRNA.* Proc Natl Acad Sci U S A, 2006. **103**(11): p. 4034-9.
31. Vickers, K.C. and A.T. Remaley, *Lipid-based carriers of microRNAs and intercellular communication.* Curr Opin Lipidol, 2012. **23**(2): p. 91-7.
32. Dhingra, R. and R.S. Vasan, *Biomarkers in cardiovascular disease: Statistical assessment and section on key novel heart failure biomarkers.* Trends Cardiovasc Med, 2017. **27**(2): p. 123-133.
33. Videira, R.F., P.A. da Costa Martins, and I. Falcao-Pires, *Non-Coding RNAs as Blood-Based Biomarkers in Cardiovascular Disease.* Int J Mol Sci, 2020. **21**(23).
34. Ghantous, C.M., et al., *Advances in Cardiovascular Biomarker Discovery.* Biomedicines, 2020. **8**(12).
35. van Wijk, X.M.R., et al., *Cardiac troponin I is present in plasma of type 1 myocardial infarction patients and patients with troponin I elevations due to other etiologies as complex with little free I.* Clin Biochem, 2019. **73**: p. 35-43.
36. Zimmermann, O., et al., *C-reactive protein in human atherogenesis: facts and fiction.* Mediators Inflamm, 2014. **2014**: p. 561428.
37. Torres-Ramalho, P., et al., *Natriuretic peptides in aortic stenosis.* Rev Port Cardiol, 2012. **31**(10): p. 655-60.
38. Villar, A.V., et al., *Myocardial and circulating levels of microRNA-21 reflect left ventricular fibrosis in aortic stenosis patients.* Int J Cardiol, 2013. **167**(6): p. 2875-81.
39. Fichtlscherer, S., A.M. Zeiher, and S. Dimmeler, *Circulating microRNAs: biomarkers or mediators of cardiovascular diseases?* Arterioscler Thromb Vasc Biol, 2011. **31**(11): p. 2383-90.
40. Navickas, R., et al., *Identifying circulating microRNAs as biomarkers of cardiovascular disease: a systematic review.* Cardiovasc Res, 2016. **111**(4): p. 322-37.
41. Zhou, S.S., et al., *miRNAS in cardiovascular diseases: potential biomarkers, therapeutic targets and challenges.* Acta Pharmacol Sin, 2018. **39**(7): p. 1073-1084.
42. Maguire, C.A., et al., *Microvesicle-associated AAV vector as a novel gene delivery system.* Mol Ther, 2012. **20**(5): p. 960-71.

43. Di Vizio, D., et al., *Large oncosomes in human prostate cancer tissues and in the circulation of mice with metastatic disease.* Am J Pathol, 2012. **181**(5): p. 1573-84.
44. Zhang, Q., et al., *Transfer of Functional Cargo in Exomeres.* Cell Rep, 2019. **27**(3): p. 940-954 e6.
45. Lotvall, J., et al., *Minimal experimental requirements for definition of extracellular vesicles and their functions: a position statement from the International Society for Extracellular Vesicles.* J Extracell Vesicles, 2014. **3**: p. 26913.
46. Doyle, L.M. and M.Z. Wang, *Overview of Extracellular Vesicles, Their Origin, Composition, Purpose, and Methods for Exosome Isolation and Analysis.* Cells, 2019. **8**(7).
47. Mobius, W., et al., *Immunoelectron microscopic localization of cholesterol using biotinylated and non-cytolytic perfringolysin O.* J Histochem Cytochem, 2002. **50**(1): p. 43-55.
48. Videira, R.F. and P.A. da Costa Martins, *Non-coding RNAs in Cardiac Intercellular Communication.* Front Physiol, 2020. **11**: p. 738.
49. Joshi, B.S., et al., *Endocytosis of Extracellular Vesicles and Release of Their Cargo from Endosomes.* ACS Nano, 2020. **14**(4): p. 4444-4455.
50. Kwok, Z.H., C. Wang, and Y. Jin, *Extracellular Vesicle Transportation and Uptake by Recipient Cells: A Critical Process to Regulate Human Diseases.* Processes (Basel), 2021. **9**(2).
51. Hirt, M.N., et al., *Deciphering the microRNA signature of pathological cardiac hypertrophy by engineered heart tissue- and sequencing-technology.* J Mol Cell Cardiol, 2015. **81**: p. 1-9.

CHAPTER 2

"The adult heart requires baseline expression of the transcription factor Hand2 to withstand RV pressure overload"

R F Videira[1,2,3], A M C Koop[4], L Ottaviani[1,2], E M Poels[1] , J M M Kocken[1,2], C Dos Remedios[5], P Mendes-Ferreira[3], K W Van De Kolk[6,7], G J Du Marchie Sarvaas[4] , A Lourenço[3], A Llucià-Valldeperas[8], D S Nascimento[9,10,11], L J de Windt[1,2], F S De Man[8], I Falcão-Pires[3], R M F Berger[4], Paula da Costa Martins [1,2,3]

[1]Department of Cardiology, CARIM School for Cardiovascular Diseases, Faculty of Health, Medicine and Life Sciences, Maastricht University, Maastricht, Netherlands.[2]Department of Molecular Genetics, Faculty of Sciences and Engineering, Maastricht University, Maastricht, The Netherlands. [3]Department of Physiology and Cardiothoracic Surgery, Faculty of Medicine, University of Porto, Porto, Portugal. [4]University of Groningen, University Medical Center Groningen, Department of Pediatrics, Center for Congenital Heart Diseases, Groningen, Netherlands. [5]University of Sidney, Sidney, and Victor Chang Cardiac Research Institute, Darlinghurst, Australia. [6]University Medical Center Groningen, The Central Animal Facility, Groningen, Netherlands. [7]University Medical Center Groningen, Gronsai (Groningen Small Animal Imaging Facility), Groningen, Netherlands. [8]Amsterdam UMC, Vrije Universiteit Amsterdam, Department of Pulmonary Medicine, PHEniX laboratory, Amsterdam Cardiovascular Sciences, Amsterdam, The Netherlands. [9]i3S-Instituto de Investigação e Inovação em Saúde, Universidade do Porto, Porto, Portugal. [10]INEB-Instituto de Engenharia Biomédica, Universidade do Porto, Porto, Portugal. [11] ICBAS-Instituto de Ciências Biomédicas de Abel Salazar, Universidade do Porto, Porto, Portugal.

Published in Cardiovasc Res. 2021 Sep 22;cvab299.

doi: 10.1093/cvr/cvab299

Abstract

Aims

Research on the pathophysiology of right ventricular (RV) failure has, in spite of the associated high mortality and morbidity, lagged behind compared to the left ventricle (LV). Previous work from our lab revealed that the embryonic basic helix-loop-helix transcription factor heart and neural crest derivatives expressed-2 (*Hand2*) is re-expressed in the adult heart and activates a 'foetal gene programme' contributing to pathological cardiac remodelling under conditions of LV pressure overload. As such, ablation of cardiac expression of *Hand2* conferred protection to cardiac stress and abrogated the maladaptive effects that were observed upon increased expression levels. In this study, we aimed to understand the contribution of Hand2 to RV remodelling in response to pressure overload induced by pulmonary artery banding (PAB).

Methods and results

In this study, *Hand2*$^{F/F}$ *and MCM- Hand2*$^{F/F}$ mice were treated with tamoxifen (control and knockout, respectively) and subjected to six weeks of RV pressure overload induced by PAB. Echocardiographic- and MRI-derived haemodynamic parameters as well as molecular remodelling were assessed for all experimental groups and compared to sham-operated controls. Six weeks after PAB, levels of *Hand2* expression increased in the control-banded animals but, as expected, remained absent in the knockout hearts. Despite the dramatic differences in *Hand2* expression, pressure overload resulted in impaired cardiac function independently of the genotype. In fact, *Hand2* depletion seems to sensitize the RV to pressure overload as these mice develop more hypertrophy and more severe cardiac dysfunction. Higher expression levels of HAND2 were also observed in RV samples of human hearts from patients with pulmonary hypertension. In turn, the LV of RV pressure-overloaded hearts was also dramatically affected as reflected by changes in shape, decreased LV mass, and impaired cardiac function. RNA-sequencing revealed a distinct set of genes that are dysregulated in the pressure-overloaded RV, compared to the previously described pressure-overloaded LV.

Conclusion

Cardiac-specific depletion of *Hand2* is associated with severe cardiac dysfunction in conditions of RV pressure overload. While inhibiting *Hand2* expression can prevent cardiac dysfunction in conditions of LV pressure overload, the same does not hold true for conditions of RV pressure overload. This study highlights the need to better understand the molecular mechanisms driving pathological remodelling of the RV in contrast to the LV, in order to better diagnose and treat patients with RV or LV failure.

Graphical Abstract

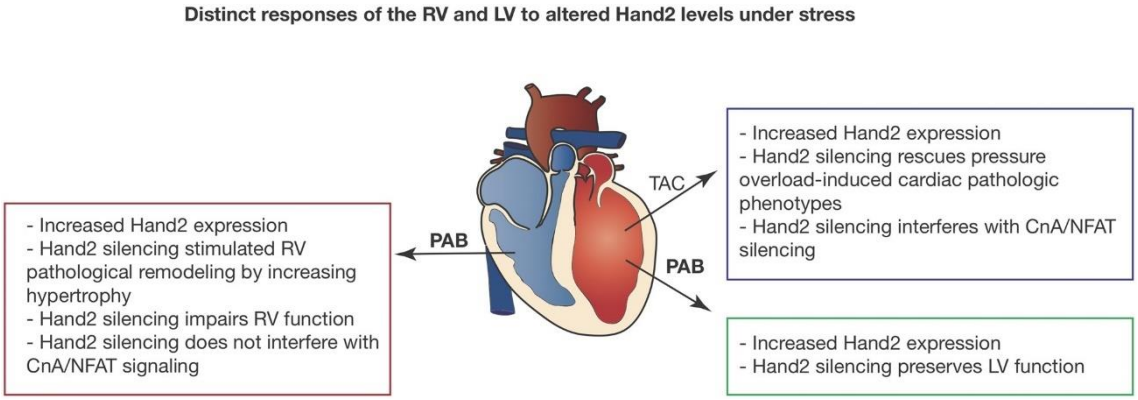

1.Introduction

Heart failure (HF), roughly described as the inability of the heart to pump blood, is a leading cause of morbidity and mortality worldwide, currently affecting more than 26 million people.[1] Commonly, HF is classified in left (LV) and right ventricular (RV) failure, depending on which ventricle is failing. The majority of the studies are focused on LV failure, whereas RV failure has received less attention. Therefore, it is not surprising that the knowledge on LV failure is greater and more accurate than on RV failure. Likewise, most of the therapies for HF are directed to the LV and commonly also administered to patients suffering from RV failure. As RV failure remains associated with poor prognosis,[2] new RV-specific therapies are urgently needed. However, our limited understanding on RV molecular pathophysiological mechanisms remains an obstacle in the development of new and more efficient drugs.

The RV has not been systematically investigated on the cellular and molecular level most likely because of the widely held opinion that the conditions governing RV and LV failure are identical or very similar and, as such, most concepts of RV failure have been shaped by the studies of the LV. However, embryological and physiological differences exist between both ventricles that support the hypothesis that gene expression patterns and their consequences differ between RV and LV failure. In fact, from embryonic development to the adult organism, both ventricles are exposed to different stimuli, including different haemodynamic forces and unique patterns of gene expression. RV is characterized by thinner walls, continuous coronary flow and is classically connected to a low-resistance pulmonary circulation, rendering it more sensitive to pressure-overload than volume-overload.[3,4]

The vertebrate heart forms from two populations of cardiac progenitor cells: the primary and the secondary heart field. The primary heart field gives rise to the cardiac crescent, left ventricle and atria.[5–7] The secondary heart field gives rise to the outflow tract, the right ventricle and atria.[5,8] During these embryological processes, transcription factors are locally expressed in the developing heart and while some can be found in both the primary and secondary heart fields, others show specific expression patterns in just one of them. T-box 5 (*TBX5*) is mostly expressed in the primary heart field with some residual expression in the RV trabeculae, but not free wall (reviewed in Steimle & Moskowitz, 2017).[9] The basic helix-loop-helix transcription factor heart and neural crest derivatives expressed-1 (*HAND1*), expressed

mainly in the primary heart field, is also found in the secondary heart field-derived myocardial outflow tract and pericardium (reviewed in George & Firulli, 2019).[10] In turn, heart and neural crest derivatives expressed-2 (*HAND2*), islet-1, fibroblast growth factor-8, fibroblast growth factor-10, and paired-like homeodomain-2 are mostly expressed in the secondary heart field.[11–14] In mice, from embryonic day 7.75, *Hand2* expression is detectable within the cardiac crescent and it becomes robustly expressed within the secondary heart field pharyngeal mesoderm that underlies and contributes to the growing heart tube.[12,15] During cardiac looping, myocardial expression of *Hand2* is very low but very accentuated in the endocardium.[16,17] Loss-of-function studies in mice revealed the importance of these transcription factors during development of the heart. Without proper expression of *Hand1*, normal development of the LV is disrupted due to a proliferation defect, and causing the mutants to die from extra-embryonic effects.[13,14,18] While, *Hand2*-null mutants show RV deficient vascularization and hypoplasia,[19,20] its overexpression in ventricles leads to absence of intraventricular septum, both observations indicating that *Hand2* expression is critical for patterning of ventricles.[21] Interestingly, two studies reported that individuals with pulmonary stenosis and congenital heart disease carry a loss-of-function mutation of the *HAND2* gene,[22,23] suggesting *HAND2* as a potential key player in RV failure pathology. Furthermore, previous work from our lab and others revealed that *Hand2* re-expression in the adult mouse heart activates a 'foetal gene programme' and contributes to pathological cardiac remodelling under conditions of LV pressure overload.[24–26] *Hand2* overexpression induces hypertrophic growth of the LV and bi-chamber dilation, again suggesting a role for this transcription factor in adult RV remodelling.[24] In agreement, ablation of cardiac expression of *Hand2* conferred protection to cardiac stress and abrogated the maladaptive effects that were observed upon increased expression levels.[24]

RV failure is a complex condition with an important impact on cardiovascular disease that still lacks accurate understanding and consequently, an efficient treatment. Here, we aim to elucidate the molecular mechanisms underlying RV failure, and decipher the intricate role of Hand2 on RV hypertrophy, by functional and molecular characterization of hearts from mice with cardiac-specific *Hand2* ablation and that were exposed to conditions of RV pressure overload.

2.Methods

Experimental procedures were reviewed and approved by the Institutional Animal Care and Use Committees and authorized by the Animal Experimental Committee of the local government in accordance to the Dutch law (DEC 2012-172) and European Directive 2010/63/EU. In addition, the investigation conforms to the Guide for the Care and Use of Laboratory Animals published by the US National Institutes of Health (NIH Publication No. 85-23, revised 1985). Approval from the Sydney Heart Bank was received for use of human RV samples (HREC #2814; HREC #7326). The use of human RV autopsy samples was approved by and performed according to guidelines of the ethics committee of Amsterdam UMC, location VUmc, and conformed to the Declaration of Helsinki principles.

2.1 Animal models and pulmonary artery banding surgery

Mice harbouring a floxed allele of *Hand2* (*Hand2*$^{F/F}$) in a B6129F1 background were described previously,[27] and crossbred with mice harbouring a tamoxifen-regulated form of Cre recombinase (MerCreMer) under control of the murine *Myh6* promoter (MHC–MerCreMer; MCM mice)[28] in a B6129F1 background to generate MCM–*Hand2*$^{F/F}$ mice. *Hand2*$^{F/F}$ and MCM–*Hand2*$^{F/F}$ were treated with either vehicle (10/90 v/v ethanol/peanut oil, Sigma P2144) or tamoxifen (45 mg kg^{-1} per day) by daily intraperitoneal injections for five consecutive days. Both male and female, adult MCM–*Hand2*$^{F/F}$ mice and *Hand2*$^{F/F}$ mice (10–12 weeks of age) were used for functional and histological analyses.

Pulmonary artery banding (PAB) was performed, as described below, in mice older than 8 weeks from both genders. Animals were anaesthetized with isofluorane/air mixture (5% induction; 2–3% maintenance), and subsequently analgesia with buprenorphine (0.01 mg/kg s.c.) was injected. Animals were placed in a supine position on a heating pad (37°C) and intubated with a 20G catheter and ventilated with room air using a Harvard mini-ventilator (model 687, Hugo Sachs, Germany; respiratory rate 180 breaths per minute and a tidal volume of 125 µL). The pulmonary artery was approached by a left lateral thoracotomy and banded with a 7–0 suture by tying over a 23G needle. Post-operative pain relief was provided with buprenorphine (0.01 mg/kg s.c.) twice daily for 2–3 consecutive days if necessary. Sham-operated animals underwent the same procedure without PAB. All protocols were reviewed and approved by the Animal Care and Use Committee of the University of Maastricht and Animal Experiments Committee of the University of Groningen and were performed according to the rules formulated in the Dutch law on care and use of experimental animals.

2.2 Haemodynamic analyses

Haemodynamic function was assessed at Week 2 and Week 6 after sham or PAB surgery, by cardiac magnetic resonance imaging (MRI) during anaesthesia with isoflurane (induction 5%; 1.5–3% maintenance) and warming at 37°C. Echocardiography to assess the PAB gradient was performed using a Vivid Dimension 7 and i13L-transducer (GE Healthcare, Waukesha, WI, USA) from a short-axis view at aortic level, at Week 2 and Week 6 after sham or PAB surgery. MRI was performed by using a vertical 9.4 T 89-mm diameter bore scanner (Bruker BioSpin, Etllingen, Germany) equipped with 1500 mT/m gradient set (Bruker BioSpin GmbH, Ellingen, Germany). Respiratory and heart rate were derived using a pressure pad placed under the chest of the mouse. The longitudinal axis of the RV was determined with two- and four-chamber scout scans,

where after axes were adjusted to actual axes. Slices of longitudinal axis, four-chamber view, and 10 or 11 slices of the short-axis of 1 mm and no slice gap were obtained. Slices were derived including complete apex and base of the right ventricle. Cine imaging was performed with a retrospectively-triggered (self-gated) gradient-echo sequence (Paravision 4.0 and IntraGate, Bruker Biopspin GmBH) with the following settings: TR = 6.8 ms, TE = 1.9 ms, number of movie frames =15, slice thickness =1 mm, matrix =256 ×256 and field of view =30 ×30. The myocardium was manually segmented by drawing the epicardial and endocardial contours, excluding the papillary muscles using QMass (version MR 7.6, Medis Medical Imaging Systems, Leiden, The Netherlands). Semiautomatic segmentation was used to determine end-diastolic volume (EDV), end-systolic volume (ESV), and wall thickness (WT). Stroke volume (SV) was calculated as EDV−ESV. Ejection fraction (EF) was calculated as (EDV−ESV)/EDV×100. Cardiac output (CO) was calculated manually as SV × mean observed heart rate. Septal flattening is expressed by the eccentricity index, both end-diastolic and end-systolic, which was calculated by dividing the diameter of the LV diameter parallel to the intraventricular septum by the diameter perpendicular to the intraventricular septum derived from short-axis at the mid-papillary level.

2.3 Tissue sampling

Animals were sacrificed by cervical dislocation and the heart, liver, and lung were excised, rinsed with ice-cold PBS and snap-frozen for further mRNA or protein expression analyses. From the hearts, we further dissected the left and right ventricle as well as the septum separately. In some cases, the hearts were perfusion-fixed with 4% paraformaldehyde for paraffin embedment. All mouse cardiac tissue samples were collected after 6 weeks of PAB.

2.4 RNA isolation, cDNA conversion, and Real-time RT–PCR

Total RNA was isolated from mouse heart tissue using Direct-zol™ reagent (ZYMO) according to manufacturer's instructions. RNA (1 ug) was then reverse-transcribed with either M-MLV reverse transcriptase (Promega, Madison, WI, USA). Quantitative real-time polymerase chain reaction (qPCR) was performed on a BioRad iCycler (Biorad) using SYBR Green reagent (VWR). Transcript quantities were compared using the relative Ct method, where the amount of target normalized to the amount of endogenous control (L7) and relative to the control sample is given by 2–ΔCt. Primer sequences for mRNA detection are depicted in Supplementary material online, *Table S1*.

2.5 Western blot analysis

SDS-PAGE electrophoresis and blotting were performed as previously described.[24] In short, whole tissue or cell lysates were produced in RIPA buffer supplemented wtih PhosSTOP (Roche) and Protease inhibitor cocktail (Roche). Subsequently, samples were boiled in 4× Leammli buffer, including 2% β-mercaptoethanol, for 5 min at 95°C. SDS-PAGE and Western blotting were performed using the Mini-PROTEAN 3 system (Bio-Rad). Blotted membranes were blocked in 5% BSA/TBS-Tween. Primary antibody labelling was performed overnight at 4°C. Secondary IgG–horseradish peroxidase (HRP)-conjugated antibodies were applied for 2 h at room temperature. After each antibody incubation, blots were washed for 3 ×10 min in TBS-Tween. Images were generated using Supersignal West Dura Extended Duration ECL Substrate (Pierce) and the LAS-3000 documentation system (FujiFilm Life Science). Stripping was performed with Restore Western blot stripping buffer (Pierce). Outputs were normalized for

loading and results are expressed as an *n*-fold increase over the values of the control group in densitometric arbitrary units. Primary antibodies that were used included rabbit polyclonal anti-Hand2 (sc-22818, Santa Cruz, 1:200), rabbit monoclonal anti-COL1A (E8I9Z, Cell Signaling Technology, 1:1000), rabbit polyclonal anti-VEGFR2 (#2472, Cell Signaling Technology, 1:1000), goat polyclonal anti-ENG (AF1320, R&D Systems, 1:1500), rabbit monoclonal antibody to PAI1 (ab222754, Abcam, 1:500), mouse monoclonal anti-alpha-tubulin (ab7291, Abcam, 1:5000), and mouse monoclonal anti-GAPDH (Millipore, 1: 10 000). Secondary antibodies included polyclonal rabbit anti-mouse IgG–HRP (DAKO, 1:5000) and polyclonal swine anti-rabbit IgG–HRP (DAKO, 1:5000).

2.6 Histology, immunohistochemistry, and immunofluorescence

For histological analysis, hearts were perfusion-fixed with 4% paraformaldehyde, embedded in paraffin and cut into 4-µm sections. Paraffin sections were stained with haematoxylin and eosin for routine histological analysis, Sirius Red for detection of fibrillar collagen and FITC-labelled wheat germ agglutinin (WGA, Sigma) to visualize and quantify the cell cross-sectional area (CSA). Modification of Isolectine B4 staining with additional fluorescence labelled-streptavidin (Dylight 595-conjugated streptavidin, Jackson Thermo, 1:100) and counterstaining with FITC-labelled WGA was performed to assess capillary to cardiomyocyte ratios. Collagen deposition, cell CSA, and capillary density were determined using ImagePro software and ImageJ software. Slides were visualized using a Leica DM2000 and a Leica DM3000 microscope for bright field and fluorescence imaging, respectively.

2.7 Library construction and sequencing

Total RNA was extracted using Direct-zol™ reagent (ZYMO), following the manufacturer's procedure. The total RNA quality and quantity were analysed by a Bioanalyzer 2100 and RNA 6000 Nano LabChip Kit (Agilent, CA, USA) with RIN number >7.0. Approximately 10 µg of total RNA was used to remove ribosomal RNA according to the manuscript of the Epicentre Ribo-Zero Gold Kit (Illumina, San Diego, USA). Following purification, the ribo-minus RNA fractions is fragmented into small pieces using divalent cations under elevated temperature. Then, the cleaved RNA fragments were reverse-transcribed to create the final cDNA library in accordance with a strand-specific library preparation by dUTP method. The average insert size for the paired-end libraries was 300 ± 50 bp. And then, we performed the pair-end 2 × 150 bp sequencing on an illumina Hiseq 4000 platform housed in the LC Sciences (Hangzhou, China) following the vendor's recommended protocol.

2.8 Bioinformatics analysis

For transcripts assembly, firstly, Cutadapt[29] and perl scripts in house were used to remove the reads that contained adaptor contamination, low-quality bases, and undetermined bases. Then, sequence quality was verified using FastQC (http://www.bioinformatics.babraham.ac.uk/projects/fastqc/). We used Bowtie2[30] and Tophat2[31] to map reads to the genome of *Mus musculus* (Version: v88). The mapped reads of each sample were assembled using StringTie.[32] Then, all transcriptomes from six samples were merged to reconstruct a comprehensive transcriptome using perl scripts and gffcompare (https://github.com/gpertea/gffcompare/). After the final transcriptome was generated, StringTie[32] and Ballgown[33] were used to estimate the expression levels of all transcripts. To

analyse the differential expression, StringTie[32] was used to perform expression level for mRNAs by calculating FPKM {FPKM=[total_exon_fragments/mapped_reads(millions) ×exon_length(kB)]}. The differentially expressed mRNAs were selected with log2 (fold change) >1 or log2 (fold change) <−1 and with parametric *F*-test comparing nested linear models (*P*-value <0.05) by R package Ballgown.[33]

2.9 Statistical analysis

All data are presented as mean ± standard error of mean. Statistical analyses were performed using prism software (GraphPad Software Inc.) and consisted of one-way analysis of variance (ANOVA), followed by Tukey's multiple comparison tests, when comparing more than two experimental groups, or of unpaired Student's *t*-test when comparing two experimental groups. Probability values $P < 0.05$ were considered statistically significant.

3.Results

3.1 Cardiac-specific deletion of *Hand2* augments RV susceptibility to increased pressure overload induced by PAB

When analysing HAND2 expression on RV tissue from patients with pulmonary hypertension (PH), we identified a significant increase of the protein in patients, compared to healthy individuals (***Figure 1A***), suggesting a role for the *HAND2* gene in the onset/development of the disease. To assess the contribution of Hand2 to the response of the RV to pressure overload, we induced deletion of a floxed *Hand2* (*Hand2$^{F/F}$*) allele using a tamoxifen-inducible Cre recombinase protein fused to two mutant oestrogen-receptor ligand-binding domains [F] under control of the cardiac-specific α-myosin heavy chain promoter (MCM-*Hand2$^{F/F}$*) in adult mice, as described by us before.[24] *Hand2$^{F/F}$* (control) and MCM-*Hand2$^{F/F}$* (knockout) mice were subjected to sham or PAB surgery for 6 weeks, a period during which cardiac function was assessed by echocardiography at Day 5 and MRI at Weeks 2 and 6 (***Figure 1B***). Whereas 5 days after PAB surgery, both *Hand2$^{F/F}$ and MCM-Hand2$^{F/F}$* mice displayed a similar increase in PA gradients (***Figure 1C***), the knockout mice showed a slight decrease in pressure 6 weeks after banding, even though it was not statistically significant. In control mice, RV pressure overload-induced myocardial *Hand2* expression by 3.5-fold in the RV and three-fold in the LV (***Figure 1D***). Elevated expression of *Hand2* in control mice subjected to PAB, is accompanied by impaired RV function as reflected by functional parameters, assessed by MRI at Week 6 (***Figure 1E– L* and *Table 1***). These results suggest that lowering *Hand2* expression could protect the heart from RV pressure overload, as also shown previously for mouse models of LV pressure overload.[24] *Hand2* silencing, however, resulted in further impairment of RV remodelling and function as reflected by increased RV EDV and ESV, respectively (***Figure 1F and G* and *Table 1***) and a subsequent decrease in RV EF (***Figure 1H* and *Table 2***). Impaired RV function was also associated with increased RV mass (***Figure 1J and K* and *Table 1***). No differences were observed within the different experimental groups regarding the response to stress between females and males (data not shown).

Overall, these data suggest an increase in sensitivity of the RV to pressure overload when *Hand2* is silenced.

3.2 Cardiac-specific silencing of *Hand2* exacerbates hypertrophic growth of the RV in response to pressure overload

Hypertrophy of the right heart was assessed by the Fulton index, the ratio of RV weight to LV plus septum weight (RV/LV+S). Whereas an increased Fulton index was observed 6 weeks after PAB in both control and knockout animals, compared to sham (***Figure 2A* and *Table 2***), the effect was more profound in the absence of *Hand2* expression. These observations were confirmed by increased CSA of cardiomyocytes derived from banded-knockout hearts when compared banded-control hearts (***Figure 2B and C***). Hypertrophic RV remodelling was associated with significantly increased mRNA expression of hypertrophic 'foetal' cardiac genes encoding natriuretic peptides atrial natriuretic factor (*Nppa*) and brain natriuretic peptide (*Nppb*), alpha-skeletal actin 1 (*Acta1*), and β-myosin heavy chain (*Myh7*) (***Figure 2D– G***). Furthermore, an increase in mRNA levels of regulator of calcineurin isoform 4 (*Rcan1.4*) confirms activation of calcineurin/NFAT signalling in the RV response to pressure overload, which was not affected by *Hand2* silencing (*Figure 2H*). At 6 weeks post-PAB, both control and *Hand2* knockout

Figure 1

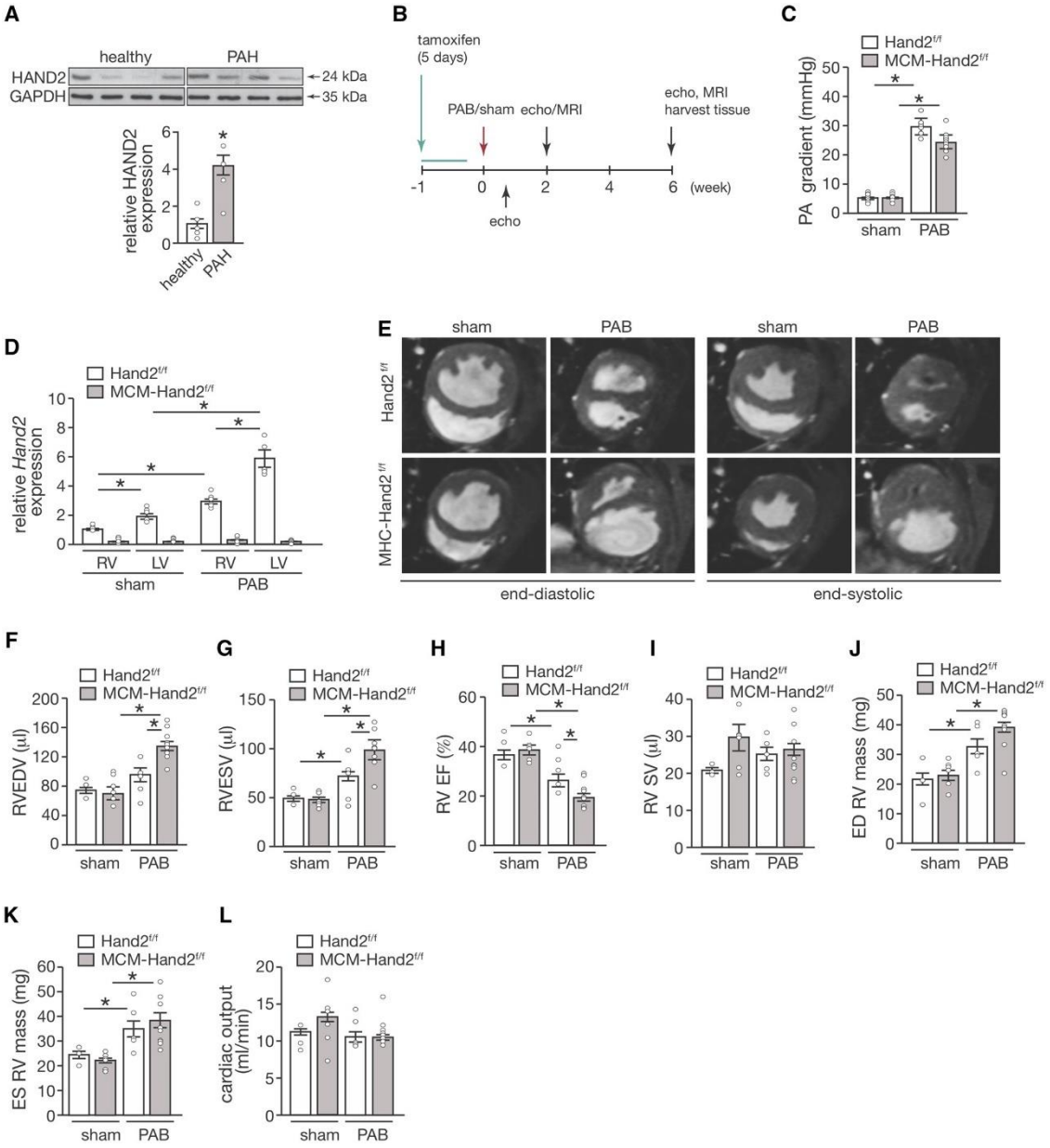

Figure 1. *Cardiac-specific depletion of Hand2 sensitizes the RV to pressure overload. (A) Western blot analysis of HAND2 and GAPDH as loading control in human heart tissue from healthy controls and pulmonary arterial hypertension patients. (B) Design of the in vivo study; (C) assessment of pulmonary artery pressure gradient in control (Hand2$^{F/F}$) and knockout (MCM-Hand2$^{F/F}$) mice 5 days after either sham or PAB surgery; (D) quantitative real-time PCR analysis of Hand2 expression in RV tissue from Hand2$^{F/F}$ and MCM-Hand2$^{F/F}$ animals either after sham or PAB surgery; (E) representative images of short-axis plan in end-diastole and end-systole hearts obtained by cardiac resonance image from Hand2$^{F/F}$ and MCM-Hand2$^{F/F}$ animals either after sham or PAB surgery Cardiac function was assessed in hearts from Hand2$^{F/F}$ and MCM-Hand2$^{F/F}$ animals either after sham or PAB surgery, and followed by quantitative analysis: (F) RV EDVs and (G) RV ESVs; (H) RV EF; (I) RV SV; (J) RV end-diastolic mass; (K) RV end-systolic mass; and (L) CO. Data are from 5–10 animals per group. Statistical analysis using one-way ANOVA with Tukey's multiple comparisons test. ∗P<0.05 between indicated groups (error bars are SEM).*

Table 1 MRI assessment of right ventricle function parameters of Hand2$^{F/F}$ and MCM-Hand2$^{F/F}$ mice at 2 and 6 weeks of sham or PAB.

	Hand2$^{F/F}$				MCM- Hand2$^{F/F}$			
	Sham		PAB		Sham		PAB	
	2 weeks	6 weeks	2 weeks	6 weeks	2 weeks	6 weeks	2 weeks	6 weeks
Stroke volume (µL)	27.0 ± 3.2	21.1 ± 1.1	24.0 ± 2.1	24.9 ± 2.4	26.9 ± 2.3	23.8 ± 4.0	25.9 ± 1.8	23.1 ± 2.8
Cardiac output (mL/min)	14.1 ± 1.3	11.1 ± 1.3	10.0 ± 0.9*	10.4 ± 0.8*	12.9 ± 0.8	13.3 ± 1.3	11.9 ± 0.6	10.6 ± 1.0*
ED volume (µL)	71.2 ± 8.9	72.0 ± 6.8	84.1 ± 12.5	91.7 ± 13.5	66.5 ± 3.1	68.8 ± 6.1	116.9 ± 7.4$^{*\#}$	117.8 ± 10.7$^{*\#}$
ES volume (µL)	44.1 ± 5.8	50.9 ± 6.1	60.1 ± 14.4	66.7 ± 12.7*	39.5 ± 3.9	45.1 ± 2.5	91.0 ± 6.2$^{*\#}$	94.7 ± 10.2$^{*\#}$
ED mass (mg)	22.6 ± 1.7	22.3 ± 4.7	30.1 ± 3.2*	32.9 ± 3.8*	22.2 ± 2.8	23.2 ± 2.0	33.9 ± 2.6*	37.8 ± 2.0*
ES mass (mg)	20.4 ± 2.1	24.3 ± 2.2	29.9 ± 4.9	36.3 ± 4.7*	19.9 ± 2.4	21.6 ± 1.4	34.4 ± 1.2*	37.6 ± 3.1*
EF (%)	38.1 ± 1.9	38.2 ± 3.8	28.6 ± 2.0	26.1 ± 2.4*	40.9 ± 3.0	34.8 ± 2.3	22.3 ± 1.3$^{*\#}$	19.4 ± 2.1$^{*\#}$

*Data are expressed as means ± SEM. ED, end-diastole; ES, end-systole; RV, right ventricle; EF, ejection fraction.*P < 0.05 vs. sham group.#P < 0.05 vs. experimental group. n.s.=5–10 animals per group.*

Table 2 Morphometric characteristics of Hand2$^{F/F}$ and MCM-Hand2$^{F/F}$ mice subjected to 6 weeks of sham or PAB.

	Hand2$^{F/F}$		**MCM- Hand2$^{F/F}$**	
	Sham	**PAB**	**Sham**	**PAB**
n	5	6	6	10
HW/BW (mg/g)	5.6 ± 0.5	7.3 ± 0.7*	5.9 ± 0.7	7.9 ± 0.3*
HW/TL (mg/mm)	7.9 ± 0.5	9.2 ± 0.4	7.9 ± 0.6	10.0 ± 0.4*
RVW (mg)	29.2 ± 2.1	39.3 ± 1.1*	26.5 ± 3.1	44.4 ± 3.9*
IVS+LV (mg)	127.1 ± 7.1	151.8 ± 9.0*	138.3 ± 5.2	150.2 ± 10.3*
Fulton index	0.18 ± 0.02	0.25 ± 0.01*	0.19 ± 0.03	0.30 ± 0.02$^{*\#}$

*Data are expressed as means ± SEM. HW, heart weight; BW, body weight; TL, tibia length; RVW, right ventricle weight; IVS, intraventricular septum; LV, left ventricle. *P < 0.05 vs. sham group. #P < 0.05 vs. experimental group. n.s.=5–10 animals per group.*

animals displayed similar levels of collagen deposition and formation of fibrotic lesions (*Figure 2I and J*). In line, no significant differences were observed for mRNA expression levels of the pro-fibrotic markers collagen type I (*Col1A*), transforming growth factor beta (*Tgfb*), and endoglin (*Eng*) between the banded animals (***Figure 2K– M***). This was also reflected at the protein levels, where no significant changes were observed for all the above markers nor plasminogen activator inhibitor-1 (PAI1), as readout of TGFβ signalling activation[34] (***Figure 2N***). Remarkably, despite silencing of *Hand2* resulting in lower levels of pro-fibrotic markers in the RV of sham animals, these levels significantly rose to control levels upon subjection to PAB.

As RV capillary rarefaction is a phenomenon that leads to maladaptive RV remodelling, we assessed the capillary to myocyte ratio of the RV in our different experimental groups. While histochemical analysis and respective quantification reflected higher capillary to myocyte ratio in control mice subjected to RV stress, a significant decrease was observed in *Hand2* knockout animals, under the same conditions (***Figure 2O***). These results were somewhat corroborated by the expression levels of vascular endothelial growth factor receptor 2 (*Vegfr2*). Whereas in control mice subjected to PAB there was a clear increase in VEGFR2 expression, the increase in the knockout mice was only mild, even if significant (***Figure 2P and Q***), and not able to promote adequate angiogenesis (***Figure 2O***).

Taken together, these data indicate that silencing of *Hand2* induces exacerbated hypertrophy while also impairing microvascular remodelling under conditions of RV pressure overload.

3.3 Effects of cardiac silencing of *Hand2* in the function and morphology of the LV under conditions of RV pressure overload

Based on interventricular interaction, any changes in RV shape will have consequences for the LV. While, we observed increased eccentricity for the banded animals at both end-diastole and end-systole, no differences were observed between control and knockout mice (***Figure 3A and B***). Increased LV eccentricity index reflects increased pressure of the RV and represents septal flattening, which affects LV function and remodelling. Pressure-overloaded animals, independent of the genotype, displayed decreased LV end-diastolic and -systolic volumes and subsequent decrease in SVs and CO (***Table 3***). No changes in systolic function were observed, as reflected by preserved LV EF throughout the different experimental groups (***Table 3***). Whereas animals subjected to PAB seem to display larger cardiomyocytes, this effect was not significant in the control or knockout mice (***Figure 3C***). In agreement, a clear up-regulation of the stress cardiac genes *Nppa, Nppb*, and *Myh7* in the LV of control-banded animals was observed but the expression levels remained at baseline in banded-knockout animals (***Figure 3D– F***). A significant down-regulation in *Acta1* mRNA expression levels in the LV, after PAB, was observed, independently of the genotype and in contrast to what was observed for the RV (***Figures 2F and 3G***). While a clear increase in *Rcan1.4* was observed in the LV of control hearts upon RV pressure overload, *Rcan1.4* mRNA levels were significantly decreased in the knockout LVs, under similar conditions, compared to the control LVs (***Figure 3H***). Although increased

collagen deposition and fibrotic lesions were observed in the LVs of the control mice subjected to PAB, this was not observed in knockout animals (***Figure 3I and J***). Similar results were obtained regarding mRNA and/or protein expression levels of *Col1a, Tgfb, Pai1*, and *Eng* in the LV tissue (***Figure 3K– N***).

Table 3 MRI assessment of LV function parameters of Hand2$^{F/F}$ and MCM-Hand2$^{F/F}$ mice at 2 and 6 weeks after PAB.

	Hand2$^{F/F}$				MCM- Hand2$^{F/F}$			
	Sham		PAB		Sham		PAB	
	2 weeks	6 weeks	2 weeks	6 weeks	2 weeks	6 weeks	2 weeks	6 weeks
Stroke volume (µL)	35.2 ± 0.9	32.3 ± 2.0	27.3 ± 3.9	23.3 ± 1.3*	38.6 ± 2.7	35.6 ± 2.4	21.7 ± 1.8*	22.1 ± 1.4*
Cardiac output (mL/min)	18.4 ± 0.4	16.9 ± 1.8	11.4 ± 1.7*	9.8 ± 0.5*	18.6 ± 0.8	17.1 ± 1.2	9.9 ± 0.7*	10.2 ± 0.6*
ED volume (µL)	92.7 ± 2.8	91.5 ± 7.7	58.9 ± 9.4*	53.7 ± 4.9*	86.3 ± 2.8	84.5 ± 4.5	47.5 ± 2.8*	52.2 ± 4.7*
ES volume (µL)	57.5 ± 3.4	59.3 ± 6.1	31.6 ± 6.2*	30.4 ± 3.9*	47.7 ± 2.8	48.8 ± 3.2	25.7 ± 1.7*	30.0 ± 4.4*
ED mass (mg)	53.7 ± 7.1	53.0 ± 1.5	38.3 ± 4.1*	39.3 ± 3.2*	54.1 ± 3.2	59.1 ± 3.2	37.8 ± 1.9*	40.3 ± 1.5*
ES mass (mg)	59.1 ± 4.5	57.7 ± 6.7	43.2 ± 3.8	42.8 ± 4.1	60.3 ± 4.0	63.4 ± 4.6	40.2 ± 2.1*	43.0 ± 2.2*
EF (%)	38.1 ± 1.9	35.5 ± 1.7	47.4 ± 3.8	44.0 ± 2.0	44.6 ± 2.5	42.3 ± 1.9	45.5 ± 2.6	42.4 ± 3.0

*2 or 6 weeks of sham or PAB. Data are expressed as means ± SEM. ED, end-diastole; ES, end-systole; LV, left ventricle; EF, ejection fraction. *P < 0.05 vs. sham group. n.s.=5–10 animals per group.*

Figure 2

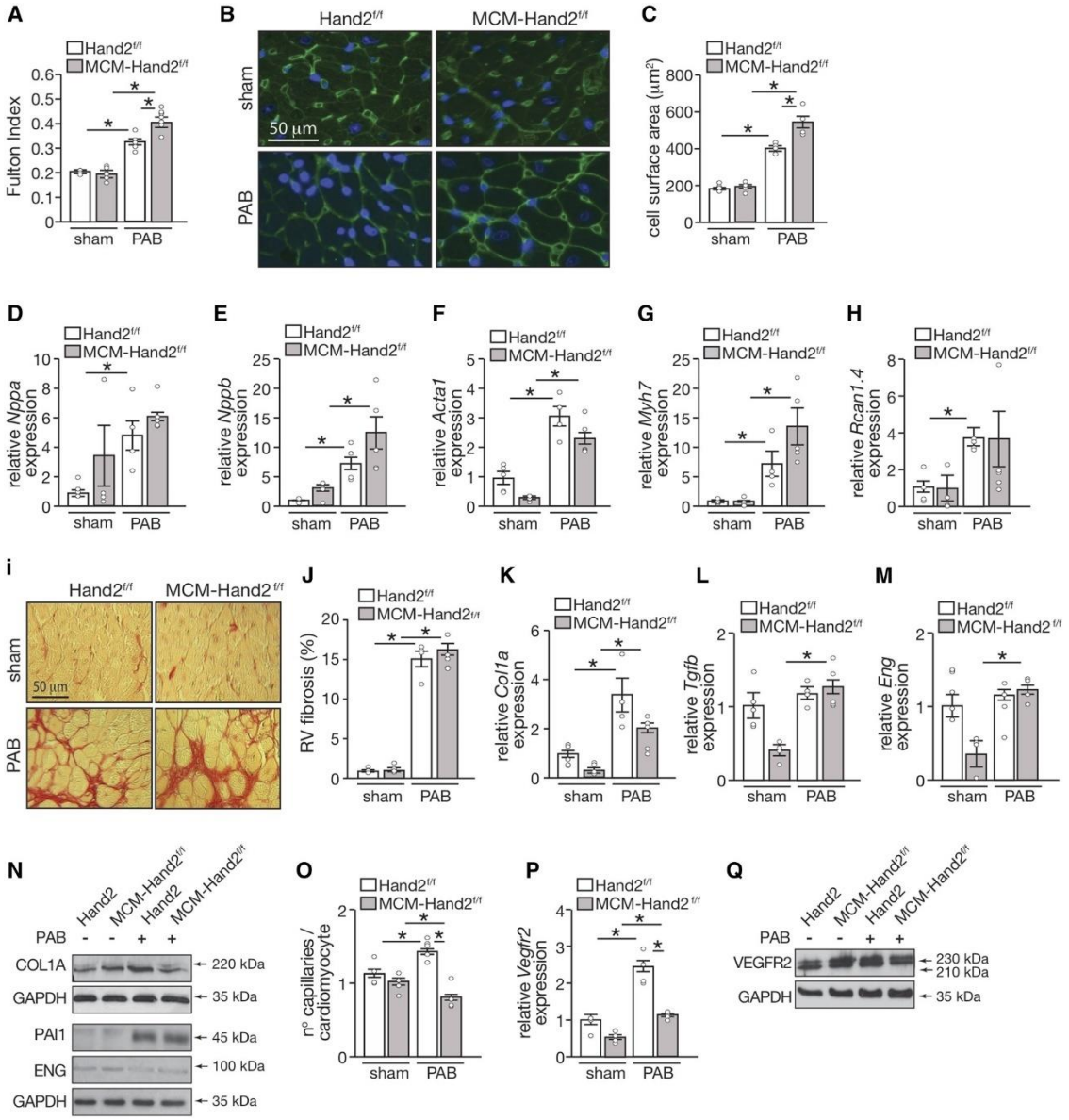

Figure 2 *Assessment of RV remodelling induced by PAB upon cardiac depletion of Hand2. (A) Fulton's index values (ratio of RV weight to LV plus septal weight) of Hand2$^{F/F}$ and MCM-Hand2$^{F/F}$ animals either after sham or PAB surgery; (B) high-magnification of representative images of histological sections stained for WGA; and (C) quantification of CSA in (B), n =30 microscopic field/heart, 3 hearts. (D–H) Quantitative real-time PCR analysis was performed to assess the expression levels of several genes known to be related to cardiac hypertrophy in RV tissue from Hand2$^{F/F}$ and MCM-Hand2$^{F/F}$ animals either after sham or PAB surgery: (D) Nppa; (E) Nppb; (F) Acta1; (G) ß-myosin heavy chain; (H) regulator of Calcineurin 1 Isoform 4; (I) high-magnification of representative images of histological sections stained for Sirius Red; (J) quantification of collagen deposition in (I), n =30 microscopic field/heart, 3 hearts. Quantitative real-time PCR analysis of (K) collagen type I alpha 1 chain; (L) Tgfb and (M) Eng; (N) representative images of western blot analysis of COL1A, PAI-1, ENG, and GAPDH as loading control in RV tissue of Hand2$^{F/F}$ and MCM-Hand2$^{F/F}$ animals subjected to either* *(continue next page).*

Figure 2. Continued *sham or PAB surgery (O) Capillaries in RV sections of Hand2$^{F/F}$ and MCM-Hand2$^{F/F}$ mice subjected to either sham or PAB surgery were identified by isolectin B4 immunohistochemistry combined with WGA and, from the images obtained, we determined (P) quantitative real-time PCR analysis of Vegfr2 expression levels in the RV of Hand2$^{F/F}$ and MCM-Hand2$^{F/F}$ animals, subjected to either sham or PAB surgery. (Q) Representative images of western blot analysis of VEGFR2 and GAPDH as loading control in RV tissue of Hand2$^{F/F}$ and MCM-Hand2$^{F/F}$ animals subjected to either sham or PAB surgery. Data are from 5–10 animals per group, except for the western blots where protein lysates from 3–5 hearts per group were pulled in one sample. Statistical analysis using one-way ANOVA with Tukey's multiple comparisons test. ∗P<0.05 between indicated groups (error bars are SEM).*

Figure 3.

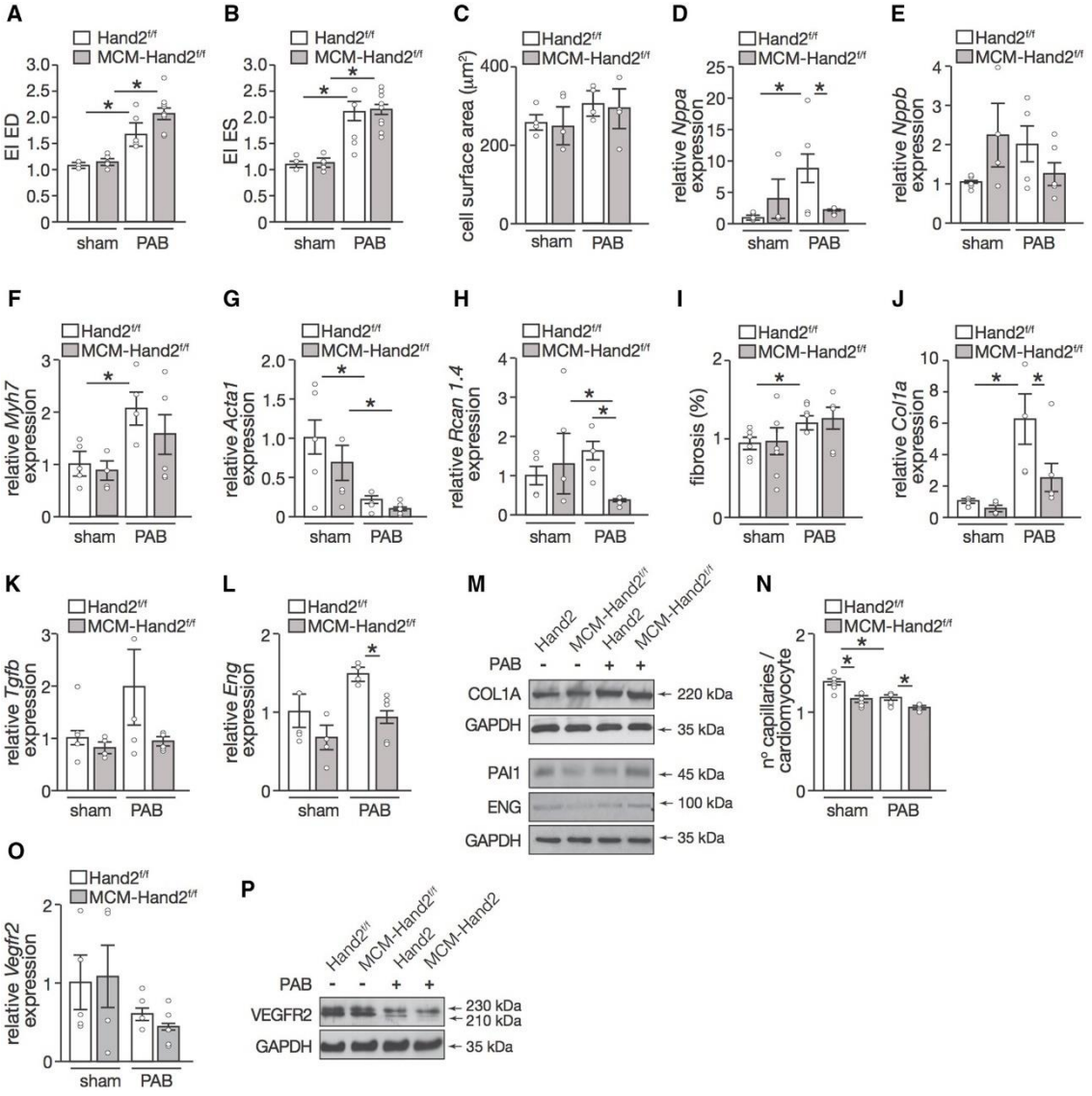

Figure 3 (previous page) *Assessment of LV remodelling induced by PAB upon cardiac depletion of Hand2. (A) Assessment of LV eccentricity index at end-diastole and (B) end-systole; (C) quantification of cardiomyocyte CSA from images of histological sections stained for WGA, n =30 microscopic field/heart, 3 hearts. (D–H) Quantitative real-time PCR analysis was performed to assess the expression levels of several genes known to be related to cardiac hypertrophy in RV tissue from Hand2$^{F/F}$ and MCM-Hand2$^{F/F}$ animals either after sham or PAB surgery: (D) Nppa; (E) Nppb; (F) β-myosin heavy chain; (G) Acta1; (H) regulator of Calcineurin 1 Isoform 4; (I) quantification of collagen deposition from images of histological sections stained for Sirius Red, n =30 microscopic field/heart, 3 hearts. (J–L) Quantitative real-time of (J) collagen type I alpha 1 chain; (K) TGFb and (L) Eng; (M) representative images of western blot analysis of COL1A, PAI-1, ENG, and GAPDH as loading control in LV tissue of Hand2$^{F/F}$ and MCM-Hand2$^{F/F}$ animals subjected to either sham or PAB surgery (N) capillaries in RV sections of Hand2$^{F/F}$ and MCM-Hand2$^{F/F}$ animals subjected to either sham or PAB surgery were identified by isolectin B4 immunohistochemistry combined with WGA and, from the images obtained, we determined the ratio of capillaries per cardiomyocyte ratios; (O) quantitative real-time PCR analysis of Vegfr2 expression levels in the RV of Hand2$^{F/F}$ and MCM-Hand2$^{F/F}$ animals, subjected to either sham or PAB surgery. (P) Representative images of western blot analysis of VEGFR2 and GAPDH as loading control in LV tissue of Hand2$^{F/F}$ and MCM-Hand2$^{F/F}$ animals subjected to either sham or PAB surgery. Data are from 5–10 animals per group, except for the western blots where protein lysates from 3–5 hearts per group were pulled in one sample. Statistical analysis using one-way ANOVA with Tukey's multiple comparisons test. ∗P<0.05 between indicated groups (error bars are SEM).*

When assessing the capillary density of the LV in our different experimental groups, we observed higher capillary density in the control mice compared to the knockout animals, in both sham and PAB groups, despite a decrease in the overloaded groups (***Figure 3O***). The lower capillary density observed at baseline in the *Hand2* knockout animals was even more reduced upon RV stress (***Figure 3O***). This was in line with the expression profile of Vegfr2, which although not significant, did show a trend to decrease in the absence of *Hand2*, either at baseline or under RV stress conditions (***Figure 3P and Q***).

These data suggest that RV pressure overload results in deformation of the LV with preserved LV function. Furthermore, while silencing of *Hand2* seems to ameliorate the molecular maladaptive response of the LV to RV stress, vascular remodelling remains slightly impaired.

3.4 Mechanisms underlying pressure overload-induced RV pathological remodelling

During RV failure, pathological remodelling is activated, as observed by an increase in cardiomyocyte hypertrophy and fibrosis, followed by a decline in cardiac function. To obtain more insight into the molecular and cellular mechanisms driving RV remodelling induced by pressure overload, we performed total RNA-sequencing in RV tissue derived from control (*Hand2$^{F/F}$*) animals subjected to either sham or PAB surgery. Transcriptomic analysis revealed 1399 genes to be differentially expressed, either up- or down-regulated, between the two groups (***Figure 4A*** **and Supplementary material online, Table S2**). Generation of a heatmap representing the 100 most differentially expressed transcripts between the experimental groups disclosed 17 down-regulated and 83 up-regulated genes in the banded WT animals (***Figure 4B***). To confirm the sequencing data, we have analysed the mRNA levels of several randomly selected

Figure 4.

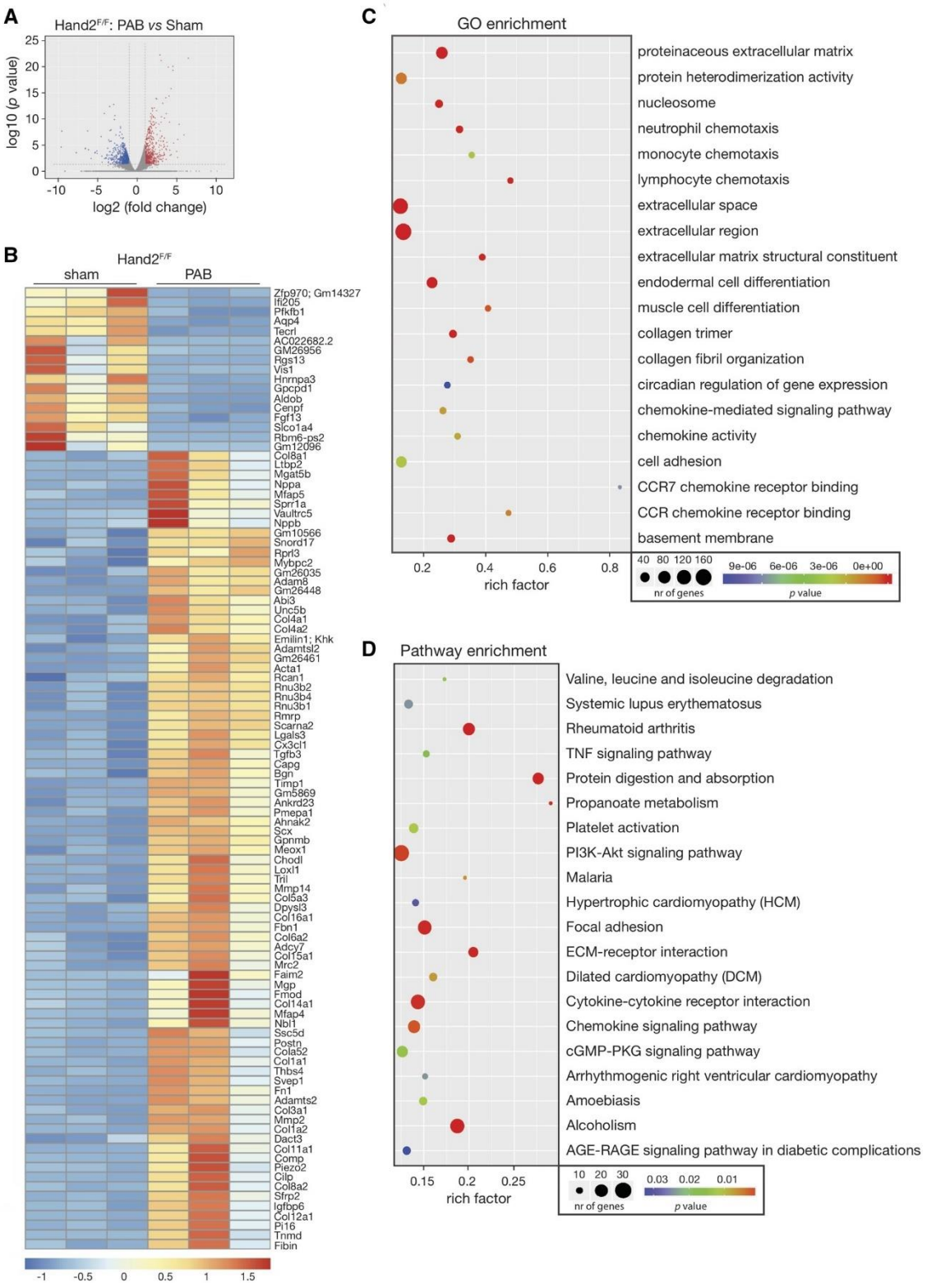
A
Hand2F/F: PAB vs Sham
log10 (p value)
log2 (fold change)
B
Hand2F/F
sham
PAB
C
GO enrichment
proteinaceous extracellular matrix
protein heterodimerization activity
nucleosome
neutrophil chemotaxis
monocyte chemotaxis
lymphocyte chemotaxis
extracellular space
extracellular region
extracellular matrix structural constituent
endodermal cell differentiation
muscle cell differentiation
collagen trimer
collagen fibril organization
circadian regulation of gene expression
chemokine-mediated signaling pathway
chemokine activity
cell adhesion
CCR7 chemokine receptor binding
CCR chemokine receptor binding
basement membrane
rich factor
nr of genes
p value
D
Pathway enrichment
Valine, leucine and isoleucine degradation
Systemic lupus erythematosus
Rheumatoid arthritis
TNF signaling pathway
Protein digestion and absorption
Propanoate metabolism
Platelet activation
PI3K-Akt signaling pathway
Malaria
Hypertrophic cardiomyopathy (HCM)
Focal adhesion
ECM-receptor interaction
Dilated cardiomyopathy (DCM)
Cytokine-cytokine receptor interaction
Chemokine signaling pathway
cGMP-PKG signaling pathway
Arrhythmogenic right ventricular cardiomyopathy
Amoebiasis
Alcoholism
AGE-RAGE signaling pathway in diabetic complications
rich factor
nr of genes
p value

Figure 4 (previous page) *Transcriptional changes in the pressure-overloaded RV. RNA-sequencing was performed to assess the transcriptomic changes in RV tissue from control (Hand2$^{F/F}$) animals subjected to either sham or PAB surgery for 6 weeks. (A) Volcano plot representation of differential expression of genes in the RV of sham and banded animals. Red and blue points mark the genes with significantly increased or decreased expression, respectively, in Hand2$^{F/F}$ sham to Hand2$^{F/F}$ PAB (FDR<0.01). The x-axis shows log2-fold expression changes and the y-axis the log10-fold likelihood of a gene being differentially expressed; (B) heatmap of the 100 top differentially expressed genes in the RV tissue of Hand2$^{F/F}$ sham compared to Hand2$^{F/F}$ PAB showing log2 FPKM (colour scale) values of dysregulated genes, with red and blue colours representing increased and decreased expression, respectively; (C) number of differentially expressed genes enriched in GO terms with P-value and rich factor shown in a scatterplot. The summarized GO terms are related to the biological processes upon PAB in the heart. Rich factor=number of differentially expressed genes in GO term/total number of genes in GO term. The larger the rich factor, the higher enrichment is. Circle size is proportional to the frequency of the GO term, whereas colour indicates the log10 P-value (red higher, blue lower); (D) KEGG pathway analysis of differentially expressed genes with P-value and rich factor shown in a scatterplot. Differentially enriched pathways in the RV tissue of control animals subjected to PAB, in comparison to sham.*

genes from both the most significantly up- and down-regulated genes by qPCR. From the down-regulated ones, we have determined the mRNA expression levels of 6-Phosphofructo-2-kinase/fructose-2,6-biphosphatase (*Pfkfb1*), Aquaporin 4 (*Aqp4*) and Centromere protein F and while all of them were decreased in mice subjected to PAB, only *Pfkfb1 and Aqp4* were significantly changed (**Supplementary material online, Figure S1a**). From the up-regulated ones, we have determined the mRNA expression levels of Collagen type VIII alpha 1 chain (*Col8a1*), Small proline rich protein 1A, and ADAM metallopeptidase domain 8 (*Adam8*) and, also here, while all of them were increased in mice subjected to PAB, only *Col8a1 and Adam8* were significantly changed (**Supplementary material online, Figure S1a**). Among the top up-regulated genes in the sequencing data, we found several collagens and fibrotic related genes (Collagen type VIII, type IV and type XVI alpha 1 chain, *Col8a1, Col4a1*, and *Col16a1*; Periostin, *Postn*; and Transforming growth factor beta-3) but also hypertrophic (natriuretic peptide A and B, *Nppa and Nppb*, respectively; Myocilin) and inflammatory genes (Interleukin 17 receptor C and Chemokine C-motif ligand 21A serine) (***Figure 4B***). After compiling our list of PAB-associated genes, we undertook a gene ontology (GO) enrichment analysis of this gene set, processing genes in terms of their associated molecular function. The top 20 GO terms based on biological processes and ranked by fold-enrichment are shown in ***Figure 4C***. This top-rank included biological processes, such as 'extracellular matrix-receptor interaction, collagen trimer, neutrophil chemotaxis, cell adhesion and chemokine signalling, receptor binding and activity'. The KEGG pathway analysis results revealed that the differentially expressed genes were highly associated with several pathways, including 'TNF-signaling pathway', 'hypertrophic cardiomyopathy', 'dilated cardiomyopathy', 'ECM-receptor interaction' as well as 'chemokine signaling' (***Figure 4D***). These results indicate that cardiac remodelling induced by PAB involves genes that are directly related to fibrosis, ECM remodelling, vascular function, and inflammation, in agreement with the RV and LV phenotypes observed in mice that were subjected to PAB.

3.5 Mechanisms underlying the role of Hand2 in pressure overload-induced RV pathological remodelling

Next, and to better understand how RV remodelling induced by pressure overload is affected by *Hand2* silencing, we performed RNA-sequencing to assess the transcriptomic changes in total RNA from RV tissue derived from control or knockout animals subjected to PAB. Transcriptome analysis identified 1783 transcripts potentially regulated by Hand2 (***Figure 5A* and Supplementary material online, Table S3**). Generation of a heatmap representing the 100 most differentially expressed transcripts between the 2 experimental groups revealed 33 down-regulated and 67 up-regulated genes in the RV of *Hand2* knockout mice (***Figure 5B* and Supplementary material online, Table S3**). To confirm the sequencing data, we have analysed the mRNA levels of several randomly selected genes from both the most significantly up- and down-regulated genes by qPCR. From the down-regulated ones, we have determined the mRNA expression levels of Caveolin 1, Matrix metallopeptidase 15, and *Adam8* and could confirm decreased expression levels in mice subjected to PAB for all of them (**Supplementary material online, Figure S1b**). From the up-regulated ones, we have determined the mRNA expression levels of Nebulette, Flavin containing dimethylaniline monooxygenase 2, and Ankyrin repeat domain 1 and while all of them showed a trend for increasing in mice subjected to PAB, these results were not significant (**Supplementary material online, Figure S1b**). The sequencing data revealed that upon silencing of Hand2, RV stress resulted in down-regulation of genes that are mostly associated with cellular components related to nucleic acid binding, regulation of transcription, and transcription factor activity (U3B small nuclear RNA 2, GINS complex subunit 2, Telomerase RNA component, and Transcription factor 7) and cell adhesion genes (*Adam8*, Angiopoietin-like protein 4, Rho GDP dissociation inhibitor alpha, Ankyrin repeat domain 63, and Ephrin B3) (***Figure 5B and C***). In turn, the up-regulated genes are associated with hypertrophy (*Nppb*; Myotrophin, and *Dmd*) and cell cycle inhibitors (Interferon activated gene 205 and cell division cycle 73) (***Figure 5B and C***). Interestingly, genes, such as Bone morphogenetic protein receptor, type II, Rho-associated coiled-coil containing protein kinase 2, and Tissue inhibitor of metalloproteinase 3, previously associated with PH, showed an even higher expression in the absence of *Hand2*. Furthermore, GO and pathway (KEGG) enrichment analysis associated the observed gene expression patterns with regulation of transcription, muscle cell differentiation, cellular response to hypoxia, as well as with development of different types of cancer and different signalling pathways in cancer, platelet activation, p53 signalling pathway, and cell communication through gap junctions (***Figure 5C and D***). These results reveal the role of Hand2 in specific molecular and cellular processes that key in the response of the RV to pressure overload.

Figure 5.

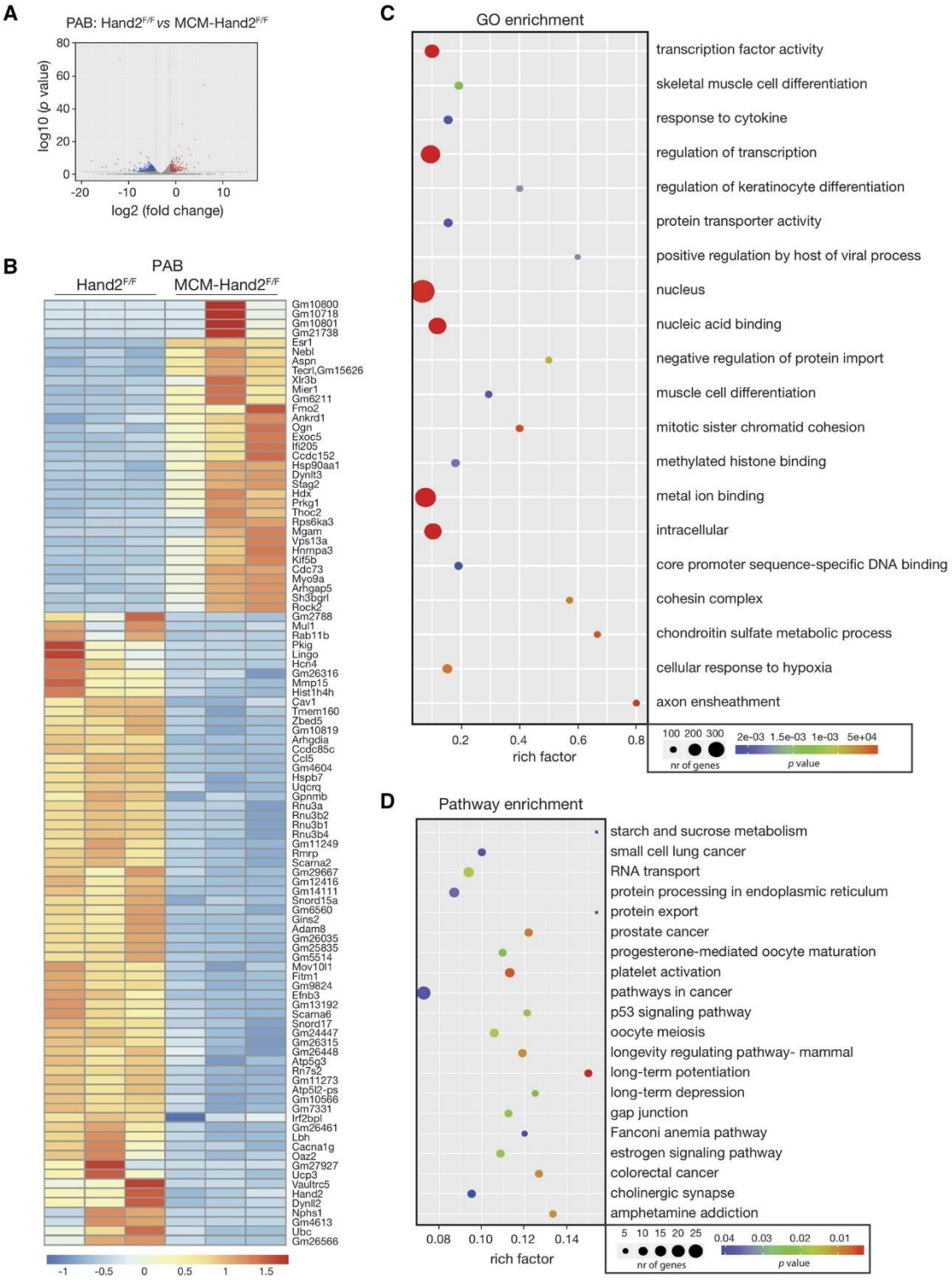
A
PAB: Hand2F/F vs MCM-Hand2F/F
log10 (p value)
log2 (fold change)
B
PAB
Hand2F/F
MCM-Hand2F/F
Gm10800
Gm10718
Gm10801
Gm21738
Esr1
Nebl
Aspn
Tecrl,Gm15626
Xlr3b
Mier1
Gm8211
Fmo2
Ankrd1
Ogn
Exoc5
Ifi205
Ccdc152
Hsp90aa1
Dynlt3
Stag2
Hdx
Prkg1
Thoc2
Rps6ka3
Mgam
Vps13a
Hnrnpa3
Kif5b
Cdc73
Myo9a
Arhgap5
Sh3bgrl
Rock2
Gm2788
Mul1
Rab11b
Pkig
Lingo
Hcn4
Gm26316
Mmp15
Hist1h4h
Cav1
Tmem160
Zbed5
Gm10819
Arhgdia
Ccdc85c
Ccl5
Gm4604
Hspb7
Uqcrq
Gpnmb
Rnu3a
Rnu3b2
Rnu3b1
Rnu3b4
Gm11249
Rmrp
Scarna2
Gm29667
Gm12416
Gm14111
Snord15a
Gm6560
Gins2
Adam8
Gm26035
Gm25835
Gm5514
Mov10l1
Fitm1
Gm9824
Efnb3
Gm13192
Scarna6
Snord17
Gm24447
Gm26315
Gm26448
Atp5g3
Rn7s2
Gm11273
Atp5l2-ps
Gm10566
Gm7331
Irf2bpl
Gm26461
Lbh
Cacna1g
Oaz2
Gm27927
Ucp3
Vaultrc5
Hand2
Dynll2
Nphs1
Gm4613
Ubc
Gm26566
-1 -0.5 0 0.5 1 1.5
C
GO enrichment
transcription factor activity
skeletal muscle cell differentiation
response to cytokine
regulation of transcription
regulation of keratinocyte differentiation
protein transporter activity
positive regulation by host of viral process
nucleus
nucleic acid binding
negative regulation of protein import
muscle cell differentiation
mitotic sister chromatid cohesion
methylated histone binding
metal ion binding
intracellular
core promoter sequence-specific DNA binding
cohesin complex
chondroitin sulfate metabolic process
cellular response to hypoxia
axon ensheathment
0.2 0.4 0.6 0.8
rich factor
100 200 300
nr of genes
2e-03 1.5e-03 1e-03 5e+04
p value
D
Pathway enrichment
starch and sucrose metabolism
small cell lung cancer
RNA transport
protein processing in endoplasmic reticulum
protein export
prostate cancer
progesterone-mediated oocyte maturation
platelet activation
pathways in cancer
p53 signaling pathway
oocyte meiosis
longevity regulating pathway- mammal
long-term potentiation
long-term depression
gap junction
Fanconi anemia pathway
estrogen signaling pathway
colorectal cancer
cholinergic synapse
amphetamine addiction
0.08 0.10 0.12 0.14
rich factor
5 10 15 20 25
nr of genes
0.04 0.03 0.02 0.01
p value

Figure 5 (next page) *Hand2-dependent transcriptional changes in the pressure-overloaded RV. RNA-sequencing was performed to assess the transcriptomic changes in RV tissue from control (Hand2$^{F/F}$) and knockout (MCM-Hand2$^{F/F}$) animals subjected to PAB. (A) Volcano plot representation of differential expression of genes in the RV of Hand2$^{F/F}$ vs. MCM-Hand2$^{F/F}$. Red and blue points mark the genes with significantly increased or decreased expression, respectively (FDR<0.01). The x-axis shows log2fold-expression changes and the y-axis the log10fold-likelihood of a gene being differentially expressed; (B) heatmap of the 100 top differentially expressed genes in the RV tissue of Hand2$^{F/F}$ sham compared to Hand2$^{F/F}$ PAB showing log2 FPKM (colour scale) values of dysregulated genes, with red and blue colours representing increased and decreased expression, respectively; (C) number of differentially expressed genes enriched in GO terms with P-value and rich factor shown in a scatterplot. The summarized GO terms are related to the biological processes upon PAB in the heart. Rich factor=number of differentially expressed genes in GO term/total number of genes in GO term. The larger the rich factor, the higher enrichment is. Circle size is proportional to the frequency of the GO term, whereas colour indicates the log10 P-value (red higher, blue lower); (D) KEGG pathway analysis of differentially expressed genes with P-value and rich factor shown in a scatterplot. Differentially enriched pathways in the RV tissue of knockout animals subjected to PAB, in comparison to control animals subjected to PAB.*

4. Discussion

Here, we aimed to unravel the role of Hand2 in RV remodelling and establish whether this transcription factor has a similar contribution to the remodelling of both ventricles in response to pressure overload. We demonstrated that RV pressure overload, by subjecting control animals (*Hand2*$^{F/F}$) to PAB, results in increased *Hand2* expression levels in both RV and LV ventricles, with the LV revealing higher levels of expression compared to the RV. Although *Hand2* is known to be expressed throughout the atrial and ventricular myocardium with its highest expression in the developing RV, these results are in line with our previous work where we have shown, in adult hearts, higher *Hand2* expression levels in the LV compared to the RV in both resting and stress conditions.[24] Whereas Hand2 participation in adult myocardial remodelling has not been thoroughly studied and understood, our studies indicate that ventricular pressure overload, either on the right or left side, induces *Hand2* expression in both ventricles, with the LV showing the highest levels. However, this contrasts with a study in mice and rats where induction of cardiac hypertrophy either by phenylephrine treatment for 3–5 days or aortic banding for 5, 14, and 21 days resulted in reduced *Hand1 and Hand2* RV expression levels.[25] In this study, we assessed Hand2 expression at 6 weeks after PAB and therefore, we cannot exclude a different expression pattern in the first days/weeks after banding as first response to the sudden cardiac stress.

As previously observed by us,[24] one would expect that correcting the expression levels of *Hand2*, which is elevated in disease, would reduce maladaptation and confer protection. Nevertheless, a loss-of-function mutation in the *Hand2* gene results in increased RV volumes at both end-diastole and end-systole, as well as decreased EF and CO in mice subjected to RV pressure overload, compared to controls, indicating an inability of the RV to adapt to pressure overload. Impaired cardiac function was associated with increased hypertrophic growth of the RV, reflected by increased heart weight to body weight ratios, increased Fulton index as well as elevated cardiomyocyte CSA. The fact that no differences were observed between male and female mice in their response to RV stress highlights the differences regarding female predisposition to PH or right HF between animals and humans. In rats, females seem to be less predisposed to develop PH and RV remodelling.[35] In humans, and even though women are more susceptible to PH than man, their RV function is better preserved.[36,37]

While collagen deposition reached similar levels in both control and *Hand2*-knockout mice subjected to RV stress, absence of *Hand2* inhibits expression of fibrosis-related genes markers early in the disease process. TGFb signalling is involved in tissue repair and scar formation[38] and not only it is an important regulator of vascular remodelling and inflammation of the lung[39] and kidney,[40] it also regulates hypertrophy and fibrosis in the heart.[41–43] While *Eng* is an established regulator of vascular remodelling,[44,45] it also plays a critical role in the development of fibrosis by serving as a coreceptor for TGFb signalling.[46,47] Their expression profiles confirm the similar collagen deposition observed in the banded animals, independently of the genotype and the fact that the *Hand2* knockout hearts display more severe hypertrophic phenotypes. These results, together with the observed increase in some of the hypertrophic gene markers, strongly suggest that absence of *Hand2* expression, under pressure overload of the RV, drives cardiac remodelling towards a more hypertrophic phenotype, without exaggerated fibrosis. Nevertheless, such a phenotype is characterized by a stronger impairment of cardiac function as reflected by the altered functional parameters measured by MRI.

Due to the pericardium and the common ventricular septum (ventricular interdependence), alterations in loading conditions of the RV are known to influence septal reconfiguration and motion towards the LV[48,49] and, in this way, affect LV performance by altering the LV pressure–volume curve.[50,51] Assessing the eccentricity index of the LV shape reflects the abnormal motion of the intraventricular septum depending on the type of RV overload, whether systolic or diastolic.[52] In our study, animals that were subjected to PAB revealed an index significantly >1.0 at both systole and diastole, which confirms right pressure overload[52] and subsequent abnormal leftward septal motion and configuration. But was the LV affected? In control mice, RV pressure overload did affect the LV as cardiomyocyte hypertrophy and mRNA expression of hypertrophic markers and pro-fibrotic genes were increased. In the absence of *Hand2* expression, the hypertrophic response was lost, with decreased cardiomyocyte CSA and associated gene expression. Whereas these results indicate some degree of protection, conferred by depletion of *Hand2*, analysis of LV function by MRI, revealed a decrease in LV volumes as well as in LV mass, reduced SVs and CO, explained by decreased preloading of the LV due to right-sided pressure overload. Previous studies have shown that impaired cardiac function is not always accompanied by transcriptional activation of the 'classical' marker genes associated either with hypertrophy or fibrosis and that it only happens once hypertrophy and/or fibrosis start to develop.[53,54] The fact that control mice subjected to RV pressure overload developed LV cardiomyocyte hypertrophy, but *Hand2* knockout hearts did not, might be explained by the absence/presence of transcriptional alterations of hypertrophic markers. In those studies, it was speculated that the absence of transcriptional deregulation and no alterations at the cellular level, such as hypertrophy and/or fibrosis, could facilitate recovery of cardiac function by specific treatments[53–55] or eventually reversing the stress. If this is the case in our study, remains to be clarified.

As LV diastolic filling is diminished in patients, and animal models, with PH,[56–59] this may cause a decrease in preloading of the LV and atrophy, and ultimately HF. In fact, reduction in LV mass was reported in disorders that are associated with chronic RV pressure overload, dysfunction, and altered LV diastolic filling.[60,61] LV atrophy is characterized by less prominent transcriptional changes in hypertrophic genes. This supports our findings in the *Hand2*-depleted animals subjected to PAB where we observed decreased LV mass, no hypertrophy, and no dramatic changes in hypertrophic gene expression. Whether the LV under these conditions becomes atrophic remains to be investigated as we would have to look at the IVS and LV separately as well as analyses the cardiomyocyte length and width in more detail.

We have previously identified differentially expressed transcripts of cardiac *Hand2* target genes in pressure-overloaded LVs from *Hand2* $^{F/F}$ *and MCM-Hand2* $^{F/F}$ animals.[24] Besides identifying several genes that had not previously been associated with cardiac hypertrophy, we also noticed a variety of genes involved in TGFb signalling as well as genes with defined functions during embryonic cardiac development.[24] Although RV remodelling due to increased pressure load is associated with increased expression of genes known to be involved in hypertrophy, fibrosis, and angiogenesis, most of those genes were not affected by silencing of *Hand2*. Unbiased approached gene analysis of *Hand2* KO hearts, subjected to RV pressure overload, revealed dysregulation of several other cardiac hypertrophy-associated genes, cell cycle inhibitors, and cellular components related to nucleic acid binding, regulation of transcription and transcription factor activity, as well as cell adhesion genes.

While in the pressure-overloaded RVs of *Hand2* KO animals, we observed differential expression of several pro-fibrotic and extracellular matrix component genes, genes involved in angiogenesis and endothelial cell function, sarcomere cytoskeleton genes, proinflammatory genes and also genes associated with cardiac hypertrophy and diastolic function; genes that are associated with embryonic development were not very prominent, in contrast to what we observed in the overloaded LVs, and suggesting that the set of *Hand2* target genes that are employed during response of the adult RV to pressure overload are very distinct from the ones engaged during cardiac embryonic development.

Altogether, our data indicate that *Hand2* depletion does not confer cardiac protection to RV pressure overload but in contrast, sensitizes the RV to stress. Furthermore, it indicates that modulation of *Hand2* expression has opposite effects in each of the ventricles and also supports the notion that each ventricle responds to stress in very dissimilar ways, involving different signalling pathways and different cellular processes. While inhibiting *Hand2* expression can prevent cardiac dysfunction in conditions of LV pressure overload, the same does not hold true for conditions of RV pressure overload, emphasizing that it is imperative to better understand the molecular mechanisms driving pathological remodelling of the RV in contrast to the LV, in order to better diagnose and treat patients with RV or LV failure.

Authors Contributions

R.F.V., A.M.C.K., L.O., E.M.P., J.M.M.K., K.W.V.D.K., D.S.N., and P.A.d.C.M.: substantial contributions to the conception of the work, acquisition and analysis of the data as well as its interpretation. Authors agreed to be accountable for parts of the work they have done. R.V.F., A.M.C.K., and P.A.d.C.M.: drafted the work. C.D.R., P.M.F., G.J.D.M.S., A.L., and A.L.-V.: substantial contribution to the design of the work, acquisition of human samples of PAH, and data interpretation. D.S.N., L.J.D.W., F.S.D.M., I.F.-P., R.M.F.B., and P.A.d.C.M.: substantial contribution to the design of the work and substantial contribution in critically revising the intellectual content of the work. All authors approved the final version of the work for publication. **Conflict of interest**: L.J.D.W. and P.A.d.C.M. are co-founders of Mirabilis Therapeutics BV.

Funding

This work was supported by the Foundation for Science and Technology of Portugal (FCT) grant (SFRH/BD/129507/2017 to R.F.V. and PTDC/BIM-MEC/4578/2014 to P.D.C.M.), by the Dutch CardioVascular Alliance (DCVA) awarded to the Phaedra consortium as well as the Impulse Grant 2018 awarded to the Phaedra IMPACT consortium (2012-08, 2014-11 to J.M.M.K., F.S.M., A.L.V., and P.D.C.M.), and by a Dutch Heart Foundation grant (NHS2010B261 to P.D.C.M.).

Translational perspective

RV failure associated with pulmonary hypertension reduces long-term survival rate to 55% within 3 years, suggesting that 3 years after diagnosis almost half of the patients will die. To revert these numbers an adequate RV-specific and, therefore, more efficient treatment is needed. Our work suggests that current therapies and potential mechanisms underlying LV failure may not be suitable for RV failure. While Hand2 deletion is favourable in LV response to

stress, it is particularly detrimental in the RV under similar conditions, and thus, highlighting potential severe consequences of not differentiating therapeutic targets or treatment for RV or LV failure.

Supplementary Figure 1.

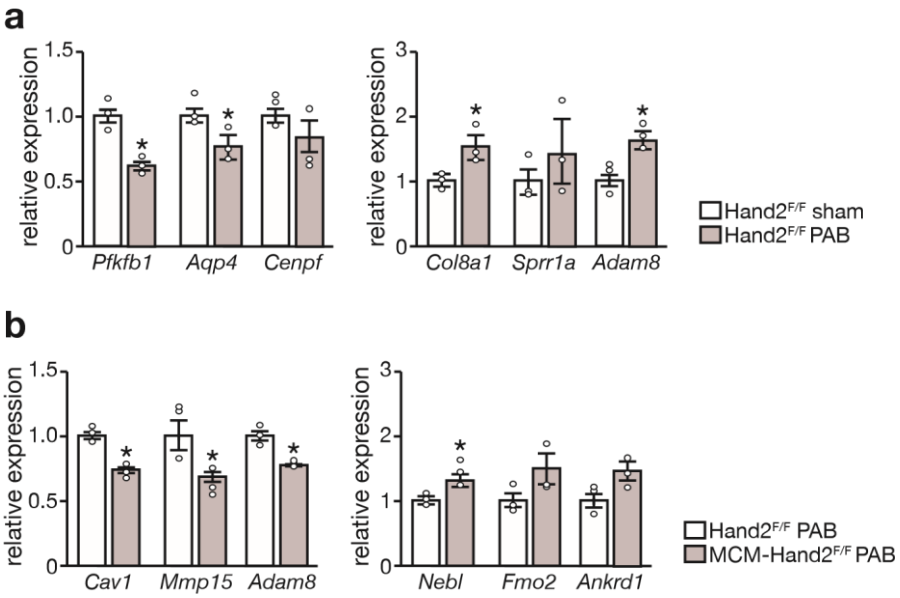

***Supplemental Figure 1**. Validation of RNA sequencing data by quantitative real-time PCR. Quantitative real-time PCR analysis was performed to assess the expression levels of several genes that were shown to be either up- or down-regulated in the sequencing data presented in figures 4 and 5. a) Expression levels of genes that were differentially expressed in RV tissue from Hand2$^{F/F}$ animals subjected to either sham or PAB surgery; b) Expression levels of genes that were differentially expressed in RV tissue from Hand2$^{F/F}$ and MCM-Hand2$^{F/F}$ animals subjected to PAB surgery. Data are from 5 animals per group and statistical analysis was performed using unpaired Student's t-test. $p < 0.05$ between indicated groups (error bars are s.e.m.).*

Supplementary Tables are available at Cardiovascular Research online

5. References

1. Ambrosy AP, Fonarow GC, Butler J, Chioncel O, Greene SJ, Vaduganathan M, Nodari S, Lam CSP, Sato N, Shah AN, Gheorghiade M. The global health and economic burden of hospitalizations for heart failure: lessons learned from hospitalized heart failure registries. J Am Coll Cardiol 2014;63:1123–1133.

2. Marques-Alves P, Baptista R, Marinho da Silva A, Peˆgo M, Castro G. Real-world, long-term survival of incident patients with pulmonary arterial hypertension. J Pulmonol 2017;23:124–131.

3. Dell'Italia LJ. The forgotten left ventricle in right ventricular pressure overload. J Am Coll Cardiol 2011;57:929–930.

4. Simon MA. Assessment and treatment of right ventricular failure. Nat Rev Cardiol 2013;10:204–218.

5. Abu-Issa R, Kirby ML. Heart field: from mesoderm to heart tube. Annu Rev Cell Dev Biol 2007;23:45–68.

6. Buckingham M, Meilhac S, Zaffran S. Building the mammalian heart from two sources of myocardial cells. Nat Rev Genet 2005;6:826–835.

7. Garry DJ, Olson EN. A common progenitor at the heart of development. Cell 2006; 127:1101–1104.

8. Meilhac SM, Esner M, Kelly RG, Nicolas JF, Buckingham ME. The clonal origin of myocardial cells in different regions of the embryonic mouse heart. Dev Cell 2004;6:685–698.

9. Steimle JD, Moskowitz IP. TBX5: A Key Regulator of Heart Development. Curr Top Dev Biol. 2017;122:195–221.

10. George RM, Firulli AB. Hand factors in cardiac development. Anat Rec 2019;302: 101–107.

11. Dyer LA, Kirby ML. The role of secondary heart field in cardiac development. Dev Biol 2009;336:137–144.

12. Barnes RM, Firulli BA, VanDusen NJ, Morikawa Y, Conway SJ, Cserjesi P, Vincentz, JW, Firulli AB. Hand2 loss-of-function in Hand1 -expressing cells reveals distinct roles in epicardial and coronary vessel development. Circ Res 2011;108:940–949.

13. Firulli AB, McFadden DG, Lin Q, Srivastava D, Olson EN. Heart and extra-embryonic mesodermal defects in mouse embryos lacking the bHLH transcription factor Hand1. Nat Genet 1998;18:266–270.

14. Riley P, Anson-Cartwright L, Cross JC. The Hand1 bHLH transcription factor is essential for placentation and cardiac morphogenesis. Nat Genet 1998;18:271–275.

15. Tsuchihashi T, Maeda J, Shin CH, Ivey KN, Black BL, Olson EN, Yamagishi H, Srivastava D. Hand2 function in second heart field progenitors is essential for cardiogenesis. Dev Biol 2011;351:62–69.

16. VanDusen NJ, Vincentz JW, Firulli BA, Howard MJ, Rubart M, Firulli AB. Loss of Hand2 in a population of Periostin lineage cells results in pronounced bradycardia and neonatal death. Dev Biol 2014;388:149–158.

17. VanDusen NJ, Casanovas J, Vincentz JW, Firulli BA, Osterwalder M, Lopez-Rios J, Zeller R, Zhou B, Grego-Bessa J, De La Pompa JL, Shou W, Firulli AB. Hand2 is an essential regulator for two notch-dependent functions within the embryonic endocardium. Cell Rep 2014;9:2071–2083.

18. McFadden DG, Charité J, Richardson J. A, Srivastava D, Firulli A B, Olson EN. A GATA-dependent right ventricular enhancer controls dHAND transcription in the developing heart. Development 2000;127:5331–5341.

19. Srivastava D, Thomas T, Lin Q, Kirby ML, Brown D, Olson EN. Regulation of cardiac mesodermal and neural crest development by the bHLH transcription factor, dHAND. Nat Genet 1997;16:154–160.

20. Srivastava D, Cserjesi P, Olson EN. A subclass of bHLH proteins required for cardiac morphogenesis. Science 1995;270:1995–1999.

21. Togi K, Yoshida Y, Matsumae H, Nakashima Y, Kita T, Tanaka M. Essential role of Hand2 in interventricular septum formation and trabeculation during cardiac development. Biochem Biophys Res Commun 2006;343:144–151.

22. Shen L, Li X-F, Shen A-D, Wang Q, Liu C-X, Guo Y-J, Song Z-J, Li Z-Z. Transcription factor HAND2 mutations in sporadic Chinese patients with congenital heart disease. Chin Med J (Engl) 2010;123:1623–1627.

23. Sun Y-M, Wang J, Qiu X-B, Yuan F, Li R-G, Xu Y-J, Qu X-K, Shi H-Y, Hou X-M, Huang R-T, Xue S, Yang Y-QA. HAND2 loss-of-function mutation causes familial ventricular septal defect and pulmonary stenosis. G3 (Bethesda) 2016;6:987–992.

24. Dirkx E, Gladka MM, Philippen LE, Armand AS, Kinet V, Leptidis S, Azzouzi HE, Salic K, Bourajjaj M, Silva GD, Olieslagers S, Nagel R, Van Der Weger RD, Bitsch N, Kisters N, Seyen S, Morikawa Y, Chanoine C, Heymans S, Volders PGA, Thum T, Dimmeler S, Cserjesi P, Eschenhagen T, Costa Martins PD, Windt LD. Nfat and miR-25 cooperate to reactivate the transcription factor Hand2 in heart failure. Nat Cell Biol 2013;15:1282–1293.

25. Thattaliyath BD, Firulli BA, Firulli AB. The basic-helix-loop-helix transcription factor HAND2 directly regulates transcription of the Atrial Naturetic Peptide gene. J Mol Cell Cardiol 2002;34:1335–1344.

26. Thattaliyath BD, Livi CB, Steinhelper ME, Toney GM, Firulli AB. HAND1 and HAND2 are expressed in the adult-rodent heart and are modulated during cardiac hypertrophy. Biochem Biophys Res Commun 2002;297:870–875.

27. Morikawa Y, D'Autré aux F, Gershon MD, Cserjesi P. Hand2 determines the noradrenergic phenotype in the mouse sympathetic nervous system. Dev Biol 2007;307: 114–126.

28. Sohal DS, Nghiem M, Crackower MA, Witt SA, Kimball TR, Tymitz KM, Penninger JM, Molkentin JD. Temporally regulated and tissue-specific gene manipulations in the adult and embryonic heart using a tamoxifen-inducible Cre protein. Circ Res 2001;89: 20–25.

29. Martin M. Cutadapt removes adapter sequences from high-throughput sequencing reads. EMBnet J 2011;17:10.

30. Langmead B, Salzberg SL. Fast gapped-read alignment with Bowtie 2. Nat Methods 2012;9:357–359.

31. Kim D, Pertea G, Trapnell C, Pimentel H, Kelley R, Salzberg SL. TopHat2: accurate alignment of transcriptomes in the presence of insertions, deletions and gene fusions. Genome Biol 2013;14:R36.

32. Pertea M, Pertea GM, Antonescu CM, Chang TC, Mendell JT, Salzberg SL. String Tie enables improved reconstruction of a transcriptome from RNA-seq reads. Nat Biotechnol 2015;33:290–295.

33. Frazee AC, Pertea G, Jaffe AE, Langmead B, Salzberg SL, Leek JT. Ballgown bridges the gap between transcriptome assembly and expression analysis. Nat Biotechnol 2015;33:243–246.

34. Datta PK, Blake MC, Moses HL. Regulation of plasminogen activator inhibitor-1 expression by transforming growth factor-b-induced physical and functional interactions between Smads and Sp1. J Biol Chem 2000;275:40014–40019.

35. Hautefort A, Mendes-Ferreira P, Sabourin J, Manaud G, Bertero T, Rucker-Martin C, Riou M, Ad~ao R, Manoury B, Lambert M, Boet A, Lecerf F, Domergue V, Bra´s-Silva C, Gomez AM, Montani D, Girerd B, Humbert M, Antigny F, Perros F. Bmpr2 mutant rats develop pulmonary and cardiac characteristics of pulmonary arterial hypertension. Circulation 2019;139:932–948.

36. Jacobs W, Veerdonk M. V D, Trip P, Man F. D, Heymans MW, Marcus JT, Kawut SM, Bogaard H-J, Boonstra A, Vonk Noordegraaf A. The right ventricle explains sex differences in survival in idiopathic pulmonary arterial hypertension. Chest 2014;145:1230–1236.

37. Thenappan T, Weir EK. Pulmonary arterial hypertension and sex in the right ventricle: it is an interesting picture! Am J Respir Crit Care Med 2020;202:928–929.

38. Massague´ J. TGF-beta signal transduction. Annu Rev Biochem 1998;67:753–791.

39. Coward WR, Saini G, Jenkins G. The pathogenesis of idiopathic pulmonary fibrosis. Ther Adv Respir Dis 2010;4:367–388.

40. Lo´ pez-Herna´ndez FJ, Lo´ pez-Novoa JM. Role of TGF-b in chronic kidney disease: an integration of tubular, glomerular and vascular effects. Cell Tissue Res 2012;347:141–154.

41. Dijke P. T, Arthur HM. Extracellular control of TGFbeta signalling in vascular development and disease. Nat Rev Mol Cell Biol 2007;8:857–869.

42. Liang H, Zhang C, Ban T, Liu Y, Mei L, Piao X, Zhao D, Lu Y, Chu W, Yang B. A novel reciprocal loop between microRNA-21 and TGFbRIII is involved in cardiac fibrosis. Int J Biochem Cell Biol 2012;44:2152–2160.

43. Goumans M, Dijke PT. TGF-b signaling in control of cardiovascular function. Cold Spring Harb Perspect Biol 2018;10:pii:a022210.

44. Li DY, Sorensen LK, Brooke BS, Urness LD, Davis EC, Taylor DG, Boak BB, Wendel DP. Defective angiogenesis in mice lacking endoglin. Science 1999;284:1534–1537.

45. Hawinkels LJAC, Kuiper P, Wiercinska E, Verspaget HW, Liu Z, Pardali E, Sier CFM, Dijke PT. Matrix metalloproteinase-14 (MT1-MMP)-mediated endoglin shedding inhibits tumor angiogenesis. Cancer Res 2010;70:4141–4150.

46. Chen K, Mehta JL, Li D, Joseph L, Joseph J. Transforming growth factor b receptor endoglin is expressed in cardiac fibroblasts and modulates profibrogenic actions of angiotensin II. Circ Res 2004;95:1167–1173

47. Shyu K-G, Wang B-W, Chen W-J, Kuan P, Hung C-R. Mechanism of the inhibitory effect of atorvastatin on endoglin expression induced by transforming growth factor beta1 in cultured cardiac fibroblasts. Eur J Heart Fail 2010;12:219–226.

48. Weyman A E, Wann S, Feigenbaum H, Dillon JC. Mechanism of abnormal septal motion in patients with right ventricular volume overload: a cross-sectional echocardiographic study. Circulation 1976;54:179–186.

49. Weber KT, Janicki JS, Shroff S, Fishman AP. Contractile mechanics and interaction of the right and left ventricles. Am J Cardiol 1981;47:686–695.

50. Bemis CE, Serur JR, Borkenhagen D, Sonnenblick EH, Urschel CW. Influence of right ventricular filling pressure on left ventricular pressure and dimension. Circ Res 1974;34:498–504.

51. Li KS, Santamore WP. Contribution of each wall to biventricular function. Cardiovasc Res 1993;27:792–800.

52. Ryan T, Petrovic O, Dillon JC, Feigenbaum H, Conley MJ, Armstrong WF. An echocardiographic index for separation of right ventricular volume and pressure overload. J Am Coll Cardiol 1985;5:918–927.

53. Grubb DR, Crook B, Ma Y, Luo J, Qian HW, Gao XM, Kiriazis H, Du XJ, Gregorevic P, Woodcock EA. The atypical 'b' splice variant of phospholipase Cb1 promotes cardiac contractile dysfunction. J Mol Cell Cardiol 2015;84:95–103.

54. Rowell J, Koitabashi N, Kass DA, Barth AS. Dynamic gene expression patterns in animal models of early and late heart failure reveal biphasic-bidirectional transcriptional activation of signaling pathways. Physiol Genomics 2014;46:779–787.

55. Matkovich SJ, Grubb DR, McMullen JR, Woodcock EA. Chronic contractile dysfunction without hypertrophy does not provoke a compensatory transcriptional response in mouse hearts. PLoS One 2016;11:e0158317.

56. Marcus JT, Vonk N. A, Roeleveld RJ, Postmus PE, Heethaar RM, Rossum ACV, Boonstra A. Impaired left ventricular filling due to right ventricular pressure overload in primary pulmonary hypertension: noninvasive monitoring using MRI. Chest 2001; 119:1761–1765.

57. Schena M, Clini E, Errera D, Quadri A. Echo-doppler evaluation of left ventricular impairment in chronic cor pulmonale. Chest 1996;109:1446–1451.

58. Krayenbuehl H, Turina J, Hess O. Left ventricular function in chronic pulmonary hypertension. Am J Cardiol 1978;41:1150–1158.

59. Lazar J, Flores A, Grandis D, Orie J, Schulman D. Effects of chronic right ventricular pressure overload on left ventricular diastolic function. Am J Cardiol 1993;72: 1179–1182.

60. Sutinen S, Pa¨a¨kko¨ P, Tienari J. Weights of the body and cardiac ventricles in pulmonary emphysema. Virchows Arch A Pathol Anat Histopathol 1985;407:249–257.

61. Gorter TM, Verschuuren EAM, Veldhuisen DV, Hoendermis ES, Erasmus ME, Bogaard HJ, Vonk Noordegraaf A, Berger RMF, Melle JV, Willems TP. Right ventricular recovery after bilateral lung transplantation for pulmonary arterial hypertension. Interact Cardiovasc Thorac Surg 2017;24:890–897

CHAPTER 3

"Non-Coding RNAs as Blood-Based Biomarkers in Cardiovascular Disease"

[1,2,3] RF Videira, [1,2,3]PA da Costa Martins, [3] I Falcão-Pires

[1] CARIM School for Cardiovascular Diseases, Faculty of Health, Medicine and Life Sciences, Maastricht University, 6229 ER Maastricht, The Netherlands, 2Department of Molecular Genetics, Faculty of Science and Engineering, Maastricht University, 6229 ER Maastricht, The Netherlands [3]Cardiovascular Research and Development Center, Faculty of Medicine, University of Porto, 4200-319 Porto, Portugal

Published in Int. J. Mol. Sci. 2020, 21(23), 9285;

doi.org/10.3390/ijms21239285

Abstract

In 2020, cardiovascular diseases (CVDs) remain a leading cause of mortality and morbidity, contributing to the burden of the already overloaded health system. Late or incorrect diagnosis of patients with CVDs compromises treatment efficiency and patient's outcome. Diagnosis of CVDs could be facilitated by detection of blood-based biomarkers that reliably reflect the current condition of the heart. In the last decade, non-coding RNAs (ncRNAs) present on human biofluids including serum, plasma, and blood have been reported as potential biomarkers for CVDs. This paper reviews recent studies that focus on the use of ncRNAs as biomarkers of CVDs.

Keywords: ncRNAs; biomarkers; cardiovascular diseases; diagnosis

Introduction

Cardiovascular diseases (CVDs) including aortic stenosis, hypertension, myocardial infarction, congenital heart diseases, aortic aneurysms, and right ventricle dysfunction can lead to heart failure (HF) and, ultimately, death. CVDs alone are responsible for more than 17.9 million deaths per year, corresponding to 31% of all deaths globally and being the first cause of morbidity and mortality worldwide (World Health Organization (WHO), data from 2019 [1]). Unfortunately, for most CVDs, treatment efficacy and outcome remain highly compromised by incorrect or late diagnosis. This unpredictability is attributed to the scarcity of obvious symptoms that indicate cardiac dysfunction, thus some CVDs are classified as "silent killers", contributing to a diagnosis that occurs after acute and/or severe symptoms episodes, usually occurring at a stage where reverting cardiac damage is no longer possible (WHO [1]).

Clinical management of CVDs could be facilitated by detection of blood-based biomarkers that reliably reflect the current condition of the heart. The term biomarker arises from the junction of the words "biological" and "marker". Biomarkers are defined by WHO as "any substance, structure, or process that can be measured in the body or its products and influence or predict the incidence of outcome or disease". Later, the definition of a biomarker was extended to "any measurement reflecting an interaction between a biological system and a potential hazard, which may be chemical, physical, or biological" [2].

Ideally, a human biomarker should be of easy access and acquirement, display a high degree of specificity and sensitivity, be stable in its environment (plasma, urine, blood, and saliva, among others), and thus have little or no variability [3]. While it is desirable that a biomarker can be determined by a simple, fast, and low-cost method [3], very few molecules satisfy these criteria and rather just meet a reduced number of these requirements. Up to date, CVD biomarkers are restricted to troponins, natriuretic peptides (namely, atrial natriuretic peptide (ANP) and brain natriuretic peptide (BNP)), matrix metalloproteases, and galectin-3, but other promising factors, such as non-coding RNAs, are slowly being introduced as both prognostic and diagnostic tools in cardiovascular clinical practice [4]. The search for ideal CVD biomarkers has deepened in the past years; however, there is still a long way to go until the golden biomarkers enter clinical practice.

In the recent years, a new class of potential biomarkers, including non-coding RNAs (ncRNAs), has received much attention in the cardiovascular field. Representing almost 60% of cell transcriptome, ncRNAs are functional RNA molecules that, despite lacking a protein-coding region, are essential players in gene regulation and, consequently, in cell function and survival [5]. The discovery of the first ncRNA lin-4, a small RNA able to decrease the translation of another gene, Lin-14, by directly binding to lin-14 RNA molecule [6], opened doors to discover many other forms of ncRNAs including microRNAs (miRNAs, miRs), long non-coding RNAs (lncRNAs), and circular RNAs (circRNAs), among others.

MiRNAs are small ncRNA (18–25 nucleotides) that inhibit the expression of their target gene(s) by sequence-specific recognition. The transcript-binding sequence is usually located in the 3'-untranslated region (3'-UTR), whereas the complementary seed sequence is located in the first two to eight nucleotides of the miRNA [7]. The degree of binding complementary between miRNA and mRNA sets the outcome of target transcript expression with high complementary, leading to transcript destabilization followed by degradation in processing

bodies (p-bodies) [8]. Meanwhile, a low complementary degree leads to translational repression, as binding to the mRNA cap prevents the translation initiation factor eIF4E, inhibiting the assembly of the ribosomal subunits or even promoting premature ribosomal drop-off and mRNA release from the ribosomal translational complex [9,10,11]. All of these regulatory mechanisms potentially enable a single miRNA to control hundreds of different target transcripts. Besides these endogenous mechanisms of action, cells can also secrete miRNAs that will be found extracellularly in human biofluids such as saliva, urine, serum, and plasma [12].

Although miRNAs are established as an important and possibly the most described group of ncRNAs, the largest portion of the ncRNA transcriptome is composed of lncRNAs. LncRNAs are a class of non-coding linear transcripts of more than 200 nucleotides in length, which frequently miss an open reading frame (ORF) and influence gene expression in a variety of manners [13]. Notwithstanding, some lncRNAs may display protein-coding functions, and several shared attributes of mRNAs such as 5' cap, more than one exon, alternative splicing, and poly(A) tails [13]. LncRNAs are commonly classified according to their genomic localization; those entirely transcribed from intronic regions of protein-coding RNA are termed intronic lncRNA, whereas the case wherein a lncRNA is transcribed from an intergenic region is named intergenic lncRNA. Additionally, a lncRNA could also be transcribed from an enhancer region, a regulatory DNA sequence of gene expression that increases promoter's activity, which are named eRNAs [14].

Similar to miRNAs, lncRNAs can also be found in different cellular compartments such as nucleus, cytoplasm, and extracellular space. In the nucleus, lncRNAs will influence transcription by recruiting regulatory factors and catalytic proteins; alternately, eRNAs drive proteins to enhancer regions, anchoring them to DNA in the right position and organizing chromatin interaction [15]. Oppositely, some lncRNAs recruit polycomb repressive complex 1 and 2 (PRC1, PRC2), promoting methylation marks and decreasing transcription [16,17]. In the cytoplasma, lncRNAs may act as miRNA sponges, preventing small ncRNAs from binding to their target transcripts or, alternatively, lncRNAs can serve as scaffolds for nucleoprotein complexes influencing mRNA translation and interfering with mRNA splicing and degradation [18,19]. Despite their many described functions, lncRNAs are still an understudied class, with many lncRNAs remaining to be identified and their functions described. Similar to miRNAs, lncRNAs can also be found in extracellular spaces and fluids, encapsulated in vesicles or bound to other particles, and have, therefore, also been studied as potential biomarkers of CVDs. Unlike protein-coding and other ncRNAs, lncRNAs sequence is poorly conserved among species, despite that the promoter regions of lncRNAs are often conserved, as well as their structure (namely their 3D conformation and shape) and their functionality [13].

A newly found class of ncRNAs is circRNAs, which, in contrast with previously reported ncRNAs, are characterized by a circular form that arises as a consequence of back splicing events [20]. CircRNAs are small, single-stranded RNA sequences with loop structures covalently closed that confer them, unlike linear ncRNAs, protection from degradation by ribonucleases [20]. CircRNAs can act as decoy elements working through protein interaction; regulate mRNA splicing processes by recruiting splicing factors; and, under special conditions, they could be translated into proteins once internal ribosome entry site (IRES) was initiated [21].

Furthermore, circRNAs are conserved among species, with some of them displaying cell-type and spatial-temporal specificity [22]. Emerging evidence suggests a myriad of mechanisms by which circRNAs can influence gene expression, participating in cell function and contributing to pathological processes, including several ones associated with CVDs [23]. Another peculiarity of circRNAs is the presence of multiple miRNA response elements (MERs), which may compete with miRNA targets for binding and, as such, serve as miRNA sponges [23].

CircRNAs can also affect gene transcription of the so-called parent gene, the gene that mRNA gives origin to the circRNA after back splicing, through interaction with RNA polymerase II and regulation of its transcriptional activity [24]. As for other ncRNAs, circRNAs can also be detected in different human biofluids, and their role as biomarkers has been recently reported in cancer [25,26].

Here, we will review the literature on the detection of ncRNAs in human samples of blood, plasma, and serum and conclude on their potential as biomarkers of CVDs.

A variety of cardiac diseases have different etiologies and specific events that can lead to the expression and circulation of cardiac-derived biomarkers.

Aortic-Related Diseases

Aortic Valve Stenosis

Aortic valve stenosis (AS) affects more than 5% of the population above 65 years old. It is defined as a narrowing of the aortic valve that progressively imposes resistance to the blood flow from the left ventricle (LV) to the aorta [27]. Unfortunately, as AS symptoms occur at an advanced disease stage, where cardiac damage is no longer reversible, the disease has a dismal prognosis in symptomatic individuals. Currently, there is no pharmacological treatment for AS and the most efficient solutions include surgical aortic valve replacement (SAVR) or trans-catheter aortic valve replacement (TAVR). However, valve replacement has been associated with risk of vascular access-site bleeding, blood transfusion-related infections, stroke, para-valvular leaks, and heart block, which also increase the risk of HF and death following valve replacement [28].

NcRNAs have been studied as prospective biomarkers of AS thanks to their potential to reflect AS pathogenesis and to be detected at an earlier AS stage. Blood-based ncRNA biomarkers could aid in patient's risk stratification and decision making, such as the timing and type of intervention (SAVR vs. TAVR), as well as in predicting AS progression.

Clinically, AS is associated with LV hypertrophy and cardiac fibrosis. In fact, a study measuring the plasma levels of miR-1, miR-133, and miR-378 in AS patients suggested that all three miRNAs were downregulated [29]. Yet, miR-378 is even lower expressed in patients with LV hypertrophy in comparison with those without hypertrophy, which indicates a strong negative correlation between miR-378 and LV mass and placing miR-378 as an independent predictor of LV hypertrophy in AS [29]. In a similar cohort of AS patients, circulating miR-210 was shown to be increased and to inversely correlate with LV end diastolic dimensions, cardiac parameters affected in AS [30]. This miRNA may also predict mortality as higher levels of miR-210 were found in patients with a high risk of mortality in follow-up studies. Although miR-210 is not established as an AS-specific marker, the results reported are comparable to data obtained

for the N-Terminal fragment of BNP levels and, when combined with other cardiovascular (CV) parameters, could help predict CV risk associated with AS [30].

Another study showed the presence of myocardial fibrosis in severe AS patients with LV preserved ejection fraction (EF). Interestingly, fibrosis directly associates with miR-21 plasma levels, suggesting that miR-21 levels reflect the degree of myocardial fibrosis [31]. Furthermore, plasma miR-21 levels provided more accuracy, sensitivity, and specificity to distinguish myocardial fibrosis when compared with common AS parameters such as global longitudinal strain and BNP levels [31]. Similar results were found by *Villar et al.*, unravelling that not only is circulating miR-21 increased in AS patients compared with healthy controls, but also an increase in circulating miR-21 increase is proportional to an increment in myocardial miR-21 expression as well as of cardiac fibrotic genes [32].

Analysis of peripheral blood collected from AS patients demonstrated that serum miR-19b levels are abnormally decreased and inversely correlated with LV stiffness and collagen cross-linking when matched to age and gender healthy controls [33]. Previously, members of the miR-17-92 cluster, to which miR-19 belongs, were reported to regulate myocardial fibrosis and angiogenesis [34]. However, the role of angiogenesis is still unclear, with some studies reporting that the degree of myocardial angiogenesis is accompanied by increased hypertrophy, worsening of systolic function, and severe AS [35,36]. On the other hand, a study demonstrated that increased angiogenesis and cardiomyocytes proliferation prevent maladaptive remodeling in a model of LV pressure-overload [37].

Interestingly, a number of different miRNAs have been related to different phenotypes of AS [38]. For example, AS patients with a low flow condition display high levels of miR-1, miR-21, and miR-133, whereas higher levels of miR-133 reflect LV hypertrophy [38]. In fact, patients with severe AS and reduced EF demonstrated increased levels of miR-1, miR-29, and miR-133 [38]. Curiously, in conditions of pressure-overload such as AS, miR-29 levels were clinically different among males and females [39]. Above the age of 50 and compared with control healthy women, women with AS showed a significant enrichment of miR-29 that is associated with increased LV mass and concentricity [39].

Despite certain circRNAs showing aortic valvular tissue specificity, and several associations that have been suggested between lncRNAs and AS pathology, to date, no studies have reported the association of AS with either plasma circRNAs or lncRNAs [40,41].

Aortic Aneurysm

Aortic aneurysm (AA) represents an important cause of death. AA is clinically characterized by an enlargement of at least 50% of an aortic segment compared with the same segment in healthy individuals and can be subdivided in thoracic aortic aneurysm (TAA) or abdominal aortic aneurysm (AAA), the latter being the most frequent [42]. AA is accompanied by progressive degeneration of the aortic wall [42]. Initially, a bulge-like dilation of a segment of the aortic wall tends to expand and increase the risk of rupture [42].

AA incidence and prognosis is associated with patient's sex and age, typically men and elderly populations are more affected by AA and demonstrate worse outcomes [42]. To date, there are no efficient pharmacological therapies against AA; therefore, when an AA progresses to a severe stage, surgery procedures are required [42].

An early and correct diagnosis could avoid surgery and improve patient's outcome. As nearly all patients are asymptomatic, an early diagnosis becomes difficult [43]. Most of the cases are detected during screenings using imaging techniques such as computerized tomography angiogram (CTA), ultrasound sonography (US), and magnetic resonance imaging (MRI) [42]. However, these techniques are expensive and incur hazards, thus new markers are needed, which encourages the exploration of ncRNAs' potential candidates. Recently, blood-based biomarkers such as tenascin-C, C-reactive protein, cystatin C, cathepsin, iron, immune system cells (lymphocytes and monocytes), genetic markers, and ncRNAs have emerged as attractive alternatives to help in AA diagnosis [44].

Among ncRNAs, miRs continue in the front of the biomarkers run as the most well described and studied ncRNAs. Therefore, it is not surprising that most AA related studies on ncRNAs focus on miRs.

In 2020, a small study described seven circulating miRs with an altered expression in AAA condition (n = 16) when compared with the control (miR-103a-3p, miR-27b-3p, miR-99a-5p, miR-375, miR-221-3p, miR-146a-5p, and miR-1260) [45]. After variable adjustment, only miR-221-3p and miR-27b-3p remained significantly overexpressed in AAA plasma, suggesting its potential as AAA biomarkers [45].

A work from *Wanhainen et al.* analyzed the circulating miRNA profile of 169 AAA patients and contrasted it against the profile of 48 healthy age and sex-matched individuals [46]. Of a predefined panel composed of the 172 most expressed miRs in plasma, 103 were found to be differentially expressed in the plasma samples of AAA patients relative to the plasma samples of healthy individuals [46]. The top altered miRs included miR-10b-5p, which displayed a specificity of 70% and a sensitivity of 60%, but, by adding let-7i-5p to the analysis, a specificity of 71% at a sensitivity of 90% was reached, allowing the discrimination between controls and AAA patients [46]. Despite improved sensitivity after combining different miRs, this result is still disappointing when compared with other studies and biomarkers.

On the other hand, lncRNAs were also reported as potential biomarkers for TAA [47]. In fact, TAA patients revealed decreased LUCAT1 and SMILR plasma levels when compared with a control group [47]. However, only LUCAT1 demonstrated an area under curve (AUC) higher than 0.65, indicating a modest potential diagnostic value for TAA [47].

More promising results were obtained by *Tian et al.*, who investigated the potential role of plasma circMARK3 to identify an advanced stage of aortic aneurysms, such as aortic dissection (when the inner aortic wall becomes tore), particularly acute aortic dissection -Standford type A (AAAD) [48]. The results showed that 506 circulating circRNAs were significantly dysregulated in AAAD cohort group compared with controls, including circRNAs that were 320 were significantly increased and 186 circRNAs that were significantly decreased [48]. From these, circMARK3 was chosen for further validation as a biomarker because of its high expression on AAAD [48]. After receiver operating characteristic (ROC) analysis, serum circMARK3 was characterized by an AUC of 0.9344 (using a cutoff value of 1.497), a sensitivity of 90.0%, and specificity of 86.7% [48]. Further combination of serum circMARK3 and miR-1273-3p revealed even improved results, namely, sensitivity and specificity were increased to 93.3% and 86.7%, respectively. The AUC of the combined ncRNAs was 0.9644 when using a cutoff value of 0.4807 [48].

Together, the results obtained by *Tian et al*. are very encouraging and highly suggest serum circMARK3 and miR-1273-3p as potential biomarkers for the AAAD condition.

Coronary Artery Disease

Often viewed as an inflammatory disorder, coronary artery disease (CAD) occurs when vessels that supply blood to the heart (coronary arteries) become damaged [49]. Artery plaque buildup due to atherosclerosis is a frequent cause of CAD, resulting in the narrowing of coronary arteries followed by myocardial ischemia and, ultimately, thrombosis and HF [49]. As the presence of plaques is influenced by age, smoking, and an unhealthy lifestyle, CAD affects mainly adults and elderly populations, displaying worse prognosis in developing countries [49]. Current therapeutic strategies are focused on pharmacological interventions to reduce the risk of atherosclerotic complications (decrease low density lipoprotein (LDL) levels, anti-thrombotic drugs) and symptoms (beta blockers and ranolazile, a drug that prevents late phase of the inward sodium current contributing to cardiac relaxation during diastole) [49]. At an advanced disease stage, mechanical interventions such as angioplasty, percutaneous coronary intervention (PCI) or coronary bypass surgery are needed to vascularize the blocked artery and to re-establish blood flow [49]. Although early CAD diagnosis is imperative to prevent plaque rupture and further associated complications, the existing methods, such as computed tomography, electrocardiogram (ECG), and echocardiography, may not be applied to the broad population owing to limited equipment availability, operated-dependent results, time constraints, and costs.

As CAD pathology is directly influenced by endothelial dysfunction, is it feasible to assume that endothelial-related miRNAs could constitute reliable biomarkers of CAD. Accordingly, miR-17 described as a negative regulator of tumor angiogenesis is highly expressed in plasma from patients with severe CAD and is a potential biomarker candidate [50]. Other miRNAs have been portrayed as potential biomarkers in plasma of CAD patients when compared with healthy control groups. Such is the case of plasma increased levels of miR-33, miR-208b, and miR-499, as well as decreased expression of miR-155, miR-145, and let-7c [51,52,53].

Notwithstanding, the levels of circulating miRNAs are not only capable of indicating the presence of CAD lesion, but also can differentiate and correlate with CAD severity, as shown for miR-206 [54]. Patients with major blocked coronary arteries or with a higher number of blocked coronary arteries have higher levels of miR-206 when compared with patients with less severe lesions or healthy controls [54]. As such, miR-206 is upregulated in individuals with three blocked coronary arteries when compared with individuals two blocked coronary arteries, and those showed enhanced levels of miR-206 when compared with individuals with only one blocked coronary artery.

Analysis of atherosclerosis- and cardiac-related lncRNAs levels in peripheral blood mononuclear cells (PBMCs) from CAD patients and healthy individuals revealed that three lncRNAs, KCNQ1OT1, HIF1A-AS2, and APO1, are significantly increased in patients when compared with the healthy controls [55]. Of the three, APO1 revealed the best diagnostic value with a sensitivity of 100% and a specificity of 80% [55]. The combination of these three lncRNAs improved the diagnostic score by increasing the specificity to 90% and maintaining the sensitivity at 100%. These results place KCNQ1OT1, HIF1A-AS2, and APO1 at the top of potential CAD biomarkers to be used in the clinics [55]. Another study revealed HOTAIR, an lncRNA

reported to be involved in vascular inflammation and age-associated-CVDs, as being upregulated in both plasma and PBMCs samples of CAD patients when compared with non-CAD patients [56]. Assessment of lncRNA expression profiles in plasma samples of both groups detected several differentially expressed lncRNAs, including lncRNAs GAS5 [57]. Although previously associated with several CVDs such as diabetes mellitus, hypertension, and valvular disease, a recent study has reported GAS5 to be significantly downregulated in CAD and diabetes mellitus, but not altered in other cardiovascular diseases such as hypertension, abnormal aortic aneurysm, viral myocarditis, atrial fibrillation, valvular disease, dilated cardiomyopathy, and peripheral artery disease [57].

A similar approach was taken by Vilades and colleagues, who categorize CAD patients according to the levels of plasma circ_0001445 (circSMARCA5), whose expression inversely correlated to coronary atherosclerosis extension and severity [58]. In fact, augmented circSMARCA5 levels are associated with a decreased segment stenosis score as well as with decreased cardiovascular risk [58]. Furthermore, RNA sequencing from plasma exosomes of CAD and non-CAD patients identified 335 exosomal circRNAs to be differentially expressed among the two groups [59]. After adjusting for risk factors, circ0005540 was upregulated in CAD patients, and displayed high sensitivity and specificity for identifying CAD patients, suggesting its potential as a CAD biomarker [59]. Similarly, circZNF609 also seems to be a promising biomarker for CAD [60]. CirZNF609 expression in peripheral blood leucocytes is decreased in CAD patients when compared with the control cohort [60]. Despite the different etiologies of CAD, overall, circZNF609 featured a specificity of 0.765 (76.5%) and a sensitivity of 0.804 (80.4%), indicating a moderate predicting value to identify CAD patients [60]. Furthermore, a microarray analysis of CAD and control PBMCs detected upregulation of circ_0001879 and circ_0004104 in CAD patients and these levels were associated not only with standard CAD biomarkers, but also with CAD risk factors [61]. Whereas both circRNAs can be individually used as biomarkers, combining both only showed an improved diagnostic value when combined with conventional CVD markers such as serum creatinine and CVD risk factors as hypertension, high LDL, smoking, and drinking, among others [61].

Myocardial Infarction

One of the consequences of CAD is the formation of a blood clot that, among other causes, occludes coronary arteries, resulting in ischemia and myocardial infarction (MI, also known as heart attack). In fact, a correlation between CAD and MI was previously established, namely on how well plasma miRNAs can predict CAD progression towards acute MI. A higher number of stenosed coronary vessels is associated with lower plasma miR-99a levels in MI patients [62]. Following PCI, miR-99 expression levels were re-established to comparable levels as observed in healthy volunteers. In MI, lower plasma miR-99 levels negatively correlated with those of cardiac troponin I and creatinine kinase (markers of cardiac dysfunction), suggesting that miR-99 expression might be necessary for proper cardiac function [62]. Similarly, miR-181a was also suggested to be a biomarker for MI as its increased plasma concentration is proportional to the severity of coronary stenotic lesions as well as deterioration of LV function [63]. Accordingly, miR-181a levels were positively correlated with creatinine kinase levels, and reduced 48 h after PCI [62,63].

Data from Centers for Disease Control and Prevention (CDC), a U.S. national public health institute, respective to the U.S. population, reported that, every 40 s, someone dies from a heart attack, and for every five occurrences, one is silent, meaning that no symptoms are recognized by the patient. Commonly, MI is diagnosed by combining an ECG test and analysis of biomarkers such as cardiac troponin I and T levels. However, ECG can only detect 30–70% of MI cases, highlighting the need for more accurate and sensitive biomarkers [64].

Various plasma miRNAs have been described as potential indicators of myocardial infarction, likely the most studied and described event among all cardiovascular diseases. Hence, miR-1, miR-126, miR-30a, miR-195, miR-26a-1, miR-146a, and miR-199a-1 were revealed to be upregulated in individuals diagnosed with acute MI (AMI) [65,66,67], with some of them, that is, miR-1, miR-126, miR-30a, and miR-195, reaching their maximal expression 8 h after the onset of symptoms [65,67,68]. In contrast, let-7b and miR-132-5p levels were decreased in acute MI patients when compared with control subjects [65]. AUC of ROC analysis only granted a modest individual value of sensitivity and specificity (below 90%), suggesting that each miRNA has moderate potential in the diagnosis of AMI patients. However, clustering of different miRNAs was more encouraging as an AUC of 0.913 was obtained when grouping miR-26a-1, miR-146a, and miR-199a-1 [66]. Other miRNAs such as miR-22-5p and miR-150-3p were also increased in MI by 36.47- and 4.09-fold, respectively, and even though they continued to be elevated for 72 h, the peak was reached at the onset of symptoms [69]. The sensitivity and specificity of the different miRNAs were calculated at different time points. Despite the fact that individual miRNAs showed a moderate power, when combined together, miR-132-5p, miR-22-5p, and miR-150-3p presented a better diagnostic value to distinguish AMI patients [69].

Microarray analysis in plasma samples of a small group of AMI patients identified 33 differentially expressed miRNAs, from which miR-30d-5p and miR-125-5p were selected for validation in a larger study population composed of 230 AMI patients and 79 healthy controls [70]. Despite the notable diagnostic value (namely specificity and sensitivity) of cardiac troponin I, the results obtained for miR-30d-5p surpassed the performance of cardiac troponin I by displaying an AUC of 0.915 [70] and highlighting the potential diagnostic use of miR-30d-5p and miR-125-5p in patients suspected of developing AMI [70].

Less promising results were reported for miR-221-3p, which, despite being upregulated by 3.89-fold in AMI [71], and an AUC of 0.881, did not reach the values of the standard marker troponin and neither improved the AUC levels when combined with troponin [71]. In line, miR-486 and miR-150 were also described as “exhibiting strong differentiation power” between healthy controls and AMI patients. However, the combination of both miR-486 and miR-150 only showed a moderated predictive power with an AUC of 0.731 [72]. Nevertheless, these two miRNAs were able to modestly classify AMI patients into ST elevation MI (STEMI) and non-ST elevation MI (NSTEMI) [72]. Typically, STEMI is associated with a more severe condition and worse prognosis.

Interestingly, even after pharmacological treatment, progression towards maladaptive remodeling occurs in approximately 30% of AMI patients [73]. A total of 14 plasma miRNAs and 16 serum miRNAs were found to be dysregulated in samples from AMI subjects [74]. Following cross data and validation (in different cohorts), only miR-30a-5p was significantly upregulated in patients with (HF) after an MI episode. Interestingly, miR-30a-5p levels at the onset of AMI

negatively correlate with LVEF six months after AMI, suggesting a prognostic value for miR-30a-5p, despite that it might also represent a marker of myocardial ischemia. The discriminatory power of miR-30a-5p to identified HF versus non-HF patients after MI was assessed by AUC calculation, resulting in an AUC of 75% [74].

As mentioned previously, one mechanism of action of lncRNAs is by competitively binding to miRNAs' target binding site, which prevents the attachment of mRNA–miRNA, thus inhibiting miRNA action. For example, lncRNA HOTAIR has a sponge like effect on miR-1, an miRNA upregulated in AMI cases [75]. HOTAIR is decreased in serum from subjects with AMI, reaching its lower expression 6 to 12 h after the onset of the first symptoms and negatively correlating with its target, miR-1 and cardiac troponin I [75]. Three days after the AMI episode, miR-1, cardiac troponin I, and HOTAIR levels are re-established [75]. Additionally, a study in mice subjected to hypoxia demonstrated that HOTAIR is myocardium-specific and that plasma HOTAIR in mice behaves similar to what was observed in humans, suggesting its myocardial origin [75].

Another myocardial enriched lncRNA is UCA1, which, similar to HOTAIR, is also decreased in the plasma of AMI individuals [76]. By clustering AMI patients according to the time from initial symptoms, it was possible to analyze the time course expression of UCA1 following an MI event [76]. While the lowest levels were reached between 6 and 12 h and remained low up to 48 h after AMI, from this point on, UCA1 levels increased and, at 96 h post-AMI, they were higher in AMI patients compared with the controls [76]. Interestingly, UCA1 also negatively correlates with miR-1 expression, but no mechanism has yet been described associating the two ncRNAs [76]. Although the predictive value of UCA1 alone is not as potent as standard biomarkers, the overall predictive power of UCA1 for AMI was increased to 0.983 AUC when combined with creatinine kinase [76].

Other lncRNAs have been attributed biomarker potential when screening for differentially expressed lncRNAs in plasma of 46 STEMI patients. While aHIF, KCNQ1OT1, and LIPCAR were found to be increased, six others, including HOTAIR, UCA1, MIAT, MALAT1, ANRIL, and CPNE3, were decreased in these patients [77]. The most promising diagnostic values were revealed for LIPCAR, with a sensitivity of 82% and a specificity of 75% in distinguishing STEMI subjects, and with LIPCAR levels positively correlating with cardiac troponin I and creatinine kinase and inversely with LV ejection fraction [77]. Notably, the increased levels of LIPCAR observed upon an STEMI event were decreased shortly after PCI [77].

Despite the relatively new role of circRNAs as biomarkers of AMI, *Deng et al*. found 160 circRNAs to be differentially expressed in AMI patients, with 87 of them being increased and 73 decreased when compared with healthy controls [78]. Among the most downregulated was circRNA_081881, showing a 12.5-fold change compared with the control group [78]. Currently, the most studied circRNA in MI is the myocardial infarction-associated circular RNA (MICRA) [79,80], which, by being decreased in plasma of MI patients, positively correlates with LV ejection fraction and accentuates the risk of LV dysfunction [79].

Congenital Heart Defects

In the past decade, prenatal testing made crucial advances and increased the survival rate up to 87% in the first year. Currently, neonatal congenital heart defects (CHDs) have an

incidence of 4–8 per 1000 births and their manifestations range from minor defects (such as small intracavitary communications) to severe defects that can even lead to prenatal lethality (CDC data, September 2020). The most common include tetralogy of fallot (TOF), atrial septal defect (ASD), ventricular septal defect (VSD) single ventricle (SV), persistent truncus arteriosus (PTA), and bicuspid aortic valve disease (BAV) [81]. A favorable CHD prognosis and reduced mortality is associated with early and correct diagnosis. However, the standard diagnostic method to detect CHD usually includes echocardiography and has an efficiency rate up to 35%, which is considerably low [82]. Additionally, some CHDs are diagnosed only after birth, during infancy, or even during adulthood. During pregnancy, several cardiogenesis-associated ncRNAs are potentially secreted by the fetus and enter into the maternal bloodstream, where they can be detected by blood analysis and used as biomarkers for CHD [83]. Multiple studies have also linked specific CHDs with an altered miRNA expression profile. In particular, children with ASD present a significant upregulation of let-7a and miR-486 and, although not statistically significant, an increase in hsa-let-7b levels when compared with healthy children [84]. Interestingly, mothers of ASD children express a similar miRNA expression pattern. In fact, because let-7a expression levels positively correlated between mothers and their offspring [84], its levels in the mother could predict ASD in children with a sensitivity of 82% and a specificity of 91%, indicating a significant diagnostic value of this miRNA in detecting ASD in children [84].

Bicuspid aortic valve disease (BAV), the most common anomaly of the human heart, results from an anomaly during valvulogenesis that is characterized by no splitting between two adjacent cusps, and it is frequently accompanied by dilation of the ascending aorta [85]. The most prominent miRNAs in adult BAV patients seem to be miR-122, miR-130a, and miR-486, and miR-718, with the latter being altered in BAV patients and inversely correlating with the diameter of the ascending aorta and, therefore, suggested as a potential biomarker of aortic dilation [86].

Overall, CHDs can be distinguished from non-CHDs through specific alterations in miRNA expression patterns [87]. Namely, miR-125b-2-3p, miR-1284, miR-142-5p, miR145-3p, miR-4426, miR-4666a-3p, and miR-4681 are downregulated, while miR-1275, miR-3664-3p, and miR4796-3p are upregulated in women pregnant with a CHD child compared with women pregnant with a non-CHD child [87]. Notably, such differences are no longer observed 24 h after delivery, supporting the hypothesis that the above miRNAs are pregnancy-related. ROC analysis demonstrated miR-142-5p to have the highest diagnostic accuracy with an AUC of 0.804 [87]. Indeed, the combination of the top four miRNAs (miR-142-5p, miR-1275, miR-4666a-3p, and miR-3664-3p) improved the accuracy in discriminating CHD from controls [87]. Interestingly, specific miRNAs can also be related to a particular CHD phenotype. For example, VSD revealed changes in miR-142-5p, miR-1275, miR-4666a-3p, and miR-3664-3p; TOF related to dysregulation of miR142-5p, miR-4666a-3p, and miR-3664-3p, while both SV and PTA were linked to miR-142-5p and miR-3664-3p differential expression [87].

A relatively small study, including 22 pregnant CHD-positive and 17 CHD-free controls, suggested miR-99a to be upregulated in the peripheral blood of the CHD-positive pregnant women when compared with the control group [88]. However, no diagnostic value was determined for this miRNA.

Yu et al. also suggested that a different group of miRNAs could identify CHDs such as ventricular septal defect (VSD), atrial septal defect (ASD), and tetralogy of fallot (TOF) [83]. The group composed of miR-19b, miR-22, miR-29c, and miR-375 is upregulated in maternal serum of CHD fetuses when compared with maternal serum of non-CHD fetuses [83]. When miRNAs were clustered according to the disease phenotype, all miRNAs were significantly upregulated in TOF, whereas only miR-19b and miR-29c were significantly increased in VSD and miR-19b, miR-29c, and miR-375 were increased in ASD [83]. Although all the miRNAs demonstrated a significant discriminatory value, and thus could be used as a disease biomarker for the detection of fetal CHD, the combination of all four miRNAs proved to be a more efficient diagnostic strategy.

Regarding lncRNAs in CHDs, HOTAIR was found to be upregulated in both myocardial tissue and plasma samples of ASD, VSD, and patent ductus arteriosus (PDA) patients when compared with healthy subjects, and thus was indicated as a potential biomarker for CHD [89]. HOTAIR seems to work through recruitment of PRC2 and inducing epigenetic modifications during embryonic heart development [89].

From a microarray-based strategy, 17,603 lncRNAs were found to be differentially present in the plasma of fetal CHD pregnant women [82]. From these, 3694 lncRNAs were significantly upregulated and 3919 were downregulated. Subsquently, this subgroup was subjected to gene ontology (GO) analysis to describe their association with specific biological processes, cellular components, and molecular functions through. GO analysis recognized 26 CHD-related lncRNAs, among which four were differentially altered in VSD, as well as another four in TOF, and two others were significantly different in ASD [82]. Overall, pregnant women with fetal CHD revealed alterations in ENST00000436681, ENST00000422826, AA584040, AA709223, and BX478947, when compared with the control group [82], all of them showing a moderated discriminating effect; therefore, it was suggested as potential lncRNA biomarkers to predict fetal CHD.

More recently, the possible value of circRNAs in the diagnosis of CHD has also been addressed. A study including 40 children with CHD (namely VSD and ASD) and 40 healthy children identified 10 upregulated and 157 downregulated circRNAs in the plasma of the CHD group. Validation by qPCR demonstrated three circRNAs, hsa_circRNA_004183, hsa_circRNA_079265, and hsa_circRNA_105039, to be significantly decreased in the affected group [90]. Hsa_circRNA_105039 presented the best diagnostic value with a sensitivity of 80%, a specificity of 100%, and AUC of 0.907, but altogether, the three circRNAs had an AUC of 0.965, suggesting a combinatorial approach to be effective in the diagnosis of CHD [90].

Right Ventricle Dysfunction

The right ventricle (RV) is responsible for pumping venous blood into the pulmonary vascular bed on the way to the LV, thereby contributing to left ventricular filling and cardiopulmonary function. Its thin walls and the direct connection with low impedance pulmonary circulation make the RV more sensitive to pressure than to volume overload [91]. Pulmonary hypertension (PH), pulmonary embolism, RV infarction, and cardiomyopathies are among the main causes of RV dysfunction and, consequently, failure [92]. Despite its critical contribution to heart function, the RV has been somewhat neglected, with only a few studies having specifically focused on RV failure. The limited knowledge of RV biology and function

contributes to the poor prognosis of RV failure (RVF) patients, with both treatment and diagnosis of RVF remaining challenging. Conventional diagnostic approaches are based on ECG, 3D-echocardiography and strain imaging, magnetic resonance imaging, and blood marker analysis such as lactate and BNP levels [93]. Although ncRNAs also recently started receiving attention in the RV field, there is still a scarce number of studies reporting on ncRNAs as biomarkers on RVF.

Arrhythmogenic cardiomyopathy (ACM) is a life-threating genetic disease where RV myocardial tissue is replaced by fibro-fatty tissue, leading to arrhythmias and, eventually, HF [94]. ACM is particularly challenging to detect because of variance expression and penetrance of the mutated gene, and as a consequence, genetics tests can result in inconclusive diagnostics [94]. miRNA profiling studies revealed miR-320a to be downregulated in ACM patients, when compared with healthy controls [94]. Intermediate values of sensitivity and specificity obtained for miR-320a were increased when combined with EGC analysis, thus improving its diagnostic potential [94]. Despite these promising results, so far, no correlation between miR-320a levels and disease severity has been found [94].

PH is a multifactorial disease, with several subgroups being characterized by an increase in RV afterload that can precede (right) HF and, eventually, death. The first report on PH-associated circulating miRNAs analyzed plasma samples from PH patients undergoing right heart catheterization [95]. MiRNAs such as miR-1, miR-26a, miR-29c, miR-34b, miR-451, and miR-1246 were found to be downregulated, whereas miR-130a, miR-133b, miR-191, miR-204, and miR-208b were profoundly upregulated in PH subjects when compared with control subjects. From all these, only miR-208b and miR-130 could be correlated with PH severity [95].

Another similar study revealed miR-451 as being significantly decreased in PH patients compared with non-PH patients (individuals diagnosed with other conditions) [96]. Although the diagnostic value of miR-451 was as moderate as the conventional Doppler-echo, combing both improved the diagnostic value of miR-451 in PH [96]. More recently, miR-424 was also linked to PH and found to be upregulated in plasma of PH patients [97], with patients with severe PH clearly displaying higher miR-424 levels when compared with individuals with less severe PH [97]. As miR-424 inversely correlates with cardiac output parameters in PH patients, it has been suggested has a potential marker of PH [97].

Pathological Reverse Remodeling

Cardiac pathological remodeling associated with the above-mentioned different cardiovascular diseases can lead to HF and, eventually, death. The severity of cardiac pathological remodeling frequently predicts treatment outcome and patient response [98]. In light of the current findings, such remodeling can be reversed and result in improved of cardiac function and, consequently, better patient prognosis and survival [99,100,101]. Reverse remodeling (RR) can be defined by any functional, structural, cellular, and/or molecular changes, resulting in improved heart function following pathological remodeling [99]. Factors contributing to the process include both pharmacological angiotensin-converting enzyme inhibitors, beta-blockers, and mechanical therapy such as cardiac resynchronization therapy (CRT), PCI, left ventricle assist device implantation (LVAD), and AVR surgery, among others [99]. Unfortunately, a fraction of patients undergoing cardiac therapy do not develop a favorable clinical response; do not show improved cardiac function; and, in some cases, cardiac condition is worsened after treatment [99,102]. Such patients, with incomplete reverse remodeling, are

classified as non-responders, while patients with improved cardiac function and complete reverse remodeling are categorized as responders [99].

Understanding the features of cardiac pathological remodeling and the cardiac response to therapy has become a major objective towards better care of CVD patients. In line, biomarkers, and more specifically ncRNAs, are claiming a greater role towards establishing reverse remodeling and predicting patient outcome upon specific therapies.

Presently, the only therapy that consistently increases survival of AS patients is AVR surgery. However, the persistence of hypertrophy after AVR surgery is a main limiting factor for patient survival and positive outcomes. Circulating miR-133a levels prior to AVR surgery are a positive predictor of LV mass normalization and subsequent decrease of cardiac hypertrophy up to one year after surgery. When combined with other clinical parameters, miR-133a yielded an AUC of 0.89 [103] and is currently considered one of the most promising biomarkers to predict LV normalization in AS patients after AVR [103].

A negatively patient outcome after mechanical therapy such as coronary artery bypass graft or AVR due to CAD and AS, respectively, is associated with high levels of serum miR-423-3p [104]. Although this is specifically significant in patients with unstable angina, when compared with individuals with stable angina or AS, the reason that miR-423-3p is particularly elevated in these patients is inconclusive [104].

Another study collectively addressed miRNA expression in the Pro-BNP Outpatient Tailored CHF Therapy (PROTECT) cohort to predict left ventricle reverse remodeling (LVRR) based on miRNAs that have been involved in human HF phenotypes or known to influence common HF signaling pathways [105]. Only 41% of the participants exhibited complete RR, considered as more than 15% reduction in LV end-systolic volume index [105]. Not only PCA analysis identified miR-423-5p and miR-212-5p as dysregulated in the plasma of systolic HF patients, they were also associated with LVRR and shared 14 target genes related to HF [105]. Together with the fact that miR-423-5p and miR-212-5p are also upregulated in myocardium tissue of end-stage HF in mice, these findings support the prospective role of miRNAs in discriminating LVRR [105].

Aside from the merit of circulating miRNAs, lncRNAs such as LIPCAR, H19, ANRIL, and MHRT have also emerged as potential biomarkers for LVRR. For example, higher plasma levels of LIPCAR and H19 in CAD patients are associated with chronic HF [106]. In HF patients, higher levels of LIPCAR are associated with a higher risk of hospitalization and mortality due to HF when compared with HF patients with lower LIPCAR levels [107]. Similarly, plasma MHRT is significantly lower in patients with HF and is able to distinguish HF from healthy subjects by presenting an AUC of 0.925 [108]. Among HF patients, lower levels of plasma MHRT significantly correlate with a lower survival rate when compared with HF patients displaying higher MHRT levels.

As previously mentioned, one treatment for CAD is coronary intervention by the use of a stent; however, 12% of patients with stent therapy showed angiographic restenosis, in-sent restenosis (ISR) [109]. ISR is defined as a “narrowing of a coronary artery at the stented segment”, and is associated with increased plasma levels of ANRIL, when compared with CAD patients without restenosis [110]. To note, ANRIL was found as an independent risk factor for

ISR incidence, with a modest diagnostic value demonstrated by an AUC of 0.749. In addition, ANRIL demonstrated a specificity of 75% and sensitivity of 68.4% after a cutoff value of 1.34 [110].

Finally, plasma circRNA MICRA was found to be a strong predictor of LV dysfunction 3 to 4 months after an AMI episode, and lower MICRA levels in MI patients are at higher risk of LV dysfunction [80].

Conclusions

Misdiagnosed CVDs have severe consequences on a patient's life quality and associated survival rate. The use of standard biomarkers for CVDs as the quantitative assessment of circulating cardiac troponins and natriuretic peptides levels it is still not specific and neither sensitive enough for early detection. Moreover, the complexity of many biological and molecular mechanisms observed on the different CVDs makes the use of a single biomarker insufficient for a correct diagnosis. Currently, circulating ncRNAs display great potential as biomarkers owing to their high abundance and stability in the blood, and ncRNAs can provide a valuable measure of heart health condition. Therefore, ncRNAs have been portrayed as potential non-invasive tools and might help on CVDs' diagnosis and prognosis, allowing tailored healthcare to each individual and a reduction of the associated societal and economic burden. However, the expression profile of ncRNAs could be influenced by age, sex, and medical drugs, which might add more complexity to our understanding of ncRNAs in CVDs. Furthermore, up to date, only a scarce number of works reported a higher individual diagnostic value of ncRNAs when compared with standard CVD markers; however, frequently, this value is improved when a set of ncRNAs is used or combined with standard CVD markers. The majority of the studies are characterized by a smaller sample size, with some possible cofounders associated (region, ethnicity, age, social status), and a short-term follow-up thwarts the hunting for the ideal biomarker. Interestingly, some ncRNAs such as muscle specific miR-1 and lncRNA HOTAIR are reported in several diseases (**Table 1**), suggesting a feature of a general CVD biomarker, while others appear to have disease-specificity (**Figure 1 and Supplementary Table S1**). New findings on ncRNAs and their role as blood-based biomarkers are reported frequently, such as the study of Viereck, who performed an extensive review on this topic [111]. Despite the vast amount of data on CVDs and plasma ncRNAs, their inclusion in medical guidelines is still far off in the upcoming years. Thus, we recommend researchers who aim to validate potential biomarkers in big cohorts to rely on the candidates derived from studies that include the largest sample sizes, on biomarkers that have the high sensitivity and specificity, and on biomarkers that show a significant correlation with cardiac parameters associated with the specific cardiovascular disease.

Figure 1.

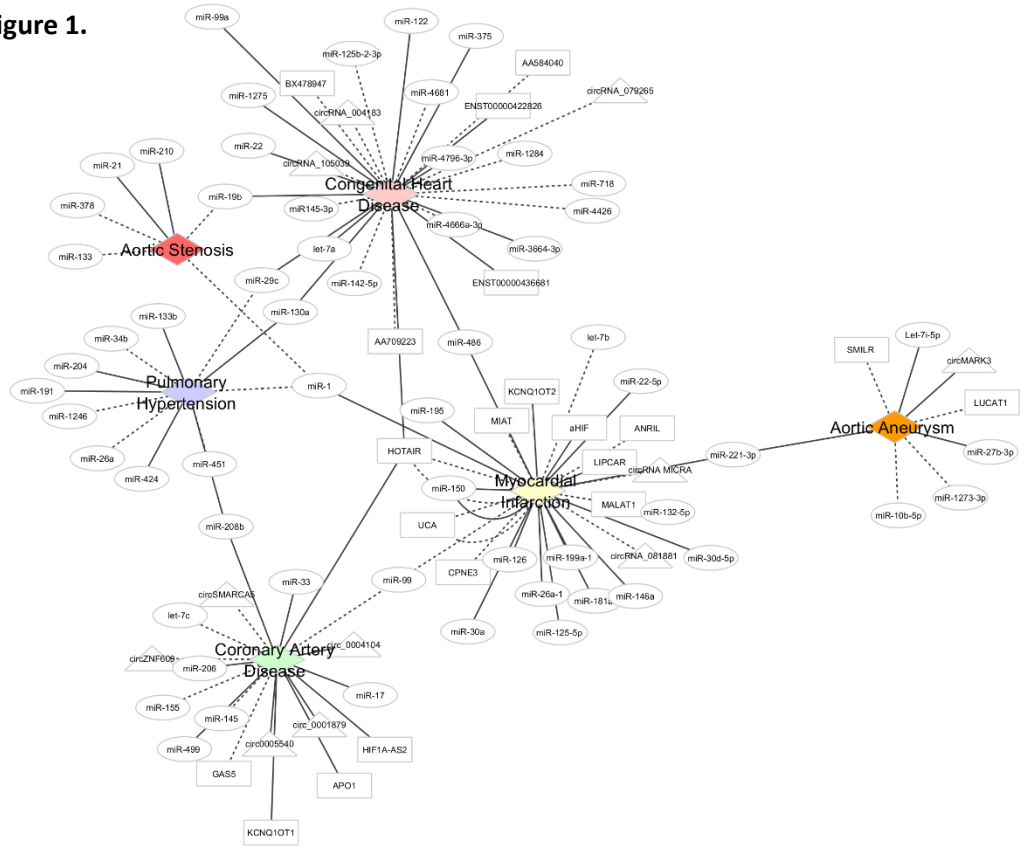

Figure 1. *Illustrative cytoscape network combining the studies reported within this review. Aortic valve stenosis (red), congenital heart disease (pink), coronary artery disease (green), myocardial infarction (yellow), aortic aneurism (orange), and pulmonary hypertension (blue) are the five central nodes (diamond shape) and specific associations to ncRNAs are denoted by edges. The different ncRNAs are represented by different edges shapes: miRNAs are in circular shape, lncRNAs are in rectangular shape, and circRNAs are in triangular shape. Dashed lines represent upregulated plasma ncRNAs, while solid lines represent downregulated ncRNAs in plasma.*

Table 1. List of non-coding RNAs (miRNAs, lncRNAs, and circRNAs) involved in multiple cardiovascular diseases. AS, aortic valve stenosis; MI, myocardial infarction; PH, pulmonary hypertension; TOF, tetralogy of fallot; VSD, ventricular septal defect; ASD, atrial septal defect; PDA, patent ductus arteriosus; BAV, bicuspid aortic valve disease; CAD, coronary artery disease. Arrows indicate the direction of miRNA variation: ↓ and ↑ correspond to a under-expression and over-expression of the miR.

NcRNA	Disease	Variation	Reference
miR-1	AS	↓	29
	MI	↑	61
	PH	↓	86
miR-150	MI	↑	62
	MI	↑	65
miR-19b	TOF	↑	74
	VSD	↑	74
	ASD	↑	74
	AS	↓	34
miR-208b	CAD	↑	
	PH	↑	86
miR-29c	TOF	↑	74
	ASD	↑	74
	PH	↓	86
	VSD	↑	74
miR-375	TOF	↑	74
	ASD	↑	74
miR-486	MI	↑	65
	ASD	↑	75
	BAV	↑	77
miR-99	CAD	↓	55
	MI	↓	55
NcRNA	Disease	Variation	Reference
HOTAIR	CAD	↑	49
	ASD	↑	80
	VSD	↑	80
	PDA	↑	80
	MI	↓	68
	MI	↓	66
KCNQ1OT1	CAD	↑	48
	MI	↑	68
UCA	MI	↓	67
	MI	↓	68
NcRNA	Disease	Variation	Reference
circRNA_004183	ASD	↓	81
	VSD	↓	81
circRNA_079265	ASD	↓	81
	VSD	↓	81
circRNA_105039	ASD	↓	81
	VSD	↓	81
circRNA MICRA	MI	↓	70
circRNA MICRA	MI	↓	71

Supplementary Table 1. Non-coding RNA (miRNAs, lncRNAs, and circRNAs) variation in several cardiovascular diseases. TAA, thoracic aortic aneurysm; AAA, abdominal aortic aneurysm; CHD, congenital heart defect.

NcRNA	Disease	Variation	Reference
let-7a	ASD	↑	[85]
let-7b	MI	↓	[66]
let-7c	CAD	↓	[52]
Let-7i-5p	AAA	↑	[47]
	AS	↓	[29]
miR-1	MI	↑	[69]
	PH	↓	[96]
miR-10b-5p	AAA	↓	[47]
miR-122	BAV	↓	[87]
miR-1246	PH	↑	[96]
miR-125-5p	MI	↓	[71]
miR-125b-2-3p	CHD	↑	[88]
miR-126	MI	↓	[68]
miR-1273-3p	AAAD	↑	[49]
miR-1275	CHD	↓	[88]
miR-1284	CHD	↑	[88]
miR-130a	BAV	↓	[87]
miR-130a	PH	↑	[96]
miR-132-5p	MI	↑	[70]
miR-133	AS	↓	[29]
miR-133b	PH	↓	[96]
miR-142-5p	CHD	↑	[88]
miR-145	CAD	↓	[52]
miR-145-3p	CHD	↓	[88]
miR-146a	MI	↓	[67]
miR-150	MI	↑	[70],[73]
miR-155	CAD	↑	[52]
miR-17	CAD	↑	[51]
miR-181a	MI	↓	[64]
miR-191	PH	↑	[96]
miR-195	MI	↑	[66]
miR-199a-1	MI	↑	[67]
	TOF	↑	[84]
miR-19b	VSD	↑	[84]
	ASD	↑	[84]

	AS	↑	[34]
miR-204	PH	↑	[96]
miR-206	CAD	↓	[55]
miR-208b	CAD	↑	[53]
	PH	↑	[96]
miR-21	AS	↑	[32]
miR-210	AS	↑	[30]
miR-22	TOF	↑	[84]
miR-221-3p	MI	↑	[72]
	AAA	↑	[46]
miR-22-5p	MI	↑	[70]
miR-26a	PH	↓	[96]
miR-26a-1	MI	↑	[67]
miR-27b-3p	AAA	↑	[46]
miR-29c	TOF	↑	[84]
	ASD	↑	[84]
	PH	↓	[96]
	VSD	↑	[84]
miR-30a	MI	↑	[66]
miR-30d-5p	MI	↑	[71]
miR-33	CAD	↑	[54]
miR-34b	PH	↓	[96]
miR-3664-3p	CHD	↑	[88]
miR-375	TOF	↑	[84]
	ASD	↑	[84]
miR-378	AS	↓	[29]
miR-424	PH	↑	[98]
miR-4426	CHD	↓	[88]
miR-451	PH	↓	[96]
		↓	[97]
miR-4666a-3p	CHD	↓	[88]
miR-4681	CHD	↓	[88]
miR-4796-3p	CHD	↑	[88]
miR-486	MI	↑	[73]
	ASD	↑	[85]
	BAV	↑	[87]
miR-499	CAD	↑	[53]
miR-718	BAV	↓	[87]
miR-99	CAD	↓	[63]
	MI	↓	[63]
miR-99a	CHD	↑	[89]
AA584040	CHD	↓	[83]
AA709223	CHD	↓	[83]
aHIF	MI	↑	[78]

ANRIL	MI	↓	[78]
APO1	CAD	↑	[56]
BX478947	CHD	↓	[83]
CPNE3	MI	↓	[78]
ENST00000422826	CHD	↑	[83]
ENST00000436681	CHD	↑	[83]
GAS5	CAD	↓	[58]
HIF1A-AS2	CAD	↑	[56]
HOTAIR	CAD	↑	[57]
	ASD	↑	[90]
	VSD	↑	[90]
	PDA	↑	[90]
KCNQ1OT1	MI	↓	[78]
	MI	↓	[76]
	CAD	↑	[56]
	MI	↑	[78]
LIPCAR	MI	↑	[78]
LUCAT1	TAA	↓	[48]
MALAT1	MI	↓	[78]
MIAT	MI	↓	[78]
SMILR	TAA	↓	[48]
UCA	MI	↓	[77]
	MI	↓	[78]
circ_0001879	CAD	↑	[62]
circ_0004104	CAD	↑	[62]
circ0005540	CAD	↑	[60]
circRNA_004183	ASD	↓	[91]
	VSD	↓	[91]
circRNA_079265	ASD	↓	[91]
	VSD	↓	[91]
circRNA_081881	MI	↓	[79]
circRNA_105039	ASD	↓	[91]
	VSD	↓	[91]
circMARK3	AAAD	↑	[49]
circRNA MICRA	MI	↓	[80,81]
circSMARCA5	CAD	↓	[59]
circZNF609	CAD	↓	[61]

References

1. Zhao Y., Henein M.Y., Mörner S., Gustavsson S., Holmgren A., Lindqvist P. Residual compromised myocardial contractile reserve after valve replacement for aortic stenosis. Eur. Heart J. Cardiovasc. Imaging. 2011;13:353–360. doi: 10.1093/ejechocard/jer246. [PubMed] [CrossRef] [Google Scholar]

2. Strimbu K., Tavel J.A. What are biomarkers? Curr. Opin. HIV AIDS. 2010;5:463–466. doi: 10.1097/COH.0b013e32833ed177. [PMC free article] [PubMed] [CrossRef] [Google Scholar]

3. Verma M., Patel P., Verma M. Biomarkers in Prostate Cancer Epidemiology. Cancers. 2011;3:3773–3798. doi: 10.3390/cancers3043773. [PMC free article] [PubMed] [CrossRef] [Google Scholar]

4. Wang J., Tan G.-J., Han L.-N., Bai Y.-Y., He M., Liu H.-B. Novel biomarkers for cardiovascular risk prediction. J. Geriatr. Cardiol. 2017;14:135–150. [PMC free article] [PubMed] [Google Scholar]

5. Djebali S., Davis C.A., Merkel A., Dobin A., Lassmann T., Mortazavi A., Tanzer A., Lagarde J., Lin W., Schlesinger F., et al. Landscape of transcription in human cells. Nature. 2012;489:101–108. doi: 10.1038/nature11233. [PMC free article] [PubMed] [CrossRef] [Google Scholar]

6. Lee R.C., Feinbaum R.L., Ambros V. The C. elegans heterochronic gene lin-4 encodes small RNAs with antisense complementarity to lin-14. Cell. 1993;75:843–854. doi: 10.1016/0092-8674(93)90529-Y. [PubMed] [CrossRef] [Google Scholar]

7. Li Z., Rana T.M. Therapeutic targeting of microRNAs: Current status and future challenges. Nat. Rev. Drug Discov. 2014;13:622–638. doi: 10.1038/nrd4359. [PubMed] [CrossRef] [Google Scholar]

8. O'Brien J., Hayder H., Zayed Y., Peng C. Overview of MicroRNA Biogenesis, Mechanisms of Actions, and Circulation. Front. Endocrinol. 2018;9:402. doi: 10.3389/fendo.2018.00402. [PMC free article] [PubMed] [CrossRef] [Google Scholar]

9. Chen S., Gao G. MicroRNAs recruit eIF4E2 to repress translation of target mRNAs. Protein Cell. 2017;8:750–761. doi: 10.1007/s13238-017-0444-0. [PMC free article] [PubMed] [CrossRef] [Google Scholar]

10. Petersen C.P., Bordeleau M.E., Pelletier J., Sharp P.A. Short RNAs repress translation after initiation in mammalian cells. Mol. Cell. 2006;21:533–542. doi: 10.1016/j.molcel.2006.01.031. [PubMed] [CrossRef] [Google Scholar]

11. Humphreys D.T., Westman B.J., Martin D.I.K., Preiss T. MicroRNAs control translation initiation by inhibiting eukaryotic initiation factor 4E/cap and poly(A) tail function. Proc. Natl. Acad. Sci. USA. 2005;102:16961–16966. doi: 10.1073/pnas.0506482102. [PMC free article] [PubMed] [CrossRef] [Google Scholar]

12. Tzimagiorgis G., Michailidou E.Z., Kritis A., Markopoulos A.K., Kouidou S., Kritis A. Recovering circulating extracellular or cell-free RNA from bodily fluids. Cancer Epidemiol. 2011;35:580–589. doi: 10.1016/j.canep.2011.02.016. [PubMed] [CrossRef] [Google Scholar]

13. Ulitsky I., Bartel D.P. lincRNAs: Genomics, Evolution, and Mechanisms. Cell. 2013;154:26–46. doi: 10.1016/j.cell.2013.06.020. [PMC free article] [PubMed] [CrossRef] [Google Scholar]

14. Ma L., Bajic V.B., Zhang Z. On the classification of long non-coding RNAs. RNA Biol. 2013;10:924–933. doi: 10.4161/rna.24604. [PMC free article] [PubMed] [CrossRef] [Google Scholar]

15. Kim T.K., Hemberg M., Gray J.M., Costa A.M., Bear D.M., Wu J., Harmin D.A., Laptewicz M., Barbara-Haley K., Kuersten S., et al. Widespread transcription at neuronal activity-regulated enhancers. Nature. 2010;465:182–187. doi: 10.1038/nature09033. [PMC free article] [PubMed] [CrossRef] [Google Scholar]

16. Gupta R.A., Shah N., Wang K.C., Kim J., Horlings H.M., Wong D.J., Tsai M.-C., Hung T., Argani P., Rinn J.L., et al. Long non-coding RNA HOTAIR reprograms chromatin state to promote cancer metastasis. Nat. Cell Biol. 2010;464:1071–1076. doi: 10.1038/nature08975. [PMC free article] [PubMed] [CrossRef] [Google Scholar]

17. Colognori D., Sunwoo H., Kriz A.J., Wang C.-Y., Lee J.T. Xist Deletional Analysis Reveals an Interdependency between Xist RNA and Polycomb Complexes for Spreading along the Inactive X. Mol. Cell. 2019;74:101–117.e10. doi: 10.1016/j.molcel.2019.01.015. [PMC free article] [PubMed] [CrossRef] [Google Scholar]

18. Shan Y., Ma J., Pan Y., Hu J., Liu B., Jia L. LncRNA SNHG7 sponges miR-216b to promote proliferation and liver metastasis of colorectal cancer through upregulating GALNT1. Cell Death Dis. 2018;9:1–13. doi: 10.1038/s41419-018-0759-7. [PMC free article] [PubMed] [CrossRef] [Google Scholar]

19. Zhang X., Wang W., Zhu W., Dong J., Cheng Y., Yin Z., Shen F. Mechanisms and Functions of Long Non-Coding RNAs at Multiple Regulatory Levels. Int. J. Mol. Sci. 2019;20:5573. doi: 10.3390/ijms20225573. [PMC free article] [PubMed] [CrossRef] [Google Scholar]

20. Greene J., Baird A.-M., Brady L., Lim M., Gray S.G., McDermott R., Finn S.P. Circular RNAs: Biogenesis, Function and Role in Human Diseases. Front. Mol. Biosci. 2017;4:38. doi: 10.3389/fmolb.2017.00038. [PMC free article] [PubMed] [CrossRef] [Google Scholar]

21. Pamudurti N.R., Bartok O., Jens M., Ashwal-Fluss R., Stottmeister C., Ruhe L., Hanan M., Wyler E., Perez-Hernandez D., Ramberger E., et al. Translation of CircRNAs. Mol. Cell. 2017;66:9–21.e7. doi: 10.1016/j.molcel.2017.02.021. [PMC free article] [PubMed] [CrossRef] [Google Scholar]

22. Zaiou M. circRNAs Signature as Potential Diagnostic and Prognostic Biomarker for Diabetes Mellitus and Related Cardiovascular Complications. Cells. 2020;9:659. doi: 10.3390/cells9030659. [PMC free article] [PubMed] [CrossRef] [Google Scholar]

23. Li H., Xu J.-D., Fang X.-H., Zhu J.-N., Yang J., Pan R., Yuan S.-J., Zeng N., Yang Z.-Z., Yang H., et al. Circular RNA circRNA_000203 aggravates cardiac hypertrophy via suppressing miR-26b-5p and miR-140-3p binding to Gata4. Cardiovasc. Res. 2019;116:1323–1334. doi: 10.1093/cvr/cvz215. [PMC free article] [PubMed] [CrossRef] [Google Scholar]

24. Li Z., Huang C., Bao C., Chen L., Lin M., Wang X., Zhong G., Yu B., Hu W., Dai L., et al. Exon-intron circular RNAs regulate transcription in the nucleus. Nat. Struct. Mol. Biol. 2015;22:256–264. doi: 10.1038/nsmb.2959. [PubMed] [CrossRef] [Google Scholar]

25. Hang D., Zhou J., Qin N., Zhou W., Ma H., Jin G., Hu Z., Dai J., Shen H. A novel plasma circular RNA circFARSA is a potential biomarker for non-small cell lung cancer. Cancer Med. 2018;7:2783–2791. doi: 10.1002/cam4.1514. [PMC free article] [PubMed] [CrossRef] [Google Scholar]

26. Wang X., Lin Y.K., Lu Z.L., Li J. Circular RNA circ-MTO1 serves as a novel potential diagnostic and prognostic biomarker for gallbladder cancer. Eur. Rev. Med. Pharmacol. Sci. 2020;24:8359–8366. [PubMed] [Google Scholar]

27. Ancona R., Comenale S. Epidemiology of aortic valve stenosis (AS) and of aortic valve incompetence (AI): Is the prevalence of AS/AI similar in different parts of the world? [(accessed

on 14 October 2020)];e-J. Cardiol. Pract. 2020 18 Available online: https://www.escardio.org/Journals/E-Journal-of-Cardiology-Practice/Volume-18/epidemiology-of-aortic-valve-stenosis-as-and-of-aortic-valve-incompetence-ai. [Google Scholar]

28. Hu P.P. TAVR and SAVR: Current Treatment of Aortic Stenosis. Clin. Med. Insights Cardiol. 2012;6:125–139. doi: 10.4137/CMC.S7540. [PMC free article] [PubMed] [CrossRef] [Google Scholar]

29. Chen Z., Li C., Xu Y., Li Y., Yang H., Rao L. Circulating Level of miR-378 Predicts Left Ventricular Hypertrophy in Patients with Aortic Stenosis. PLoS ONE. 2014;9:e105702. doi: 10.1371/journal.pone.0105702. [PMC free article] [PubMed] [CrossRef] [Google Scholar]

30. Røsjø H., Dahl M.B., Bye A., Andreassen J., Jørgensen M., Wisløff U., Christensen G., Edvardsen T., Omland T. Prognostic Value of Circulating MicroRNA-210 Levels in Patients with Moderate to Severe Aortic Stenosis. PLoS ONE. 2014;9:e91812. doi: 10.1371/journal.pone.0091812. [PMC free article] [PubMed] [CrossRef] [Google Scholar]

31. Fabiani I., Scatena C., Mazzanti C.M., Conte L., Pugliese N.R., Franceschi S., Lessi F., Menicagli M., De Martino A., Pratali S., et al. Micro-RNA-21 (biomarker) and global longitudinal strain (functional marker) in detection of myocardial fibrotic burden in severe aortic valve stenosis: A pilot study. J. Transl. Med. 2016;14:248. doi: 10.1186/s12967-016-1011-9. [PMC free article] [PubMed] [CrossRef] [Google Scholar]

32. Villar A.V., García R., Merino D., Llano M., Cobo M., Montalvo C., Martín-Durán R., Hurlé M.A., Nistal J.F. Myocardial and circulating levels of microRNA-21 reflect left ventricular fibrosis in aortic stenosis patients. Int. J. Cardiol. 2013;167:2875–2881. doi: 10.1016/j.ijcard.2012.07.021. [PubMed] [CrossRef] [Google Scholar]

33. Beaumont J., López B., Ravassa S., Hermida N., José G.S., Gallego I., Valencia F., Gómez-Doblas J.J., De Teresa E., Díez J., et al. MicroRNA-19b is a potential biomarker of increased myocardial collagen cross-linking in patients with aortic stenosis and heart failure. Sci. Rep. 2017;7:40696. doi: 10.1038/srep40696. [PMC free article] [PubMed] [CrossRef] [Google Scholar]

34. Iaconetti C., Polimeni A., Sorrentino S., Sabatino J., Pironti G., Esposito G., Curcio A., Indolfi C. Inhibition of miR-92a increases endothelial proliferation and migration in vitro as well as reduces neointimal proliferation in vivo after vascular injury. Basic Res. Cardiol. 2012;107:1–14. doi: 10.1007/s00395-012-0296-y. [PubMed] [CrossRef] [Google Scholar]

35. Lee S.-P., Kim H.-K., Kim Y.-J., Oh S., Sohn D.-W. Association of Myocardial Angiogenesis with Structural and Functional Ventricular Remodeling in Aortic Stenosis Patients with Normal Ejection Fraction. J. Cardiovasc. Ultrasound. 2014;22:72–79. doi: 10.4250/jcu.2014.22.2.72. [PMC free article] [PubMed] [CrossRef] [Google Scholar]

36. Selvam S.N., Bowman M., Inglis M., Kloosterman R., Grabell J., Casey L., Johri A.M., James P.D. Patients with aortic stenosis have von Willebrand factor abnormalities and increased proliferation of endothelial colony forming cells. J. Thromb. Haemost. 2020;18:593–603. doi: 10.1111/jth.14715. [PubMed] [CrossRef] [Google Scholar]

37. Mohammadi M.M., AbouIssa A., Isyatul A., Xie Y., Cordero J., Shirvani A., Gigina A., Engelhardt M., Trogisch F.A., Geffers R., et al. Induction of cardiomyocyte proliferation and angiogenesis protects neonatal mice from pressure overload & ndash; associated maladaptation. JCI Insight. 2019;4:5. doi: 10.1172/jci.insight.128336. [PMC free article] [PubMed] [CrossRef] [Google Scholar]

38. Fabiani I., Pugliese N.R., Calogero E., Conte L., Mazzanti M.C., Scatena C., Scopelliti C., Tantillo E., Passiatore M., Angelillis M., et al. MicroRNAs distribution in different phenotypes of Aortic Stenosis. Sci. Rep. 2018;8:1–10. doi: 10.1038/s41598-018-28246-8. [PMC free article] [PubMed] [CrossRef] [Google Scholar]

39. García R., Salido-Medina A.B., Gil A., Merino D., Gómez J., Villar A.V., González-Vilchez F., Hurlé M.A., Nistal J.F. Sex-Specific Regulation of miR-29b in the Myocardium Under Pressure Overload is Associated with Differential Molecular, Structural and Functional Remodeling Patterns in Mice and Patients with Aortic Stenosis. Cells. 2020;9:833. doi: 10.3390/cells9040833. [PMC free article] [PubMed] [CrossRef] [Google Scholar]

40. Chen J., Wang J., Jiang Y., Gu W., Ni B., Sun H., Gu W., Chen L., Shao Y. Identification of circular RNAs in human aortic valves. Gene. 2018;642:135–144. doi: 10.1016/j.gene.2017.10.016. [PubMed] [CrossRef] [Google Scholar]

41. Wang J., Wang Y., Gu W., Ni B., Sun H., Yu T., Gu W., Chen L., Shao Y. Comparative Transcriptome Analysis Reveals Substantial Tissue Specificity in Human Aortic Valve. Evol. Bioinform. 2016;12:EBO.S37594-84. doi: 10.4137/EBO.S37594. [PMC free article] [PubMed] [CrossRef] [Google Scholar]

42. Mathur A., Mohan V., Ameta D., Gaurav B., Haranahalli P. Aortic aneurysm. J. Transl. Intern. Med. 2016;4:35–41. doi: 10.1515/jtim-2016-0008. [PMC free article] [PubMed] [CrossRef] [Google Scholar]

43. Spin J.M., Li D.Y., Maegdefessel L., Tsao P.S. Non-coding RNAs in aneurysmal aortopathy. Vasc. Pharmacol. 2019;114:110–121. doi: 10.1016/j.vph.2018.06.008. [PubMed] [CrossRef] [Google Scholar]

44. Moris D., Mantonakis E., Avgerinos E.D., Makris M., Bakoyiannis C., Pikoulis E., Georgopoulos S. Novel Biomarkers of Abdominal Aortic Aneurysm Disease: Identifying Gaps and Dispelling Misperceptions. BioMed Res. Int. 2014;2014:1–13. doi: 10.1155/2014/925840. [PMC free article] [PubMed] [CrossRef] [Google Scholar]

45. Plana E., Gálvez L., Medina P., Navarro S., Fornés-Ferrer V., Panadero J., Miralles M. Identification of Novel microRNA Profiles Dysregulated in Plasma and Tissue of Abdominal Aortic Aneurysm Patients. Int. J. Mol. Sci. 2020;21:4600. doi: 10.3390/ijms21134600. [PMC free article] [PubMed] [CrossRef] [Google Scholar]

46. Wanhainen A., Mani K., Vorkapic E., De Basso R., Björck M., Länne T., Wågsäter D. Screening of circulating microRNA biomarkers for prevalence of abdominal aortic aneurysm and aneurysm growth. Atherosclerosis. 2017;256:82–88. doi: 10.1016/j.atherosclerosis.2016.11.007. [PubMed] [CrossRef] [Google Scholar]

47. Patamsytė V., Žukovas G., Gečys D., Žaliaduonytė D., Jakuška P., Benetis R., Lesauskaitė V. Long Noncoding RNAs CARMN, LUCAT1, SMILR, and MALAT1 in Thoracic Aortic Aneurysm: Validation of Biomarkers in Clinical Samples. Dis. Markers. 2020;2020:1–6. doi: 10.1155/2020/8521899. [PMC free article] [PubMed] [CrossRef] [Google Scholar]

48. Tian C., Tang X., Zhu X., Zhou Q., Guo Y., Zhao R., Wang D., Gong B. Expression profiles of circRNAs and the potential diagnostic value of serum circMARK3 in human acute Stanford type A aortic dissection. PLoS ONE. 2019;14:e0219013. doi: 10.1371/journal.pone.0219013. [PMC free article] [PubMed] [CrossRef] [Google Scholar]

49. Boudoulas K.D., Triposkiadis F., Geleris P., Boudoulas H. Coronary Atherosclerosis: Pathophysiologic Basis for Diagnosis and Management. Prog. Cardiovasc. Dis. 2016;58:676–692. doi: 10.1016/j.pcad.2016.04.003. [PubMed] [CrossRef] [Google Scholar]

50. Chen J., Xu L., Hu Q., Yang S., Zhang B., Jiang H. MiR-17-5p as circulating biomarkers for the severity of coronary atherosclerosis in coronary artery disease. Int. J. Cardiol. 2015;197:123–124. doi: 10.1016/j.ijcard.2015.06.037. [PubMed] [CrossRef] [Google Scholar]

51. Faccini J., Ruidavets J.-B., Cordelier P., Martins F., Maoret J.-J., Bongard V., Ferrières J., Roncalli J., Elbaz M., Vindis C. Circulating miR-155, miR-145 and let-7c as diagnostic biomarkers of the coronary artery disease. Sci. Rep. 2017;7:srep42916. doi: 10.1038/srep42916. [PMC free article] [PubMed] [CrossRef] [Google Scholar]

52. Wang W., Li T., Gao L., Li Y., Sun Y., Yao H.-C. Plasma miR-208b and miR-499: Potential Biomarkers for Severity of Coronary Artery Disease. Dis. Markers. 2019;2019:1–7. doi: 10.1155/2019/9842427. [PMC free article] [PubMed] [CrossRef] [Google Scholar]

53. Reddy L.L., Shah S.A.V., Ponde C.K., Rajani R.M., Ashavaid T.F. Circulating miRNA-33: A potential biomarker in patients with coronary artery disease. Biomarkers. 2018;24:36–42. doi: 10.1080/1354750X.2018.1501760. [PubMed] [CrossRef] [Google Scholar]

54. Zehtabian S.H., Alibakhshi R., Seyedena S.Y., Rai A.R. Relationship between microRNA-206 plasma levels with the severity of coronary artery conflicts in patients with coronary artery disease. Bratisl. Med. J. 2019;120:581–585. doi: 10.4149/BLL_2019_095. [PubMed] [CrossRef] [Google Scholar]

55. Zhang Y., Zhang L., Wang Y., Ding H., Xue S., Yu H., Hu L., Qi H., Wang Y., Zhu W., et al. KCNQ1OT1, HIF1A-AS2 and APOA1-AS are promising novel biomarkers for diagnosis of coronary artery disease. Clin. Exp. Pharmacol. Physiol. 2019;46:635–642. doi: 10.1111/1440-1681.13094. [PubMed] [CrossRef] [Google Scholar]

56. Avazpour N., Hajjari M., Yazdankhah S., Sahni A., Foroughmand A.M. Circulating HOTAIR LncRNA Is Potentially Up-regulated in Coronary Artery Disease. Genomics Inform. 2018;16:e25. doi: 10.5808/GI.2018.16.4.e25. [PMC free article] [PubMed] [CrossRef] [Google Scholar]

57. Yin Q., Wu A., Liu M. Plasma Long Non-Coding RNA (lncRNA) GAS5 is a New Biomarker for Coronary Artery Disease. Med. Sci. Monit. 2017;23:6042–6048. doi: 10.12659/MSM.907118. [PMC free article] [PubMed] [CrossRef] [Google Scholar]

58. Vilades D., Martínez-Camblor P., Ferrero-Gregori A., Bär C., Lu D., Xiao K., Vea À., Nasarre L., Vega J.S., Leta R., et al. Plasma circular RNA hsa_circ_0001445 and coronary artery disease: Performance as a biomarker. FASEB J. 2020;34:4403–4414. doi: 10.1096/fj.201902507R. [PubMed] [CrossRef] [Google Scholar]

59. Wu W.-P., Pan Y.-H., Cai M.-Y., Cen J.-M., Chen C., Zheng L., Liu X., Xiong X.-D. Plasma-Derived Exosomal Circular RNA hsa_circ_0005540 as a Novel Diagnostic Biomarker for Coronary Artery Disease. Dis. Markers. 2020;2020:1–7. doi: 10.1155/2020/3178642. [PMC free article] [PubMed] [CrossRef] [Google Scholar]

60. Liang B., Li M., Deng Q., Wang C., Rong J., He S., Xiang Y., Zheng F. CircRNA ZNF609 in peripheral blood leukocytes acts as a protective factor and a potential biomarker for coronary artery disease. Ann. Transl. Med. 2020;8:741. doi: 10.21037/atm-19-4728. [PMC free article] [PubMed] [CrossRef] [Google Scholar]

61. Wang L., Shen C., Wang Y., Zou T., Zhu H., Lu X., Li L., Yang B., Chen J., Chen S., et al. Identification of circular RNA Hsa_circ_0001879 and Hsa_circ_0004104 as novel biomarkers for coronary artery disease. Atherosclerosis. 2019;286:88–96. doi: 10.1016/j.atherosclerosis.2019.05.006. [PubMed] [CrossRef] [Google Scholar]

62. Yang S.-Y., Wang Y.-Q., Gao H.-M., Wang B., He Q. The clinical value of circulating miR-99a in plasma of patients with acute myocardial infarction. Eur. Rev. Med. Pharmacol. Sci. 2016;20:5193–5197. [PubMed] [Google Scholar]

63. Zhu J., Yao K., Wang Q., Guo J., Shi H., Ma L., Liu H., Gao W., Zou Y., Ge J. Circulating miR-181a as a Potential Novel Biomarker for Diagnosis of Acute Myocardial Infarction. Cell. Physiol. Biochem. 2016;40:1591–1602. doi: 10.1159/000453209. [PubMed] [CrossRef] [Google Scholar]

64. Garvey J.L., Zegre-Hemsey J., Gregg R., Studnek J.R. Electrocardiographic diagnosis of ST segment elevation myocardial infarction: An evaluation of three automated interpretation algorithms. J. Electrocardiol. 2016;49:728–732. doi: 10.1016/j.jelectrocard.2016.04.010. [PMC free article] [PubMed] [CrossRef] [Google Scholar]

65. Long G., Wang F., Duan Q., Yang S., Chen F., Gong W., Yang X., Wang Y., Chen C., Wang D.W. Circulating miR-30a, miR-195 and let-7b Associated with Acute Myocardial Infarction. PLoS ONE. 2012;7:e50926. doi: 10.1371/journal.pone.0050926. [PMC free article] [PubMed] [CrossRef] [Google Scholar]

66. Xue S., Zhu W., Liu D., Su Z., Zhang L., Chang Q., Li P. Circulating miR-26a-1, miR-146a and miR-199a-1 are potential candidate biomarkers for acute myocardial infarction. Mol. Med. 2019;25:18. doi: 10.1186/s10020-019-0086-1. [PMC free article] [PubMed] [CrossRef] [Google Scholar]

67. Hu H., Yuan H., Li C., Yu H., Chen Y. Association of Gene Polymorphisms in the Human MicroRNA-126 Gene with Plasma-Circulating MicroRNA-126 Levels and Acute Myocardial Infarction. Genet. Test. Mol. Biomarkers. 2019;23:460–467. doi: 10.1089/gtmb.2018.0282. [PubMed] [CrossRef] [Google Scholar]

68. Zhang R., Niu H., Ban T., Xu L., Li Y., Wang N., Sun L., Ai J., Yang B. Elevated plasma microRNA-1 predicts heart failure after acute myocardial infarction. Int. J. Cardiol. 2013;166:259–260. doi: 10.1016/j.ijcard.2012.09.108. [PubMed] [CrossRef] [Google Scholar]

69. Li H., Zhang P., Li F., Yuan G., Wang X., Zhang A., Li F. Plasma miR-22-5p, miR-132-5p, and miR-150-3p Are Associated with Acute Myocardial Infarction. BioMed Res. Int. 2019;2019:1–13. doi: 10.1155/2019/5012648. [PMC free article] [PubMed] [CrossRef] [Google Scholar]

70. Jia K., Shi P., Han X., Chen T., Tang H., Wang J. Diagnostic value of miR-30d-5p and miR-125b-5p in acute myocardial infarction. Mol. Med. Rep. 2016;14:184–194. doi: 10.3892/mmr.2016.5246. [PMC free article] [PubMed] [CrossRef] [Google Scholar]

71. Coskunpinar E., Cakmak H.A., Kalkan A.K., Tiryakioglu N.O., Erturk M., Ongen Z. Circulating miR-221-3p as a novel marker for early prediction of acute myocardial infarction. Gene. 2016;591:90–96. doi: 10.1016/j.gene.2016.06.059. [PubMed] [CrossRef] [Google Scholar]

72. Zhang R., Lan C., Pei H., Duan G., Huang L., Li L. Expression of circulating miR-486 and miR-150 in patients with acute myocardial infarction. BMC Cardiovasc. Disord. 2015;15:51. doi: 10.1186/s12872-015-0042-0. [PMC free article] [PubMed] [CrossRef] [Google Scholar]

73. Savoye C., Equine O., Tricot O., Nugue O., Segrestin B., Sautière K., Elkohen M., Pretorian E.M., Taghipour K., Philias A., et al. Left Ventricular Remodeling After Anterior Wall Acute Myocardial Infarction in Modern Clinical Practice (from the REmodelage VEntriculaire [REVE] Study Group) Am. J. Cardiol. 2006;98:1144–1149. doi: 10.1016/j.amjcard.2006.06.011. [PubMed] [CrossRef] [Google Scholar]

74. Maciejak A., Kostarska-Srokosz E., Gierlak W., Dluzniewski M., Kuch M., Marchel M., Opolski G., Kiliszek M., Matlak K., Dobrzycki S., et al. Circulating miR-30a-5p as a prognostic biomarker of left ventricular dysfunction after acute myocardial infarction. Sci. Rep. 2018;8:1–11. doi: 10.1038/s41598-018-28118-1. [PMC free article] [PubMed] [CrossRef] [Google Scholar]

75. Gao L., Liu Y., Guo S., Yao R., Wu L., Xiao L., Wang Z., Liu Y., Zhang Y. Circulating Long Noncoding RNA HOTAIR is an Essential Mediator of Acute Myocardial Infarction. Cell. Physiol. Biochem. 2017;44:1497–1508. doi: 10.1159/000485588. [PubMed] [CrossRef] [Google Scholar]

76. Yan Y., Zhang B., Liu N., Qi C., Xiao Y., Tian X., Li T., Liu B. Circulating Long Noncoding RNA UCA1 as a Novel Biomarker of Acute Myocardial Infarction. BioMed Res. Int. 2016;2016:1–7. doi: 10.1155/2016/8079372. [PMC free article] [PubMed] [CrossRef] [Google Scholar]

77. Li M., Wang Y.-F., Yang X.-C., Xu L., Li W.-M., Xia K., Zhang D.-P., Wu R.-N., Gan T. Circulating Long Noncoding RNA LIPCAR Acts as a Novel Biomarker in Patients with ST-Segment Elevation Myocardial Infarction. Med. Sci. Monit. 2018;24:5064–5070. doi: 10.12659/MSM.909348. [PMC free article] [PubMed] [CrossRef] [Google Scholar]

78. Deng Y.-Y., Zhang W., She J., Zhang L., Chen T., Zhou J., Yuan Z. GW27-e1167 Circular RNA Related to PPARγ Function as ceRNA of microRNA in Human Acute Myocardial Infarction. J. Am. Coll. Cardiol. 2016;68:C51–C52. doi: 10.1016/j.jacc.2016.07.189. [CrossRef] [Google Scholar]

79. Salgado-Somoza A., Zhang L., Vausort M., Devaux Y. The circular RNA MICRA for risk stratification after myocardial infarction. IJC Heart Vasc. 2017;17:33–36. doi: 10.1016/j.ijcha.2017.11.001. [PMC free article] [PubMed] [CrossRef] [Google Scholar]

80. Vausort M., Salgado-Somoza A., Zhang L., Leszek P., Scholz M., Teren A., Burkhardt R., Thiery J., Wagner D.R., Devaux Y. Myocardial Infarction-Associated Circular RNA Predicting Left Ventricular Dysfunction. J. Am. Coll. Cardiol. 2016;68:1247–1248. doi: 10.1016/j.jacc.2016.06.040. [PubMed] [CrossRef] [Google Scholar]

81. Xie N., Wang H., Liu Z., Fang J., Yang T., Zhou S., Wang A., Qin J., Xiong L. Perinatal outcomes and congenital heart defect prognosis in 53313 non-selected perinatal infants. PLoS ONE. 2017;12:e0177229. doi: 10.1371/journal.pone.0177229. [PMC free article] [PubMed] [CrossRef] [Google Scholar]

82. Gu M., Zheng A., Tu W., Zhao J., Li L., Li M., Han S.-P., Hu X., Zhu J., Pan Y., et al. Circulating LncRNAs as Novel, Non-Invasive Biomarkers for Prenatal Detection of Fetal Congenital Heart Defects. Cell. Physiol. Biochem. 2016;38:1459–1471. doi: 10.1159/000443088. [PubMed] [CrossRef] [Google Scholar]

83. Zhu S., Cao L., Zhu J., Kong L., Jin J., Qian L., Zhu C., Hu X., Li M., Guo X., et al. Identification of maternal serum microRNAs as novel non-invasive biomarkers for prenatal detection of fetal congenital heart defects. Clin. Chim. Acta. 2013;424:66–72. doi: 10.1016/j.cca.2013.05.010. [PubMed] [CrossRef] [Google Scholar]

84. Song Y., Higgins H., Guo J., Harrison K., Schultz E.N., Hales B.J., Moses E.K., Goldblatt J., Pachter N., Zhang G. Clinical significance of circulating microRNAs as markers in detecting and predicting congenital heart defects in children. J. Transl. Med. 2018;16:1–11. doi: 10.1186/s12967-018-1411-0. [PMC free article] [PubMed] [CrossRef] [Google Scholar]

85. Girdauskas E., Petersen J., Neumann N., Naito S., Gross T., Jagodzinski A., Reichenspurner H., Zeller T. Novel Approaches for BAV Aortopathy Prediction—Is There a Need for Cohort Studies and Biomarkers? Biomolecules. 2018;8:58. doi: 10.3390/biom8030058. [PMC free article] [PubMed] [CrossRef] [Google Scholar]

86. Martínez-Micaelo N., Beltrán-Debón R., Baiges I., Faiges M., Alegret J.M. Specific circulating microRNA signature of bicuspid aortic valve disease. J. Transl. Med. 2017;15:1–12. doi: 10.1186/s12967-017-1176-x. [PMC free article] [PubMed] [CrossRef] [Google Scholar]

87. Gu H., Chen L., Xue J., Huang T., Wei X., Liu D., Ma W., Cao S., Yuan Z. Expression profile of maternal circulating microRNAs as non-invasive biomarkers for prenatal diagnosis of congenital heart defects. Biomed. Pharmacother. 2019;109:823–830. doi: 10.1016/j.biopha.2018.10.110. [PubMed] [CrossRef] [Google Scholar]

88. Kehler L., Biro O., Lazar L., Rigo J., Nagy B. Elevated hsa-miR-99a levels in maternal plasma may indicate congenital heart defects. BioMed Rep. 2015;3:869–873. doi: 10.3892/br.2015.510. [PMC free article] [PubMed] [CrossRef] [Google Scholar]

89. Jiang Y., Mo H., Luo J., Zhao S., Liang S., Zhang M., Yuan J. HOTAIR Is a Potential Novel Biomarker in Patients with Congenital Heart Diseases. BioMed Res. Int. 2018;2018:1–7. doi: 10.1155/2018/2850657. [PMC free article] [PubMed] [CrossRef] [Google Scholar]

90. Wu J., Li J., Liu H., Yin J., Zhang M., Yu Z., Miao H. Circulating plasma circular RNAs as novel diagnostic biomarkers for congenital heart disease in children. J. Clin. Lab. Anal. 2019;33:e22998. doi: 10.1002/jcla.22998. [PMC free article] [PubMed] [CrossRef] [Google Scholar]

91. Friedberg M.K., Redington A.N. Right versus left ventricular failure: Differences, similarities, and interactions. Circulation. 2014;129:1033–1044. doi: 10.1161/CIRCULATIONAHA.113.001375. [PubMed] [CrossRef] [Google Scholar]

92. Lang I.M. Management of acute and chronic RV dysfunction. Eur. Heart J. Suppl. 2007;9:H61–H67. doi: 10.1093/eurheartj/sum020. [CrossRef] [Google Scholar]

93. Ibrahim B.S. Right ventricular failure. EJ Cardiol. Pract. 2016;14:32. [Google Scholar]

94. Sommariva E., D'Alessandra Y., Farina F.M., Casella M., Cattaneo F., Catto V., Chiesa M., Stadiotti I., Brambilla S., Russo A.D., et al. MiR-320a as a Potential Novel Circulating Biomarker of Arrhythmogenic CardioMyopathy. Sci. Rep. 2017;7:1–10. doi: 10.1038/s41598-017-05001-z. [PMC free article] [PubMed] [CrossRef] [Google Scholar]

95. Wei C., Henderson H., Spradley C., Li L., Kim I.-K., Kumar S., Hong N., Arroliga A.C., Gupta S. Circulating miRNAs as Potential Marker for Pulmonary Hypertension. PLoS ONE. 2013;8:e64396. doi: 10.1371/journal.pone.0064396. [PMC free article] [PubMed] [CrossRef] [Google Scholar]

96. Song X.-W., Zou L.-L., Cui L., Li S.-H., Qin Y.-W., Zhao X.-X., Jing Q. Plasma miR-451 with echocardiography serves as a diagnostic reference for pulmonary hypertension. Acta Pharmacol. Sin. 2018;39:1208–1216. doi: 10.1038/aps.2018.39. [PMC free article] [PubMed] [CrossRef] [Google Scholar]

97. Baptista R., Marques C., Catarino S., Enguita F.J., Costa M.C., Matafome P., Zuzarte M., Castro G., Reis A., Monteiro P., et al. MicroRNA-424(322) as a new marker of disease progression in pulmonary arterial hypertension and its role in right ventricular hypertrophy by targeting SMURF1. Cardiovasc. Res. 2018;114:53–64. doi: 10.1093/cvr/cvx187. [PubMed] [CrossRef] [Google Scholar]

98. Puls M., Beuthner B.E., Topci R., Vogelgesang A., Bleckmann A., Sitte M., Lange T., Backhaus S.J., Schuster A., Seidler T., et al. Impact of myocardial fibrosis on left ventricular remodelling, recovery, and outcome after transcatheter aortic valve implantation in different haemodynamic subtypes of severe aortic stenosis. Eur. Heart J. 2020;41:1903–1914. doi: 10.1093/eurheartj/ehaa033. [PMC free article] [PubMed] [CrossRef] [Google Scholar]

99. Rodrigues P.G., Leite-Moreira A., Falcao-Pires I. Myocardial reverse remodeling: How far can we rewind? Am. J. Physiol. Circ. Physiol. 2016;310:H1402–H1422. doi: 10.1152/ajpheart.00696.2015. [PubMed] [CrossRef] [Google Scholar]

100. Kitai T., Grodin J.L., Mentz R.J., Hernandez A.F., Butler J., Metra M., McMurray J.J., Armstrong P.W., Starling R.C., O'Connor C.M., et al. Insufficient reduction in heart rate during hospitalization despite beta-blocker treatment in acute decompensated heart failure: Insights from the ASCEND-HF trial. Eur. J. Heart Fail. 2016;19:241–249. doi: 10.1002/ejhf.629. [PubMed] [CrossRef] [Google Scholar]

101. Schmid F., Schlager O., Keller P., Seifert B., Huang R., Fröhlich G.M., Lüscher T.F., Ruschitzka F., Enseleit F. Prognostic value of long-term blood pressure changes in patients with chronic heart failure. Eur. J. Heart Fail. 2017;19:837–842. doi: 10.1002/ejhf.805. [PubMed] [CrossRef] [Google Scholar]

102. Abraham W.T., Fisher W.G., Smith A.L., Delurgio D.B., Leon A.R., Loh E., Kocovic D.Z., Packer M., Clavell A.L., Hayes D.L., et al. Cardiac Resynchronization in Chronic Heart Failure. N. Engl. J. Med. 2002;346:1845–1853. doi: 10.1056/NEJMoa013168. [PubMed] [CrossRef] [Google Scholar]

103. García R., Villar A.V., Cobo M., Llano M., Martín-Durán R., Hurlé M.A., Nistal J.F. Circulating Levels of miR-133a Predict the Regression Potential of Left Ventricular Hypertrophy After Valve Replacement Surgery in Patients With Aortic Stenosis. J. Am. Heart Assoc. 2013;2:e000211. doi: 10.1161/JAHA.113.000211. [PMC free article] [PubMed] [CrossRef] [Google Scholar]

104. Miyamoto S., Usami S., Kuwabara Y., Horie T., Baba O., Hakuno D., Nakashima Y., Nishiga M., Izuhara M., Nakao T., et al. Expression Patterns of miRNA-423-5p in the Serum and Pericardial Fluid in Patients Undergoing Cardiac Surgery. PLoS ONE. 2015;10:e0142904. doi: 10.1371/journal.pone.0142904. [PMC free article] [PubMed] [CrossRef] [Google Scholar]

105. Shah R., Ziegler O., Yeri A., Liu X., Murthy V., Rabideau D., Xiao C.Y., Hanspers K., Belcher A., Tackett M., et al. MicroRNAs Associated With Reverse Left Ventricular Remodeling in Humans Identify Pathways of Heart Failure Progression. Circ. Heart Fail. 2018;11:e004278. doi: 10.1161/CIRCHEARTFAILURE.117.004278. [PMC free article] [PubMed] [CrossRef] [Google Scholar]

106. Zhang Z., Gao W., Long Q.-Q., Zhang J., Lian-Sheng W., Liu D.-C., Yan J.-J., Yang Z.-J., Wang L.-S. Increased plasma levels of lncRNA H19 and LIPCAR are associated with increased risk of coronary artery disease in a Chinese population. Sci. Rep. 2017;7:1–9. doi: 10.1038/s41598-017-07611-z. [PMC free article] [PubMed] [CrossRef] [Google Scholar]

107. Santer L., López B., Ravassa S., Baer C., Riedel I., Chatterjee S., Moreno M.U., González A., Querejeta R., Pinet F., et al. Circulating Long Noncoding RNA LIPCAR Predicts Heart Failure Outcomes in Patients Without Chronic Kidney Disease. Hypertension. 2019;73:820–828. doi: 10.1161/HYPERTENSIONAHA.118.12261. [PubMed] [CrossRef] [Google Scholar]

108. Zhang L.-E., Wu Y.-J., Zhang S.-L. Circulating lncRNA MHRT predicts survival of patients with chronic heart failure. J. Geriatr. Cardiol. 2019;16:818–821. [PMC free article] [PubMed] [Google Scholar]

109. Cassese S., Byrne R.A., Tada T., Pinieck S., Joner M., Ibrahim T., King L.A., Fusaro M., Laugwitz K.-L., Kastrati A. Incidence and predictors of restenosis after coronary stenting in 10 004 patients with surveillance angiography. Heart. 2014;100:153–159. doi: 10.1136/heartjnl-2013-304933. [PubMed] [CrossRef] [Google Scholar]

110. Wang F., Su X., Liu C., Wu M., Li B. Prognostic Value of Plasma Long Noncoding RNA ANRIL for In-Stent Restenosis. Med. Sci. Monit. 2017;23:4733–4739. doi: 10.12659/MSM.904352. [PMC free article] [PubMed] [CrossRef] [Google Scholar]

111. Viereck J., Thum T. Circulating Noncoding RNAs as Biomarkers of Cardiovascular Disease and Injury. Circ. Res. 2017;120:381–399. doi: 10.1161/CIRCRESAHA.116.308434. [PubMed] [CrossRef] [Google Scholar]

CHAPTER 4

"MicroRNAs as Plasma Biomarkers for Reverse Remodeling after Aortic Valve Replacement: a Portuguese-sample case study"

[1,2,3] RF Videira, [1,2,3]PA da Costa Martins, [3] I Falcão-Pires

[1] Department of Cardiology, CARIM School for Cardiovascular Diseases, Faculty of Health, Medicine and Life Sciences, Maastricht University, Maastricht, Netherlands;[2]Department of Molecular Genetics, Faculty of Sciences and Engineering, Maastricht University, Maastricht, The Netherlands; [3]Department of Physiology and Cardiothoracic Surgery, Faculty of Medicine, University of Porto, Porto, Portugal.

(In preparation)

Abstract

Recent advances in medical care allow for cardiac reverse remodeling (RR) and, consequently, for saving the heart from adverse phenotypes and eventually failing. RR is defined by any changes that lead to improved function following pathological cardiac remodeling. Unfortunately, a significant fraction of patients (33%*)[1, 2] that goes under treatment, namely aortic valve replacement (AVR), fails to show complete RR, does not show improved cardiac function, and develops an unfavorable clinical response. Patients with complete RR exhibit recovered cardiac function with improved prognosis and survival.

MicroRNAs (miRs) have evolved as potential biomarkers of cardiac pathological remodeling. More recently, circulating miRs were shown to play a greater role in predicting RR and patient outcomes under specific therapies.

The present work aims to identify and understand miR expression profiles associated with cardiac RR in aortic stenosis (AS). We investigated the contribution of circulating miRs as potential predictors of cardiac RR by preselecting plasma miRs that were previously associated with aortic pathologies and miR primer lab availability. The selected miR panel was further quantified by RT-qPCR in plasma samples from a Portuguese cohort of AS patients undergoing AVR. The results indicate that let-7b-3p and miR-133a-3p are differentially present in samples from complete in comparison to incomplete RR.

Interestingly, the AUC for all of these miRs individually is higher than 0.85, indicating a potentially good predictive value. After valve replacement, RR is crucial to evade heart failure; however, not being able to predict RR outcome hampers the improvement of precision and personalized medicine. Our data indicate miR-133a-3p and let-7b-3p as potentially strong biomarkers of complete RR after AVR surgery.

*This number could change according to the study population, parameters used by the observer, and type of treatment.

Introduction

Aortic stenosis (AS) is a common pathology described as the narrowing of the aortic valve that progressively imposes resistance to the blood flow from the left ventricle (LV) to the aorta [3]. As a result, the cardiac leaflets become calcified, which seriously compromises leaflet motion and ultimately leads to blood flow obstruction. The increased pressure precedes maladaptive LV hypertrophic, myocardial fibrosis, and eventually heart failure [3]. Concomitantly with compromising cardiac function and promoting heart failure, AS is also an important risk factor for perioperative mortality and morbidity in noncardiac surgery [4].

AS alone affects more than 5% of the population above 65 years old and together with other cardiovascular diseases account for more than 30% of all deaths globally (WHO), data from 2019 [5]. These numbers are increasing, and it is estimated that in 2050 symptomatic severe AS will affect 2.1 million Europeans [6]. Up to date, surgical aortic valve replacement (SAVR) or transcatheter aortic valve replacement (TAVR) are recommended as the most efficient treatments for AS. Still, both procedures entail numerous risks including heart failure and death [7].

Due to the scarcity of obvious symptoms linked to cardiac dysfunction, most AS patients are diagnosed late. The late-stage diagnosis occurs when cardiac damage is no longer reversible. Consequently, a poor prognosis is associated with AS symptomatic individuals contributing to a decrease in treatment efficacy and outcome [8, 9]. Moreover, not all patients who undergo AS treatment, including SAVR, benefit from the procedure. It is estimated that, after SAVR, there is a 54.8% risk of the composite outcome of all-cause mortality, stroke, or myocardial infarction [10]. Therefore, it is crucial to understand the mechanisms, determine which patients can benefit from SAVR, and estimate the occurrence of favorable LV remodeling.

Ideally, valve replacement triggers myocardial reverse remodeling (RR), which is accompanied by regression of LV hypertrophy by 20-30% (LV mass), and improvement of LV function [11]. However, a study on SAVR patients reported that this reversal is incomplete in most patients at 1-year post AVR, and the extent of RR is highly variable [12]. While some patients respond to therapy by decreasing LV mass and recovering cardiac function, thereby presenting improved prognosis and survival [13]. Others fail to respond, present signs of incomplete RR (increased LV mass and cardiac dysfunction), and thus develop an unfavorable clinical response [13].

In AS patients, reliable cardiac condition assessment by detecting blood-based biomarkers could aid in AS clinical management. Briefly, a blood-based biomarker is any blood measurement that reflects an interaction between a biological system and a potential hazard [14]. This correlation should feature a high degree of specificity and sensitivity; however, these criteria are not met by the clinical use of biomarkers troponins and natriuretic peptides since they are used on a panoply of diseases [15]. In order to overcome this, new prognostic and diagnostic tools, namely, miRs, are being investigated to further use in cardiovascular clinical practice.

MiRs are a class of conserved single-stranded small non-coding RNAs (~22 nucleotides) that regulate gene expression at a post-transcriptional level, usually through mRNA silencing [16]. It has been observed that alteration of miRs' expression levels contributes to the development of several pathologies, including AS [16, 17]. Similarly, reestablishing miR physiologic levels can

hamper disease progression, and their modulation arises as promising therapeutic tools [18, 19]. Meanwhile, miRs have been identified in different cellular compartments and extracellularly in human biofluids such as blood, serum, and plasma [20, 21]. In fact, miRs have been studied as prospective AS biomarkers due to their potential to reflect AS pathogenesis and be detected in blood at an earlier AS stage [22].

This work contributes to elucidating the potential use of plasma miRs as biomarkers for RR after AVR in patients with AS. Furthermore, patients' miR profiles could be used to guide AS diagnosis including patient's risk stratification and treatment decision making, as it may help in predicting AS progression and evaluating the benefit of AVR surgery.

Methods

a) Data mining

To better understand the role of miRs in cardiac RR, we carried out a search on PubMed and Google Scholar with no date restrictions to collect all articles that have reported miRs involved in the LV reverse remodeling by using the following keywords: “microRNAs” or “miRs” and “reverse remodeling”, “reverse remodelling”, “aortic valve replacement”, “cardiac recovery”, “myocardial recovery” and “aortic constriction”. Searches were performed between February and June of 2017.

Articles with a high relevance were retrieved and further analyzed in an unblinded standardly manner by two independent investigators. After careful revision, a list of pre-selected articles was elaborated by excluding articles without: i) full-size text in English, ii) association with left ventricle iii) clinical information iv) reference to reverse remodeling or mortality, v) pathological-induced reverse remodeling, and vi) direct correlation between microRNA expression and subject outcome.

After the elimination process, articles that provided sufficient sensitivity and specific information were suitable for data mining.

An Excel spreadsheet was generated, and data from each study was categorized in: “miR ID”, “human homology” (yes or no, if applicable), “variation” (+, - or unchanged), “fold change” (if applicable), “p-value” (if applicable), “sample type” (plasma, myocardial biopsies, left ventricle biopsies or cardiomyocytes), “clinical outcome” (maladaptive remodeling, recovery, if applicable), “experimental approach” (the event that triggered reverse remodeling), “sample size” (number of enrolled subjects), “specie” (human, mice or rat), “sampling time”, “methodology” (microarray or RT-PCR), “control condition”, “miR target” and “reference”.

To cope with the broad heterogeneity, each microRNA from different articles was individually annotated and further sorted and pooled data sub-grouped into the main events that motivate reverse remodeling. Reported microRNAs without human homology or studies with divergent results were also eliminated from our analysis. Finally, let-7b-3p, miR-21-3p, miR-23a-3p, miR-26a-5p and miR-133a-3p were chosen to further validation.

b) Patient Characterization

The local ethics committee approved the study protocol (CES 35/17) and written informed consent was obtained from all patients. This study complies with the Declaration of Helsinki. Patients undergoing aortic valve replacement (AVR) surgery and previously diagnosed with AS (aortic valve area <1 cm^2 or mean trans aortic gradient >40 mmHg) were recruited from Hospital de São João Porto, Portugal. Between June 2017 and June 2018, 19 plasma samples were collected at the time of surgery. Patients were followed by a 6-month period where different clinical parameters were assessed including sex, age, LV mass, ejection fraction (EF), and disease stage, among others. Individuals were sorted into complete and incomplete RR accordingly with the percentage of left ventricle mass regression (LVMR) assessed by echocardiography. Incomplete RR was considered when the percentage of LVM variation [(Follow-up LVM–Baseline LVM)/Baseline LVM x 100] was higher than -5%, while RR was considered complete whenever this value was lower than -15%.

c) Echocardiographic characterization

All patients were echocardiographically examined before and ~6-months after surgery. The examinations were performed using M-mode, two-dimensional, pulsed, continuous, color-flow, and tissue Doppler echocardiography. All measurements were performed according to the recommendations of the European Association of Echocardiography (EAE)/American Society of Echocardiography (ASE) [23].

LV mass (LVM) was estimated using Devereux's formula for ASE measurements in diastole: LV mass=0.8 x (1.04 x ([LV internal dimension + posterior wall thickness + interventricular septal thickness]3 – [LV internal dimension]3) + 0.6 g. Left ventricular hypertrophy (LVH) was defined by LV mass index greater than 115 g/m^2 in men and 95 g/m^2 in women. A value of LVM between 43-95 g/m^2 is considered a normal healthy value for women and between 49-115 g/m^2 a normal healthy value for men [24].

All indexed values were obtained by dividing by the body surface area following the Mosteller method [25].

d) Plasma collection and miR quantification

Venous blood samples were collected in ethylenediaminetetraacetic acid (EDTA) containing tubes from AS patients immediately before valve surgery. Blood samples were span at 5000 r.p.m. for 15 min at 4 °C and plasma was separated and frozen at -80°C until further processed for total RNA isolation. Plasma samples with a visible degree of hemolysis were excluded from our analysis. Total RNA was extracted from 100 µL of plasma following the manufacturer's protocol using the miRNeasy Serum/Plasma kit (Qiagen 217,184). Nanodrop 2000 (Thermo Fischer Scientific) was used to ensure equal RNA input amounts. Next, cDNA was produced from purified total RNA according to the manufacturer's instructions of TaqMan Advanced miRNA cDNA Synthesis (A28007). Four reactions were performed, including Poly(A) Tailing, Adapter Ligation, Reverse Transcription, and miR-Amplification. Briefly, for the first reaction 12 ng of total RNA sample was used and incubated with Poly(A) Reaction Mix for 45 min at 37°C followed by 10 min at 65°C. The next step consisted of the Adapter Ligation and was achieved by adding 10µl ligation reaction mix to 5 µl of Poly(A) Tailing product and incubating for 60 min at 16°C. Immediately after, Reverse Transcription was performed by adding 45 µl reverse transcription reaction mix to 5 µl Adapter Ligation product and thermally cycled for 15 min at 42°C, and inactivated at 85°C for 5 min. Finally, miR-Amplification was achieved by incubating 5 µl of reverse transcription product with 45 µl and exposed to 95°C for 5 min; at 3 sec 95°C for and 30 sec 60°C for 14 cycles and 99°C for 10 min.

e) Real-Time quantitative Poly Chain Reaction Analysis and Normalization

Out of these 19, only 13 samples (8 complete RR group and 5 incomplete RR group) showed a sufficient amount of material for miR analysis and thus were included in the subsequent analysis. MiRs selection for RT-qPCR analysis was chosen based on published literature as previously described in a). Circulating let-7b-3p, miR-21-3p, miR-23a-3p, miR-26a-5p and miR-133a-3p levels were quantified by RT-qPCR in plasma samples of 13 diagnosed AS patients (including patients with incomplete and complete RR) by using TaqMan Advanced miRNA Assays

(Thermofisher A25576), and Applied Biosystems™ TaqMan™ Fast Advanced Master Mix under fast cycling conditions. In brief, the miR-Amp product was diluted 1:5 in 0.1x TE added to 15 uL PCR reaction mix and cycled 20 s at 95 °C for enzyme activation; 1 sec at 95°C for denaturation, and 20 s at 60 °C for 40 times for annealing and extensionthe reaction was then stopped by increasing the temperature at 99 °C for 10 minutes. For each sample, qPCR reactions were performed in triplicates. Relative expression values were calculated using the 2 -ΔΔCt method.

Normalization: Analysis of plasma RNA is difficult due to the inexistence of constant levels of specific RNAs. Previously, a set of miRs was described as good endogenous control [26-28]; however, after performing the Bestkeeper analysis, no miR was above the cut-off value [29]. Therefore, as previously described, no housekeeping miR was used as endogenous control [30, 31]. All the reaction conditions were maintained constant and uniform throughout the assays. Finally, the diagnostic value was assessed via receiver operating characteristic curve (ROC) analysis.

f) Statistical Analysis

All data are presented as mean ± standard error of mean (SEM). The variables were analyzed using student t-test to assess statistical significance between groups. The diagnostic ability of each miR was assessed by plotting receiving operating curve (ROC) analysis in GraphPad Prism v.7., including Area Under the Curve (AUC). Probability values $p<0.05$ were considered statistically significant.

Results

a) Patient Population Characterization

To understand if different plasma miR profiles could aid in discriminating among patients with complete and incomplete remodeling, 13 patients diagnosed with AS were included in this study. Patients' clinical characterization before surgery (baseline) and at the 6-month follow-up are depicted in **Table 1**. Patients' mean age was 71,5±7,8 years, with a percentage of 61.5% women. At 6-month follow-up patients were classified as previously described as having complete RR (n=8) or incomplete RR (n=5). The complete RR group had a range of ages of 57 and 80 (37.5% male), while the incomplete RR group displays ages between 70 and 85 (40% male). Neither sex nor age was significantly different between groups. Echocardiographic data were collected before surgery and at the 6-months follow-up consultation. Complete and incomplete RR groups showed similar degrees of aortic valve stenosis as no significant differences were found in aortic valvular gradient, average aortic gradient, initial LV mass, initial EF, and natriuretic brain peptide (BNP) levels before SAVR (**Table 1**). As expected and due to the classification imposed, only the percentage of LVMR after surgery was significantly lower in the incomplete versus complete RR group. AS is usually associated with other comorbidities, **Table 2.** illustrates patients' comorbidities, 7 out of 8 of the complete RR group of patients had arterial hypertension (AHT), 3 had diabetes mellitus, and 4 had dyslipidemia (DL). Moreover, chronic obstructive pulmonary disease (COPD), renal insufficiency (RI), and syncope were observed in 3 out of 5 of the patients from the complete RR group and 1 has been diagnosed with angina. By contrast, the incomplete RR group is composed of 1 smoker, 4 with AHT, and 3 with DL. No significant differences were found between groups. Additionally, angina, RI, and syncope were present in 2 individuals in the population of incomplete RR patients, while COPD affects 1 patient in the incomplete RR group of patients. In summary, at time of the intervention, there were no demographic or clinical data that allowed to predict RR since there were no statistically significant differences between the two groups. As such, these results support the need for a strategy to differentiate which patients benefit from an earlier AVR intervention to prevent incomplete RR.

b) Plasma levels of let-7b-3p and miR-133a-3p are downregulated in incomplete RR group of patients

To determine the clinical significance of plasma miRs, we performed a literature search. Based on their potential as biomarkers, we selected let-7b-3p, miR-21-3p, miR-23a-3p, miR-26a-5p and miR-133a-3p to be validated on our group study.

Quantitative PCR analysis revealed that incomplete RR presented significant decreased levels of let-7b-3p and miR-133a-3p when compared to complete RR, as evident by their higher CT values (30.76 ± 1.3 vs 27.17 ± 0.81, $p = 0.0318$ and 38.61 ± 0.54 vs 34.24± 1.1, $p = 0.0107$, respectively, **Figure 1**). Contrarily, no significant differences were found in miR-21-3p, miR-23a-3p, miR-26a-5p. These results suggested that downregulated levels of let-7b-3p and miR-133a-3p are associated with incomplete RR after SAVR.

Table 1. Clinical Data of Patients with Complete and Incomplete RR.

	Complete RR	Incomplete RR	p
Age (years)	68.25± 7.36	76.6±5.77	ns
Male Sex	3/8	2/5	ns
Body Surface Area (m^2)	1.76±0.23	1.7±0.15	ns
Initial EF	57.38±13.84	60.18±15.42	ns
Final EF	60.52±13.76	61.55±8.47	ns
(Initial) Peak aortic valve velocity (cm/s)	456.78±41.91	413.68±71.42	ns
(Initial) Mean aortic transvalvular pressure gradient (mmHg)	52.1±9.47	39.8±14.37	ns
Initial LV Mass (g/m^2)	132.88±46.46	129.08±10.61	ns
Final LV Mass (g/m^2)	87.72±23.35	137.53±27.95	0.005
% of LV Mass Regression	-31.95	6.18±17.95	0.0003
Initial BNP (pg/mL)	302.72±114.91	374.25±271.95	ns

LV- Left Ventricle

EF- Ejection Fraction

BNP- Brain Natriuretic Peptide

Table 2. Comorbidities of Patients with Complete and Incomplete RR.

	Complete RR	Incomplete RR	p
Smoking	0/8	1/5	ns
AHT	7/8	4/5	ns
DM	3/8	0/5	ns
DL	4/8	3/5	ns
COPD	3/8	1/5	ns
RI	3/8	2/5	ns
Angina	1/8	2/5	ns
Syncope	3/8	1/5	ns
EuroScore	3.35±4.12	2.78±2.03	ns

AHT- Arterial Hypertension

DM- Diabetes Mellitus

DL-Dislipidemia

COPD- Chronic obstructive pulmonary disease

PAD- Peripheral Arterial Disease

RI- Renal Insuficiency

Figure 1.

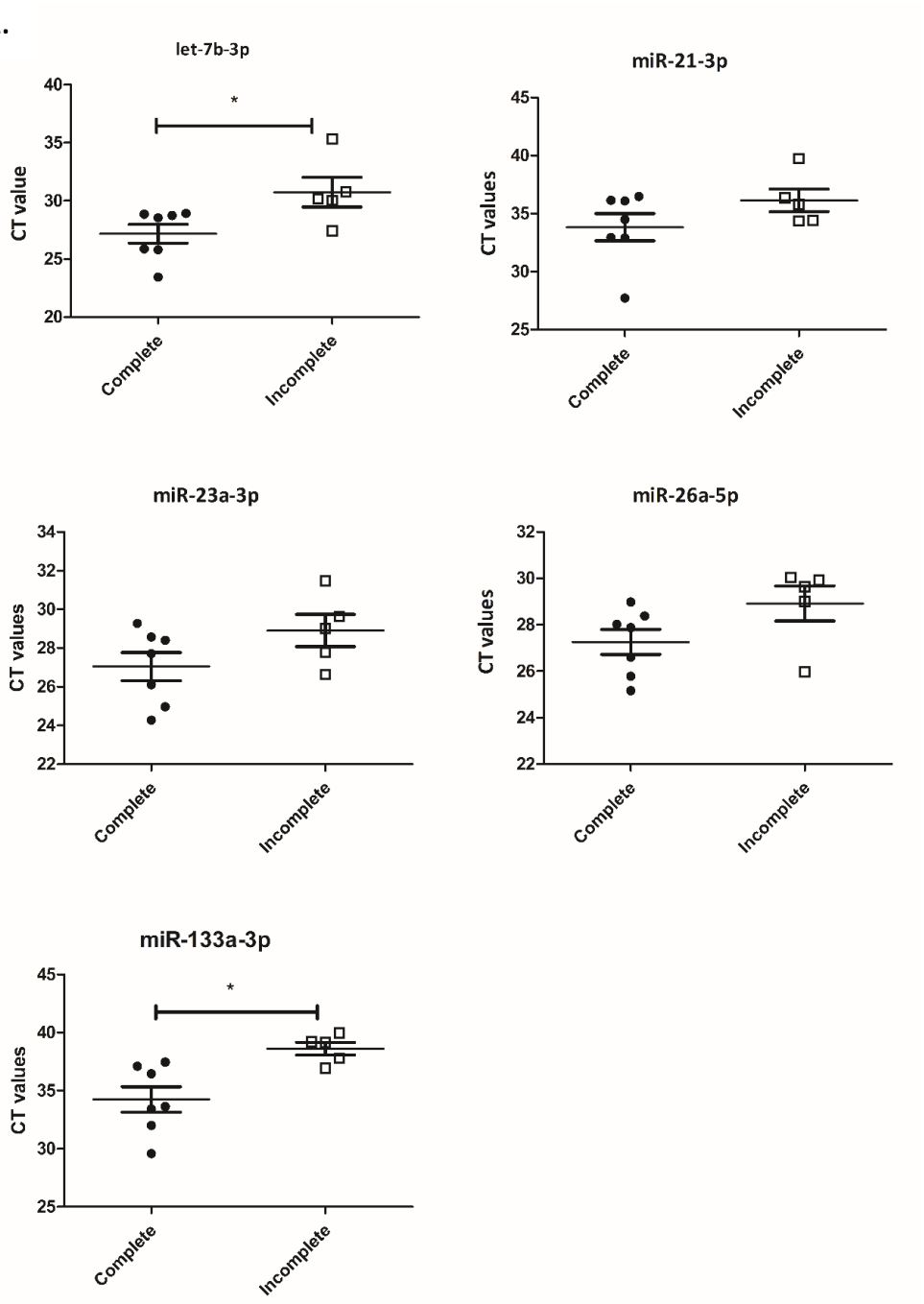

Figure 1. *Graphs representing RT-qPCR analysis of the respective miR CT values. Dark circles correspond to complete RR group and empty squares corresponds to incomplete RR group. T-student test was used to assess difference between groups. Data is represented in mean+/- SEM, *p<0.05.*

c) Sensitivity and Specificity of miRs for complete RR after SAVR

Incomplete RR diagnostic value of let-7b-3p and miR-133a-3p was investigated by the ROC curve and AUC (**Figure 2**). Let-7b-3p demonstrated an AUC of 0.88 ± 0.11, a 95% confidence interval (CI) of [0.66-1.1] and a p-value of 0.028. However, the highest AUC value was obtained by miR-133a-3p, which corresponds to 0.94, a 95% CI [0.81-1.07], and a p-value of 0.012. Qualitatively, let-7b-3p has a diagnostic accuracy of "very good" while miR-133a-3p is classified as "excellent" [32]. The cut-off values for 80% sensitivity and 100% specificity of let-7b-3p, and miR-133a-3p were 29.49 and 37.62, respectively. Although miR-133a-3p has proven the highest sensitivity and specificity and is probably more efficient in predicting incomplete remodeling after SAVR. Also, let-7b-3p is a good candidate, and we can speculate that if combined, the diagnostic value can be further increased.

Figure 2.

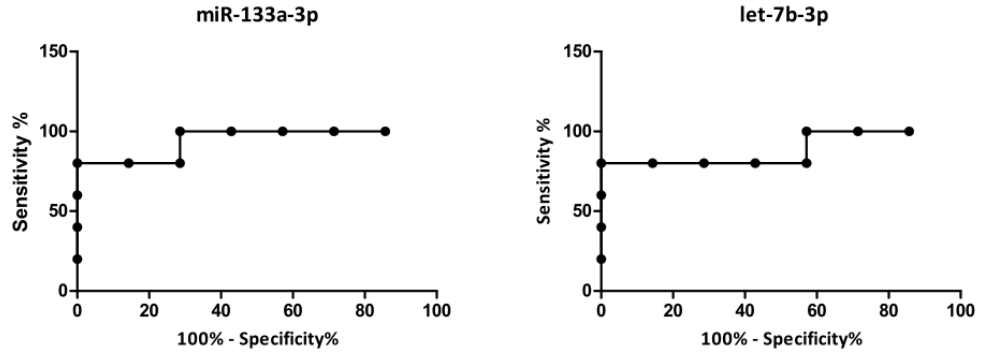

Figure 2. *ROC curve of the respective miR and the respective area under the curve (AUC) is represented with a 95 %confidence interval. Let-7b-3p and miR-133a-3p have an AUC of 0.8857, 0.8571 and 0.9429 and p-value of 0.0284 and 0.01186, respectively. All graphs were generated with Prism 5 (GraphPad).*

Discussion

Aortic stenosis is one of the most common valvular diseases and, by the year 2050, will affect 2.1 million Europeans [33]. Late symptoms or even asymptomatic individuals are associated with a delayed diagnosis and, consequently, poor prognosis [9, 34]. Ultimately, AS compromises heart function and structure and can lead to heart failure; hence, RR is crucial to evade this fate. Currently, there is no efficient pharmacological treatment for AS, and so far, clinical management includes valve replacement to promote RR [9]. However, not all patients benefit from this procedure, and some patients show worse cardiac function and structure after valve replacement. These patients are classified as incomplete RR, whereas a complete RR is observed in patients where cardiac function and structure improve significantly. Not being able to predict RR outcome hampers the improvement of personalized adjuvant treatments after valve replacement. Therefore, it is important to develop more effective strategies to predict the type of RR upon SAVR. So far, blood-based biomarkers, such as troponins and natriuretic peptides, are used in clinical practice, but these are not sufficiently sensitive to predict RR. Recently, miRs emerged as new potential plasma biomarkers for RR since a high degree of correlation between plasma and tissue miR expression profiles has been shown [35]. Although BNP has been used as a marker to predict patients' outcomes after SAVR, in our sample case study, there were no statistically significant differences in plasma BNP levels that could help identify incomplete RR group of patients [36].

Our study investigates the role of plasma let-7b-3p, miR-21-3p, miR-23a-3p, miR-26a-5p, and miR-133a-3p as discriminating factors for RR after SAVR in a Portuguese subpopulation. Our data indicate that miR-133a-3p and let-7b-3p are differentially expressed among AS patients. The diagnostic value of this miR panel was evaluated by ROC analysis followed by AUC calculation; interestingly, both miRs had values superior to 0.85, and in fact, let-7b-3p was classified as "very good" and miR-133a-3p was classified as "excellent" in the scale of diagnostic accuracy [32]. Thus, our results suggested miR-133a and let-7b-3p downregulation as a potentially strong biomarker of incomplete RR based on LVM regression.

The literature supports our results since previous associations were made between let-7b-3p and miR-133a-3p, particularly with AS. *Wang et al.* described that several members of the let-7 family, including let-7b, were decreased in the calcific aortic valve, which precedes AS [37]. Let-7b was also described as downregulated in the unloaded myocardium of rat model of reverse remodeling (induced by heterotopic transplantation of a heart previously subjected to abdominal aortic constriction) compared to non-transplanted hypertrophic hearts [38]. In another study, in mice, traverse aortic constriction was used to induce hypertrophy, which led to overexpression of cardiac let-7b [39]. Among our studied miR panel, miR-133a is by far the most studied. MiR-133a is a muscle-specific miR and one of the most abundant in the heart. MiR-133a controls pathological signaling of cardiac pathological hypertrophic growth and extracellular matrix remodeling both in mouse models and human pathological conditions [22, 40]. MiR-133a is considered a crucial player for maintaining the heart under normal conditions; a decrease in miR-133a levels contributes to the adverse remodeling response under pressure-overload conditions and, consequently, cardiac hypertrophy [22, 40]. MiR-133a was upregulated in plasma samples of patients with heart failure [41], risk of AS [42], and hypertrophic cardiomyopathy [42], when compared to healthy individuals. In another study, where circulating exosomal miR-133a levels were measured in patients with mitral regurgitation (and associated

LV hypertrophy) undergoing mitral clip surgery (suturing of mitral valve leaflets), it was described that miR-133a is upregulated in patients that recover (complete RR) when compared to non-recovery patients (incomplete RR) [43]. Similar to what we describe, *Villar et al.* described that plasma levels of miR-133a could predict the regression potential of LV hypertrophy after AVR since higher preoperative plasma levels of miR-133a are associated with complete RR [22, 44].

This work presents several limitations, such as the small sample size of patients and plasma samples included in this study. An increase in the number of patients might have helped strengthen the diagnostic value of the reported miRs. One limitation is patients' dropout throughout this study, which hinders clarifying if the observed differences are long-term biologically significant. Additionally, poor quality of the samples associated with very low concentrations of miRs in plasma is often observed as indicated by the extremely high CT values of all miRs in all the samples, directly influencing the miR expression level and translating into deficient diagnostic accuracy [45, 46]. Another limitation relates to the absence of a normalizer gene for this group of patients. Currently, the normalization of miR expression lacks definitive guidelines and, consequently, different normalization strategies could lead to different results [45, 47]. One of the miR normalization strategies is based on endogenous miRs, using the average Cq value of all the analyzed miRNAs in experiments that assayed large numbers of miRNAs or in which stable reference miRs are unknown. However, after measuring the expression of stable reference miRs as reported in [26-28] and following the Bestkeeper algorithm analysis, none of the suggested miRs was above the cut-off value [29]. As mentioned before, we decided not to use a housekeeping miR, similar to what was previously described [30, 31].

Nevertheless, we minimize the possibility of technical variables introduced during the experimental steps of this study. Thus, the starting sample amount, collection modality, storage conditions, equal RNA amount previous to cDNA synthesis, and cDNA previous to RT-qPCR were kept constant throughout the different samples to obtain results that translate into true biological responses.

Ideally, the perfect biomarker should be specific for a certain disease. A major issue of this study is that miRs reported by us were previously linked to AS but also to other diseases, some in the opposite spectrum of AS. So care must be taken when analyzing these data since let-7b and miR-133a-3p have been reported in other contexts besides AS. For example, let-7b-3p was found to be enriched in circulating serum extracellular vesicles of patients with colon cancer, and it was suggested as a promising biomarker to detect early-stage colon cancer [48].

Finally, the expression level of certain miRs might be influenced by patients' comorbidities (diabetes, hypertension, obesity), medication, and other factors and thereby impact RR after SAVR.

In conclusion, RR is crucial to evading heart failure; however, not being able to predict RR outcome hampers precision medicine approaches. Our data indicate that miR-133a and let-7b-3p are potential biomarkers of complete RR after AVR surgery. Individually, miR miR-133a and let-7b-3p are not enough to be used in clinical practice since each miR could only add a small

value in predicting RR. Therefore, our data should be combined with patient clinical parameters to help improve patients' diagnosis, treatment, and prognosis.

References

1. Allen, C.J., et al., *Baseline NT-proBNP Accurately Predicts Symptom Response to Transcatheter Aortic Valve Implantation.* J Am Heart Assoc, 2020. **9**(23): p. e017574.
2. Puri, R., et al., *TAVI or No TAVI: identifying patients unlikely to benefit from transcatheter aortic valve implantation.* Eur Heart J, 2016. **37**(28): p. 2217-25.
3. Gosev, I., et al., *Epigenome alterations in aortic valve stenosis and its related left ventricular hypertrophy.* Clin Epigenetics, 2017. **9**: p. 106.
4. Samarendra, P. and M.P. Mangione, *Aortic stenosis and perioperative risk with noncardiac surgery.* J Am Coll Cardiol, 2015. **65**(3): p. 295-302.
5. Pinto, R.A.S.C., *Epidemiology of aortic valve stenosis (AS) and of aortic valve incompetence (AI): is the prevalence of AS/AI similar in different parts of the world?* e-Journal of Cardiology Practice, 2020. **18**(10).
6. Osnabrugge, R.L., et al., *Aortic stenosis in the elderly: disease prevalence and number of candidates for transcatheter aortic valve replacement: a meta-analysis and modeling study.* J Am Coll Cardiol, 2013. **62**(11): p. 1002-12.
7. Hu, P.P., *TAVR and SAVR: Current Treatment of Aortic Stenosis.* Clin Med Insights Cardiol, 2012. **6**: p. 125-39.
8. Zhao, Y., et al., *Residual compromised myocardial contractile reserve after valve replacement for aortic stenosis.* Eur Heart J Cardiovasc Imaging, 2012. **13**(4): p. 353-60.
9. Marquis-Gravel, G., et al., *Medical Treatment of Aortic Stenosis.* Circulation, 2016. **134**(22): p. 1766-1784.
10. Jorgensen, T.H., et al., *Eight-year outcomes for patients with aortic valve stenosis at low surgical risk randomized to transcatheter vs. surgical aortic valve replacement.* Eur Heart J, 2021. **42**(30): p. 2912-2919.
11. Poulsen, S.H., et al., *Recovery of left ventricular systolic longitudinal strain after valve replacement in aortic stenosis and relation to natriuretic peptides.* J Am Soc Echocardiogr, 2007. **20**(7): p. 877-84.
12. Magalhaes, M.A., et al., *Outcome of Left-Sided Cardiac Remodeling in Severe Aortic Stenosis Patients Undergoing Transcatheter Aortic Valve Implantation.* Am J Cardiol, 2015. **116**(4): p. 595-603.
13. Trindade, F., et al., *Preoperative myocardial expression of E3 ubiquitin ligases in aortic stenosis patients undergoing valve replacement and their association to postoperative hypertrophy.* PLoS One, 2020. **15**(9): p. e0237000.
14. Strimbu, K. and J.A. Tavel, *What are biomarkers?* Curr Opin HIV AIDS, 2010. **5**(6): p. 463-6.
15. Wang, J., et al., *Novel biomarkers for cardiovascular risk prediction.* J Geriatr Cardiol, 2017. **14**(2): p. 135-150.
16. Videira, R.F., P.A. da Costa Martins, and I. Falcao-Pires, *Non-Coding RNAs as Blood-Based Biomarkers in Cardiovascular Disease.* Int J Mol Sci, 2020. **21**(23).
17. Santos-Faria, J., et al., *MicroRNAs and ventricular remodeling in aortic stenosis.* Rev Port Cardiol (Engl Ed), 2020. **39**(7): p. 377-387.
18. Imamura, T., et al., *Depleted tumor suppressor miR-107 in plasma relates to tumor progression and is a novel therapeutic target in pancreatic cancer.* Sci Rep, 2017. **7**(1): p. 5708.

19. van der Ree, M.H., et al., *Miravirsen dosing in chronic hepatitis C patients results in decreased microRNA-122 levels without affecting other microRNAs in plasma.* Aliment Pharmacol Ther, 2016. **43**(1): p. 102-13.
20. Ntelios, D., et al., *Elevated plasma levels of miR-29a are associated with hemolysis in patients with hypertrophic cardiomyopathy.* Clin Chim Acta, 2017. **471**: p. 321-326.
21. Zhang, C., H. Wang, and B. Yang, *miR-146a regulates inflammation and development in patients with abdominal aortic aneurysms by targeting CARD10.* Int Angiol, 2020. **39**(4): p. 314-322.
22. Garcia, R., et al., *Circulating levels of miR-133a predict the regression potential of left ventricular hypertrophy after valve replacement surgery in patients with aortic stenosis.* J Am Heart Assoc, 2013. **2**(4): p. e000211.
23. Lang, R.M., et al., *Recommendations for chamber quantification: a report from the American Society of Echocardiography's Guidelines and Standards Committee and the Chamber Quantification Writing Group, developed in conjunction with the European Association of Echocardiography, a branch of the European Society of Cardiology.* J Am Soc Echocardiogr, 2005. **18**(12): p. 1440-63.
24. Kinno, M., Waller, A., and Gardin, J. , *Approaches to Echocardiographic Assessment of Left Ventricular Mass what does Echocardiography add.* American College of Cardiology, 2016.
25. Mosteller, R.D., *Simplified calculation of body-surface area.* N Engl J Med, 1987. **317**(17): p. 1098.
26. Marabita, F., et al., *Normalization of circulating microRNA expression data obtained by quantitative real-time RT-PCR.* Brief Bioinform, 2016. **17**(2): p. 204-12.
27. Song, J., et al., *Identification of suitable reference genes for qPCR analysis of serum microRNA in gastric cancer patients.* Dig Dis Sci, 2012. **57**(4): p. 897-904.
28. Hu, Z., et al., *Serum microRNA profiling and breast cancer risk: the use of miR-484/191 as endogenous controls.* Carcinogenesis, 2012. **33**(4): p. 828-34.
29. Pfaffl, M.W., et al., *Determination of stable housekeeping genes, differentially regulated target genes and sample integrity: BestKeeper--Excel-based tool using pair-wise correlations.* Biotechnol Lett, 2004. **26**(6): p. 509-15.
30. Martins-Ferreira, R., et al., *Circulating microRNAs as potential biomarkers for genetic generalized epilepsies: a three microRNA panel.* Eur J Neurol, 2020. **27**(4): p. 660-666.
31. Wang, G., et al., *Serum and urinary cell-free MiR-146a and MiR-155 in patients with systemic lupus erythematosus.* J Rheumatol, 2010. **37**(12): p. 2516-22.
32. Simundic, A.M., *Measures of Diagnostic Accuracy: Basic Definitions.* EJIFCC, 2009. **19**(4): p. 203-11.
33. Ancona R., C.S. *Epidemiology of aortic valve stenosis (AS) and of aortic valve incompetence (AI): Is the prevalence of AS/AI similar in different parts of the world?* . e-J. Cardiol. Pract. 2020 [cited 18; Available from: https://www.escardio.org/Journals/E-Journal-of-Cardiology-Practice/Volume-18/epidemiology-of-aortic-valve-stenosis-as-and-of-aortic-valve-incompetence-ai.
34. Lancellotti, P., et al., *Outcomes of Patients With Asymptomatic Aortic Stenosis Followed Up in Heart Valve Clinics.* JAMA Cardiol, 2018. **3**(11): p. 1060-1068.
35. Han, J., et al., *Identification of plasma miR-148a as a noninvasive biomarker for hepatocellular carcinoma.* Clin Res Hepatol Gastroenterol, 2019. **43**(5): p. 585-593.

36. Iwahashi, N., et al., *Usefulness of plasma B-type natriuretic peptide in the assessment of disease severity and prediction of outcome after aortic valve replacement in patients with severe aortic stenosis.* J Am Soc Echocardiogr, 2011. **24**(9): p. 984-91.
37. Wang, H., et al., *MicroRNA Expression Signature in Human Calcific Aortic Valve Disease.* Biomed Res Int, 2017. **2017**: p. 4820275.
38. Wang, J., et al., *MicroRNA: novel regulators involved in the remodeling and reverse remodeling of the heart.* Cardiology, 2009. **113**(2): p. 81-8.
39. Sayed, D., et al., *MicroRNAs play an essential role in the development of cardiac hypertrophy.* Circ Res, 2007. **100**(3): p. 416-24.
40. Care, A., et al., *MicroRNA-133 controls cardiac hypertrophy.* Nat Med, 2007. **13**(5): p. 613-8.
41. Wang, E., et al., *Circulating miRNAs reflect early myocardial injury and recovery after heart transplantation.* J Cardiothorac Surg, 2013. **8**: p. 165.
42. Roncarati, R., et al., *Circulating miR-29a, among other up-regulated microRNAs, is the only biomarker for both hypertrophy and fibrosis in patients with hypertrophic cardiomyopathy.* J Am Coll Cardiol, 2014. **63**(9): p. 920-7.
43. Kasner, M., et al., *Circulating exosomal microRNAs predict functional recovery after MitraClip repair of severe mitral regurgitation.* Int J Cardiol, 2016. **215**: p. 402-5.
44. Villar, A.V., et al., *Myocardial gene expression of microRNA-133a and myosin heavy and light chains, in conjunction with clinical parameters, predict regression of left ventricular hypertrophy after valve replacement in patients with aortic stenosis.* Heart, 2011. **97**(14): p. 1132-7.
45. Faraldi, M., et al., *Normalization strategies differently affect circulating miRNA profile associated with the training status.* Sci Rep, 2019. **9**(1): p. 1584.
46. Chen, Y., et al., *Reproducibility of quantitative RT-PCR array in miRNA expression profiling and comparison with microarray analysis.* BMC Genomics, 2009. **10**: p. 407.
47. Faraldi, M., et al., *Free Circulating miRNAs Measurement in Clinical Settings: The Still Unsolved Issue of the Normalization.* Adv Clin Chem, 2018. **87**: p. 113-139.
48. Min, L., et al., *Evaluation of circulating small extracellular vesicles derived miRNAs as biomarkers of early colon cancer: a comparison with plasma total miRNAs.* J Extracell Vesicles, 2019. **8**(1): p. 1643670.

CHAPTER 5

"Non-coding RNAs in Cardiac Intercellular Communication"

Raquel Figuinha Videira[1,2,3] and Paula A. da Costa Martins[1,2,4*]

[1]CARIM School for Cardiovascular Diseases, Faculty of Health, Medicine and Life Sciences, Maastricht University, Maastricht, Netherlands [2]Department of Molecular Genetics, Faculty of Science and Engineering, Maastricht University, Maastricht, Netherlands [3]Cardiovascular Research and Development Center, Faculty of Medicine, University of Porto, Porto, Portugal [4]Department of Physiology and Cardiothoracic Surgery, Faculty of Medicine, University of Porto, Porto, Portugal

Published in Front. Physiol., 09 September 2020

https://doi.org/10.3389/fphys.2020.00738

Abstract

Intercellular communication allows for molecular information to be transferred from cell to cell, in order to maintain tissue or organ homeostasis. Alteration in the process due to changes, either on the vehicle or the cargo information, may contribute to pathological events, such as cardiac pathological remodeling. Extracellular vesicles (EVs), namely exosomes, are double-layer vesicles secreted by cells to mediate intercellular communication, both locally and systemically. EVs can carry different types of cargo, including non-coding RNAs (ncRNAs), which, are major regulators of physiological and pathological processes. ncRNAs transported in EVs are functionally active and trigger a cascade of processes in the recipient cells. Upon cardiac injury, exosomal ncRNAs can derive from and target different cardiac cell types to initiate cellular and molecular remodeling events such as hypertrophic growth, cardiac fibrosis, endothelial dysfunction, and inflammation, all contributing to cardiac dysfunction and, eventually, heart failure. Exosomal ncRNAs are currently accepted as crucial players in the process of cardiac pathological remodeling and alterations in their presence profile in EVs may attenuate cardiac dysfunction, suggesting that exosomal ncRNAs are potential new therapeutic targets. Here, we review the current research on the role of ncRNAs in intercellular communication, in the context of cardiac pathological remodeling.

Introduction

Cardiac homeostasis is achieved through a complex network of interactions between the different cells of the myocardium, including cardiomyocytes, cardiac fibroblasts, neurons, cardiac endothelial, and immune cells. Upon injury, this homeostatic state is damaged and intercellular communications are rearranged toward cardiac maladaptive remodeling (Xin et al., 2013), normally characterized by cardiac hypertrophic growth, capillary rarefaction, and scar-induced events such as exacerbated inflammation, interstitial fibrosis, and ventricular dilation (Xin et al., 2013).

Cardiac communication between different types of cells can occur *via* (i) cell–matrix interactions, where cells respond to mechanical and extracellular matrix (ECM) stress; (ii) synaptic signaling, usually associated with electric and chemical neuronal signals released at the synapse site; (iii) endocrine signaling, a long distance communication where signaling factors are released into the blood stream (Kamo et al., 2015); but mostly (iv) *via* paracrine signaling, a short-range crosstalk mechanism where signals are diffused through the extracellular space before being incorporated in recipient cells and instigating a response (Bang et al., 2015). While paracrine factors have been confined for a long-time to soluble factors released from the cells, such as cytokines, in the past few years, growing evidence suggests more controlled and protected signaling mechanisms mediated by extracellular vesicles (EVs) (Hervera et al., 2019).

The classic concept of EVs containing cell debris or being markers of cell death was recently revolutionized when healthy cells were also shown to be capable of releasing these vesicles and, today, they are considered crucial mediators of both physiological and pathological cellular and molecular events. While EV is a generic term to describe a double-layer vesicle endogenously secreted by cells, their different origin, size and surface markers allow us to categorize them into three main groups: microvesicles, exosomes, and apoptotic bodies (Raposo and Stoorvogel, 2013). In contrast to microvesicles (100–1000 nm in diameter, MVs), which are formed by direct budding of the plasma membrane and, therefore, express selectins, integrins, and CD40l; exosomes (40–120 nm in diameter) originate through the cellular endocytic pathway and express markers such as CD81, CD63, CD9 (tetraspanins), flotillin, and Alix (Raposo and Stoorvogel, 2013). To date, only MVs and exosomes have been associated with intercellular communication.

Recently, a new class of EVs named exomeres has been characterized as non-encapsulated nanoparticles due to the absence of an external membrane structure, a low lipidic composition and a smaller size (up to 50 nm in diameter) (Zhang et al., 2018). The same study also distinguished two subtypes of exosomes: small exosomes (exo-S) and large exosomes (exo-L), primarily according to their size which varies from 60 to 80 nm and 90 to 120 nm, respectively. Although exo-S and exo-L present the typical exosome marker proteins Alix and Tsg101, exo-S preferentially express tetraspanins and their cargo is mainly composed of proteins associated with endosomes, multivesicular bodies, vacuoles, and phagocytic vesicles whereas Exo-L are enriched in proteins that make up the plasma membrane, cell junctions, late-endosome, and trans-Golgi network (Zhang et al., 2018). Given that a distinct set of proteins is found among the different exosomes, it is not surprising that they also show different degrees of stiffness and charge (Zhang et al., 2018). Due to their novelty, differences among exosomes subtypes were not taking into consideration on the studies reported in this review and, therefore,

discrimination between exo-S and exo-L was not included in their reported analysis. Indeed, exosomes are generalized and referred to as a major class, without differentiation according to their subtypes, throughout this review.

Notably, exosomes can transport both proteomic and genetic cargo that are functionally active once within the recipient cell (Raposo and Stoorvogel, 2013). A great component of exosomal cargo is made up of non-coding RNAs (ncRNAs), which are major regulators of cell homeostasis and are the main players in a variety of diseases, namely cardiovascular diseases and heart failure (Dhanoa et al., 2018). ncRNAs are a heterogenous class of RNAs, classified mostly according to their size: small (miRNAs) or long (lncRNAs); shape: linear or circular (circRNAs), and cell position: nucleolar (snoRNAs) or cytoplasmic (Santosh et al., 2015; **Figure 1**). From bacteria to humans, ncRNAs are present in a wide range of organisms, in fact, the "baby boom" of ncRNAs occurred after the first report on the lin-4 gene in *Caenorhabditis elegans* (Lee et al., 1993). Since then, multiple reports have implicated miRNAs in the negative regulation of gene expression at a post-transcriptional level, in biological processes ranging from cellular proliferation, migration, and apoptosis and thus, also in pathological processes such as maladaptive cardiac remodeling leading to heart failure (Liao et al., 2018; Huang S. et al., 2019; Yang et al., 2019). Typically, a miRNA selectively binds to the 3'UTR of mRNA targets and either induces their degradation or prevents them from being translated into protein, in a process that is dependent on the complementarity between the miRNA and the respective mRNA target (Li and Rana, 2014). In turn, miRNAs can be regulated by linear lncRNAs that present multiple miRNA-binding sites and which, by allowing the recruitment of several molecules at once, generate a sponge-like effect (Greene et al., 2017; Zhou and Yu, 2017). lncRNAs can also structurally facilitate mRNA decay, mRNA splicing, and translation by functioning as a dock for the "mRNA-lncRNA-Staufen-1," a complex responsible for mRNA degradation and accumulation/assembly of specific factors of the splicing machinery by promoting the association of the mRNA 5'UTR with the polysome (Gong and Maquat, 2011; Uchida and Dimmeler, 2015). At the DNA level, lncRNAs can contribute to epigenetic modifications, namely histone and DNA methylation, by recruiting chromatin remodeling complexes such as the polycomb repressive complex 2 (PRC2) or H3K27me3 and lead to transcriptional repression (Gupta et al., 2010). In contrast to miRNAs, with their exclusive non-coding function, recent reports described a potential dual role for lncRNA as both non-coding and protein coding genes (Matsumoto et al., 2017). Recently, several lncRNAs were found to be enriched in EVs secreted by colorectal cancer cells and were shown to control gene expression patterns in the recipient cells (Hinger et al., 2018). The export of RNAs through exosomes seems to be a controlled rather than a passive or random mechanism. Despite miRNAs and lncRNAs being both incorporated in EVs, miRNAs are exported in greater quantities, and often intact, suggesting a more regulated control of exosomal miRNA content (Hinger et al., 2018).

Exosome-mediated shuttling of ncRNAs between cells is not the only mechanism of ncRNAs transference, as shown for miRNAs which can also leave the cell bound to either lipid particles such as cholesterol (Tabet et al., 2014), ribonucleic complex (Arroyo et al., 2011), and other vesicles (Chen et al., 2019). Being incorporated into vesicles grants higher miRNA longevity by conferring protection from degradation by nucleases (Arroyo et al., 2011). However, the relative abundance of cardiac secreted miRNAs within exosomes and/or other vesicles remains debatable. While Chen et al. (2020) described higher plasma levels of miR-126 in the exosomal

fraction compared to the non-exosomal fraction, another study suggests that plasmatic exosomal miRNAs are only a minority, with 90% of the plasmatic miRNAs being present in a non-membrane-bound form, possibly bound to a ribonucleoprotein complex (Arroyo et al., 2011).

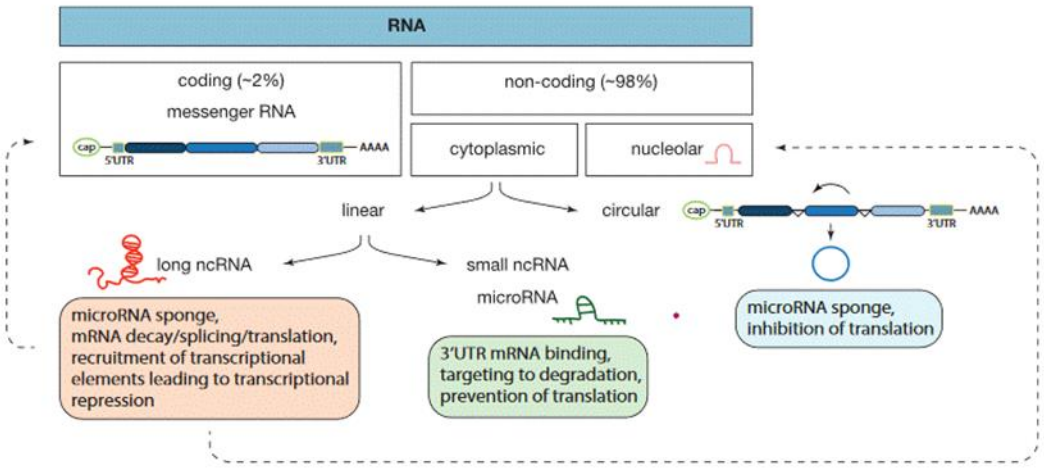

Figure 1. *Classes of RNAs and their mechanisms of action. In our genome, approximately 98% of the transcribed RNA is ncRNA, a diverse class of RNAs thatdoes not encode for a protein. ncRNAs are divided according to their localization: nucleus or cytoplasm; shape: circular or linear and size: small or long. EachncRNA is a unique form and mechanism of action, as described inside of each box. In this review we focused on microRNAs, long non-coding, and circular RNAs.Dashed lines represent findings that need further validation.*

Similar to lncRNAs, circular RNAs (circRNAs) can also inhibit miRNAs using the "sponge" effect strategy. circRNAs are ncRNAs (exon- or intron-derived) where the 3' and 5' ends, usually free in a linear RNA, are linked together forming a continuous loop (Greene et al., 2017). Recently, these structurally different RNAs were associated with cardiovascular diseases and were shown to also serve as EV cargo (Zhou and Yu, 2017; Huang S. et al., 2019). In fact, an altered circRNA pattern was found in EVs derived from ischemic heart tissue when compared to EVs derived from healthy myocardium (Ge et al., 2019). The enriched circRNAs in ischemic heart tissue were associated with the metabolic process of vesicle generation while the depleted circRNAs were involved in transforming growth factor beta (TGF-β) signaling, commonly, associated with cardiac fibrosis and inflammation (Ge et al., 2019).

Here, we review the current research on the role of ncRNAs in intercellular communication, in the context of cardiac pathological remodeling.

Cross TALK of ncRNAs in Cardiac Hypertrophy

Cardiomyocytes, the most prominent cell type of the myocardium (Zhou and Pu, 2016) can grow either via hyperplasia, which results in increased number of cells, or via hypertrophy where cell size increases while the cell number remains the same. In mammalians, adult cardiac growth occurs mainly through cardiomyocyte hypertrophy as cardiomyocytes exit the cell cycle, shortly after birth, hampering them to proliferate as an adult (Xin et al., 2013). Although physiological hypertrophic growth may be necessary to prevent cardiac atrophy during pregnancy or intense exercise, (Pu et al., 2003) hypertrophic growth is normally a maladaptive

remodeling process that eventually progresses toward heart failure, depending on the nature, length, and intensity of the initial cardiac stress (Samak et al., 2016).

Intense exercise and pregnancy often result in cardiac hypertrophic growth through a process regulated by the phosphoinositide 3-kinase/protein kinase B (PI3K/AKT) signaling pathway and insulin growth factor (IGF) (Frey and Olson, 2003). As cardiac morphology and contractile function are both preserved, this is considered to be an adaptive or physiological process (Frey and Olson, 2003). In pathologic hypertrophy, where contractile function is compromised, activation of G-protein coupled receptors (GPCRs), mitogen-activated protein kinase (MAPK), and the calcineurin/nuclear factor activated cells (Cn/NFAT) pathway leads to suppression of fatty acid oxidation, increased cell growth, fibrosis, and inflammation toward heart failure (Frey and Olson, 2003). Pathological hypertrophy often develops as a consequence of chronic hypertension, valvular disease, or cardiomyopathies. Briefly, the ventricular wall is exposed to elevated mechanical stress which is perceived by the sarcomeric Z-disks in the cardiac muscle cells to trigger the activation of signaling pathways including the Cn/NFAT pathway, inducing, in turn, cardiomyocytes to become hypertrophic and ventricle walls to reach excessive dimensions (Lyon et al., 2015). Initially, an increase in size is matched with a higher heart rate as the heart tries to maintain its normal cardiac output. However, if the pathologic stimuli remains, the heart can no longer cope with the stress, and without enough oxygen due to insufficient coronary perfusion, hypertrophy becomes a maladaptive, rather than an adaptive process (Frey and Olson, 2003). In fact, the Heart Outcomes Prevention Evaluation (HOPE) trial, a study assessing the efficiency of ramipril, an angiotensin-converting enzyme (ACE) inhibitor, in preventing future cardiovascular events in high-risk patients, showed that inhibition or regression of cardiac hypertrophy is able to decrease heart failure and stroke events as well as increase survival rate, thus questioning whether hypertrophy is ever an adaptive process at all (Mathew et al., 2001).

Not only cardiomyocytes but also cardiac fibroblasts and endothelial cells are affected by hypertrophic stimuli, and their orchestrated response can promote cardiomyocyte growth mostly by the release of a variety of pro-hypertrophic paracrine factors. In line with this, lower levels of such factors will hamper cell growth. Inhibition of nitric oxide (NO) synthesis by endothelial cells is followed by a reduction in cardiomyocyte size (Jaba et al., 2013). Another well-described paracrine factor is TGF-β, secreted by cardiac fibroblasts. Conditioned medium of cardiac pressure overload-derived fibroblasts was shown to be sufficient to induce hypertrophic growth of cardiomyocytes in culture – an effect that could be abrogated by blockade of TGF- β receptors (Cartledge et al., 2015). These findings highlight the role of intercellular communication in the heart and its importance in the cardiac response to stress.

Hypertrophic signaling is also influenced by the transfer of ncRNAs through crosstalk between cardiomyocytes and non-cardiomyocytes (**Figure 2**). Fibroblast-derived exosomes were shown to be enriched in miR-21∗ which can be taken up by cardiomyocytes and can induce their hypertrophic growth by targeting cytoskeletal proteins, namely sorbin and SH3 domain-containing protein 2 (SORBS2) and PDZ and LIM domain 5 (PDLIM5) (Tian et al., 2018). In line with this, blocking of miR-21∗ in mice subjected to chronic administration of angiotensin II (AngII) reduced cardiomyocyte growth, underlining fibroblast-derived miR-21∗ as a key player toward a pathologic cardiac response to chronic stress (Tian et al., 2018). More recently, miR-

34a, along with miR-27a and miR-28a were reported to be preferentially incorporated into exosomes secreted by cardiac fibroblasts after tumor necrosis factor alpha (TNF-α) treatment (Tian et al., 2018). These miRNAs are secreted from cardiac fibroblasts and transferred to cardiomyocytes where they not only induce expression of hypertrophic genes but also have as a common target an antioxidant enzyme, Kelch-like ECH-associated protein 1-nuclear factor erythroid 2-related factor 2 (Nrf2), previously shown to be downregulated in chronic heart failure (Tian et al., 2018). By being upregulated in chronic heart failure, miR-27a, miR-28a, and miR-34a may contribute to the development of the disease through the inhibition of Nrf2 (Tian et al., 2018).

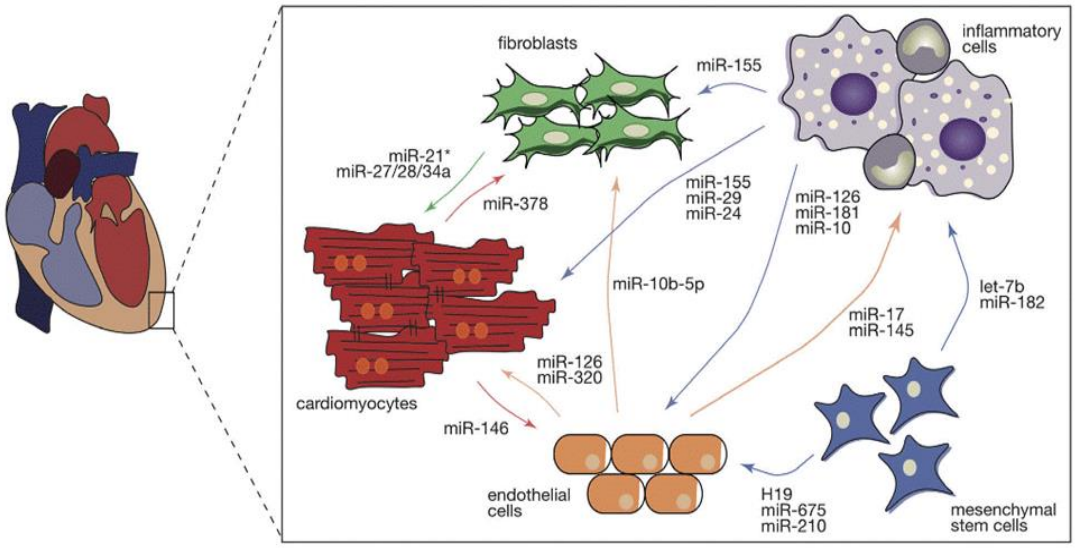

Figure 2. *Classes of RNAs and their mechanisms of action. In our genome, approximately 98% of the transcribed RNA is ncRNA, a diverse class of RNAs thatdoes not encode for a protein. ncRNAs are divided according to their localization: nucleus or cytoplasm; shape: circular or linear and size: small or long. EachncRNA is a unique form and mechanism of action, as described inside of each box. In this review we focused on microRNAs, long non-coding, and circular RNAs.Dashed lines represent findings that need further validation.*

Similarly, macrophages are also able to influence the cardiomyocyte response to stress by transferring macrophage-derived miR-155 (Halkein et al., 2013). *In vitro*, the hypertrophic phenotype of cardiomyocytes treated with the pro-hypertrophic factor endothelin 1 (ET1) was attenuated by exposing the cells to conditioned media derived from miR-155-deficient macrophages (Wang C. et al., 2017). *In vivo*, specific genetic ablation of miR-155 on macrophages hampered cardiac hypertrophy and inflammation in a mouse model of hypertrophy (Wang C. et al., 2017). Regarding endothelial cells, it was shown that in peripartum cardiomyopathy, a cardiac disease initiated by a cleaved prolactin fragment (16-kDa N-terminal prolactin fragment, 16K PRL), increased expression of miR-146 hampering angiogenesis (Halkein et al., 2013). However, miR-146 was also found in endothelial cell-derived exosomes and was shown to be transferred to cardiomyocytes where it negatively regulates Erb-B2 Receptor Tyrosine Kinase 4 (Erbb4), known to be involved in cardiac hypertrophy and metabolism. Chemical inhibition of miR-146 in a mouse model of peripartum cardiomyopathy attenuated cardiac dysfunction (Halkein et al., 2013).

Cardiac hypertrophy, a fundamental risk factor for heart failure, develops as an orchestrated response of several types of cells where ncRNAs act as paracrine factors manipulating the behavior of both donor and recipient cells (**Figure 2**).

Cross TALK of ncRNAs in Cardiac Capillary Rarefaction

As shown for several vascular diseases such as atherosclerosis, vessel restenosis, and primary hypertension, the vasculature is mostly capable of adapting itself in response to different stimuli to maintain vascular function and structure after injury (Su et al., 2017). However, pathologic stimulation of the cardiac vessels results in increased rigidity and a decline of vessel compliance as maladaptive vascular remodeling that will ultimately further contribute to cardiomyocyte hypertrophy and fibrosis (Su et al., 2017). Larger cardiomyocytes require more oxygen and nutrients and to cope with this increased demand, the cardiac vasculature must expand accordingly. In an initial phase, proangiogenic signals are released from damaged cardiomyocytes and capillaries are able to adapt to the increased demand, however, if the stress persists leading to exaggerated hypertrophy, these mechanisms fail to further stimulate vascular growth (Gogiraju et al., 2019). In pressure overload-induced hypertrophy, an increase in p53 expression leads to apoptosis of endothelial cells, deficient vasculature, and diminished capillary density – all contributing to tissue hypoxia and subsequent scar formation (Gogiraju et al., 2019).

One of the mainstays of cardiac vascularization and function is the vascular endothelial growth factor (VEGF) signaling pathway. Constitutive expression of VEGF-A in mice is able to enhance cardiac angiogenesis and improve basal cardiac function and vice versa, while its depletion results in defective vascularization, thinner cardiac walls, and contractile dysfunction (Lee et al., 2017). The VEGF signaling is also under the control of miRNAs including miR-374, shown to target VEGF receptor 1 (VEGFR1) and its downstream factor protein kinase G1 (PKG1), a regulator of calcium release from endoplasmatic reticulum that, indirectly, promotes hypertrophy (Lee et al., 2017). Depletion of miR-126, another miRNA regulating angiogenesis, in endothelial cells leads to partial embryonic lethality (40%) due to vascular defects (Wang et al., 2008). Similarly, in mice subjected to myocardial infarction (MI), miR-126 deletion contributed to a decrease in the VEGF signaling pathway (Yang et al., 2017). Following MI, the ischemic myocardium responds by increasing VEGF and fibroblast growth factor (FGF) expression, two potent angiogenic factors that are crucial for the development of collateral vessels and contribute to the reperfusion of the damaged myocardium (Cochain et al., 2013). MiR-126 silencing promotes the expression of its target Sprouty Related EVH1 Domain Containing 1 (SPRED1), an inhibitor of the RAF proto-oncogene serine/threonine-protein kinase (RAF1) and VEGF/ERK angiogenic pathway (Fish et al., 2008). Interestingly, miR-126 was reported to be depleted in exosomes derived from type 2 diabetic rat cardiomyocytes, while miR-320 was found to be highly enriched (Wang et al., 2014). Uptake of these miR-320-enriched exosomes by cardiac endothelial cells compromised their proliferative, migratory, and tube formation capacity (Wang et al., 2014). In contrast, inhibition of miR-320 or pharmacological inhibition of exosome formation were sufficient to abrogate the deleterious effects of miR-320 expression on angiogenesis – indicative of an anti-angiogenic and exosome-dependent role for this miRNA (Wang et al., 2014).

Moreover, depletion of miR-17 and miR-145 from exosomes derived from macrophages that were exposed to AngII, interferes with the capacity of cells to incorporate those exosomes

(Leisegang et al., 2017). In endothelial cells, exosomal depletion of miR-17 and miR-145 increased the expression of two previously described targets known to be involved in inflammation, intercellular adhesion molecule 1 (ICAM-1), and plasminogen activator inhibitor 1 (PAI-1) (Osada-Oka et al., 2017). These results underline miRNAs as pathological cargo of exosomes, emphasizing their role in promoting pro-inflammatory signaling pathways in endothelial cells.

Similar to miRNAs, lncRNAs can also act as regulators of angiogenesis. CRISPR/Cas9-mediated genetic deletion of a lncRNA that is normally found upregulated in vascular pathologies (Leisegang et al., 2017), MANTIS, in human umbilical vein endothelial cells (HUVECs), compromised their tube formation and sprouting capacity through the downregulation of several angiogenic-related genes (Leisegang et al., 2017).

Interestingly, exposing neonatal rat cardiomyocytes to hypoxic conditions induced the release of exosomes that are enriched in circRNAs, namely, circHIPK3 (Wang et al., 2019b). Conditioned media derived from hypoxic cardiomyocytes led to upregulation of this circRNA in cardiac microvascular endothelial cells (CMVECs). In contrast, circHIPK3 is downregulated when CMVECs are exposed to H_2O_2. In these cells, circHIPK3 acts as a sponge for miR-29, that in turn, targets the insulin-like growth factor 1 (IGF-1) pathway, involved in reactive oxygen species (ROS) production and apoptosis (Yanagisawa-Miwa et al., 1992). In fact, re-expression of IGF-1, due to enrichment of circHIPK3, promoted survival of CMVECs exposed to H_2O_2 and decreased ROS production, suggesting that cardiomyocyte exosome-derived circHIPK3 is a regulator of endothelial function and capillary rarefaction during hypoxic conditions (Wang et al., 2019b).

A defective vasculature is typical of the maladaptive cardiac remodeling process observed in different pathologies, including MI, hypertension, or cardiomyopathy (Cochain et al., 2013). Increased capillary density after cardiac injury has been shown to prevent cardiac remodeling and improve cardiac function, establishing angiogenesis as an appealing therapeutic target (Yanagisawa-Miwa et al., 1992). Besides being effective regulators of angiogenesis, incorporation of ncRNAs into exosomes protects them and facilitates their intercellular transfer, making them attractive tools for angiogenic therapy (Huang P. et al., 2019).

CrossTALK of ncRNAs in Cardiac Fibrosis

The very limited regenerative capacity of the mammalian adult heart due to low proliferative capacity and defective angiogenesis leads to the formation of a permanent scar after ischemic injury (Xin et al., 2013). Cardiac fibrosis is the main cellular event leading to scar formation and is characterized by an accumulation of ECM in the myocardium (Beltrami et al., 2003). In healthy conditions, ECM is responsible for transmission of the contractile force and serves as scaffolding for cardiac cells conferring mechanical support to the heart, and as such, cardiac contraction and relaxation firmly depends on ECM (Michel, 2003; Bildyug, 2019). Cardiac ECM is predominantly composed of collagens I and III (ColI and ColIII), glycosaminoglycans, glycoproteins, latent growth factors, and proteases (Kong et al., 2014), and is under constant turnover of sustained degradation and synthesis processes (Lajiness and Conway, 2014). Dysregulation of this tightly controlled process may impair both systolic and diastolic function as result of uncoordinated cardiomyocyte contraction, and/or cardiomyocyte displacement associated with ventricular dilation, and, ultimately cause ventricular stiffness and arrhythmias. The hallmarks of the cardiac fibrotic response include activation of fibrillary collagen and

myofibroblast differentiation from either fibroblasts, hematopoietic, or endothelial cells (Davis and Molkentin, 2014). Myofibroblasts display contractile stress fibers and a large endoplasmic reticulum – associated with secretion of large amounts of ECM proteins – and are very sensitive to growth factors and pro-inflammatory molecules (Davis and Molkentin, 2014). Despite being essential for myocardium repair, continuous presence of myofibroblasts in response to persistent inflammatory signals may result in excessive scarring and impairment of both systolic and diastolic function (Davis and Molkentin, 2014).

The molecular mechanisms underlying cardiac fibrosis are very dependent on the type of primary myocardial injury; however, there are fibrogenic signals consistently activated during fibrosis such as increased levels of TGF-β and AngII, among several others (Kong et al., 2014). TGF-β is a cytokine present as three different isoforms (TGF-β1, 2, and 3) and, while in the heart TGF-β1 is mainly present as a latent complex, once it is activated upon injury through the matrix metalloproteases 9 and 2 (MMP-9, MMP-2), it will cause alterations in the ECM composition (Ignotz and Massague, 1986). While overexpression of TGF-β1 promotes collagen deposition and ventricular fibrosis, its loss of function attenuates myocardial fibrosis in a rat model of pressure-overload (Koitabashi et al., 2011).

Several studies have indicated cardiac fibrosis to be under control of ncRNAs. In fact, TGF-β1 activity is regulated by miR-21, which by targeting Jagged1, a ligand for Notch receptor 1, affects trans-differentiation of cardiac fibroblasts into myofibroblasts and subsequently, myocardial fibrosis (Zhou et al., 2018).

Global lncRNA expression profiling in cardiac fibroblasts revealed lncRNA Meg3 to be specifically enriched in cardiac fibroblasts (Piccoli et al., 2017). Upon pressure overload, Meg3 regulates MMP-2 expression by stabilizing p53 at its binding site on the MMP-2 promoter, resulting in cardiac fibrosis and diastolic dysfunction (Piccoli et al., 2017). Silencing of lncRNA Meg3 with gapmers, prevented MMP2 activation and had a protective effect in pressure-overloaded hearts, partially due to attenuation of fibrosis (Piccoli et al., 2017). Given the emerging importance of circRNAs in myocardial function, Zhou and Yu (2017) analyzed the circRNA expression pattern in myocardial tissue of diabetic mice. A circRNA microarray screening identified circRNA_010567 as one of the top upregulated circRNAs in cardiac fibroblasts and its inhibition in cardiac fibroblasts exposed to AngII suppressed fibrosis-associated genes such as Col I, Col III, and alpha smooth muscle actin (α-SMA) (Zhou and Yu, 2017). circRNA_010567 was shown to have multiple binding sites for miR-141, that in turn targets TGF-β1. In fact, silencing of circRNA_010567, increased miR-141 expression, decreased TGF-β1 expression and its downstream targets, attenuating myocardial fibrosis (Zhou and Yu, 2017).

Apart from fibroblast-derived ncRNAs, there are other ncRNAs that originate from different cell types and are implicated in cardiac fibrosis through paracrine signaling. A recent study demonstrated that mechanical stress due to pressure-overload promotes transfer of cardiomyocyte-derived miR-378 to cardiac fibroblasts in an EV-dependent manner (Yuan et al., 2018). Loss- and gain-of function of miR-378 in cardiomyocytes, via targeting of the TGF-β1 pathway, accentuated collagen deposition but inhibited cardiac fibroblast proliferation. Similar effects were observed when EV secretion was impaired by administration of a sphingomyelin phosphodiesterase inhibitor, GW4869 (Yuan et al., 2018), suggesting that the mechanism used

by cardiomyocytes to release miR-378 and to exert its function in cardiac fibroblasts, is dependent on intercellular communication via exosomes.

As mentioned, myofibroblast activation is a key contributor to cardiac fibrosis and cardiac pathological remodeling, and the transition between fibroblasts and myofibroblast can be regulated by exosomal miRNAs, namely, cardiomyocyte-derived miR-195 (Morelli et al., 2019). Upon cardiac ischemic injury, cardiomyocytes release exosomes that are enriched in miR-195. *In vitro* exposure of cardiac fibroblasts to conditioned medium derived from myocardial infarction (MI)-hypoxic cardiomyocytes, led to an increase in the levels of miR-195, as well as in myofibroblast and fibrotic markers such as periostatin, alpha smooth muscle actin (α-SMA), and ColI and III on cardiac fibroblasts. Mechanistically, miR-195 targets the α-SMA inhibitor mothers against decapentaplegic homolog 7 (SMAD7), promoting the transcription of α-SMA and other myofibroblast associated genes (Morelli et al., 2019). Inhibition of EV release or inhibition of miR-195, via administration of the GW4869 or miR-195 inhibitor, respectively, abrogated myofibroblast activation. These observations established miR-195 as an important player during MI-induced pathological remodeling through myocyte-fibroblast communication (Morelli et al., 2019).

Macrophages, in turn, are able to affect cardiac fibrosis by transferring miR-155 into cardiac fibroblasts (Wang C. et al., 2017). An increment in exosome secretion by macrophages is accompanied by an increase in miR-155 expression in cardiac fibroblasts while deletion of miR-155 on macrophages leads to a reduction of miR-155 levels in cardiac fibroblasts. However, abrogation of miR-155 expression in cardiac fibroblasts did not interfere with their endogenous levels of miR-155, suggesting that the origin of miR-155 in cardiac fibroblasts derives from an external source, namely, macrophages. In cardiac fibroblasts, increased miR-155 expression prevents cell proliferation and increases inflammation by targeting fibrotic and inflammatory genes, simultaneously. Genetic deletion of miR-155 *in vivo* attenuated inflammation but accelerated cardiac fibroblast proliferation after MI, inhibiting myocardial rupture and improving cardiac function (Wang C. et al., 2017).

While the concept of exosomal miRNAs in myocardial fibrosis is well established, implication of exosomal lncRNAs and/or exosomal circRNAs transfer during cardiac fibrosis were still not reported, highlighting the need for better understanding of the molecular mechanisms driving cardiac fibrosis as a dichotomous event, in order to pursue more efficient therapeutic targets.

CrossTALK of ncRNAs in Cardiac Inflammation

Inflammation is a common ground for maladaptive cardiac remodeling, independent of the disease etiology. Inflammation occurs in all stages of tissue repair including initiation, maintenance, resolution, and clearing out the damaged tissue. A vast variety of cells, including monocytes, macrophages, dendritic cells, T-cells, B-cells, NK cells, and others, compose the immune system and regulate the inflammatory response. Both MI and hypertension activate an inflammatory cardiac response; however, the mechanisms induced by these two types of injury are very distinct.

In MI, inflammation is initiated following the typical hallmarks of ischemic injury, cardiomyocyte death, and interstitial fibrosis, both involved in the generation of reactive

oxidative species and activation of the complement pathway (Prabhu and Frangogiannis, 2016). Subsequently, endothelial dysfunction leads to increased vessel permeability followed by leukocyte infiltration. Finally, remodeling of the ECM, along with damaged cardiac cells' release of interleukins (IL) like IL one alpha (IL-1α) and heat shock proteins (HSP) that act as damage-associated molecular patterns (DAMPs), takes place (Prabhu and Frangogiannis, 2016). When secreted to the extracellular environment these danger signals bind to pattern recognition receptors activating leukocytes (Prabhu and Frangogiannis, 2016). Hearts subjected to pressure overload either by hypertension or aortic stenosis, show a profound vascular remodeling accompanied by perivascular fibrosis and inflammation but no significant cardiomyocyte loss (Xia et al., 2009). Cardiac hypertrophy is followed by transient activation of the inflammatory response, starting with the release of pro-inflammatory cytokines such as IL-1β, IL-6, and TNF-α and rapidly progressing to macrophage infiltration and upregulation of TGF-β. Long term inflammation is replaced by fibrosis and the initial cardiac response develops into both diastolic and systolic dysfunction (Xia et al., 2009).

Macrophages display different inflammatory states. Usually, M1 macrophages are associated with a pro-inflammatory phenotype by releasing IL-1β, IL-6, and TNF-α, while M2 phenotype transition is linked to immunomodulation and secretion of anti-inflammatory cytokines such as IL-10. Notably, M1 to M2 macrophage transition might be influenced by bone marrow-derived mesenchymal stem cells (BMSCs)-derived exosomes (Xu et al., 2019) as myocardial injection of such exosomes in the border zone of ischemic hearts, significantly decreased M1/M2 ratio and attenuated cardiac inflammation. These protective effects were enhanced by exosomes derived from BMSCs after preconditioning with lipopolysaccharide (LPS) stimulation (Xu et al., 2019). Similar to BMSCs, LPS preconditioning of mesenchymal stromal cells can also guide M1 to M2 macrophage activation along with the upregulation of anti-inflammatory cytokines through exosomal release (Ti et al., 2015). Interestingly, exosomes derived from LPS-activated MSCs are enriched with let-7b which regulates macrophage plasticity via toll-like receptor 4 (TLR4), and *in vivo*, increases diabetic cutaneous wound healing and attenuates inflammation (Ti et al., 2015). Another report on mesenchymal stromal cells-derived exosomes highlighted the cardioprotective and immunomodulatory effect of exosomal miRNAs on M1/M2 macrophage shuttle (Zhao et al., 2019). Under inflammatory conditions, such as myocardial ischemia/reperfusion, miR-182 is loaded in MSCs-derived exosomes and further incorporated into macrophages (Zhao et al., 2019). Similar to let-7b, miR-182 also targets the TLR4 pathway and activates the PI3K/AKT signaling pathway, an important step in the conversion of M1 into anti-inflammatory M2 phenotype (Zhao et al., 2019).

Reduction of the inflammatory process and improved immunomodulatory response were shown upon addition of endothelial cell-derived EV to monocytes (Njock et al., 2015). Endothelial cells exert their anti-inflammatory effect by secreting EVs loaded with miR-126, miR-181b, and miR-10. Once taken up by monocytes, miR-10 induced the strongest anti-inflammatory effect by repressing the nuclear factor κB (NF-κB) pathway and increasing the levels of immunomodulatory genes (Njock et al., 2015). This supports an essential role of the crosstalk between different cell types such as endothelial cells and monocytes, during cardiac inflammation cardiac, mediated by miRNAs enclosed in secreted EVs.

Inter-Organ Crosstalk

The primary function of the heart is to pump blood to the rest of the body, yet, recent studies demonstrate that the heart could have other functions and acts as an endocrine organ (de Bold et al., 1981; Nakamura et al., 1991). Through endocrine signaling, the heart is able to maintain whole body homeostasis and, in this way, peripheral organs are able to respond to stress stimuli that originate in the heart (**Figure 3**).

Most likely, the best described cardiac endocrine factor is the atrial natriuretic peptide (ANP), the expression of which is increased after myocardial stretching (Hardy-Rando and Fernandez-Patron, 2019). A previous study reported that upon corticosterone stimulation, astrocytes release "ANPergic vesicles" (vesicles enriched in ANP) (Chatterjee and Sikdar, 2013). In the brain, ANP acts as an inhibitory signal that regulates astrocyte mobility, neuron signaling and blood flow to the brain due to its vasoregulatory action (Chatterjee and Sikdar, 2013). Although no evidence of ANP vesicles has been reported in the heart, it is possible that ANP-containing vesicles constitutes a mechanism of ANP transport and action within the cardiovascular system, as well as modulators of heart-kidney communication and particularly, blood pressure-control.

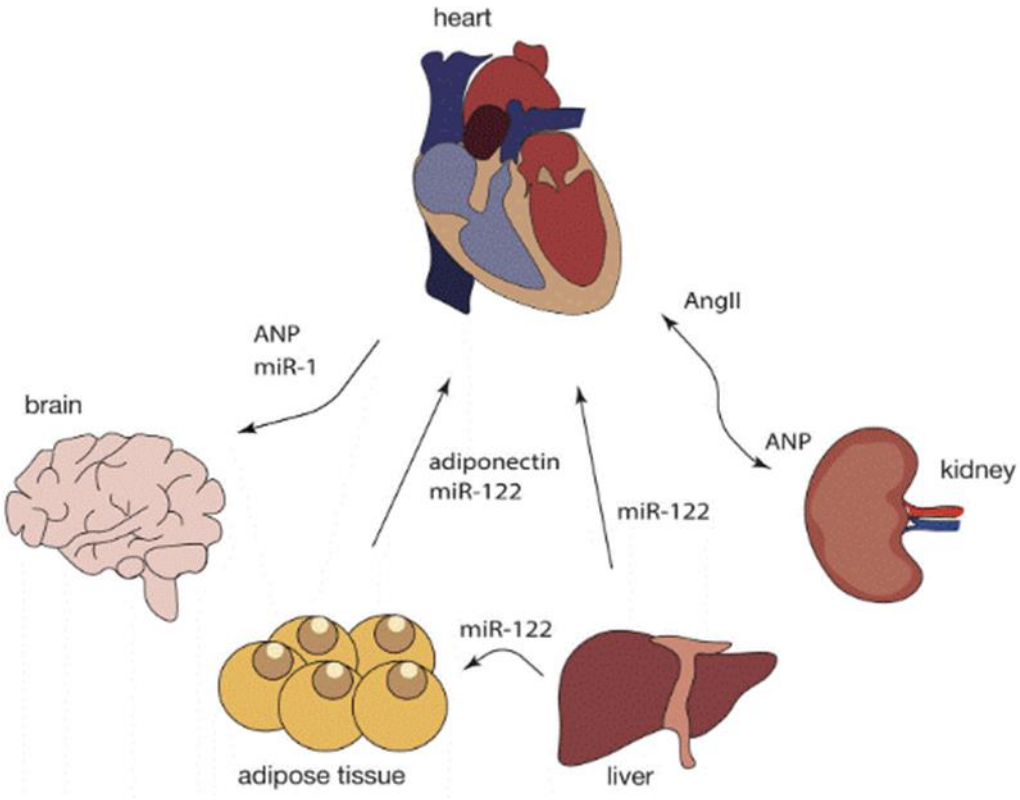

***Figure 3**. Crosstalk between the heart and peripheral organs during cardiac pathological remodeling. Response to cardiac injury is a multi-organ process as itaffects not only the heart but also the brain, kidneys, adipose tissue, and the liver, among others. In turn, a variety of other tissues can contribute to cardiacpathological remodeling, not only by secreting specific chemokines but also by releasing exosomal ncRNAs into the blood stream and further affecting cardiacfunction through intricate signaling networks. Dashed lines represent findings that need further validation.*

Atrial natriuretic peptide can influence and suppress the sympathetic activity in the heart through a decrease in the activity of chemo and baroreceptors, which leads to lower heart rate and cardiac output (McGrath et al., 2005). Since adipose tissue presents ANP receptors, the release of ANP by the heart, can trigger lipolysis, energy expenditure and shifting of adipokine production and release (Gruden et al., 2014). In mice subjected to MI, miR-214, typically enriched in adipose-derived regenerative cells (ADRCs), is transferred into cardiomyocytes, where it suppresses apoptotic gene expression such as Bcl-2-like protein 11 (Bcl2l11) and solute carrier family 8 member A1 (Slc8a1), preventing cardiac rupture (Eguchi et al., 2019). Cardiomyocytes can also uptake miR-214 derived from ADRCs, suggesting that EVs containing miR-214 are endocytosed through a clathrin-mediated endocytosis process triggered by MI-induced hypoxia (Eguchi et al., 2019).

However, the opposite can also occur. For example, in obesity, metabolic stress induces changes in adipose tissue, and increased secretion of adipokines is perceived by the heart and impacts on its function. One of these adipokines, adiponectin, is decrease in several cardiovascular diseases, including MI (Shojaie et al., 2009), and hypertension (Wang et al., 2012; Brambilla et al., 2013). In cardiomyocytes, adiponectin is able to activate the adenosine monophosphate-activated protein kinase signaling pathway inhibiting pressure-overload induced hypertrophy (Turdi et al., 2011).

An increase in heart rate and contractility is regulated by the sympathetic system, namely, postganglionic efferent neurons that communicate with cardiomyocytes by releasing noradrenaline and cause the activation of β-adrenergic receptors (Bang et al., 2015). In contrast, heart rate decrease is under the control of the parasympathetic system via acetylcholine, which binds to muscarinic receptors, and dysregulation of these hormones could lead to arrhythmias (Bang et al., 2015).

Besides the adipose tissue and the brain, the heart also communicates with the kidneys through the renin-angiotensin system (RAS), mainly associated with regulation of blood pressure (Jahng et al., 2016). In a healthy heart, low blood pressure stimulates the kidneys to produce renin, which, in turn, leads to increased AngII, followed by sodium and water retention. Finally, an increase in blood volume and increased pressure stimulate cardiomyocytes to release ANP into the circulation, through which it will reach the kidneys (Song et al., 2015). Here, ANP activates excretion of salts and water reducing both blood volume and pressure. In hypertension, this system is overly activated and the heart is not able to decrease the blood pressure, causing continuous secretion of ANP and subsequently maladaptive cardiac remodeling (Orsborne et al., 2017).

Interestingly, not only proteins participate in cardiac inter-organ communication. In obese mice, cardiac injury can be induced by liver-derived exosomal miR-122 (Wang et al., 2019a). MiR-122 is liver-specific and, upon accumulation of visceral fat, miR-122 is released in liver-derived exosomes and transported to the heart, where it interferes with mitochondrial adenosine triphosphate (ATP) production, and eventually, left ventricle (LV) function (Wang et al., 2019a). Deletion of hepatic miR-122 significantly improved LV function parameters in obese mice (Wang et al., 2019a). This miRNA, by also being enriched in plasmatic exosomes from obese humans, is a promising target against obese-induced cardiac injury.

As discussed before, the heart can also send signals to other organs, including the brain. Upon MI, cardiomyocytes increase the release of exosomes enriched in miR-1 (Sun et al., 2018). These exosomes are carried through the blood flow and incorporated by the hippocampus to induce neuronal microtubule damage (Sun et al., 2018). Genetic ablation of cardiomyocyte-derived miR-1 significantly attenuated neuronal damage in mice subjected to MI, suggesting that miR-1 acts as an endocrine factor (Sun et al., 2018).

To date no other classes of ncRNAs have been reported to have an endocrine effect to or from the heart.

Therapeutic Potential of Cardiac Exosomal ncRNAs

Exosomal ncRNAs constitute a new form of paracrine signaling that seems to be more protected, directed, and therefore, most likely also more efficient. Naturally, exosomes are endogenously produced by cells, but systemic isolation of exosomes that are secreted by one specific cell type is still difficult. Therefore, all the studies reported in this review are based on exosomes that were produced *in vitro* and then administrated *in vivo*. Consequently, these cell culture-derived exosomes are of exogenous origin, relative to the recipient mouse, which, in turn are also able to naturally produce endogenous exosomes. These exogenous exosomes may have an enormous therapeutic potential. In fact, exosomes revolutionized the delivery strategies of therapeutics as the use of these vectors in cell-free medicine will, most likely, overcome the barriers associated with cell transplantation such as contamination and cell death (Toma et al., 2002) and decrease the risk of tumorigenicity and immune rejection (Chen Y. et al., 2017). The smaller size of exosomes allows immediate and easy circulation through capillaries, opposed to what was observed for cell-based therapies such as mesenchymal stem cell (MSC) transplantation, where many cells do not manage to pass the first capillary bed (Phinney and Pittenger, 2017). Exosomes can potentially carry the same miRNA profile of the donor cell, which may potentiate the beneficial effects observed in traditional cell transplantation (Shao et al., 2017). Likewise, in a mouse model of MI it was shown that the protective effect of MSC transplantation was promoted by exosomal miR-125, which, by targeting p53 reduced the apoptotic flux and, consequently, cell death, while its deletion abrogated these effects (Xiao et al., 2018). Transplantation of MSC-derived exosomes alone, revealed to be sufficient to recapitulate MSC-associated beneficial effects. Furthermore, exosomal ncRNA content can be, partially, modulated by transfecting donor cells with a specific ncRNA mimic or inhibitor (Xiao et al., 2018) that will be, in turn, naturally released in exosomes, improving therapy efficacy, as demonstrated by Zhu et al. (2019). The presence of lncRNA MALAT-1 in exosomes derived from umbilical cord MSCs is able to alter NF-κB signaling and exert cardioprotection in an *in vitro* model of aging (Zhu et al., 2019). The facility in obtaining MSCs, isolating their released exosomes and modeling their miRNA content, are particularly attractive features for their therapeutic use.

In fact, MSCs, have been extensively studied as therapeutic targets for MI, due to their reparative capacity (Przybyt and Harmsen, 2013; Chen L. et al., 2017; Luger et al., 2017). Since transplantation of MSCs has high risks, a therapy based on EVs could be advantageous. Analysis of the MSC-derived exosome contents revealed enrichment of miR-24 and miR-29 and depletion of miR-130, miR-378, and miR-34 (Shao et al., 2017). While the enriched miRNAs positively associate with the regulation of cardiac function, the depleted miRNAs were negative regulators.

Interestingly, addition of MSCs-derived exosomes to cardiomyocyte cultures was sufficient to stimulate cardiomyocyte proliferation (Shao et al., 2017). Another study reported that hypoxic preconditioning enhances the protective effect of MSCs, manifested by decreased scar size and improved cardiac function after MI, through exosome-mediated signaling (Zhu et al., 2018). Exosomes secreted by MSCs can be incorporated into cardiac endothelial cells, increase their angiogenic capacity and, ultimately, improve cardiac function (Zhu et al., 2018). MSC-derived exosomes are also enriched in miR-210, known as the "master hypoxamir," (Chan et al., 2012) which overexpression promotes to tube formation but its depletion fails to promote angiogenesis on endothelial cells (Zhu et al., 2018). Furthermore, Wang K. et al. (2017) unraveled that the mechanism whereby endometrium-derived MSCs (EndMSC) can exert their cardiac protective effect is by exosomal release of miRNAs, namely, miR-21. EndMSC secrete miR-21 that is shuttled to both cardiomyocytes and endothelial cells, preventing apoptosis and promoting angiogenesis after MI, respectively (Wang K. et al., 2017).

In turn, lncRNA H19 was shown to have a paracrine effect upon atorvastatin (AT)-conditioned (MSC) treatment, as AT treatment induced MSCs to produce exosomes that were enriched in lncRNA H19 and miR-675, that once internalized by endothelial cells enhanced their migratory, proliferative and sprouting capacity and therefore, angiogenesis (Huang P. et al., 2019). In fact, in a mouse model of MI, administration of H19-enriched, MSC-derived exosomes, significantly reduced infarct size and increased left ventricle ejection fraction (Huang P. et al., 2019).

Due to their high proliferative capacity, endothelial colony forming-cells (ECFCs), progenitor of endothelial cells, are able to reduce fibrosis after MI, making them an attractive target for cell-based therapies, even though their beneficial effect is hampered under hypoxic conditions (Liu et al., 2018). ECFCs have shown to enhance vascularization by stabilizing the perivascular area and secretion of angiogenic molecules (e.g., VEGF-A), to attenuate fibrosis, and to increase cardiomyocyte survival possibly due to increased expression of IGF-1, an anti-apoptotic factor (Liu et al., 2018). ECFC-derived exosomes are thought to be the mediators of the observed protective effects. Adding exosomes derived from ECFCs exposed to normoxia to cardiac fibroblast cultures, significantly reduced fibroblast activation, TGF-β stimulation, and the fibroblast expression levels of Col-Iα and α-SMA (Liu et al., 2018). Exposing cardiac fibroblasts to hypoxic ECFCs-derived exosomes increased fibrosis and showed a similar effect to treatment of TGF-β alone. miRNA content analysis revealed miR-10b-5p as the most enriched miRNA in normoxia ECFCs-derived exosomes when compared to hypoxia ECFCs-derived exosomes, which, curiously, targets the downstream factors of the TGF-β pathway, SMAD ubiquitylation regulatory factor 1 (SMURF1) and histone deacetylase 4 (HDAC4) (Liu et al., 2018).

A study reported that intravenously and intraperitoneal injections of exogenous exosomes does not induce toxicity (no body weight or behavioral changes) nor an alteration of hematological and biochemical parameters (Zhu et al., 2017). As EVs were only detectable at low levels in the spleen and not detectable at all in the liver or spleen, this indeed suggests that there is no toxicity or severe immune response (Zhu et al., 2017). Nevertheless, not only is more research needed to draw a conclusion on exosome cardiotoxicity, a better understanding of miRNA off-targets effects is also necessary before exomiRs reach clinical practice.

Conclusion

Intercellular communication in the heart contributes to both the maintenance of cardiac function and the development of cardiac pathologies, characterized by cardiac hypertrophy, fibrosis, inflammation, and deficient vasculature. Communication between cardiomyocytes, fibroblasts, inflammatory cells, and endothelial cells in the heart is not unidirectional but bi/multidirectional, as each cell type profoundly influences each other's behavior. Most of the mechanisms driving this cell-to-cell crosstalk are relatively unknown, thus, analyzing the changes in cell signaling upon a pathological stimulus may yield new information to prevent or reverse pathological remodeling. Although intercellular communication can occur in a variety of forms, here we focused on the paracrine signaling through EVs, namely, exosomes. Many reports have been focused on how the modulation of ncRNAs can successfully prevent and even reverse cardiac maladaptive remodeling. Despite the promising value of several miRNAs, lncRNAs, and circRNAs, as new therapeutic targets, to date, miR-122 is the only ncRNA that has reached a phase II clinical trial.

Interestingly, ncRNAs can be loaded into EVs and further incorporated into others cell types, where they are still capable of efficiently exert their action and consequently, trigger a response. However, since the majority of the current studies were based on the isolation of vesicles from cellular cultures, there is a considerable gap in the *in vivo* EV characterization, as well as in understanding their spatial and temporal secretion in the heart. Furthermore, exosomal ncRNAs have an unpredictable toxicity when administrated *in vivo* due to the short-observation span of the majority of the studies. Finally, we believe that understanding and mimicking the action of EVs, by modifying EV ncRNA content, will constitute a future therapeutic target.

References

Arroyo, J. D., Chevillet, J. R., Kroh, E. M., Ruf, I. K., Pritchard, C. C., Gibson, D. F., et al. (2011). Argonaute2 complexes carry a population of circulating microRNAs independent of vesicles in human plasma. Proc. Natl. Acad. Sci. U.S.A. 108, 5003–5008. doi: 10.1073/pnas.1019055108

Bang, C., Antoniades, C., Antonopoulos, A. S., Eriksson, U., Franssen, C., Hamdani, N., et al. (2015). Intercellular communication lessons in heart failure. Eur. J. Heart Fail. 17, 1091–1103. doi: 10.1002/ejhf.399

Beltrami, A. P., Barlucchi, L., Torella, D., Baker, M., Limana, F., Chimenti, S., et al. (2003). Adult cardiac stem cells are multipotent and support myocardial regeneration. Cell 114, 763–776. doi: 10.1016/s0092-8674(03)00687-1

Bildyug, N. (2019). Extracellular matrix in regulation of contractile system in cardiomyocytes. Int. J. Mol. Sci. 20:5054. doi: 10.3390/ijms20205054

Brambilla, P., Antolini, L., Street, M. E., Giussani, M., Galbiati, S., Valsecchi, M. G., et al. (2013). Adiponectin and hypertension in normal-weight and obese children. Am. J. Hypertens 26, 257–264. doi: 10.1093/ajh/hps033

Cartledge, J. E., Kane, C., Dias, P., Tesfom, M., Clarke, L., McKee, B., et al. (2015). Functional crosstalk between cardiac fibroblasts and adult cardiomyocytes by soluble mediators. Cardiovasc. Res. 105, 260–270. doi: 10.1093/cvr/cvu264

Chan, Y. C., Banerjee, J., Choi, S. Y., and Sen, C. K. (2012). miR-210: the master hypoxamir. Microcirculation 19, 215–223. doi: 10.1111/j.1549-8719.2011.00154.x

Chatterjee, S., and Sikdar, S. K. (2013). Corticosterone treatment results in enhanced release of peptidergic vesicles in astrocytes via cytoskeletal rearrangements. Glia 61, 2050–2062. doi: 10.1002/glia.22576

Chen, L., Zhang, Y., Tao, L., Yang, Z., and Wang, L. (2017). Mesenchymal stem cells with eNOS over-expression enhance cardiac repair in rats with myocardial infarction. Cardiovasc. Drugs Ther. 31, 9–18. doi: 10.1007/s10557-016-6704-z

Chen, M., Xu, R., Rai, A., Suwakulsiri, W., Izumikawa, K., Ishikawa, H., et al. (2019). Distinct shed microvesicle and exosome microRNA signatures reveal diagnostic markers for colorectal cancer. PLoS One 14:e0210003. doi: 10.1371/journal.pone.0210003

Chen, S., Shiesh, S. C., Lee, G. B., and Chen, C. (2020). Two-step magnetic bead-based (2MBB) techniques for immunocapture of extracellular vesicles and quantification of microRNAs for cardiovascular diseases: a pilot study. PLoS One 15:e0229610. doi: 10.1371/journal.pone.0229610

Chen, Y., Zhao, Y., Chen, W., Xie, L., Zhao, Z. A., Yang, J., et al. (2017). MicroRNA-133 overexpression promotes the therapeutic efficacy of mesenchymal stem cells on acute myocardial infarction. Stem Cell Res. Ther. 8:268.

Cochain, C., Channon, K. M., and Silvestre, J. S. (2013). Angiogenesis in the infarcted myocardium. Antioxid Redox Signal. 18, 1100–1113. doi: 10.1089/ars.2012.4849

Davis, J., and Molkentin, J. D. (2014). Myofibroblasts: trust your heart and let fate decide. J. Mol. Cell Cardiol. 70, 9–18. doi: 10.1016/j.yjmcc.2013.10.019

de Bold, A. J., Borenstein, H. B., Veress, A. T., and Sonnenberg, H. (1981). A rapid and potent natriuretic response to intravenous injection of atrial myocardial extract in rats. Life Sci. 28, 89–94. doi: 10.1016/0024-3205(81)90370-2

Dhanoa, J. K., Sethi, R. S., Verma, R., Arora, J. S., and Mukhopadhyay, C. S. (2018). Long non-coding RNA: its evolutionary relics and biological implications in mammals: a review. J. Anim. Sci. Technol. 60:25. doi: 10.1016/b978-1-78548-265-6.50002-2

Eguchi, S., Takefuji, M., Sakaguchi, T., Ishihama, S., Mori, Y., Tsuda, T., et al. (2019). Cardiomyocytes capture stem cell-derived, anti-apoptotic microRNA-214 via clathrin-mediated endocytosis in acute myocardial infarction. J. Biol. Chem. 294, 11665–11674. doi: 10.1074/jbc.ra119.007537

Fish, J. E., Santoro, M. M., Morton, S. U., Yu, S., Yeh, R. F., Wythe, J. D., et al. (2008). miR-126 regulates angiogenic signaling and vascular integrity. Dev. Cell 15, 272–284. doi: 10.1016/j.devcel.2008.07.008

Frey, N., and Olson, E. N. (2003). Cardiac hypertrophy: the good, the bad, and the ugly. Annu. Rev. Physiol. 65, 45–79. doi: 10.1146/annurev.physiol.65.092101.142243

Ge, X., Meng, Q., Zhuang, R., Yuan, D., Liu, J., Lin, F., et al. (2019). Circular RNA expression alterations in extracellular vesicles isolated from murine heart post ischemia/reperfusion injury. Int. J. Cardiol. 296, 136–140. doi: 10.1016/j.ijcard.2019.08.024

Gogiraju, R., Bochenek, M. L., and Schafer, K. (2019). Angiogenic endothelial cell signaling in cardiac hypertrophy and heart failure. Front. Cardiovasc. Med. 6:20. doi: 10.3389/fcvm.2019.00020

Gong, C., and Maquat, L. E. (2011). lncRNAs transactivate STAU1-mediated mRNA decay by duplexing with 3' UTRs via Alu elements. Nature 470, 284–288. doi: 10.1038/nature09701

Greene, J., Baird, A. M., Brady, L., Lim, M., Gray, S. G., McDermott, R., et al. (2017). Circular RNAs: biogenesis, function and role in human diseases. Front. Mol. Biosci. 4:38. doi: 10.3389/fmolb.2017.00038

Gruden, G., Landi, A., and Bruno, G. (2014). Natriuretic peptides, heart, and adipose tissue: new findings and future developments for diabetes research. Diabetes Care 37, 2899–2908. doi: 10.2337/dc14-0669

Gupta, R. A., Shah, N., Wang, K. C., Kim, J., Horlings, H. M., Wong, D. J., et al. (2010). Long non-coding RNA HOTAIR reprograms chromatin state to promote cancer metastasis. Nature 464, 1071–1076. doi: 10.1038/nature08975

Halkein, J., Tabruyn, S. P., Ricke-Hoch, M., Haghikia, A., Nguyen, N. Q., Scherr, M., et al. (2013). MicroRNA-146a is a therapeutic target and biomarker for peripartum cardiomyopathy. J. Clin. Invest. 123, 2143–2154. doi: 10.1172/jci64365

Hardy-Rando, E., and Fernandez-Patron, C. (2019). Emerging pathways of communication between the heart and non-cardiac organs. J. Biomed. Res. 33, 145–155.

Hervera, A., Santos, C. X., De Virgiliis, F., Shah, A. M., and Di Giovanni, S. (2019). Paracrine mechanisms of redox signalling for postmitotic cell and tissue regeneration. Trends Cell Biol. 29, 514–530. doi: 10.1016/j.tcb.2019.01.006

Hinger, S. A., Cha, D. J., Franklin, J. L., Higginbotham, J. N., Dou, Y., Ping, J., et al. (2018). Diverse long RNAs are differentially sorted into extracellular vesicles secreted by colorectal cancer Cells. Cell Rep. 25, 715.e4–725.e4.

Huang, P., Wang, L., Li, Q., Tian, X., Xu, J., Xu, J., et al. (2019). Atorvastatin enhances the therapeutic efficacy of mesenchymal stem cells derived exosomes in acute myocardial infarction via up-regulating long non-coding RNA H19. Cardiovasc. Res. 116, 353–367.

Huang, S., Li, X., Zheng, H., Si, X., Li, B., Wei, G., et al. (2019). Loss of super-enhancer-regulated circRNA Nfix induces cardiac regeneration after myocardial infarction in adult mice. Circulation 139, 2857–2876. doi: 10.1161/circulationaha.118.038361

Ignotz, R. A., and Massague, J. (1986). Transforming growth factor-beta stimulates the expression of fibronectin and collagen and their incorporation into the extracellular matrix. J. Biol. Chem. 261, 4337–4345.

Jaba, I. M., Zhuang, Z. W., Li, N., Jiang, Y., Martin, K. A., Sinusas, A. J., et al. (2013). NO triggers RGS4 degradation to coordinate angiogenesis and cardiomyocyte growth. J. Clin. Invest. 123, 1718–1731. doi: 10.1172/jci65112

Jahng, J. W., Song, E., and Sweeney, G. (2016). Crosstalk between the heart and peripheral organs in heart failure. Exp. Mol. Med. 48:e217. doi: 10.1038/emm.2016.20

Kamo, T., Akazawa, H., and Komuro, I. (2015). Cardiac nonmyocytes in the hub of cardiac hypertrophy. Circ. Res. 117, 89–98. doi: 10.1161/circresaha.117.305349

Koitabashi, N., Danner, T., Zaiman, A. L., Pinto, Y. M., Rowell, J., Mankowski, J., et al. (2011). Pivotal role of cardiomyocyte TGF-beta signaling in the murine pathological response to sustained pressure overload. J. Clin. Invest. 121, 2301–2312. doi: 10.1172/jci44824

Kong, P., Christia, P., and Frangogiannis, N. G. (2014). The pathogenesis of cardiac fibrosis. Cell Mol. Life Sci. 71, 549–574.

Lajiness, J. D., and Conway, S. J. (2014). Origin, development, and differentiation of cardiac fibroblasts. J. Mol. Cell Cardiol. 70, 2–8. doi: 10.1016/j.yjmcc.2013.11.003

Lee, J. S., Song, D. W., Park, J. H., Kim, J. O., Cho, C., and Kim, D. H. (2017). miR-374 promotes myocardial hypertrophy by negatively regulating vascular endothelial growth factor receptor-1 signaling. BMB Rep. 50, 208–213. doi: 10.5483/bmbrep.2017.50.4.165

Lee, R. C., Feinbaum, R. L., and Ambros, V. (1993). The C. elegans heterochronic gene lin-4 encodes small RNAs with antisense complementarity to lin-14. Cell 75, 843–854. doi: 10.1016/0092-8674(93)90529-y

Leisegang, M. S., Fork, C., Josipovic, I., Richter, F. M., Preussner, J., Hu, J., et al. (2017). Long noncoding RNA MANTIS facilitates endothelial angiogenic function. Circulation 136, 65–79. doi: 10.1161/circulationaha.116.026991

Li, Z., and Rana, T. M. (2014). Therapeutic targeting of microRNAs: current status and future challenges. Nat. Rev. Drug Discov. 13, 622–638. doi: 10.1038/nrd4359

Liao, B., Chen, R., Lin, F., Mai, A., Chen, J., Li, H., et al. (2018). Long noncoding RNA HOTTIP promotes endothelial cell proliferation and migration via activation of the Wnt/beta-catenin pathway. J. Cell Biochem. 119, 2797–2805. doi: 10.1002/jcb.26448

Liu, W., Zhang, H., Mai, J., Chen, Z., Huang, T., Wang, S., et al. (2018). Distinct anti-fibrotic effects of exosomes derived from endothelial colony-forming cells cultured under normoxia and hypoxia. Med. Sci. Monit. 24, 6187–6199. doi: 10.12659/msm.911306

Luger, D., Lipinski, M. J., Westman, P. C., Glover, D. K., Dimastromatteo, J., Frias, J. C., et al. (2017). Intravenously delivered mesenchymal stem cells: systemic anti-inflammatory effects improve left ventricular dysfunction in acute myocardial infarction and ischemic cardiomyopathy. Circ. Res. 120, 1598–1613. doi: 10.1161/circresaha.117.310599

Lyon, R. C., Zanella, F., Omens, J. H., and Sheikh, F. (2015). Mechanotransduction in cardiac hypertrophy and failure. Circ. Res. 116, 1462–1476. doi: 10.1161/circresaha.116.304937

Mathew, J., Sleight, P., Lonn, E., Johnstone, D., Pogue, J., Yi, Q., et al. (2001). Reduction of cardiovascular risk by regression of electrocardiographic markers of left ventricular

hypertrophy by the angiotensin-converting enzyme inhibitor ramipril. Circulation 104, 1615–1621. doi: 10.1161/hc3901.096700

Matsumoto, A., Pasut, A., Matsumoto, M., Yamashita, R., Fung, J., Monteleone, E., et al. (2017). mTORC1 and muscle regeneration are regulated by the LINC00961-encoded SPAR polypeptide. Nature 541, 228–232. doi: 10.1038/nature21034

McGrath, M. F., de Bold, M. L., and de Bold, A. J. (2005). The endocrine function of the heart. Trends Endocrinol. Metab. 16, 469–477.

Michel, J. B. (2003). Anoikis in the cardiovascular system: known and unknown extracellular mediators. Arterioscler Thromb. Vasc. Biol. 23, 2146–2154. doi: 10.1161/01.atv.0000099882.52647.e4

Morelli, M. B., Shu, J., Sardu, C., Matarese, A., and Santulli, G. (2019). Cardiosomal microRNAs are essential in post-infarction myofibroblast phenoconversion. Int. J. Mol. Sci. 21:201. doi: 10.3390/ijms21010201

Nakamura, S., Naruse, M., Naruse, K., Kawana, M., Nishikawa, T., Hosoda, S., et al. (1991). Atrial natriuretic peptide and brain natriuretic peptide coexist in the secretory granules of human cardiac myocytes. Am. J. Hypertens 4, 909–912. doi: 10.1093/ajh/4.11.909

Njock, M. S., Cheng, H. S., Dang, L. T., Nazari-Jahantigh, M., Lau, A. C., Boudreau, E., et al. (2015). Endothelial cells suppress monocyte activation through secretion of extracellular vesicles containing antiinflammatory microRNAs. Blood 125, 3202–3212. doi: 10.1182/blood-2014-11-611046

Orsborne, C., Chaggar, P. S., Shaw, S. M., and Williams, S. G. (2017). The renin-angiotensin-aldosterone system in heart failure for the non-specialist: the past, the present and the future. Postgrad. Med. J. 93, 29–37. doi: 10.1136/postgradmedj-2016-134045

Osada-Oka, M., Shiota, M., Izumi, Y., Nishiyama, M., Tanaka, M., Yamaguchi, T., et al. (2017). Macrophage-derived exosomes induce inflammatory factors in endothelial cells under hypertensive conditions. Hypertens Res. 40, 353–360. doi: 10.1038/hr.2016.163

Phinney, D. G., and Pittenger, M. F. (2017). Concise review: MSC-Derived exosomes for cell-free therapy. Stem Cells 35, 851–858. doi: 10.1002/stem.2575

Piccoli, M. T., Gupta, S. K., Viereck, J., Foinquinos, A., Samolovac, S., Kramer, F. L., et al. (2017). Inhibition of the cardiac fibroblast-enriched lncRNA Meg3 prevents cardiac fibrosis and diastolic dysfunction. Circ. Res. 121, 575–583. doi: 10.1161/circresaha.117.310624

Prabhu, S. D., and Frangogiannis, N. G. (2016). The biological basis for cardiac repair after myocardial infarction: from inflammation to fibrosis. Circ. Res. 119, 91–112. doi: 10.1161/circresaha.116.303577

Przybyt, E., and Harmsen, M. C. (2013). Mesenchymal stem cells: promising for myocardial regeneration? Curr. Stem Cell Res. Ther. 8, 270–277. doi: 10.2174/1574888x11308040002

Pu, W. T., Ma, Q., and Izumo, S. (2003). NFAT transcription factors are critical survival factors that inhibit cardiomyocyte apoptosis during phenylephrine stimulation in vitro. Circ. Res. 92, 725–731. doi: 10.1161/01.res.0000069211.82346.46

Raposo, G., and Stoorvogel, W. (2013). Extracellular vesicles: exosomes, microvesicles, and friends. J. Cell Biol. 200, 373–383. doi: 10.1083/jcb.201211138

Samak, M., Fatullayev, J., Sabashnikov, A., Zeriouh, M., Schmack, B., Farag, M., et al. (2016). Cardiac hypertrophy: an introduction to molecular and cellular basis. Med. Sci. Monit. Basic Res. 22, 75–79.

Santosh, B., Varshney, A., and Yadava, P. K. (2015). Non-coding RNAs: biological functions and applications. Cell Biochem. Funct. 33, 14–22. doi: 10.1002/cbf.3079

Shao, L., Zhang, Y., Lan, B., Wang, J., Zhang, Z., Zhang, L., et al. (2017). MiRNA-sequence indicates that mesenchymal stem cells and exosomes have similar mechanism to enhance cardiac repair. Biomed. Res. Int. 2017:4150705.

Shojaie, M., Sotoodah, A., and Shafaie, G. (2009). Is adiponectin associated with acute myocardial infarction in Iranian non obese patients? Lipids Health Dis. 8:17. doi: 10.1186/1476-511x-8-17

Song, W., Wang, H., and Wu, Q. (2015). Atrial natriuretic peptide in cardiovascular biology and disease (NPPA). Gene 569, 1–6. doi: 10.1016/j.gene.2015.06.029

Su, S. A., Xie, Y., Fu, Z., Wang, Y., Wang, J. A., and Xiang, M. (2017). Emerging role of exosome-mediated intercellular communication in vascular remodeling. Oncotarget 8, 25700–25712. doi: 10.18632/oncotarget.14878

Sun, L. L., Duan, M. J., Ma, J. C., Xu, L., Mao, M., Biddyut, D., et al. (2018). Myocardial infarction-induced hippocampal microtubule damage by cardiac originating microRNA-1 in mice. J. Mol. Cell Cardiol. 120, 12–27. doi: 10.1016/j.yjmcc.2018.05.009

Tabet, F., Vickers, K. C., Cuesta Torres, L. F., Wiese, C. B., Shoucri, B. M., Lambert, G., et al. (2014). HDL-transferred microRNA-223 regulates ICAM-1 expression in endothelial cells. Nat. Commun. 5:3292.

Ti, D., Hao, H., Tong, C., Liu, J., Dong, L., Zheng, J., et al. (2015). LPS-preconditioned mesenchymal stromal cells modify macrophage polarization for resolution of chronic inflammation via exosome-shuttled let-7b. J. Transl. Med. 13:308.

Tian, C., Gao, L., Zimmerman, M. C., and Zucker, I. H. (2018). Myocardial infarction-induced microRNA-enriched exosomes contribute to cardiac Nrf2 dysregulation in chronic heart failure. Am. J. Physiol. Heart Circ. Physiol. 314, H928–H939.

Toma, C., Pittenger, M. F., Cahill, K. S., Byrne, B. J., and Kessler, P. D. (2002). Human mesenchymal stem cells differentiate to a cardiomyocyte phenotype in the adult murine heart. Circulation 105, 93–98. doi: 10.1161/hc0102.101442

Turdi, S., Kandadi, M. R., Zhao, J., Huff, A. F., Du, M., and Ren, J. (2011). Deficiency in AMP-activated protein kinase exaggerates high fat diet-induced cardiac hypertrophy and contractile dysfunction. J. Mol. Cell Cardiol. 50, 712–722. doi: 10.1016/j.yjmcc.2010.12.007

Uchida, S., and Dimmeler, S. (2015). Long noncoding RNAs in cardiovascular diseases. Circ. Res. 116, 737–750. doi: 10.1161/circresaha.116.302521

Wang, C., Zhang, C., Liu, L., Xi, A., Chen, B., Li, Y., et al. (2017). Macrophage-derived mir-155-containing exosomes suppress fibroblast proliferation and promote fibroblast inflammation during cardiac injury. Mol. Ther. 25, 192–204. doi: 10.1016/j.ymthe.2016.09.001

Wang, K., Jiang, Z., Webster, K. A., Chen, J., Hu, H., Zhou, Y., et al. (2017). Enhanced cardioprotection by human endometrium mesenchymal stem cells driven by exosomal MicroRNA-21. Stem Cells Transl. Med. 6, 209–222. doi: 10.5966/sctm.2015-0386

Wang, L., Manson, J. E., Gaziano, J. M., Liu, S., Cochrane, B., Cook, N. R., et al. (2012). Plasma adiponectin and the risk of hypertension in white and black postmenopausal women. Clin. Chem. 58, 1438–1445. doi: 10.1373/clinchem.2012.191080

Wang, S., Aurora, A. B., Johnson, B. A., Qi, X., McAnally, J., Hill, J. A., et al. (2008). The endothelial-specific microRNA miR-126 governs vascular integrity and angiogenesis. Dev. Cell 15, 261–271. doi: 10.1016/j.devcel.2008.07.002

Wang, X., Huang, W., Liu, G., Cai, W., Millard, R. W., Wang, Y., et al. (2014). Cardiomyocytes mediate anti-angiogenesis in type 2 diabetic rats through the exosomal transfer of miR-320 into endothelial cells. J. Mol. Cell Cardiol. 74, 139–150. doi: 10.1016/j.yjmcc.2014.05.001

Wang, Y., Jin, P., Liu, J., and Xie, X. (2019a). Exosomal microRNA-122 mediates obesity-related cardiomyopathy through suppressing mitochondrial ADP-ribosylation factor-like 2. Clin. Sci. 133, 1871–1881. doi: 10.1042/cs20190558

Wang, Y., Zhao, R., Liu, W., Wang, Z., Rong, J., Long, X., et al. (2019b). Exosomal circHIPK3 released from hypoxia-pretreated cardiomyocytes regulates oxidative damage in cardiac microvascular endothelial Cells via the miR-29a/IGF-1 pathway. Oxid Med. Cell Longev. 2019:7954657.

Xia, Y., Lee, K., Li, N., Corbett, D., Mendoza, L., and Frangogiannis, N. G. (2009). Characterization of the inflammatory and fibrotic response in a mouse model of cardiac pressure overload. Histochem. Cell Biol. 131, 471–481. doi: 10.1007/s00418-008-0541-5

Xiao, C., Wang, K., Xu, Y., Hu, H., Zhang, N., Wang, Y., et al. (2018). Transplanted mesenchymal stem cells reduce autophagic flux in infarcted hearts via the exosomal transfer of miR-125b. Circ. Res. 123, 564–578. doi: 10.1161/circresaha.118.312758

Xin, M., Olson, E. N., and Bassel-Duby, R. (2013). Mending broken hearts: cardiac development as a basis for adult heart regeneration and repair. Nat. Rev. Mol. Cell Biol. 14, 529–541. doi: 10.1038/nrm3619

Xu, R., Zhang, F., Chai, R., Zhou, W., Hu, M., Liu, B., et al. (2019). Exosomes derived from pro-inflammatory bone marrow-derived mesenchymal stem cells reduce inflammation and myocardial injury via mediating macrophage polarization. J. Cell Mol. Med. 23, 7617–7631. doi: 10.1111/jcmm.14635

Yanagisawa-Miwa, A., Uchida, Y., Nakamura, F., Tomaru, T., Kido, H., Kamijo, T., et al. (1992). Salvage of infarcted myocardium by angiogenic action of basic fibroblast growth factor. Science 257, 1401–1403. doi: 10.1126/science.1382313

Yang, H. H., Chen, Y., Gao, C. Y., Cui, Z. T., and Yao, J. M. (2017). Protective effects of MicroRNA-126 on human cardiac microvascular endothelial cells against Hypoxia/Reoxygenation-induced injury and inflammatory response by activating PI3K/Akt/eNOS signaling pathway. Cell Physiol. Biochem. 42, 506–518. doi: 10.1159/000477597

Yang, W., Han, Y., Yang, C., Chen, Y., Zhao, W., Su, X., et al. (2019). MicroRNA-19b-1 reverses ischaemia-induced heart failure by inhibiting cardiomyocyte apoptosis and targeting Bcl2 l11/BIM. Heart Vessels 34, 1221–1229. doi: 10.1007/s00380-018-01336-3

Yuan, J., Liu, H., Gao, W., Zhang, L., Ye, Y., Yuan, L., et al. (2018). MicroRNA-378 suppresses myocardial fibrosis through a paracrine mechanism at the early stage of cardiac hypertrophy following mechanical stress. Theranostics 8, 2565–2582. doi: 10.7150/thno.22878

Zhang, H., Freitas, D., Kim, H. S., Fabijanic, K., Li, Z., Chen, H., et al. (2018). Identification of distinct nanoparticles and subsets of extracellular vesicles by asymmetric flow field-flow fractionation. Nat. Cell Biol. 20, 332–343.

Zhao, J., Li, X., Hu, J., Chen, F., Qiao, S., Sun, X., et al. (2019). Mesenchymal stromal cell-derived exosomes attenuate myocardial ischaemia-reperfusion injury through miR-182-regulated macrophage polarization. Cardiovasc. Res. 115, 1205–1216. doi: 10.1093/cvr/cvz040

Zhou, B., and Yu, J. W. (2017). A novel identified circular RNA, circRNA_010567, promotes myocardial fibrosis via suppressing miR-141 by targeting TGF-beta1. Biochem. Biophys. Res. Commun. 487, 769–775. doi: 10.1016/j.bbrc.2017.04.044

Zhou, P., and Pu, W. T. (2016). Recounting cardiac cellular composition. Circ. Res. 118, 368–370. doi: 10.1161/circresaha.116.308139

Zhou, X. L., Xu, H., Liu, Z. B., Wu, Q. C., Zhu, R. R., and Liu, J. C. (2018). miR-21 promotes cardiac fibroblast-to-myofibroblast transformation and myocardial fibrosis by targeting Jagged1. J. Cell Mol. Med. 22, 3816–3824. doi: 10.1111/jcmm.13654

Zhu, B., Zhang, L., Liang, C., Liu, B., Pan, X., Wang, Y., et al. (2019). Stem cell-derived exosomes prevent aging-induced cardiac dysfunction through a novel exosome/lncRNA MALAT1/NF-kappaB/TNF-alpha signaling pathway. Oxid. Med. Cell Longev. 2019:9739258.

Zhu, J., Lu, K., Zhang, N., Zhao, Y., Ma, Q., Shen, J., et al. (2018). Myocardial reparative functions of exosomes from mesenchymal stem cells are enhanced by hypoxia treatment of the cells via transferring microRNA-210 in an nSMase2-dependent way. Artif. Cells Nanomed. Biotechnol. 46, 1659–1670.

Zhu, X., Badawi, M., Pomeroy, S., Sutaria, D. S., Xie, Z., Baek, A., et al. (2017). Comprehensive toxicity and immunogenicity studies reveal minimal effects in mice following sustained dosing of extracellular vesicles derived from HEK293T cells. J. Extracell Vesicles. 6:1324730. doi: 10.1080/20013078.2017.1324730

CHAPTER 6

"The Cre-LoxP system in 3D Cardiac Communication –

Is it possible to trace EVs transfer on Engineered Human Myocardium?"

[1,2,3] RF Videira, [1,2]L.Ottaviani, [4]B. Berecic, [3]I Falcão-Pires ,[5]H. Fernandes, [4]M. Tiburcy, [1,2,3]PA da Costa Martins

[1] Department of Cardiology, CARIM School for Cardiovascular Diseases, Faculty of Health, Medicine and Life Sciences, Maastricht University, Maastricht, Netherlands;[2]Department of Molecular Genetics, Faculty of Sciences and Engineering, Maastricht University, Maastricht, The Netherlands; [3]Department of Physiology and Cardiothoracic Surgery, Faculty of Medicine, University of Porto, Porto, Portugal.[4] Institute of Pharmacology and Toxicology, University Medical Center Göttingen, Göttingen, Germany, [5] Faculty of Medicine, University of Coimbra, Coimbra, Portugal.

(In preparation)

Abstract

Extracellular vesicles (EVs) play a major role in cardiac communication, representing an essential mechanism to maintain heart homeostasis that is frequently altered under cardiovascular pathologies. Several studies in 2D showed that EV uptake results in cargo (e.g. mRNA, miRs, or proteins) transfer to recipient cells that interfere with recipient cell behavior. Despite the promising outcomes of EVs' research, translation into the clinical setting remains a key challenge. To overcome this limitation, more and better methods to monitor EVs transfer are needed. Here, we investigated a novel method based on the Cre-LoxP recombination system to visualize and screen cardiac intercellular EV transfer. For that, we used a 3D human heart model composed of human cardiomyocytes (iPSCs-CMs) and stromal cells (iPSC-SCs). We showed that the Cre-LoxP recombination system can be used to trace cardiac EVs both in 2D and 3D models and to quantify the relative number of EVs' recipient cells. Additionally, we also confirmed that EVs cargo, namely *Cre mRNA* was functionally active in recipient cells. However, our data also raised important questions on whether some cells are more susceptible to iPSCs-CMs-derived EVs or even if the cargo carried by EVs is differentially processed depending on the recipient cell type. These results may significantly impact the development of EV-based therapies against cardiac pathologies.

Introduction

Cardiomyocytes work together in a synchronized beating manner to carry out the contractile function of the heart. However, the cellular composition of the heart is complex, including cardiomyocytes, fibroblasts, stromal cells, endothelial cells, nervous cells, inflammatory cells, and smooth muscle cells. Despite being responsible for keeping a normal cardiac structure and function [1], the percentage and contribution of each of these cell types remain to be defined. While some studies reported endothelial cells as the major cell population in the heart [1], recent literature describes fibroblast as the most abundant cell type after cardiomyocytes [2].

The concept of a multicellular organ implies effective communication between the different cell types to maintain homeostasis and respond to adverse situations. Many hypotheses have been posed for cardiac communication, including extracellular vesicle-mediated communication. Extracellular vesicles (EVs) are small lipid bilayer-delimited particles endogenously released by almost all mammalian cell types and, therefore, found in cell-conditioned media and all biological fluids. Although EVs comprise apoptotic bodies, microvesicles, and exosomes, only the last two have been associated with intercellular communication [3, 4].

Multiple factors can aid in distinguishing microvesicles from exosomes, such as their size, biogenesis, and the presence of specific surface markers. Firstly, exosomes (30-150 nm in size) are substantially smaller than microvesicles (100–1000 nm); and secondly, while exosomes are of endocytic origin and are formed in the multivesicular bodies (MVBs), microvesicles are produced by direct budding from the plasma membrane [3]. The endocytic pathway starts with invagination of the plasma membrane-deriving endosomes, then proteins like endosomal sorting complexes required for transport (ESCRT) protein family attach to the surface of the late endosomes. The ESCRT is responsible for sorting cargo such as proteins, mRNAs, and miRs. After cargo selection, the endosomal membrane curves inwards, generating intraluminal vesicles (ILV) and, therefore, the late endosome becomes known as MVB containing ILV. MVBs can be degraded if they fuse with lysosomes or released to the extracellular space by exocytosis if their membrane fuse with the plasma cell membrane (exosomes). In addition to ESCRT, tetraspanins and sphingolipid ceramides can regulate the type of MVB cargo [3]. Therefore, exosomal markers include tetraspanins (CD81, CD63, CD9), flotillin, and Alix. Tetraspanins are transmembrane proteins that were suggested to be involved in forming membrane-curved structures, namely due to their cytoskeleton connections, which may influence vesicles' fission process [5]. Ceramides are lipids composed of sphingosines and fatty acids present on the membranes and necessary for exosome formation [6]. In turn, microvesicle biogenesis starts upon stimuli such as cytokines release and calcium signals and implies the trafficking of molecular cargo to the plasma membrane [7]. After vesicle pinching, there is redistribution of the lipids and proteins in the membrane, membrane remodeling, and loss of its asymmetry. Because the outer layer of MVs is formed from the cell plasma membrane, it remains difficult to find specific markers for MVs. Nevertheless, suggested MVs' markers include selectins, integrins (proteins involved in cell adhesion), CD40l, and proteins containing post translational modification [8-10].

EVs encapsulate cargo such as DNA, RNA, including non-coding RNA, proteins, lipids, and metabolites that will be transferred into the recipient cells, modulate the downstream signaling pathways, and interfere with cell function. A study described the transfer of EVs cargo as a selective process and not random since specific cargo content is higher in EVs than in the host cell, supporting the hypothesis of selective EV load [11]. It has been implied that some post-translational modifications such as ubiquitination, phosphorylation, oxidation, and glycosylation of certain protein residues serve

as a signal for cargo transport into EVs. Similarly, RNA-containing selected motifs are suggested to be preferentially sorted into EVs [11]. As previously described [12], certain pathological conditions, such as cardiac hypertrophy, may alter cardiac cell communication by modifying EV sorting preferences, leading to modifications in the recipient cell. While EVs are active participants in cardiac communication, they have also recently emerged as attractive delivery tools and potential drug-delivery vehicles [13]. They are suggested to be better alternatives to cell therapies due to their low immunogenicity, high bioavailability, biocompatibility, and lower costs. Therefore, it is essential to understand better the biodistribution and kinetics of EV release and uptake [13].

Current models to study cardiac communication through EVs cannot truthfully recapitulate human heart physiology while allowing for accessibility and high-resolution visualization of EVs in real-time and are, therefore, considered inadequate [13]. Despite retaining cardiac physiology, animal models may not provide translation to human clinical situations as control and tracking administered EVs is challenging [14]. Typically evaluation methods of EV biodistribution imply the staining of EV membranes with fluorescent lipophilic dyes, followed by EV tracking via diverse imaging systems like optical imaging and nuclear imaging [15]. Despite being affordable, optical imaging (through absorption and scattering of photons) has a small depth of penetration and thus it is only feasible to track EV biodistribution in small animals and cannot be used as a quantitative tool. While nuclear imaging solves the problem of absolute quantification, it is not easy to access due to the high price and equipment necessary [15]. Furthermore, EV membrane labeling could give a false positive result of EV uptake since there is a risk of leakage from EV lipids to the recipient cell membrane, without a true uptake. At last, EVs and their associated cargo could follow the lysosomal pathway suggesting that EV content is not functionally active in recipient cells and may be immediately degraded [16].

In contrast, *in vitro* models have evolved to patient-specific cell technologies (namely, human induced pluripotent stem cells -iPSCs) allowing easier control and access. However, these models lack myocardial cell heterogeneity and their intrinsic complex interactions and often cannot recapitulate disease pathophysiology [17].

Recently, engineered models of human myocardium (EHM) have emerged as promising tools by combining human cells (usually iPSC-derived) and biomaterials to mimic the human heart's heterogeneous cellular composition and function in physiology and pathological conditions. When compared to *in vivo* models, EHM facilitates control of environmental factors and easy access to EVs and cells that compose the EHM. Moreover, EHMs do not face strict ethical approval and due to closer proximity to the human heart composition, EHMs are now being used in clinical trials to test the safety of a treatment for end-stage heart failure (BioVAT-HF-DZHK20 trial). Thus, if the outcomes of the BioVAT-HF-DZHK20 trial are successful, EHM readouts will be eventually considered more clinically relevant than any other human heart model. Moreover, EHM can also aid in improving the development of personalized medicine and contribute to the establishment of patient-specific models by using patient-derived hiPSCs [18, 19].

Previously work from Prof. Zimmermann’s lab used an EHM model to study the role of EVs on cardiac injury [20]. For this reason, this study will use a similar model composed of iPSCs- derived cardiomyocytes (iPSCs-CMs) and iPSCs-derived stromal cells (iPSCs-SCs) with or without iPSCs-derived endothelial cells (iPSCs-ECs) to monitor EV transfer in a cardiac environment.

Here, we aim to investigating cardiac intercellular communication through EVs in an engineered human myocardium (EHM) model. This model has been previously described as a

promising human heart model with the 3D novelty, since allows the evaluation of cardiac contractile function, promotes the maturation of cardiomyocytes, and displays a cellular organization that mirrors human myocardium tissue. Thereby, it can be used in disease modeling, drug screening, and possibly cardiac communication [21, 22]. This model was first established by *Tiburcy et al.,* in 2017, where EHMs generated from defined cell populations (high purity cardiomyocytes and fibroblasts) enhanced robustness for disease modeling and allowed to specifically address cell-cell interaction [22].

The Cre-loxP method allows monitoring of vesicle transfer through color switch of the recipient cells, giving an insight into the biodistribution, timing, and release of the Cre-enriched EVs. These findings are the first step towards a more complex *in-vivo* EV tracking in the heart and will contribute to uncovering the biological functions of cardiac vesicle transfer, opening new avenues for the development of novel therapeutic strategies. For that, we used two viral constructs that were previously reported by *Zommer et al.* [23]. First, we generated an adeno-associated virus 6 (AAV6) harboring a cyan fluorescence reporter protein (CFP) and Cre 25nt that allows cellular Cre export through EVs under the cardiac troponin T promoter control. Secondly, we used a lentivirus harboring the reporter protein DsRed immediately followed by a stop codon, flanked by two Lox P sites. Downstream the second LoxP site, there is an enhanced green fluorescence protein (eGFP) under cytomegalovirus (CMV) promoter control. These constructs will help to visualize how cardiomyocytes infected with AAV6-CFP-Cre will secrete EVs enriched in *Cre* that, in turn, will be taken up by cells expressing LoxP-DsRed-stop-LoxP-eGFP. Once in the host cells, Cre will mediate excision and removal of DsRed-stop, promoting the expression of eGFP and allowing for visualization of cardiomyocyte-derived EV-mediated cellular transfer.

Methods

Construction and production of viral vectors

The packing construct pcDNA3-CMV-CFP; Ubc-Cre-25nt plasmid (Addgene, #65727) was cloned into pTrek1-CMV-MCS plasmid. The pTrek1-CMV-MCS plasmid and the helper plasmids pDP9RS and pDP6RS were provided by Dr. Roger Hajjar (Icahn School of Medicine at Mount Sinai, New York) [24]. Production of recombinant AAV6, rAAV6, was performed as previously described (Ramanujam *et al.* Mol Therapy 2016). The viral particles were produced by transient transfection of HEK293-T cells. Prior to transfection, cells were cultured in Nunc Cell Factory 10 trays (#140400; ThermoFisher Scientific, Bonn, Germany) for 24 hours in Dulbecco's modified essential medium (DMEM) containing 10% fetal bovine serum (FBS) and 1% penicillin/streptomycin (P/S) (Gibco-ThermoFisher Scientific, Bonn, Germany). Transfection was achieved using polyethyleneimine 'Max' (#24765; Polysciences Warrington PA) and incubating cells with 420 g of the transgene plasmid and 1.5 mg of the helper plasmid for 72 hours. The supernatant of the cell lysates was incubated with 50 U/mL of benzonase (#E1014; Sigma-Aldrich, Taufkirchen, Germany) for 30 minutes at 37°C, followed by ultracentrifugation over an iodixanol density gradient (Optiprep; Fresenius Kabi Norge, Oslo, Norway) to purify the viruses. High-titer stocks were obtained by centrifuging in Vivaspin 20 columns (#VS2042; Sartorius Stedim, Goettingen, Germany) Ringer lactate buffer (Braun, Melsungen, Germany). At last, rAAV6 titer was quantified by real-time quantitative polymerase chain reaction.

Twenty-four hours before lentivirus genesis, $6x10^6$ human embryonic kidney (HEK) 293T cells were plated into a $25cm^2$ flask and cultured at 37°C with 5%CO_2. The next day, 3.5µg plasmid containing the packing construct (LoxP-dsRed-stop codon-LoxP-eGFP), 1.23 µg pMD2.G, and 2.27 µg psPax2 were transfected into HEK293T by using MEM and Turbofect transfecting reagents. The media was refreshed the next day and after 96 hours, the virus was harvested by centrifuging the supernatant at 500G for 5 min.

In vitro iPSCs-CMs differentiation, culture, and infection

IPSCs-CMs were obtained by direct differentiation of human iPSCs TC1133 cell line into iPSCs-CMs performed by WNT signaling modulation as described in [21, 25].

Briefly, 45 minutes before starting differentiation, flasks were coated with Matrigel (1:120 BD Cat 354230) and incubated at 37°C. At 80%–90% confluence, cells were stimulated for 48h by incubation with cardio differentiation medium composed of basal medium (RPMI 1640 with Glutamax (Thermo Fisher Scientific), 2% B27 (Thermo Fisher Scientific), 1% sodium pyruvate (Invitrogen) and 0.2 mg/ml L-ascorbic acid 2-phosphate (Sigma)) and treatment with 1 µM CHIR (Calbiochem), 5 ng/ml BMP4 (R&D systems), 9 ng/ml Activin A (R&D systems) and 5 ng/ml bFGF (Stemgent). At day 3, were incubated with cardiac differentiation medium composed of RPMI 1640 with Glutamax, 2% B27 with Insulin (Thermo Fisher Scientific), 1% sodium pyruvate (Invitrogen), and 0.2 mg/ml L-ascorbic acid 2-phosphate (Sigma) plus 5µM IWP4 (Stemgent). At day 10 iPSCs-CMs IWP4 is removed from the medium and after 48 hours iPSCs-CMs selection medium constituted of RPMI 1640 with Glutamax (Thermo Fisher Scientific), 2.2 mM sodium lactate (Sigma), and 0.1 mM 2-mercaptoethanol (Invitrogen) has added to the cells. After day 17, iPSCs-CMs selection media is replaced by basal medium until EHM generation. Finally, iPSC-CMs' purity was quantified by flow cytometry analysis.

After 4 weeks iPSCs-CMs were re-plated on a monolayer as previously described and cultured for 4 days before AAV6 infection. iPSCs-CMs were treated with 5 µM of polybrene (Merck Millipore) for 30 minutes followed by incubation with AAV6 (at MOI 10^4 or 10^5), after 24 hours media was

refreshed and renewed every two days for fourteen days. Viral efficiency was evaluated by fluorescence microscopy and quantified by flow cytometry.

Detachment of iPSCs-CMs was achieved by incubating cells at room temperature (RT) with 6mL of Accutase (Thermo Scientific) until cells are visibly detached followed by adding 12 mL of cardiomyocyte medium composed of RMPI 1640 (Invitrogen, Cat 61870-010) supplemented with L-ascorbic acid 2 phosphate sesquimagnesium salt hydrate (ASC) (Sigma, Cat A8960-5G) 1% Penicillin-Streptomycin (Thermofisher) and centrifuged at 200G for 7 min. Next, cells were resuspended in 10mL of cardiomyocyte medium and strained with a 100 µm strainer before replating, EHM casting, or FACS protocol.

iPSCs-ECs differentiation, culture, and infection

IPSCs-ECs were obtained by direct differentiation of human iPSCs TC 1133 into iPSCs-ECs by mesodermal induction, vascular specification, and EC amplification as described in [26]. In brief, 24 hours prior to mesoderm induction, 2500 cells/cm^2 were plated in Matrigel-coated flasks (1:120 BD Cat 354230) and grown in StemMACS iPS Brew (Miltenyi Biotech, Cat 130-104-368). Then differentiation was initiated by incubating cells with mesodermal induction medium (MIM) composed of DMEM-F12 (ThermoFisher, Cat 11320033), 10% Fetal Bovine Serum (Gibco), 1 % penicillin/streptomycin (Invitrogen, Cat 15140122) and 4 µM CHIR (Stemgent, Cat 04-0004) and renewed next day. At day 2, vascular specification was started with Endothelial Cell Basal Medium MV2 (EBM-2 PromoCell, Cat C-22221) and supplemented with 5ng/ml bFGF (Miltenyi Biotech, Cat 130-093-841) and 10 ng/ml VEGFA (Peprotech, Cat AF-100-20) and renewed next day. Media was changed to Endothelial Cell Growth Medium (EGM-2 Promo Cell, Cat C-22022) supplemented with 10 ng/ml VEGFA (Peprotech) and renewed every other day. After 12 days, iPSCs-ECs were purified via magnetic-activated cell sorting (MACS) following the manufacturer's protocol. In summary, cells were digested with prewarmed 0.125% trypsin-EDTA (Gibco 25200056) and incubated for 5 minutes at 37^oC, next EGM-2 supplemented with 20% FBS was used to neutralize the reaction, and cells were centrifuged for 5 minutes at 300G. Pooled cells were washed in phosphate-buffered saline (PBS) (Gibco, A1285601) and resuspended in a concentration of 1×10^7 cells per 60 µL of medium and 20 µL of FcR Blocking Reagent (130-059-901, Miltenyi), after vortex, 20 µL of CD31 MicroBeads (130-091-935, Miltenyi) was added to the mixture and incubated at 4^oC. After 15 minutes, 1mL of medium was added and centrifuge cells at 300G for 3 min. An LS (130-042-401, Miltenyi) was placed in the magnetic field of a MidiMACS Separator (Miltenyi) and washed before use. The cell suspension was passed into the column and washed 3x before removing the column from the separator. At last, 5 mL of media were added onto the column and magnetically labeled cells were immediately flushed out by pushing the plunger into the column. Cells were counted and plated in matrigel pre-coated flasks/ plates with EGM-2 supplemented with 5 µM ROCKi (Stemolecule, Cat.: 04001210). At 80% confluency iPSCs-ECs were pre-treated with 5 µM of polybrene for 30 minutes and infected with 10, 50, 100, or 300 µL of ADV stock viral in EGM-2 media, after 24 hours media was renewed every other day. Infection efficiency was assessed by fluorescence microscopy and quantified by flow cytometry.

Differentiation and culture iPSCs-SCs

Four days prior to stromal cell differentiation, iPSCs (TC1133 cell line) were plated as a monolayer in a plate or flask pre-coated with Matrigel. At day 0, iPSCs were washed with RPMI and incubated with a stromal cell induction medium composed of RPMI 1640 GlutaMax with 1% sodium pyruvate (Invitrogen, Cat 11360), 0.1% L-asc, 2% B27 minus Insulin (B27 supplement, Thermo

Scientific), 1 µM CHIR (Stemgent, Cat 04-0004), 5 ng/ml BMP4 (R&D Systems), 9 ng/ml Activin A (R&D Systems), 5 ng/ml bFGF (Peprotech) for 48 hours. At day 2 of differentiation, cells were incubated in stromal cell differentiation medium made of RPMI with Glutamax plus 1% Pyruvate, 0.1% L-Asc, 2% B-27 minus Insulin, and 5 µM IWP4 (Stemgent, Cat 04-0036) and after 24 hours cells were detached with TrypLE select (Thermo Scientific). Cells were incubated at 37°C for up to 15 minutes, next culture medium was added to the pooled cells followed by centrifugation at 300G for 5 min at RT and plating in a pre-coated flask and appropriate culture medium. After 3 days, the medium was replaced by a stromal cell specification medium containing, RPMI 1640 with Glutamax, 1% sodium pyruvate, 2 % B27 supplement (Thermo Scientific), 200uM L-Asc, 1% of P/S, 50 ng/ml BMP4, 4 µmol/L retinoic acid (Sigma: R2625) and 1 µM CHIR for 48 hours. Then, cells were expanded with a stromal cell expansion medium composed of KO DMEM (Thermo Scientific), 1% Glutamin (Thermo Scientific), 10% KO Serum Replacement (Thermo Scientific), 50 ng/ml FGF, and 25 ng/ml VEGF. At day 21, cells were re-plated as previously described but with the following modifications: cells were incubated with Accutase at RT for 10 -20 minutes followed by the addition of Versene at 37°C for 5 minutes. IPSCs-SCs were continuously expanded until day 28, after which cells were either frozen or used for viral infection.

Generation and maintenance of Engineered Human Myocardium (EHM)

EHMs were generated following a previously described protocol [21]. In brief, a cell mix ($5x10^5$ cells/ EHM) composed of hiPSCs-CMs and hiPSCs-SCs (EHM-1), or alternatively hiPSCs-CMs, hiPSCs-SCs and iPSCs-ECs (EHM-2) was gently reconstituted on ice with collagen hydrogel (180 µL/EHM) and cast into a 48 well plate (myriamed GmbH). The cell-hydrogel mix was incubated for 1h at 37°C to condense, and EHM medium (as prepared in [21]) supplemented with 5 ng/ml TGF-β1 was added and refreshed daily. After 3 days, EHM medium without TGF-β1 was added, and spontaneously beating of EHMs was observed. From here on, the EHM medium was renewed every day. A ratio of 7 to 3 (hiPSCs-CMs to hiPSCs-SCs) was used in EHM-1 and a ratio of 2:1:1 (hiPSCs-CMs to hiPSCs-SCs to iPSCs-ECs) was used in EHM-2.

Heart failure mimicking on EHM

Heart failure protocol was induced through noradrenaline (NA) and TGF-ß1 stimulation. In brief, at day 14 EHM were incubated with an EHM hypertrophic medium composed of aMEM GlutaMax (Thermofisher) supplemented with B27 minus insulin, Non-Essential Amino Acids (Thermofisher), Pen/Strep, VEGF, FGF, and IGF-1. After 2 weeks, EHMs were treated with an EHM hypertrophic medium supplemented with L-noradrenaline (NA, Sigma-Aldrich) and TGF-ß1 (Peprotech, Cat. #AF-100-21C) to a final concentration of 10 µM and 5 ng/ml, respectively, for another 2 weeks. EHM hypertrophy-inducing medium was changed every day.

Flow cytometry analysis

For flow cytometry analysis of iPSC-CMs and iPSCs-ECs, the cells were dissociated with Accutase and 0.1% Trypsin-EDTA into single cells, centrifuged at 500G for 7 minutes and 300G for 3min, respectively, and resuspended in (100µL-1000µL) PBS. Alternatively, EHMs were dissociated as described in [22]. In brief, EHMs were treated with collagenase I (2 mg/ml in calcium-containing PBS in the presence of 20% fetal bovine serum) for 1-2 hours at 37 °C. After washing with PBS, EHMs were incubated in Accutase mix solution (0.025% Trypsin and 20 µg/ml DNAse I) and mechanically dissociated. At last, separated cells were centrifuge at 300G for 5 minutes at 4°C and resuspended in 100µL of PBS with SYTOX™ Red Dead Cell Stain (1:10000, #S34859, Thermofisher).

Subsequently, cells were analyzed using the LSRII flow cytometer (BD Biosciences), and non-infected cells were used as a negative control. At least 5,000-10,000 events were analyzed per sample.

Optical Measurements Analysis

Optical measurements were performed to monitor EHM contraction activity following the previously described protocol [1] with some modifications. Each EHM was measured and recorded inside a 37°C climate chamber resolution until at least 3600 frames were reached. Surface Area (SA) was represented by white pixels at time t, next SA was converted to fractional area change (FAC) by dividing the maximum sa of a contraction cycle. Time-points of maximal FAC representing contraction peaks were identified automatically. Analysis of each file was performed using MATLAB compiler runtime.

Imaging of EHMs and Cells

Images of EHMs after viral infection were obtained with a LUMAR stereoscope (Zeiss). Imaging of monolayer cells was performed with a confocal scanning laser microscope (Zeiss LSM710).

Extracellular Vesicles Isolation

Extracellular vesicles were isolated by ultracentrifugation based on the previously described protocol [27]. Briefly, for the removal of dead cells and cell debris, the conditioned medium was centrifuged for 20 minutes at 2.000G. Next, the supernatant was centrifuged for 30 minutes at 10.000G for the removal of large vesicles, followed by EVs precipitation at 100 000G, for 2 hours. The pellet containing the small EVs was washed in PBS at 100 000G, for 2 hours. At last, the pellet was resuspended in 50 µL of PBS and stored at -80°C. All centrifugation steps were performed at 4°C using Beckman Coulter ultracentrifuge with a Si32TW ultracentrifuge rotor.

RNA isolation, cDNA synthesis, and PCR

Total RNA was isolated by Trizol (Thermofisher) method following the manufacturer's protocol. RNA was then reverse-transcribed using M-MLV reverse transcriptase (Promega). Polymerase chain reaction (PCR) was performed by using FastDNA green (Promega) on a thermocycler (Applied Biosystems)). To measure mRNA Cre expression the following primers were used:5'CTA GAG CCT TTG CAC GTT C 3' and 5'GTT CGC AAG AAC CTG ATG GAC A 3' and cycled at 95°C for 3 min for enzyme activation, 30 sec 95°C for denaturation and 30s 54 C and 30s at 72°C for 37 times for annealing and extension. Amplified products were run in a 1.5% agarose gel at 120mV for 90 minutes, a 1kB ladder was used. Gel images were acquired on a Gel Doc XR (Biorad) using Quantity One Software.

Statistical Analysis

Data are presented as mean ± standard error of the mean. A two-way ANOVA followed by Bonferroni posttest was used to assess statistical differences in EHMs' contractile function (only if n>3 in all groups). Statistical testing was performed with GraphPad Prism 5.

Results

Study Design

The screening of cardiac vesicles' transfer is crucial to gaining insights into EVs' biodistribution, uptake, and release. To monitor cardiac EVs, we proposed to use the Cre-LoxP recombination system [23], a method based on color switch in the recipient cells, and to test it on engineered human myocardium (EHM), a human model, which parallels 2D human cell cultures by allowing intercellular interactions and a higher degree of structural complexity.

Our proposed study design described the Cre-LoxP system as follows: firstly, we generated an AAV6 harboring a cTNT-CFP-CRE construct, and secondly, an adenovirus (ADV) or a lentivirus harboring a CMV-LoxP-DsRed-LoxP-eGFP construct (**Figure 1A**). Human iPSCs-CMs infected with AAV6-cTNT-CFP-CRE promoted cardiomyocyte-specific CFP and Cre expression, with subsequent release of Cre^+ EVs (**Figure 1B left**). In turn, human iPSCs-ECs or human iPSCs-SCs transduced with ADV-CMV-LoxP-DsRed-LoxP-eGFP were capable of expressing eGFP after recognition and excision of LoxP sites by Cre. Hence, after incorporating Cre^+ EVs, recipient cells stopped expression of DsRed and expressed eGFP (**Figure 1B right**).

Optimization of viral infection of iPSCs-CMs, iPSCs-ECs and iPSCs-SCs

The establishment of optimal transduction is an important step in understanding the efficiency of Cre-LoxP recombination system, and, it was achieved by testing different incubations' times and concentrations of viral particles (given by multiplicity of infection (MOI)). To this end, after iPSCs-CMs infection, the number of CFP^+ iPSCs-CMs was quantified by flow cytometry. As illustrated in **Figure 2**, iPSCs-CMs were infected with either ten thousand (condition B- MOI 10^4) or one hundred thousand (condition C-MOI 10^5) viral particles per cell, and CFP expression was measured on days 3, 7, or 14 after infection.

Three days post-infection, condition C displayed a CFP^+ iPSCs-CMs percentage of 71.25%, while in condition B, only 35.1% of the live cell population were CFP^+. At day 7, transduction efficiency increased to 51.2% in condition B and 94.5% in condition C. Both conditions showed an increased number of CFP^+ cells over time, being the maximum efficiency reached on day 14, as shown by the 81.4% and 98.8% of CFP^+ cells of conditions B and C, respectively. As control, iPSCs-CMs only exposed to polybrene were used and are represented on condition A.

The results suggested that condition C had the best performance regarding cell transduction efficiency and, therefore, an MOI of one hundred thousand was used in the following experiments.

Similarly, optimal transduction efficiency was explored in iPSCs-ECs; for that, hiPSCs-ECs were incubated with 0, 100 µL, or 300 µL of ADV CMV-LoxP-DsRed-LoxP-eGFP (per 1 mL of media), represented by conditions A, B, and C, respectively. After 3 days of infection, DsRed expression was observed under fluorescence microscopy and $DsRed^+$ cells were quantified by flow cytometry. The results demonstrated that the addition of 100uL/mL showed 85.8% of $DsRed^+$ cells suggesting a good transduction efficiency, whereas adding 300uL/mL promoted 85.2% of cells expressing DsRed (**Supplementary Figure 1**), indicating that the percentage of positive cells will not increase with higher viral concentration. Our data suggested that 100uL/mL of media was the best ratio to perform ADV infection, and consequently, in posterior experiments, this ratio will be used.

Figure 1.

A)

B)

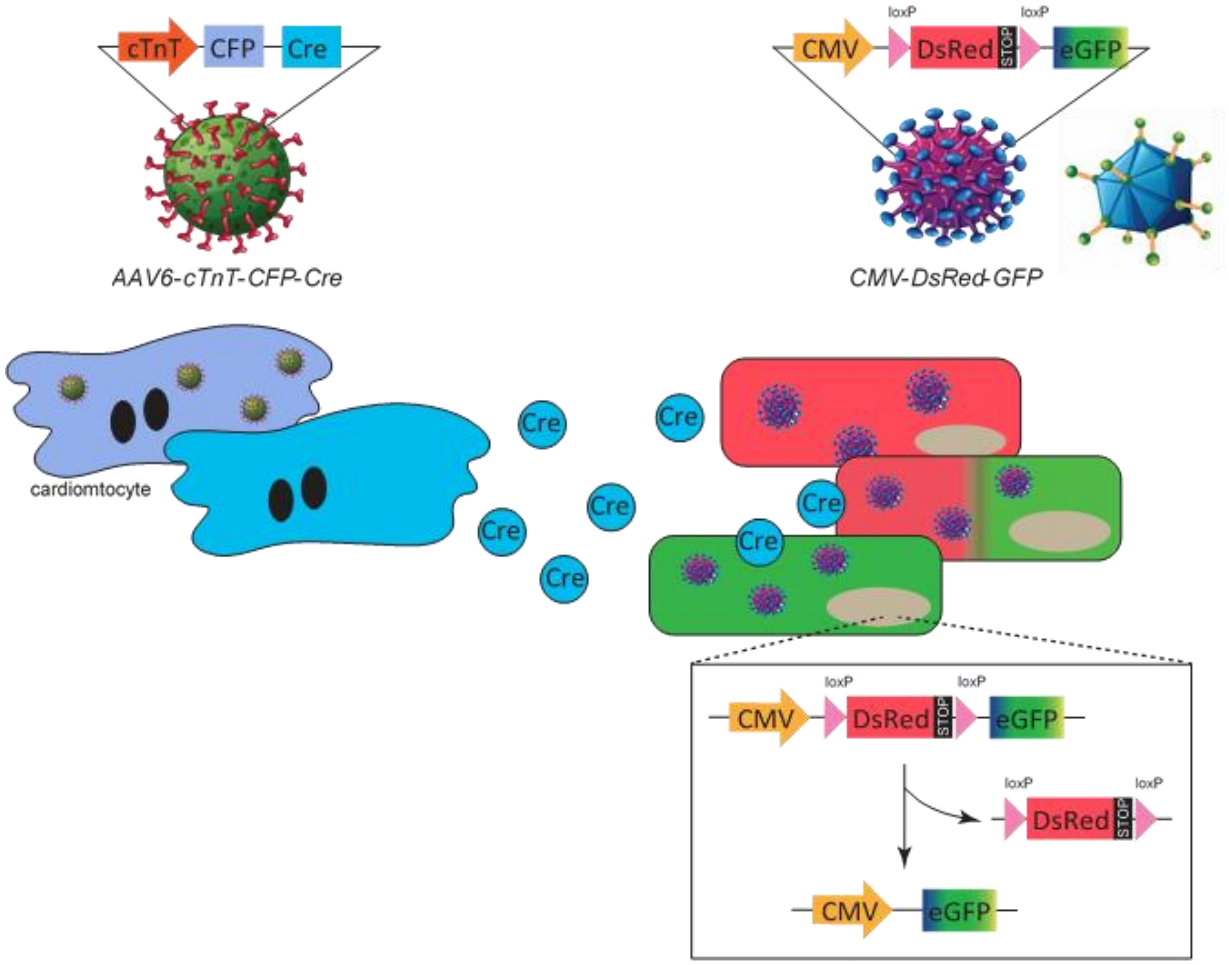

Figure 1*. *Intercellular Cardiac EVs transfer could be traced by Cre-LoxP System*. *A. *Viral Vector Composition of AAV6-CFP-Cre (left) and Lentivirus-LoxP-DsRed-stop-codon- LoxP-eGFP (right)* ***B.*** *Sketch illustrating the Cre-LoxP system used to report the transfer of Cre recombinase (Cre) activity. IPSCs-CMs expressing CFP^{+} secrete Cre^{+} enriched EVs (left) that are transfered into the recipient non-myocyte cells DsRed^{+} inducing red-to-green color switch (right).*

Optimization of EV reporter strategy in EHM

Next, we employed the EHM model composed of iPSCs-CMs and iPSCs-SCs (EHM-1), or iPSCs-CMs, iPSCs-ECs, and iPSCs-SCs (EHM-2) to assess structural and functional consequences of EHM AAV6 and ADV viral exposure and posteriorly, EVs transfer in a 3D model.

The presence of ADV in iPSC-SCs and iPSCs-ECs used on EHM construction (both EHM-1 and EHM-2) prevented proper EHMs condensation as represented by a cloud-like structure (**Figure 3A**). The lack of solidification might be explained by a toxic effect that ADV had on cells, which led to cell death, and, as proved in **Figures 3A and B**, there was a significant decrease in the DsRed signal. ADV toxicity may decrease EHM cell number to below the threshold limit, preventing hydrogel collagen condensation (**Figure 3B**). Our findings of a deficient EHM were confirmed by optical measurements analyses with no peaks being detected by the software. In contrast to ADV infected cells, AAV6 infected iPSCs-CMs were able to keep their CFP expression constant in a 3D structure (**Figure 3B**), generating EHMs with a proper morphology. The apparent toxicity of ADV in non-myocytes prevents proper EHM formation, given the critical role for non-myocytes, as previously described in [22]. To circumvent the ADV-associated toxicity we tested a lentiviral approach to stably integrate the CMV-LoxP-DsRed-LoxP-eGFP cassette into non-myocytes (iPSC-SC, iPSC-EC).

Analysis of EHM contractile function revealed that EHMs containing AAV6- iPSCs-CMs performed worst regarding *EHM's shortening*, a parameter that displays the strength over time, and *EHM's contraction period*, a parameter that indicates the time needed for a contraction (**Supplementary Figure 2**). There were no statistically significant differences regarding *EHM´s base pole distance*, a parameter that expresses the EHM basal contraction, which is commonly decreased over time due to a compression of the EHM tissue (**Supplementary Figure 2**). Also, no differences were observed regarding *EHM´s beating frequency*. Hence, AAV6 infected iPSCs-CMs were associated with a poor contraction when embedded in a 3D structure like EHM.

Since EHM model has been suggested as a good model to mimic cardiac pathologies, we further investigated if the current HF model led to functional changes in EHM and whether these changes were preserved under AAV6 infection conditions. *EHM's shortening* was decreased in both infected and non-infected EHM under HF conditions suggesting a decrease in EHM's force (**Supplementary Figure 2**). Also, in both HF conditions, there was an increase in EHM's base pole distance possibly indicating that EHM's structure expanded, and thus, there was a decrease in the EHM's contraction ability (**Supplementary Figure 2**).

EHM's contraction period was also lower in both viral conditions, which could be explained due to activation of a compensatory mechanism, where a decrease in *EHM's shortening* (less "area" to contract) leads to a diminished contraction period. In all of the previous parameters, HF had a higher impact on non-infected cells when compared to virus-treated cells, already with an impaired contraction capacity (**Supplementary Figure 2**).

Also, EHM beating frequency was altered under HF conditions, and a decline indicating cardiac failure was observed in EHM with infected cells. However, EHMs of non-infected cells showed an increase in the beating frequency not typical of HF (**Supplementary Figure 2**). At the initial stage of cardiac remodeling, the cardiac muscle may increase its beating frequency to avoid heart failure and maintain cardiac output. Therefore, the rise in beating frequency observed in non-infected EHM might

Figure 2.

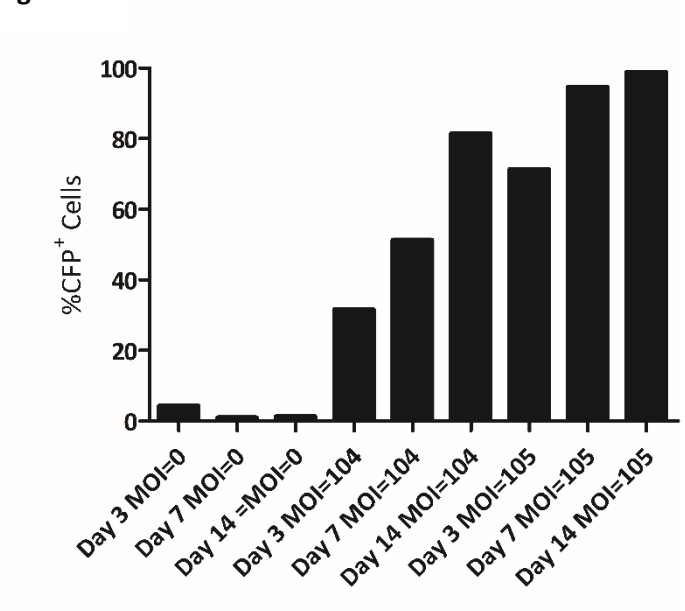

Figure 2. Optimization of AAV6 transduction efficiency*. Graph of live iPSCs-CMs illustrating in black the percentage of CFP⁺ cells regarding control (MOI=0), AAV6 transduced iPSCs-CMs with a MOI=10^4 (condition B) and a MOI=10^5 (condition C) at days 3, 7 and 14 after transduction.*

Figure 3.

A)

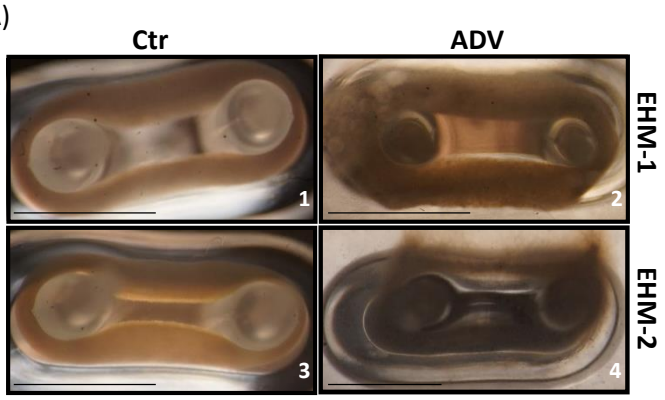

B)

Figure 3 A. *Illustrative pictures of EHM-1 (top) and EHM-2 (bottom). Non-infected EHMs (control EHMs) are represented on numbers 1 and 3. EHMs infected with ADV display a cloudy-like shape due to lack of condensation (numbers 2 and 4).* ***B.*** *Representative stereoscopic images of CFP⁺ iPSCs-CMs EHM-1, DsRed⁺ EHM-1 and DsRed⁺ EHM-2, under CFP and DsRed filter, respectively. AAV6 infected cardimyocytes are alive on EHM as observed by CFP⁺. The lack of DsRed⁺ signal indicates the death of ADV infected cells in both EHM-1 and EHM-2. Scale=2.5mm*

be another compensatory mechanism to cope with failing. These results noted that our model of HF leads to functional alterations in EHM of non-infected cells. Unfortunately, since AAV6 infected EHM implies a poor basal contraction, it does not represent a good 3D model for HF. Consequently, AAV6-infected iPSCs-CMs are associated with a deficient contraction when embedded in a 3D structure.

At last, to understand if the lentiviral treatment inherent in the Cre-LoxP system affects EHM contractile function, optical measurements were performed every week for 21 days on EHMs. For that, EHMs were exposed to three 3 different viral conditions A, B, and C. EHMs belonging to condition A were composed of iPSCs-SCs infected with lentivirus-LoxP-DsRed-LoxP-eGFP and AAV6-CFP-Cre iPSCs-CMs. In contrast, EHM that belonged to condition B were composed by iPSCs-SCs infected with lentivirus-LoxP-DsRed-LoxP-eGFP and control (non-infected) iPSCs-CMs. Condition C was used as control, and thereby these EHMs were generated using both control (non-infected) iPSCs-CMs and iPSCs-SCs.

"Virus vs Time" interaction was firstly assessed by performing a two-way ANOVA followed by Bonferroni posttest. A statistically significant interaction between these two factors was observed in *EHM's shortening* and *EHM's contraction period* parameters suggesting that "time of experiment" had a different effect among the different "viral treatments". Thus, care must be taken when interpreting the impact of "time" and "virus" alone. As previously observed and discussed, disregarding the viral treatment, time affected EHM's shortening, *EHM´s beating frequency*, and *EHM's contraction period* parameters that increased throughout time (**Supplementary Figure 3**). Regarding the "viral treatment" effect per se, no differences were observed in *EHM's Beating Frequency* and *EHM's Base Pole Distance* parameters. However, both *EHM's shortening* and *EHM's contraction period* parameters displayed statistically significant differences between viral treatments. In *EHM's shortening* condition A, values were drastically affected by the presence of both AAV6 and lentivirus, while in condition B there was an improvement in contraction capacity and an approximation to control values (condition C) throughout time. Another indicator of substantial contraction impairment in condition A was the low values on *EHM's contraction period* parameter compared to conditions B and C (control). Altogether, optical measurements analyses suggested that both AAV6 and lentivirus used on the Cre-LoxP system compromised EHM's contractile function.

CFP$^+$ IPSCs-CMs release EVs enriched in mRNA Cre that is functional in recipient cells in 2D

Our hypothesis proposed to investigate intercellular EV transfer (namely from cardiomyocytes to non-myocyte cells), a hallmark of cardiac communication, by using the Cre-LoxP system. To this end, after AAV6 infection, iPSCs-CMs conditioned medium was collected and EVs presented in the medium were isolated by the ultracentrifugation method. Results revealed that EVs carried *Cre mRNA* (**Figure 4A**), as shown by the presence of a dark band on CFP$^+$ iPSCs-CMs and the absence of any band on the control condition. Thus, PCR analysis of isolated EVs indicated that *Cre mRNA* particles are incorporated into EVs and released by CFP$^+$ iPSCs-CMs.

Next, we intended to determine if Cre$^+$ EVs are uptake and functionally active in the recipient cells. For that DsRed$^+$ iPSCs-SCs and DsRed$^+$ iPSCs-ECs were incubated with Cre$^+$ EVs, or alternatively CFP$^+$ cardiomyocyte conditioned medium. After 6 days of treatment, eGFP$^+$ cells were found in both DsRed$^+$ iPSCs-SCs and DsRed$^+$ iPSCs-ECs conditions (**Figura 4B and C**). Interestingly, iPSC-SCs showed a fast response to both Cre$^+$ EVs and conditioned medium, within two days of treatment DsRed$^+$ cells turn into eGFP$^+$ cells, but, treatment with CFP$^+$ iPSCs-CMs conditioned media showed fewer GFP$^+$ cells when compared to EVs only condition.

In opposition, only a few DsRed$^+$ iPSCs-ECs became eGFP$^+$ and this turnover was observed after five days of EV treatment but no eGFP$^+$ cells were detected in the "CFP$^+$ cardiomyocyte conditioned media" condition (**Figure 4B and C**). While iPSCs-SCs manifested only one color at the same time: red (DsRed$^+$) or green (eGFP$^+$), an iPSC-EC could simultaneously express DsRed$^+$ and eGFP$^+$, proposing a slower degradation of DsRed$^+$ signal (**Figure 4B and C**). Importantly, eGFP$^+$ cell number increased throughout this experiment, denoting that after color switch, eGFP$^+$ cells can multiply and thus increase eGFP$^+$ cells number without occurring "DsRed to eGFP" turnover.

These results confirmed that Cre$^+$ EVs were indeed incorporated in recipient cells and corroborated our hypothesis that *Cre mRNA* was translated into protein and became functionally active in these cells leading to a color shift in the recipient cell. Hence, cardiac EV transfer can be reported by the Cre-LoxP system in 2D.

CFP$^+$ IPSCs-CMs release EVs enriched in mRNA Cre that is functional in recipient cells in 3D

Next, to confirm that the observed color shift mediated by the Cre-LoxP system in 2D was also valid in 3D, we employed the EHM model composed of iPSCs-CMs and iPSCs- SCs (EHM-1) and evaluated color switch in three different conditions (A, B and C). Condition A was constituted of AAV6-CFP iPSCs-CMs and lentivirus-DsRed iPSCs-SCs, condition B was composed of control iPSCs-CMs and lentivirus-DsRed iPSCs-SCs and condition C was composed of control iPSCs-CMs and control iPSCs-SCs. After 21 days, transduced cells were visualized in an EHM 3D structure (**Figure 5A**). EHMs from condition A expressed both DsRed and CFP proteins, while EHMs from condition B only expressed DsRed, and condition C's EHMs were negative for both fluorescence proteins (**Figure 5A**). Due to spectral overlap, the potential presence of eGFP$^+$ cells could not be distinguished in stereoscopic pictures of the EHM.

To detect and quantify the number of eGFP$^+$ cells within the EHM, single cells from EHM were isolated by enzymatic digestion and analyzed by flow cytometry of live cells. Results belonging to condition A showed that 67.6% of total live cells expressed CFP$^+$, which identified iPSCs-CMs, whereas DsRed$^+$ cells represented 23.8% of the live cell population, identifying iPSCs-SCs (**Figure 5B**). Notably, the iPSCs-CMs and iPSCs-SCs values obtained by FACS, were similar to the 70%/30% ratio of iPSCs-CMs/ iPSCs-SCs used upon EHM casting, suggesting that the number of cells was not greatly altered after 3 weeks of EHM culture. To determine the percentage of eGFP$^+$ cells, we excluded the CFP$^+$ population to avoid spectral overlap. In brief, gating for total cells was used by side and forward scatter indicating granularity and size (complexity) (P1), followed by live-cell selection by SYTOX red, a dead cell stain, and gating for forward scatter and Allophycocyanin-APC (far-red, P2). Then CFP$^+$ iPSCs-CMs (P3) were identified by using Alexa Fluor 700 (infra-red) versus Pacific-blue (CFP$^+$) while iPSCs-SCs DsRed$^+$ were detected by selecting (P5) on Phycoerythrin-PE versus Fluorescein isothiocyanate-FITC of the non-CM population. Finally, PE vs FICT was used to identify non-cardiomyocytes double-positive cells (P4). This gating strategy showed that 2.7% of cells non- iPSCs-CMs population was double-positive (DsRed$^+$/eGFP$^+$) implying that Cre-LoxP system worked in a cardiac 3D model, particularly, in EHM model constituted of iPSCs-CMs/ iPSCs-SCs (**Figure 5B**). Additionally, neither double-positive cells (DsRed$^+$/eGFP$^+$) were observed in condition B nor in condition C (data not shown).

In conclusion, the Cre-LoxP recombination system could track EV transfer and promote color switch in 3D EHMs.

Figure 4.

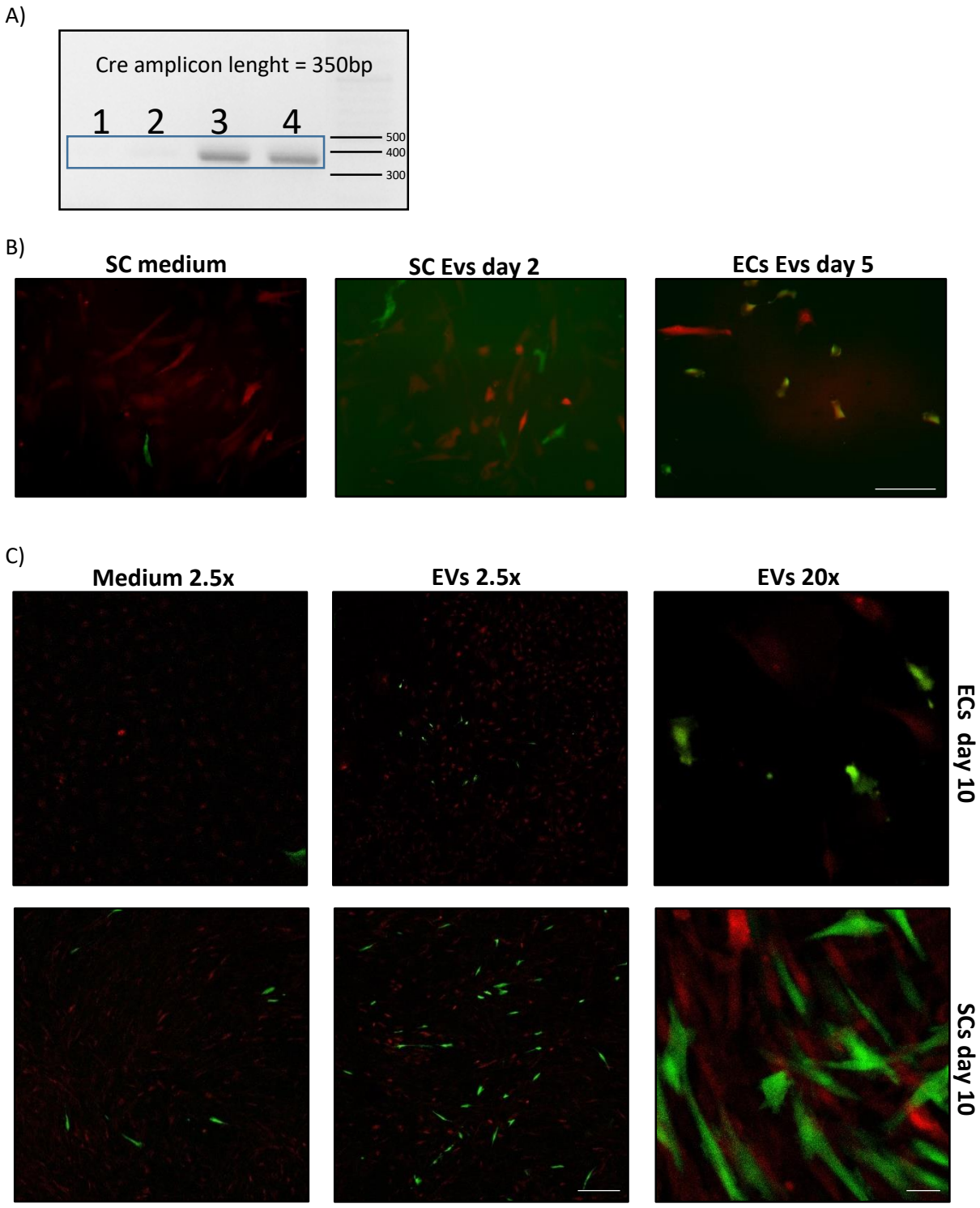

Figure 4. CFP⁺ IPSCs-CMs release exosomes enriched in Cre mRNA that induce color switch in recipient cells. A. *RT-PCR for Cre mRNA of EVs isolated from control iPSC-CMs conditioned media (1 and 2) and EVs isolated from CFP⁺ iPSC-CMs conditioned media (3 and 4). Dark bands at 350bp indicate amplification product of Cre mRNA.* ***B****. Illustrative images highlighting the first day eGFP (green) was detected on DsRed⁺ (red) cells. iPSCs-SCs treated with cardiomyocyte conditioned media (left), iPSCs-SCs treated with EVs (middle) and iPSCs-ECs treated with EVs****. Images were acquired with a 10x magnification. Scale Bar= 50mm* ***C.*** *Representative pictures of DsRed⁺ cells at day 10 after treatment with iPSC-CMs conditioned media or EVs. Images were acquired with a 2.5x or 20x magnification, respectively. Scale Bar=500 µm (2.5x) and 50µm (20x).*

Figure 5.

A)

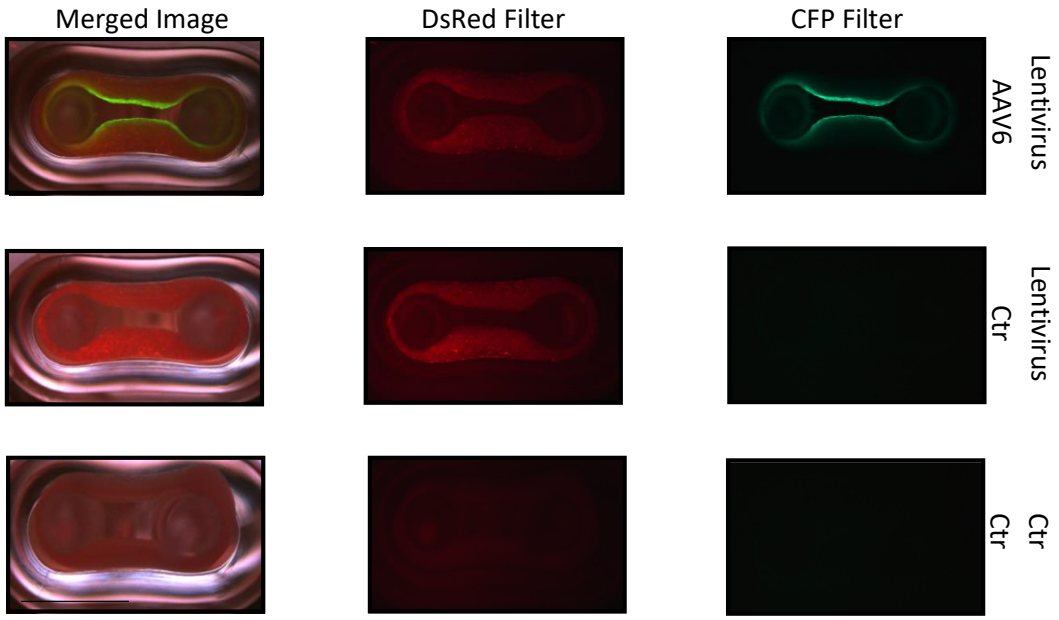
Merged Image
DsRed Filter
CFP Filter
Lentivirus AAV6
Lentivirus Ctr
Ctr Ctr

B)

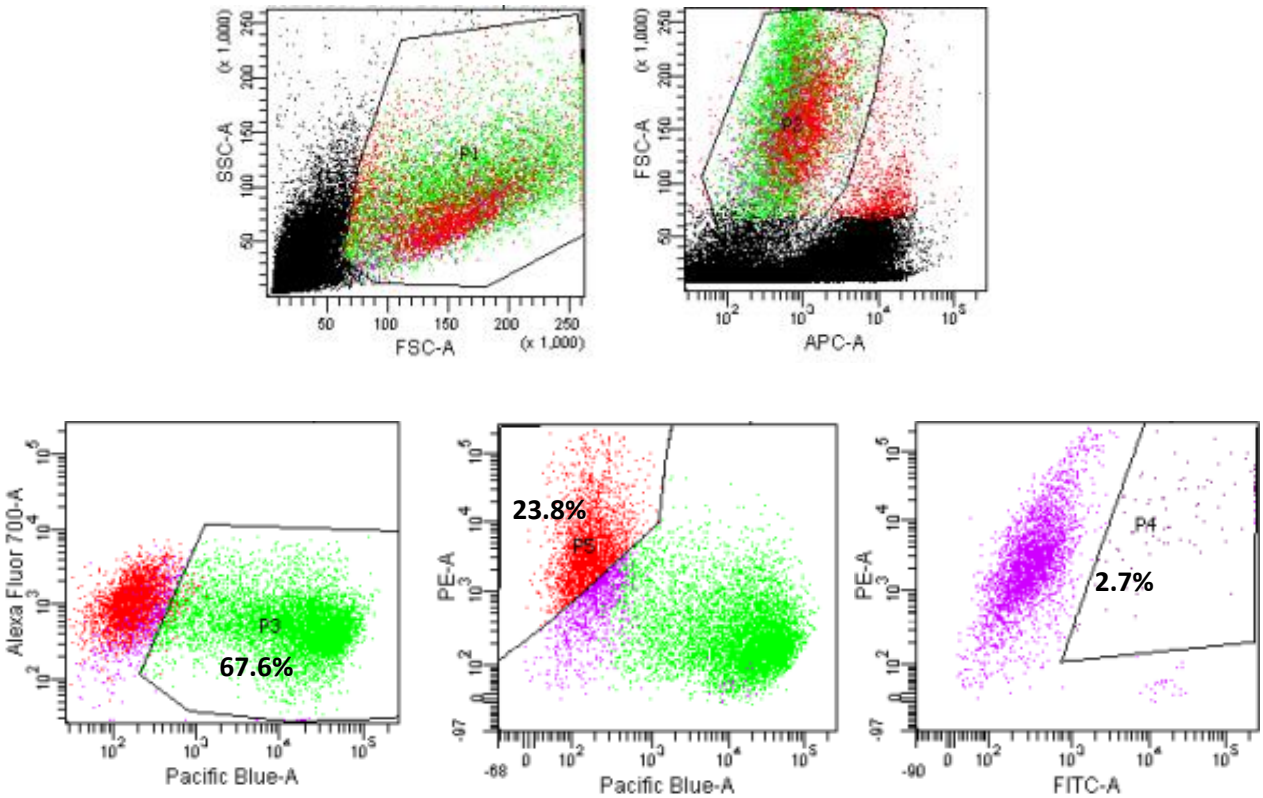
SSC-A
FSC-A
P1
FSC-A
APC-A
P2
Alexa Fluor 700-A
Pacific Blue-A
P3
67.6%
PE-A
Pacific Blue-A
23.8%
P5
PE-A
FITC-A
P4
2.7%

Figure 5. (Previous page) Cre-LoxP system is functional in 3D model A. *Representative images of EHMs composed of AAV6-CFP iPSCs-CMs and Lentivirus-DsRed iPSCs-SCs (top-condition A), control iPSCs-CMs and Lentivirus-DsRed iPSCs-SCs (middle-condition B) or control iPSCs-CMs and control iPSCs-SCs (bottow-condition C), under Brightfield merged with DsRed Filter and CFP Filter (right), only DsRed Filter (middle) and only CFP filter (left)* ***B.*** *Illustrative FACS plots of separated cells derived from EHM condition A (at day 23). P1 and P2 correspond to live cells after size and metabolic exclusion, P3 green population identifies CFP expressing iPSCs-CMs population, P4 purple population represents eGFP and DsRed^{+} (iPSCs-SCs) cells and P5 red population identifies DsRed^{+} cells (iPSCs-SCs). Scale bar EHMs= 2.5mm*

Discussion

Cardiac communication is essential to maintain cardiac homeostasis and function. CVDs are associated with altered cardiac communication, namely through EVs [12]. In recent years, EVs have shown tremendous potential in CVDs, both as biomarkers, therapeutic targets, or even drug delivery tools [13]. Before cardiac EVs reach a clinical setting, it is important to monitor EVs transfer; however, methods tracing endogenous cardiac EVs are needed. Here, we proposed a new method based on the Cre-LoxP system to trace endogenous cardiac EVs in a 3D human myocardium model.

In brief, the Cre-LoxP recombination system relied on two viral constructs, the first construct (AAV6-CFP-Cre, EV-donor) was infected into host cells (iPSCs-CMs) which promoted the expression of CFP and the release of Cre-enriched EVs. These EVs induced a color switch on recipient cells (iPSCs-SCs), previously infected with the second construct (EV-reporter construct: LoxP-DsRed-stop-codon-LoxP-eGFP), allowing the excision between LoxP sites by Cre, the removal of DsRed-stop-codon, and thereby, the expression of eGFP (**Figure 1**). Cre-LoxP recombination system is particularly attractive since its rationale avoided external manipulation of EVs and thus granted the study of endogenous EV cardiac population.

Viral transduction was optimized in different cell types in 2D; unfortunately, when converted to 3D, ADV was revealed to be unsuitable for our study. As a result, ADV was replaced by lentivirus encoding the EV-reporter. Similarly, we began our study focused on iPSCs-ECs, however, EHM comprising iPSCs-ECs still needed optimization, subsequently, iPSCs-ECs were excluded from our 3D pilot study, but expectantly, they will be again the focus of our research after the optimization step is achieved.

We were able to prove Evs' interaction in both 2D and 3D *in vitro* models and with different cell types. However, in 2D, different responses of iPSCs-SCs and iPSCs-ECs were observed upon exposure to Cre^+ EVs, but, the reasons underlying these behaviors are still to be investigated. It could be hypothesized that iPSCs-ECs are less susceptible to infection and EVs absorption. Another hypothesis is that iPSCs-CMs-derived EVs have a higher affinity for iPSCs-SCs than iPSCs-ECs and, therefore, are also more easily uptake by iPSCs-SCs.

In contrast to what was observed in 2D, only a small percentage of the iPSCs-SCs population switches color and uptakes Cre^+ EVs derived from iPSCs-CMs, possibly indicating that, despite cardiac communication occurring through EV transfer, in EHMs this communication may be altered. Results could also imply that after EHM assembly, cells may have their metabolism decreased as well as their cell cycle arrested, but, it is also possible that EHM collagen-based matrix interfered with EVs transfer and other alternative mechanisms are used for cardiac communication. Moreover, the intrinsic features of EHM as collagen gel may interfere with cell membrane properties, a possible change in cell cycle metabolism, which was previously reported in [22]. Nevertheless, the EHM model may benefit from an "arrested cell cycle", since it decreases the number of false-positive obtained in 2D, where $eGFP^+$ cell clones may be observed and consequently, hides a proper "DsRed to eGFP" turnover and associated EV transfer. Akin, viruses' influence on EHM contractile should not be overlooked, Cre LoxP system is suboptimal, and if possible Cre-LoxP system should be avoided in studies that seek to compare the effect of different EVs on cardiac contractile function.

Given the exploratory nature of this chapter, it was not possible to perform all the required experiments to draw solid conclusions, we will next formulate future perspectives of this study.

An important aspect of this study is to characterize EVs from EHMs exposed to HF and control conditions following ISEV guidelines and elaborating on EV size, number, membrane markers, membrane potential, structure, density, and other properties. The content of EVs, particularly, their miRnome is especially important and needs to be investigated, thus Evs' miRnome is currently under analysis in our lab.

Rather than just mimicking HF on EHMs, it would be interesting to research on EHMs composed of iPSCs-CMs or iPSCs-SCs derived CVD patients (e.g. HF patients) and assess whether cardiac communication is altered in these patients.

Based on our data, it is possible to speculate if iPSCs-CMs derived EVs are preferentially incorporated into specific cell types compared to others and if this preference is shifted or maintained upon HF conditions.

In conclusion, our results are the first step toward detecting and dissecting cardiac communication by EV transfer in a 3D model. Both the Cre-loxP recombination system and the EHM model are exciting tools for studying cardiac communication and EV transfer, thus, they may help to find new therapeutic and diagnostic approaches to HF.

Supplementary Figure 1.

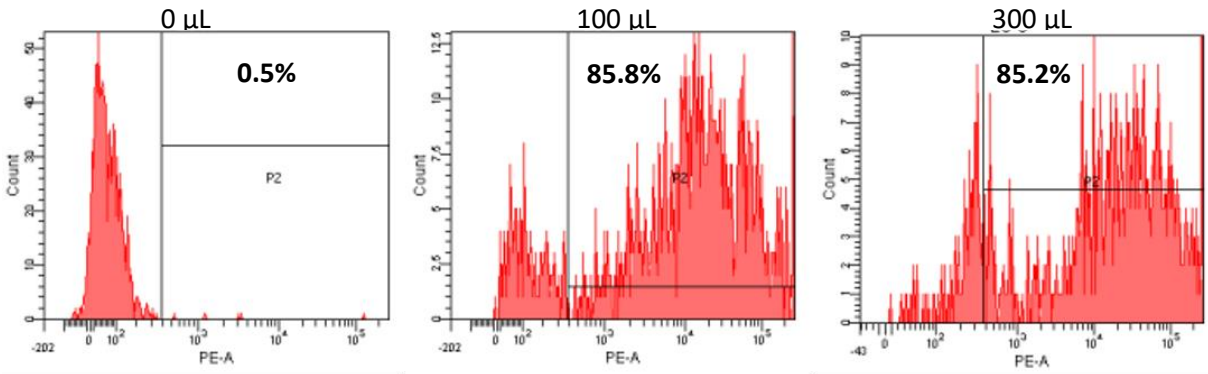

Supplementary Figure 1. *Illustrative FACS plots of hiPSCs-ECs of control (EC-A), ADV transduced with 100uL (EC-B) or 300uL (EC-C). P2 population indicates the percentage of DsRed⁺ cells.*

Supplementary Figure 2.

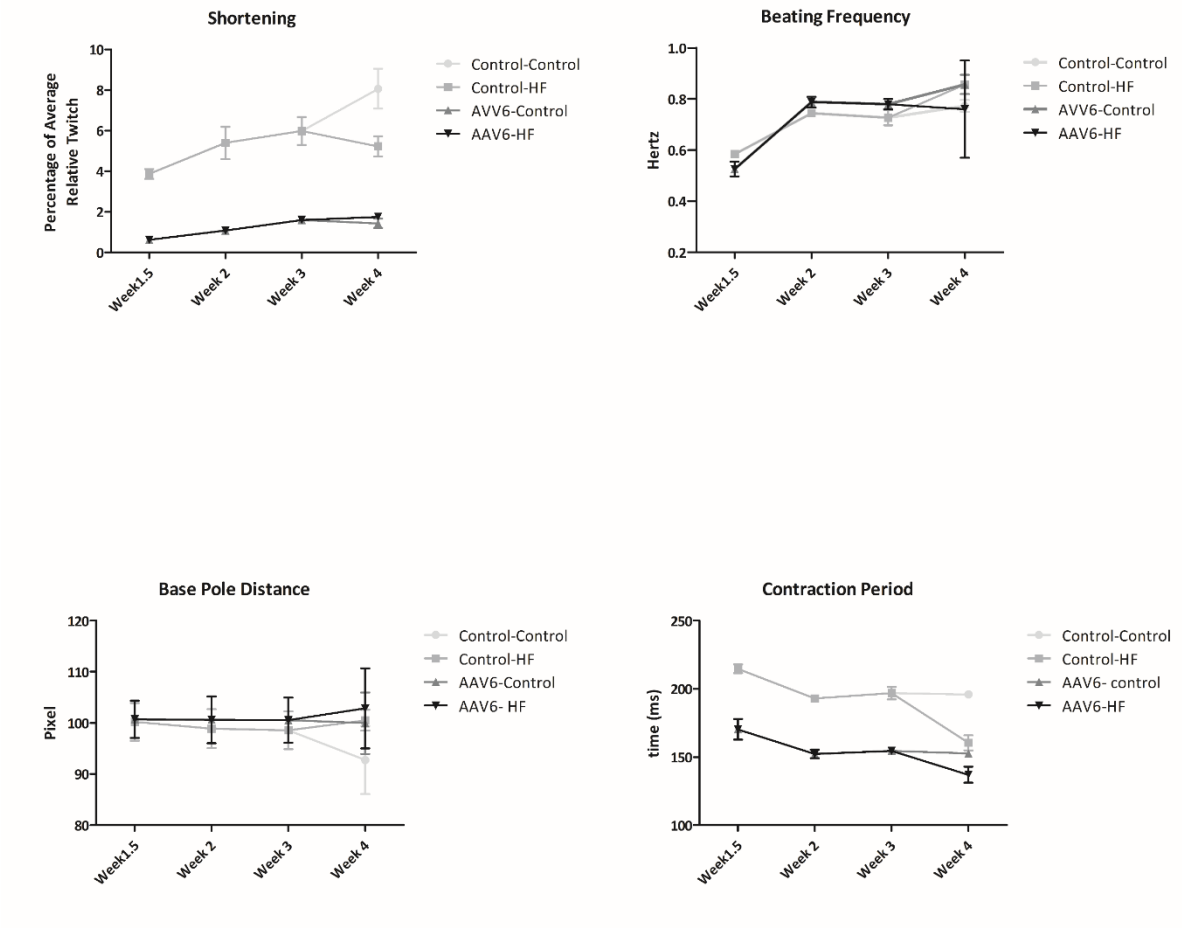

Supplementary Figure 2. (Previous page) *Graphs illustrating EHM contractile function including parameters of EHM's shortening, EHM's beating frequency, EHM's base pole distance and EHM's contraction period. Light grey circles and grey squares correspond to EHMs composed of non-infected (control) iPSCs-CMs exposed to control medium or heart failure medium, respectively. While dark grey triangles and black inverted triangles correspond to AAV6 infected iPSCs-CMs exposed to control medium or heart failure medium, respectively. n=2-6*

Supplementary Figure 3.

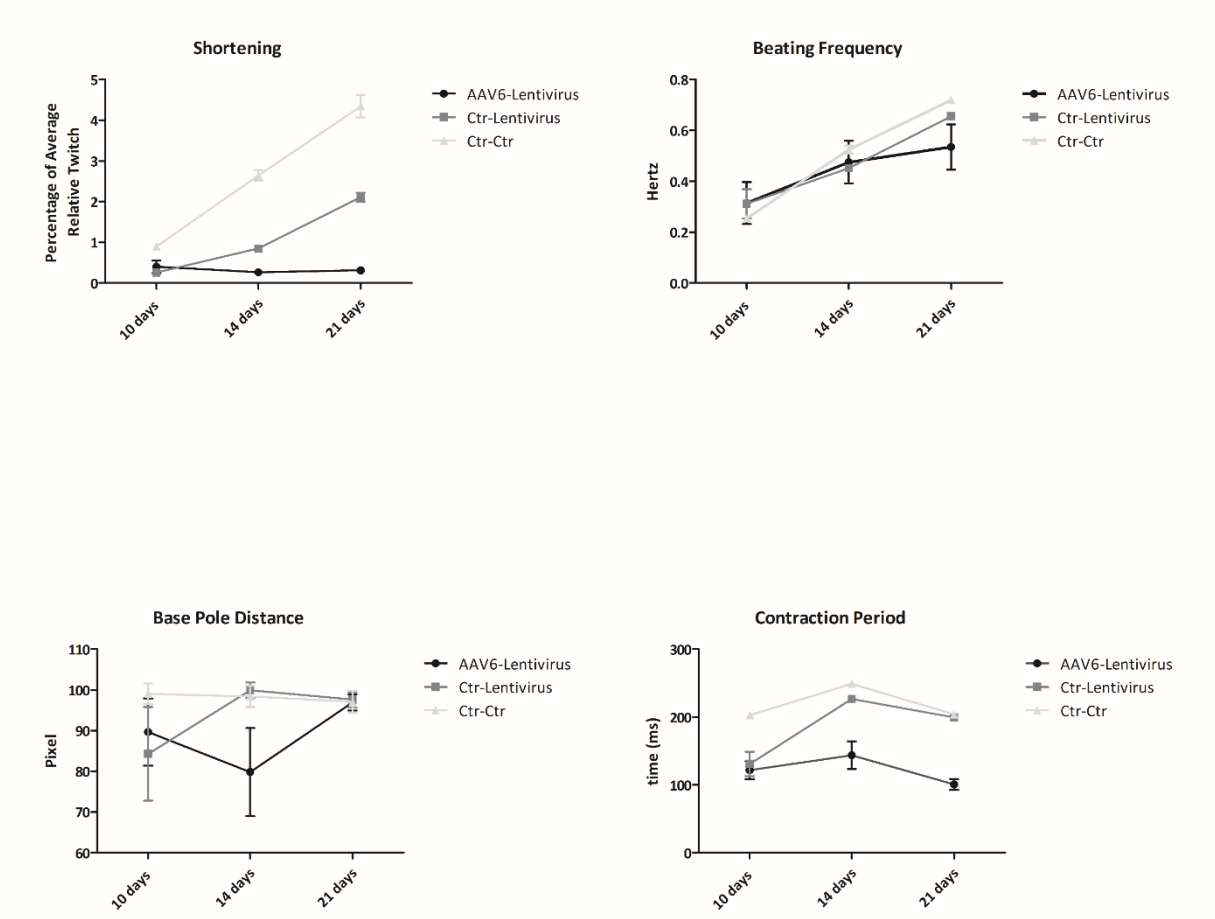

Supplementary Figure 3*. Graphs illustrating EHM contractile function including parameters of EHM's shortening, EHM's beating frequency, EHM's base pole distance and EHM's contraction period. Black circles, dark grey squares and light grey triangles correspond to EHMs composed of AAV6-CFP iPSCs-CMs and Lentivirus-DsRed iPSCs-SCs, control iPSCs-CMs and Lentivirus-DsRed iPSCs-SCs or control iPSCs-CMs and control iPSCs-SCs, respectively. Results are represented mean+SEM, two-way ANOVA, *p<0.05 relative to control (condition C), n=11-12 per group.*

References

1. Pinto, A.R., et al., *Revisiting Cardiac Cellular Composition.* Circ Res, 2016. **118**(3): p. 400-9.
2. Litvinukova, M., et al., *Cells of the adult human heart.* Nature, 2020. **588**(7838): p. 466-472.
3. Raposo, G. and W. Stoorvogel, *Extracellular vesicles: exosomes, microvesicles, and friends.* J Cell Biol, 2013. **200**(4): p. 373-83.
4. Berumen Sanchez, G., et al., *Extracellular vesicles: mediators of intercellular communication in tissue injury and disease.* Cell Commun Signal, 2021. **19**(1): p. 104.
5. Andreu, Z. and M. Yanez-Mo, *Tetraspanins in extracellular vesicle formation and function.* Front Immunol, 2014. **5**: p. 442.
6. Elsherbini, A. and E. Bieberich, *Ceramide and Exosomes: A Novel Target in Cancer Biology and Therapy.* Adv Cancer Res, 2018. **140**: p. 121-154.
7. Colombo, F., et al., *Cytokines Stimulate the Release of Microvesicles from Myeloid Cells Independently from the P2X7 Receptor/Acid Sphingomyelinase Pathway.* Front Immunol, 2018. **9**: p. 204.
8. Stahl, A.L., et al., *Exosomes and microvesicles in normal physiology, pathophysiology, and renal diseases.* Pediatr Nephrol, 2019. **34**(1): p. 11-30.
9. Tricarico, C., J. Clancy, and C. D'Souza-Schorey, *Biology and biogenesis of shed microvesicles.* Small GTPases, 2017. **8**(4): p. 220-232.
10. Doyle, L.M. and M.Z. Wang, *Overview of Extracellular Vesicles, Their Origin, Composition, Purpose, and Methods for Exosome Isolation and Analysis.* Cells, 2019. **8**(7).
11. Wei, H., et al., *Regulation of exosome production and cargo sorting.* Int J Biol Sci, 2021. **17**(1): p. 163-177.
12. Videira, R.F. and P.A. da Costa Martins, *Non-coding RNAs in Cardiac Intercellular Communication.* Front Physiol, 2020. **11**: p. 738.
13. de Abreu, R.C., et al., *Native and bioengineered extracellular vesicles for cardiovascular therapeutics.* Nat Rev Cardiol, 2020. **17**(11): p. 685-697.
14. Saludas, L., et al., *Extracellular Vesicle-Based Therapeutics for Heart Repair.* Nanomaterials (Basel), 2021. **11**(3).
15. Kang, M., et al., *Biodistribution of extracellular vesicles following administration into animals: A systematic review.* J Extracell Vesicles, 2021. **10**(8): p. e12085.
16. Eitan, E., et al., *Impact of lysosome status on extracellular vesicle content and release.* Ageing Res Rev, 2016. **32**: p. 65-74.
17. Jantaree, P., et al., *From 3D Back to 2D Monolayer Stomach Organoids-on-a-Chip.* Trends Biotechnol, 2021. **39**(8): p. 745-748.
18. Stein, J.M., C.L. Mummery, and M. Bellin, *Engineered models of the human heart: Directions and challenges.* Stem Cell Reports, 2021. **16**(9): p. 2049-2057.
19. Meyer, T., M. Tiburcy, and W.H. Zimmermann, *Cardiac macrotissues-on-a-plate models for phenotypic drug screens.* Adv Drug Deliv Rev, 2019. **140**: p. 93-100.
20. Del Campo, C.V., et al., *Regenerative potential of epicardium-derived extracellular vesicles mediated by conserved miRNA transfer.* Cardiovasc Res, 2022. **118**(2): p. 597-611.
21. Tiburcy, M., et al., *Generation of Engineered Human Myocardium in a Multi-well Format.* STAR Protoc, 2020. **1**(1): p. 100032.
22. Tiburcy, M., et al., *Defined Engineered Human Myocardium With Advanced Maturation for Applications in Heart Failure Modeling and Repair.* Circulation, 2017. **135**(19): p. 1832-1847.

23. Zomer, A., et al., *In Vivo imaging reveals extracellular vesicle-mediated phenocopying of metastatic behavior.* Cell, 2015. **161**(5): p. 1046-1057.
24. Ramanujam, D., et al., *Viral Vector-Based Targeting of miR-21 in Cardiac Nonmyocyte Cells Reduces Pathologic Remodeling of the Heart.* Mol Ther, 2016. **24**(11): p. 1939-1948.
25. Chen, V.C., et al., *Development of a scalable suspension culture for cardiac differentiation from human pluripotent stem cells.* Stem Cell Res, 2015. **15**(2): p. 365-75.
26. Liu, X., et al., *Differentiation of functional endothelial cells from human induced pluripotent stem cells: A novel, highly efficient and cost effective method.* Differentiation, 2016. **92**(4): p. 225-236.
27. Thery, C., et al., *Isolation and characterization of exosomes from cell culture supernatants and biological fluids.* Curr Protoc Cell Biol, 2006. **Chapter 3**: p. Unit 3 22.

CHAPTER 7

“Summary and General Discussion”

The health system has been tremendously affected by COVID-19 and its associated deaths in the last years. Despite this, the nominator for one of the largest causes of death remains constant: cardiovascular diseases (CVDs). CVDs include a broad group of diseases that affect the heart and vessels that, when left untreated, can progress to heart failure (inability of the heart to pump enough blood) and eventually death.

The impact of Hand2 in RVF and LVF – different roads to the same destination

Heart failure (HF) is an end-stage of many CVDs, which are commonly divided HF into left ventricular (LVF) or right ventricular failure (RVF). The differences in LVF and RVF can be partly explained by each ventricle's intrinsic and specific characteristics, and their responses to damage are distinct, therefore requiring specific treatment. Despite RVF's severity, to date, studies on RVF are significantly less compared to LVF. RVF is a complex condition that requires accurate knowledge of its mechanisms and effective treatment. **Chapter 2** investigated the molecular mechanisms underlying RVF and studied the contribution of the transcription factor Hand2 to RV remodeling in response to pressure overload injury. Specific cardiac Hand2 depletion was associated with severe cardiac dysfunction under conditions of RV pressure overload. Hand2 depletion sensitized the RV to cardiac injury, as observed in animal models that developed more severe cardiac hypertrophy and dysfunction. Higher expression levels of HAND2 were also observed in RV samples from human heart samples of patients with pulmonary hypertension, usually associated with RVF. Although inhibition of Hand2 expression can prevent cardiac dysfunction under conditions of LV pressure overload, the same could not be valid for conditions of RV pressure overload. Hypertrophy is a common ground factor for both LV and RV responses to pressure overload. However, the pathways that activate and withstand hypertrophy may be different. Initially, pressure overload leads to calcineurin activation in both ventricles, but in LV, NFAT is dephosphorylated and translocates to the nucleus; it activates the expression of hypertrophic genes such as RCAN1.4 [23]. In the RV, it is suggested that myocyte enhancer factor 2 (MEF2) transcription factor is responsible to promote the transcription of hypertrophic genes [65].

Triggering the exact same injury in both ventricles might be challenging comparing previous work [1] with **Chapter 2**, different types of needles and time endpoints are used and thus, there is a possibility that the extent of injured LV and RV is different. Additionally, the baseline differences in pressure in the LV and RV may also explain the different responses to stress [2].

Other reports on humans with PAH, show that, initially, the ventricular pressure in RV leads to a stretch on the right ventricular wall followed by an increase in muscle mass. Sustained pressure overload is not supported by the RV as it cannot maintain an "adaptive hypertrophy" and will ultimately enter into a dilated phase [3, 4]. Later stages of the disease showed a decline of RV function and a decrease in RV stroke volume, but also a deformation of RV/LV septum, which is shifted towards the left, resulting in a reduction of LV filling volume and altogether contributes to decreased cardiac output [4, 5]. **Chapter 2** reported an increase in cardiac cell size and deterioration of RV function parameters but preserved cardiac output, suggesting that the used model did not reach an advanced disease stage like observed in severe PH, which is usually associated with RVF. Consequently, the results observed in **Chapter 2** are possibly valid for a mild form of RVF and PH. There is a possibility that Hand2 has different roles and significances during the different stages of PH and RVF. Nevertheless, the results of Chapter 2 suggested that there are multiple pathways to HF and also multiple pathways to avoid HF, remarking the importance of looking at HF both as a whole and individually at RVF and LVF.

MicroRNAs and EVs as Mirrors of Cardiac Condition

Rescuing the heart from HF is now possible by inducing reverse remodeling (RR) through cardiac therapy and medical treatments [6]. MicroRNAs (miRs) are a class of small non-coding RNAs found both in cellular and extracellular spaces. Due to their ability to mirror cardiac conditions, they have recently emerged as potential therapeutic tools and biomarkers [7]. MiR expression is altered during cardiac pathological conditions and identification of miR expression profiles within extracellular fluids could potentially facilitate CVDs' diagnosis [8-10]. Moreover, circulating miRs are an attractive class of potential biomarkers owing to their high abundance and stability in the blood and other biologic fluids [11]. The intrinsic complexity of CVDs and their diverse mechanisms toward pathological conditions limit the use of a single biomarker for a correct diagnosis. To understand the current position of miRs and other non-coding RNAs **Chapter 3** summarized up-to-date research on the use of ncRNAs, including miRs, in human blood, plasma, and serum samples as biomarkers of CVDs, also discussing their weaknesses and potential. Many papers described a direct association between miR expression profiles and CVDs, including aortic-related diseases, myocardial infarction, right ventricle dysfunction, and also cardiac RR, with some ncRNAs such as muscle-specific miR-1 and lncRNA HOTAIR being reported in different CVDs [12-17]. However, several obstacles should be overcome, namely the small sample size of the study, with some possible cofounders associated (region, ethnicity, age, sex) and short-term follow-up, which might contribute to the general lack of reproducibility [18]. There is still a long road until miRs eventually reach clinical practice. While **Chapter 3** reviewed and concluded on the potential of miRs as biomarkers of CVDs, and their ability to mirror the cardiac condition, it did not critically assess the origin of these miRs. This gap was filled by **Chapter 5**, which reported on the source, vehicle, and destination cell of ncRNAs, including miRs, upon cardiac pathological remodeling. **Chapter 5** reviewed the current research on the role of ncRNAs in intercellular communication that use extracellular vesicles (EVs) as vehicles. EVs are double-layer vesicles secreted by cells to mediate intercellular communication [19] and may help maintain cardiac homeostasis. EVs transport cargo as ncRNAs coming from the host cell and may be functionally active on target cells. When the cardiac injury occurs, EV ncRNAs expression is altered and EVs-ncRNAs can act on recipient cells to promote remodeling processes such as cardiac hypertrophy, fibrosis, capillary rarefaction, inflammation, and others, leading to heart failure [20-23]. Therefore, modifications on EV ncRNA content contribute to and reflect the current cardiac condition. It has been suggested that modulation of ncRNAs can successfully prevent and even reverse cardiac maladaptive remodeling, however, so far, miR-122 is the only ncRNA that has reached a phase II clinical trial [24]. These findings highlight that pathological conditions imply complex crosstalk between different cell types extensively mediated by EVs. Analysis of the miR content of EVs or even miRs alone can contribute to understanding the heart condition at a specific time point.

MicroRNAs as Biomarkers for Reverse Remodeling in Aortic Stenosis -a dead-end road

MiRs have a pivotal role in regulating gene expression at a post-transcriptional level, but a new door was opened after discovering miRs in extracellular fluids namely plasma and serum [11]. Their features are particularly attractive due to the easy and minimally-invasive access to body fluids and rapid identification. Furthermore, extracellular miRs are remarkably stable in body fluids and, as previously discussed, they acutely mirror the present cardiac condition. The reason underlying miRs stability is still unknown; however, it is hypothesized that they are resistant to RNase A activity due to either EV encapsulation, being bound to high-density lipoprotein (HDL), or complexed with the AGO protein family [11]. Despite cardiac symptoms and the available biomarkers such as natriuretic peptides and troponins may indicate pathological cardiac conditions, more specific and sensitive

markers are still urgently needed [25]. In this regard, **Chapter 3** demonstrated that miRs are promising biomarkers and may increase the diagnostic capacity of cardiac pathological conditions if combined with other factors. Not only CVDs are associated with changes in miR levels but medical interventions, including aortic valve replacement (AVR), manifested alterations in miR expression profiles [26, 27]. Therefore, miRs have proven to be of diagnostic and prognostic value, possibly helping to predict the outcome (and consequently the type of RR) of a cardiac intervention such as AVR. Simultaneously, it has been observed that patients respond differently to therapy and it is necessary to predict the outcome of RR to improve the time of intervention, thus, aiming for personalized medicine strategies [6]. **Chapter 4** focused on identifying the expression of plasma miRs that emerged as potential biomarkers of complete RR after AVR surgery in a case study of a Portuguese sample. MiR-133a-3p and let-7b-3p were found significantly decreased in plasma samples from patients with incomplete RR (patients who do not show improvement in cardiac function and an unfavorable clinical response) compared with patients with complete RR (patients with recovered cardiac function). Qualitatively, the diagnostic accuracy of let-7b-3p is "very good", while miR-133a-3p is rated "excellent". Thus, our data suggested miR-133a-3p and let-7b-3p as potentially good biomarkers of complete RR after AVR surgery. Previously, miR-133a was also reported by *Nistal et al*. as a good predictor of LV RR after AVR in patients with aortic stenosis, which corroborates our results [27]. Our results also suggested that let-7b-3p could potentially be a new marker to recognize the RR type of remodeling and identify patients who benefit from SAVR. Given the exploratory nature of this project, the results obtained were not sufficient to recommend the use of miR-133a-3p and let-7b-3p in clinical practice but are strongly suggested to be further tested in larger cohorts. Despite the large potential of miRs to be used as biomarkers tools not only for CVD diagnosis but also prognosis, the standardization of plasma collection (fasting vs postprandial status, current sickness, physical activity) and storage (time and temperature) remains important, as well as miR isolation and detection methods. While no clinical trials with the appropriate study designs and strict timepoints to reach reproducible results are made, miRs will not reach clinical practice and continue on this “dead end” road that was reached years ago.

The Cre Lox-P system- a new road to track EVs in a 3D model

Increasing evidence has placed EVs at the center of CVDs since they have a significant role in mediating intercellular communication and, consequently, maintaining cardiac physiology [28, 29]. EVs are secreted from numerous cardiac cell types and alteration in their content or route could have a tremendous impact on heart homeostasis. Recent preclinical work on the ischemic heart using EVs as therapeutic tools generated promising results at a preclinical stage [30]. Some EV-based treatments evolved and are now at a clinical trial stage [31]. However, most current studies of EVs are based on the isolation of vesicles from cell cultures and therefore do not truly mimic the physiology of the human heart while retaining track of EVs behavior. Hence tracking EVs in a cardiac context is crucial to gain insights into their intricate biogenesis, release, biodistribution, timing, and trafficking. To better understand these aspects of EV biology, in **Chapter 6,** we proposed a new viral method using a 3D modified cardiac muscle-engineered human myocardium (EHM) model to monitor the intercellular transfer of vesicles by color change in recipient cells. The Cre-LoxP method uses two viral constructs previously reported by *Zommer et al*. [32] to help visualize how cardiomyocyte-derived EV-mediated cellular transfer occurs. An adeno-associated virus 6 (AAV6) harboring a cyan fluorescence reporter protein (CFP) and Cre 25nt that indicates cell secretion via EVs and a lentivirus harboring the reporter protein DsRed immediately followed by a stop codon, flanked by two Lox P sites and followed by an enhanced green fluorescence protein (eGFP) were used. Upon EV release by cardiomyocytes, recipient cells, namely stromal cells, can incorporate EV cargo, specifically the *Cre* recombinase. If EV cargo is

functionally active, recombination occurs and a change of color from red to green will be observed in recipient cells. Results reported in **Chapter 6** suggested that this Cre-LoxP method works in the cardiac context and could be a pilot proof towards a more complex *in vivo* EV tracking in the heart. It also elucidated whether up EVs cargo is guided to degradation by the endolysosomal system or if cargo is functionally active on recipient cells. The use of EHM allows the study of EVs transfer in a "human" HF setting and, therefore, contributes to understanding how cardiac communication via EVs is altered under HF conditions, particularly the miR composition within EVs. Since EHMs are composed of different types of cells, such as cardiomyocytes and stromal cells, the study of EVs using the EHM HF model facilitates research on how HF can compromise cardiac function, namely through cardiac fibrosis and cardiac hypertrophy, limiting events for cardiac recovery and RR. These findings could be further used to investigate the role of miRs on cardiac pathological remodeling. Simultaneously, the use of different cell types on EHM elucidates the uptake affinity of cardiomyocyte-derived EVs by different cell types. At last, **Chapter 6** described whether promising models such as EHMs can be used to study EV cardiac communication. Despite the preliminary nature of these data, the results obtained are very encouraging to continue more research based on the Cre-LoxP method beyond EHMs, perhaps *in vivo*, and use EHMs as a systematic model to study EVs transfer. Overall, we present a new tracking method for cardiac EVs biodistribution and understanding of their fluctuation throughout time according to different pathologies.

Challenges and Future Perspectives:

CVDs comprise a diverse group of cardiac pathologies and, it is important to perceive them as complex processes. The lack of efficient treatments for CVDs might be partially explained by our limited understanding of the mechanisms driving HF, often looked at by the effect of a "tunnel vision". Although relevant, the findings in this thesis may suffer from several limitations. In **Chapter 2** we used mice models that although currently accepted and used in basic cardiac science, still lack human translation. In contrast, in **Chapter 6**, we employed a human model. However, since it is an *in vitro* model composed of a hydrogel matrix, it cannot precisely recapitulate the human cardiac environment. Another major challenge presented in **Chapter 4** is the absence of direct evidence that the circulating miRs were initially released from cardiac cells. Transversal to all chapters, there are constraints on research design or methodology, for example, the low number of subjects. However, even the smallest progress in basic science may contribute to advances in clinical treatments. Being so, advances in plasma miR profiling and their use in clinical practice before mechanical interventions, as suggested in **Chapter 4**, may lead to personalized patient profiles and therefore, allow more targeted treatments. Moreover, this study reported the tracking of cardiac endogenous EVs by using the Cre-LoxP recombination system, a method that does not modify either EVs' biogenesis or morphology. EVs have tremendous potential in CVDs as biomarkers, therapeutic targets, and drug-delivery tools; therefore, it is crucial to understand the endogenous behavior of EVs but also standardize EVs isolation protocols, EVs administration routes, and EVs concentrations.

With this thesis, we worked on exploring the complexity of pathological cardiac remodelling at multiple levels ranging from basic mechanisms to diagnostic tools.

References

1. Dirkx, E., et al., *Nfat and miR-25 cooperate to reactivate the transcription factor Hand2 in heart failure.* Nat Cell Biol, 2013. **15**(11): p. 1282-93.
2. Friedberg, M.K. and A.N. Redington, *Right versus left ventricular failure: differences, similarities, and interactions.* Circulation, 2014. **129**(9): p. 1033-44.
3. Bogaard, H.J., et al., *The right ventricle under pressure: cellular and molecular mechanisms of right-heart failure in pulmonary hypertension.* Chest, 2009. **135**(3): p. 794-804.
4. Vonk Noordegraaf, A. and N. Galie, *The role of the right ventricle in pulmonary arterial hypertension.* Eur Respir Rev, 2011. **20**(122): p. 243-53.
5. Vonk-Noordegraaf, A., et al., *Interventricular mechanical asynchrony due to right ventricular pressure overload in pulmonary hypertension plays an important role in impaired left ventricular filling.* Chest, 2005. **128**(6 Suppl): p. 628S-630S.
6. Allen, C.J., et al., *Baseline NT-proBNP Accurately Predicts Symptom Response to Transcatheter Aortic Valve Implantation.* J Am Heart Assoc, 2020. **9**(23): p. e017574.
7. Cortez, M.A. and G.A. Calin, *MicroRNA identification in plasma and serum: a new tool to diagnose and monitor diseases.* Expert Opin Biol Ther, 2009. **9**(6): p. 703-711.
8. Fabiani, I., et al., *MicroRNAs distribution in different phenotypes of Aortic Stenosis.* Sci Rep, 2018. **8**(1): p. 9953.
9. Beaumont, J., et al., *MicroRNA-19b is a potential biomarker of increased myocardial collagen cross-linking in patients with aortic stenosis and heart failure.* Sci Rep, 2017. **7**: p. 40696.
10. Wang, W., et al., *Plasma miR-208b and miR-499: Potential Biomarkers for Severity of Coronary Artery Disease.* Dis Markers, 2019. **2019**: p. 9842427.
11. Sohel, M.H., *Extracellular/Circulating MicroRNAs: Release Mechanisms, Functions and Challenges.* Achievements in the Life Sciences, 2016. **10** p. 175–186.
12. Chen, Z., et al., *Circulating level of miR-378 predicts left ventricular hypertrophy in patients with aortic stenosis.* PLoS One, 2014. **9**(8): p. e105702.
13. Zhang, R., et al., *Elevated plasma microRNA-1 predicts heart failure after acute myocardial infarction.* Int J Cardiol, 2013. **166**(1): p. 259-60.
14. Wei, C., et al., *Circulating miRNAs as potential marker for pulmonary hypertension.* PLoS One, 2013. **8**(5): p. e64396.
15. Avazpour, N., et al., *Circulating HOTAIR RNA Is Potentially Up-regulated in Coronary Artery Disease.* Genomics Inform, 2018. **16**(4): p. e25.
16. Jiang, Y., et al., *HOTAIR Is a Potential Novel Biomarker in Patients with Congenital Heart Diseases.* Biomed Res Int, 2018. **2018**: p. 2850657.
17. Gao, L., et al., *Circulating Long Noncoding RNA HOTAIR is an Essential Mediator of Acute Myocardial Infarction.* Cell Physiol Biochem, 2017. **44**(4): p. 1497-1508.
18. Garcia, R., et al., *Sex-Specific Regulation of miR-29b in the Myocardium Under Pressure Overload is Associated with Differential Molecular, Structural and Functional Remodeling Patterns in Mice and Patients with Aortic Stenosis.* Cells, 2020. **9**(4).
19. Raposo, G. and W. Stoorvogel, *Extracellular vesicles: exosomes, microvesicles, and friends.* J Cell Biol, 2013. **200**(4): p. 373-83.
20. Fish, J.E., et al., *miR-126 regulates angiogenic signaling and vascular integrity.* Dev Cell, 2008. **15**(2): p. 272-84.

21. Zhao, J., et al., *Mesenchymal stromal cell-derived exosomes attenuate myocardial ischaemia-reperfusion injury through miR-182-regulated macrophage polarization.* Cardiovasc Res, 2019. **115**(7): p. 1205-1216.
22. Zhou, B. and J.W. Yu, *A novel identified circular RNA, circRNA_010567, promotes myocardial fibrosis via suppressing miR-141 by targeting TGF-beta1.* Biochem Biophys Res Commun, 2017. **487**(4): p. 769-775.
23. Tian, C., et al., *Myocardial infarction-induced microRNA-enriched exosomes contribute to cardiac Nrf2 dysregulation in chronic heart failure.* Am J Physiol Heart Circ Physiol, 2018. **314**(5): p. H928-H939.
24. Titze-de-Almeida, R., C. David, and S.S. Titze-de-Almeida, *The Race of 10 Synthetic RNAi-Based Drugs to the Pharmaceutical Market.* Pharm Res, 2017. **34**(7): p. 1339-1363.
25. Rehan, R. and S. Patel, *Plasma microRNAs in human left ventricular reverse remodelling.* Open Med (Wars), 2020. **15**(1): p. 586-588.
26. Marfella, R., et al., *Circulating microRNA changes in heart failure patients treated with cardiac resynchronization therapy: responders vs. non-responders.* Eur J Heart Fail, 2013. **15**(11): p. 1277-88.
27. Garcia, R., et al., *Circulating levels of miR-133a predict the regression potential of left ventricular hypertrophy after valve replacement surgery in patients with aortic stenosis.* J Am Heart Assoc, 2013. **2**(4): p. e000211.
28. Sahoo, S., et al., *Therapeutic and Diagnostic Translation of Extracellular Vesicles in Cardiovascular Diseases: Roadmap to the Clinic.* Circulation, 2021. **143**(14): p. 1426-1449.
29. Fu, S., et al., *Extracellular vesicles in cardiovascular diseases.* Cell Death Discov, 2020. **6**: p. 68.
30. Gallet, R., et al., *Exosomes secreted by cardiosphere-derived cells reduce scarring, attenuate adverse remodelling, and improve function in acute and chronic porcine myocardial infarction.* Eur Heart J, 2017. **38**(3): p. 201-211.
31. Ciferri, M.C., R. Quarto, and R. Tasso, *Extracellular Vesicles as Biomarkers and Therapeutic Tools: From Pre-Clinical to Clinical Applications.* Biology (Basel), 2021. **10**(5).
32. Zomer, A., et al., *In Vivo imaging reveals extracellular vesicle-mediated phenocopying of metastatic behavior.* Cell, 2015. **161**(5): p. 1046-1057.

CHAPTER 8

“Abstract in Portuguese- Sumário”

Nos últimos anos, o sistema de saúde foi tremendamente afetado pela COVID-19 e consequentemente pelas mortes por ela provocadas. Apesar disso, o denominador para uma das maiores causas de morte manteve-se constante: doenças cardiovasculares (DCVs).

As DCVs incluem um amplo grupo de doenças que afetam o coração e os vasos e quando não tratadas, podem progredir para insuficiência cardíaca (incapacidade do coração bombear o sangue eficazmente) e, eventualmente, a morte. A insuficiência cardíaca (IC) é um estádio final de muitas DCVs com múltiplas vias, que comumente dividem a IC em insuficiência ventrículo esquerdo (IVE) ou insuficiência do ventrículo direito (IVD). As diferenças de IVE e IVD podem ser em parte explicadas pelas caraterísticas intrínsecas e específicas de cada ventrículo. No entanto, as suas respostas ao dano são diferentes e por isso requerem um tratamento distinto. Apesar da gravidade da IVD, até ao momento, os estudos sobre IVD são significativamente menores quando comparados com a IVE. A IVD é uma condição complexa que necessita de um conhecimento preciso e de um tratamento eficaz.

O **Capítulo 2** investigou os mecanismos moleculares subjacentes à IVD e estuda a contribuição do fator de transcrição Hand2 para a remodelação do VD em resposta à lesão por sobrecarga de pressão. De fato, a específica deleção de Hand2 no coração está associada a disfunção cardíaca grave em condições de sobrecarga de pressão do VD, uma vez que a deleção de Hand2 sensibiliza o VD à lesão cardíaca, como observado em animais que desenvolveram mais hipertrofia e disfunção cardíaca mais grave. Os níveis de expressão mais elevados de HAND2 foram também detetados em amostras de VD de corações humanos de pacientes com hipertensão pulmonar, geralmente associada a IVD. Embora a inibição da expressão de Hand2 possa prevenir a disfunção cardíaca em condições de sobrecarga de pressão do VE, o mesmo não é verdadeiro para as condições de sobrecarga de pressão do VD. Assim, os resultados do capítulo 2 sugerem que existem múltiplas vias para a IC e também múltiplos caminhos para evitar a IC.

Restaurar o coração de IC é agora possível pela indução da remodelagem reversa (RR) através de terapia e tratamentos médicos cardíacos. No entanto, tem sido observado que os pacientes respondem de forma diferente à terapia e é necessário prever o resultado da RR para melhorar a precisão de um tratamento e obter uma medicina personalizada. Os microARNs (miRs) são uma classe de pequenos ARNs não codificantes encontrados tanto no espaço celular quanto no espaço extracelular, devido à sua capacidade de espelhar a condição cardíaca. Recentemente, os miRs surgiram como biomarcadores, nomeadamente, na RR cardíaca.

O **Capítulo 3** resumiu a pesquisa atual sobre o uso de ncARNs, incluindo miRs, em amostras humanas de sangue, plasma e soro como biomarcadores de DCVs, discutindo também as suas fragilidades e potenciais.

O **Capítulo 4** transitou do geral para o particular, identificando a expressão de miRs plasmáticos que emergiram como potenciais biomarcadores de RR completa após cirurgia de substituição da valvula aórtica (SVA), num estudo de casos de uma amostra portuguesa. Verificou-se que o miR-133a-3p e let-7b-3p são diferencialmente expressos em amostras de plasma de pacientes com RR incompleta (pacientes que não apresentam melhoria da função cardíaca e desenvolvem uma resposta clínica desfavorável), quando comparados com pacientes com RR completa (pacientes com função cardíaca recuperada). Qualitativamente, a precisão diagnóstica de let-7b-3p é "muito boa", enquanto miR-133a-3p é classificado como "excelente". Assim, os nossos dados sugerem miR-133a-3p e let-7b-3p como potencialmente bons biomarcadores de RR completo após cirurgia SVA. O **Capítulo 4** focou-se em miRs plasmáticos secretados, no entanto, não descreveu todos os caminhos possíveis

da secreção de miRs das células para o espaço extracelular. Na verdade, existem muitas vias para as células secretarem miRs, nomeadamente através de vesículas extracelulares (VEs). As VEs, incluindo exossomas, são vesículas de dupla camada secretadas pelas células para mediar a comunicação intercelular, tanto local quanto sistemicamente.

O **Capítulo 5** fez uma revisão geral da literatura atualizada sobre o papel dos ARNncs na comunicação intercelular, nomeadamente no contexto da remodelação patológica cardíaca. Contudo, a maioria dos estudos atuais de comunicação cardíaca por vesículas extracelulares foram baseados no isolamento de vesículas de culturas celulares, por isso não mimetizam verdadeiramente a fisiologia do coração humano nem mantêm a acessibilidade e a alta resolução espacial e temporal da secreção de VEs temporal no coração. Para ultrapassar estes obstáculos, **O Capítulo 6** estudou um novo método viral, usando um modelo 3D do músculo cardíaco modificado (MCM), que permite monitorizar a transferência intercelular de vesículas pela mudança de cor nas células recetoras. Através do MCM é possível estudar a transferência de VEs em ambientes de IC e, portanto, compreender como a comunicação de VEs é alterada em condições de IC. Simultaneamente, este capítulo discute se modelos promissores como o MCM podem espelhar com precisão a comunicação cardíaca através de VEs.

Assim, os capítulos desta tese surgem como vários caminhos para a IC.

CHAPTER 9

"Impact Paragraph"

Ethics, Economy and Society

Cardiovascular diseases (CVDs) are the number one cause of mortality worldwide. In 2019 alone, CVDs were accountable for 17.9 million deaths (WHO data, 2021)[1] predominantly due to heart failure and stroke. Nevertheless, it is estimated that this number will rise to 23 million by 2030 (WHO data)[2]. Furthermore, the concept that CVDs only affect high-income countries and the elderly population is wrong, as 75% of deaths caused by CVD occur in low and middle-income countries, and 38% of premature deaths (under 70 years old) in non-communicable diseases are caused by CVDs (WHO data, 2021)[1].

With the advances in medical care, life expectancy is increasing, and a person lives on average 80 years[3]. However, this does not translate into healthy life expectancy as, in fact, with increased life expectancy, the life quality dramatically decreases, and the last years of an individual are marked by severe disability, and dementia, among others[4]. Therefore, better treatments are essential to improve the survival rate of each patient and the quality of life by decreasing the comorbidities associated with CVDs. Overall, this thesis may be a small step toward a healthier society. Therefore, firstly, it focused on RVF patients by highlighting the divergences between right and left heart failure and how ventricle-specific treatment might be needed when treating HF, particularly in RVF patients. Secondly, it contributed more data that might directly impact the life quality and expectancy of patients with aortic stenosis (a pathology that belongs to the CVDs group) by predicting if patients could benefit from aortic valve replacement surgery. Finally, by creating new models of HF, we will gain knowledge of new cardiac pathophysiological mechanisms, and ultimately, this will help discover new treatments for HF patients.

CVDs without an efficient treatment can have a massive impact on health care systems by draining large quantities of money from the society and governmental organizations that support it. Within the European Union, overall CVD costs up to €210 billion per year (EHN 2017), being that €111 billion are spent on health care costs, 54 billion are due to productivity losses, and 45 billion on informal care[5]. A better treatment will directly reflect on the health care system, directly decrease the costs associated with patient therapy, and indirectly improve its community's economic status. The results obtained within this thesis will contribute to finding an adequate and more efficient treatment against CVDs, directly and indirectly improving the economic and social state of individuals, communities, and nations.

Moreover, the work reported within this thesis was performed through a double degree agreement and in collaboration between two countries, The Netherlands and Portugal, joining efforts and combining different expertise to increase the network within labs and opening doors for future collaborations working towards a common goal. Besides helping to increase the soft power of both countries, it contributes to cultivating values of openness, pluralism, empathy, freedom, and diplomacy among the European Union.

Peers, Scientific Community and Pharmaceutical Industry

The survival rate of a patient with heart failure is 45.5% at 5 years, but this value drastically decreases to 12.7% at 15 years[6]. Also, a study from Coimbra, Portugal, reported that the long-term survival rate (at 3 years) of individuals with pulmonary hypertension (PH) from different classes such as idiopathic, hereditable, or drug-related PH is only 55%, indicating that

3 years after diagnosis almost half of the patients will die[7]. Both pathologies show frightening survival rates and still lack efficient treatment.

Beyond the comorbidities and the high mortality rate, patients suffering from CVDs are more prone to other diseases. For example, in 2020, the COVID 19 pandemic had a drastic impact on people with CVDs; therefore, these patients constitute a group risk, lowering their chances of survival. Therefore, it is imperative to decrease the number of risk groups and the number of individuals that belong to these groups. In this direction, the work developed within this thesis allowed us to increase our understanding of RV vs LV pathological remodeling. Precisely, we found that potential targets of LV failure due to pressure overload are not suitable for RV failure, as is the case of Hand2. Also, we were able to amplify our knowledge of epigenome transference between cells, namely miRs, during cardiac injury.

The content of this thesis affects a broad spectrum of areas within the CVD field, including the following topics: disease-associated information on RV failure; pulmonary hypertension; heart failure; cardiac reverse remodeling biomarkers to basic fields, including differences between left and right ventricle response to injury and cardiac intercellular communication between different types of cells both in physiological situations.

Up to date, there is no treatment for heart failure and the ultimate goal of my research is to find potential therapeutic targets to improve the efficacy and efficiency of current treatments. Each year the use of miRs as therapeutic agents becomes closer to clinical practice, as it is already happening with Miravirsen, an antagomiR targeting miR-122, crucial in preventing the multiplication of hepatitis C virus in the liver[8,9]. Miravirsen is currently in clinical phase II, and it is expected to be used routinely in clinical practice in the next few years[9], thus influencing the pharmaceutical sector.

However, the results reported here can be applied to other fields. For example, extracellular vesicles (EVs) are a common ground for several types of cancers, neurological diseases, and diabetes, among other pathologies. Furthermore, while EVs have been accepted as potential biomarkers[10,11], recent research has been focused on EVs as new drug-delivery tools[12]. The attractive features of EVs include large bioavailability and exceptional biocompatibility paired with a low immunogenic response assuming a “safe-to-use” platform[13]. Interestingly, EVs can also cross the blood-brain barrier, usually a hindrance to drug delivery, and in this way allow drug access to brain tissues[14]. To further increase target efficacy and stability, EVs can also be engineered and modified regarding their structure, composition, and content[15,16] creating a promising future for EVs as delivery tools in multiple contexts.

Finally, knowledge is only valuable to the world if it is shared. During the last years, the findings reported in this thesis were disseminated by attending international meetings from the European Society of Cardiology and others, where I had the opportunity to expose our data in posters and oral presentations. Furthermore, the scientific data was used to elaborate four papers, including original articles and reviews, submitted to journals in the cardiovascular field, facilitating knowledge spreading throughout all scientific community and academia.

References

1- https://www.who.int/en/news-room/fact-sheets/detail/cardiovascular-diseases-(cvds) uploaded in 11/06/2021 and visited in 22/02/2022

2- *World Health Organization, Global Health Estimates Summary Tables: Projection of Deaths by Cause, Age & Sex (2013) assessed by* https://pharma.bayer.com/economic-and-societal-impact-cardiovascular-disease?fbclid=IwAR0b1o49W9hAygfFxIwojjUfbzipoPd-HB6NT-gD6cTqPTPriPznrrN1dkw

3- *ONS visited on* https://www.gov.uk/government/publications/health-profile-for-england/chapter-1-life-expectancy-and-healthy-life-expectancy

4- ONS (2016) Estimates of the very old (including centenarians), UK: 2002 to 2015. Office for National Statistics

5- *European Heart Network, European cardiovascular disease statistics 2017*

6- Taylor, Clare J., et al. "Trends in survival after a diagnosis of heart failure in the United Kingdom 2000-2017: population based cohort study." *bmj* 364 (2019).

7- Marques-Alves, P., et al. "Real-world, long-term survival of incident patients with pulmonary arterial hypertension." *Revista Portuguesa de Pneumologia (English Edition)* 23.3 (2017): 124-131.

8- Gebert, Luca FR, et al. "Miravirsen (SPC3649) can inhibit the biogenesis of miR-122." *Nucleic acids research* 42.1 (2014): 609-621.

9- Ottosen, Søren, et al. "In vitro antiviral activity and preclinical and clinical resistance profile of miravirsen, a novel anti-hepatitis C virus therapeutic targeting the human factor miR-122." *Antimicrobial agents and chemotherapy* 59.1 (2015): 599-608.

10- Lee, Seongju, Sakulrat Mankhong, and Ju-Hee Kang. "Extracellular vesicle as a source of Alzheimer's biomarkers: opportunities and challenges." *International Journal of Molecular Sciences* 20.7 (2019): 1728.

11- Liu, Qingyun, et al. "Circulating exosomal microRNAs as prognostic biomarkers for non-small-cell lung cancer." *Oncotarget* 8.8 (2017): 13048.

12- Herrmann, Inge Katrin, Matthew John Andrew Wood, and Gregor Fuhrmann. "Extracellular vesicles as a next-generation drug delivery platform." *Nature nanotechnology* 16.7 (2021): 748-759.

13- McVey MJ, Weidenfeld S, Maishan M, Spring C, Kim M, Tabuchi A, Srbely V, Takabe-French A, Simmons S, Arenz C, Semple JW, Kuebler WM. Platelet extracellular vesicles mediate transfusion-related acute lung injury by imbalancing the sphingolipid rheostat. Blood. 2021 Feb 4;137(5):690-701. doi: 10.1182/blood.2020005985. PMID: 33232973.

14- García-Romero, Noemí, et al. "DNA sequences within glioma-derived extracellular vesicles can cross the intact blood-brain barrier and be detected in peripheral blood of patients." *Oncotarget* 8.1 (2017): 1416.

15- Piffoux, Max, et al. "Extracellular Vesicle Production Loaded with Nanoparticles and Drugs in a Trade-off between Loading, Yield and Purity: Towards a Personalized Drug Delivery System." *Advanced Biosystems* 1.5 (2017): 1700044.

16- de Abreu, R.C., Fernandes, H., da Costa Martins, P.A. *et al.* Native and bioengineered extracellular vesicles for cardiovascular therapeutics. *Nat Rev Cardiol* **17,** 685–697 (2020). https://doi.org/10.1038/s41569-020-0389-5

CHAPTER 10

“Biography and Acknowledgments”

Raquel Figuinha Videira was born on 16th of November of 1993 in Coimbra, Portugal. There, she studied Sciences and Technologies finishing high school (Jose Falcao High School, Coimbra, PT) in 2011 with a final grade of 18 out of 20 and therefore being part of the merit students' school board.

From 2011 to 2014, Raquel studied at the University of Coimbra, where she graduated with a Bachelor of Science in Biology. Raquel was awarded twice with 3% Best Students of the University of Coimbra during this time. Raquel continued her academic career and pursued a Master of Science in Cellular and Molecular Biology at the University of Coimbra, and in 2016, she obtained her master's degree with a final classification of 18 out of 20. During her master thesis, Raquel's work focused on "Cardiac ischemia-reperfusion injury: in vitro models and regulation by microRNAs," under the supervision of Miguel Mano (UC-Biotech, Cantanhede, Portugal); this work obtained a 19 out of 20 final scores.

Her passion for molecular cardiovascular sciences led her to search for a master's fellowship to work with Inês Falcão Pires and Paula da Costa Martins. In 2018, Raquel was awarded a PhD Scholarship from FCT (Fundação para a Ciência e Tecnologia, Portuguese Science Ministry) to develop her work on cardiovascular sciences and enrolled in a joint PhD between the University of Maastricht (CARIM) and the University of Porto (FMUP). During her PhD, Raquel received a travel grant to attend Basic Science Summer School promoted by the European Society of Cardiology and an HS-BAFTA PhD Talented Student Scholarship promoted by CARIM. Raquel has continued her research on engineered heart muscle in Göttingen, Germany, in the group of Dr. Prof. Zimmermann and Dr. Prof. Malte Tiburcy. Raquel's work focused on broad aspects of heart failure, including:

- studying ventricle dichotomy response to cardiac hypertrophy with particular attention to the right ventricle and Hand2.
- finding new biomarkers for predicting reverse remodeling on aortic stenotic patients that have a high degree of cardiac hypertrophy,
- finding new tools to study and understand cardiac communication

List of Publications

1. Videira, R. F., Koop, A. M. C., Ottaviani, L., Poels, E. M., Kocken, J. M., Dos Remedios, C., ... & da Costa Martins, P. A. (2021). The adult heart requires baseline expression of the transcription factor Hand2 to withstand right ventricular pressure overload. *Cardiovascular Research*.

2. Videira, R. F., da Costa Martins, P. A., & Falcão-Pires, I. (2020). Non-Coding RNAs as Blood-Based Biomarkers in Cardiovascular Disease. *International journal of molecular sciences*, *21*(23), 9285.

3. Videira, R. F., & da Costa Martins, P. A. (2020). Non-coding RNAs in Cardiac Intercellular Communication. *Frontiers in Physiology*, *11*, 738.

4. Bär, C., Chatterjee, S., Falcão Pires, I., Rodrigues, P., Sluijter, J. P., Boon, R. A., ... & Thum, T. (2020). Non-coding RNAs: Update on mechanisms and therapeutic targets from the ESC Working Groups of Myocardial Function and Cellular Biology of the Heart. *Cardiovascular Research*, *116*(11), 1805-1819.

Acknowledgments

During these four years, I had the opportunity to reinvent myself and my PhD project numerous times. I lived some less good and good moments, but I am thankful for all of them. Like most of us, I can now say that my PhD was not what I expected. Still, I cannot say it was a boring one. From the several courses I did, the conferences and meetings that I attended, the countries I visited and the three lived in, the four labs I worked in, and the people I met. To all the people who contribute to my work and my personal growth, thank you, without you, this PhD could not be possible without you.

Paula, thank you for being my supervisor. Your knowledge and expertise were invaluable in pushing me to complete my thesis and work to a higher level. I also want to thank you for your always nice feedback, positivity, flexibility, and constant worries with me as a person and not only as a PhD student. Above all, thank you for believing in me; I hope our friendship doesn't finish here.

Inês, my "Portuguese" supervisor, thank you for your suggestions and your imprinting on this thesis. It was nice to work with you. Thank you also to Prof. Adelino and all of the members of the Unic lab.

Leon, Martina, and Servé, thank you for receiving me into your group; it was a pleasure to be part of it. Your feedback was extremely important for this thesis, and your questions pushed me to be a better professional.

Hugo and Lino, it was not on my plans to move to Coimbra when I did, but your kindness and work ethic made everything more accessible. A sincere thank you for being so flexible and always treating me as a group member. Thank you for your scientific questions and enthusiasm during this thesis; although things didn't go as planned, I have learned a lot. Thank you to all of the members of the Stem cell lab; it was very nice to have lunch with you and share some good laughs.

Prof. Wolfram Zimmermann and all the Toxicology and Pharmacology department members, thank you for accepting me into your department and for all the help that it was given. I had a good time there.

Malte Tiburcy, thank you for receiving into your group and integrating me as your student. I felt very supported by you, and thanks to you, my laboratory adaption was very simple. Laura Zelarayan, thank you for your input on extracellular vesicles and viral particles; you always found time to meet me and to help me; thank you.

For those who don't know how Claudia and I became friends, she purposely locked herself outside her house just to spend the night at my place. Claudia, my cute, hard worker, and stubborn criceto; I didn't feel your energy when I met you for the first time, but as they say "primeiro estranha-se depois entranha-se" (look for it). After one or two days of you being in the lab, we became inseparable; from that point on, I was always on your ass, "cric bring a jacket", "cric did you have lunch", "cric, another bruise?", "cric you need to stand up for yourself", but my favorite is "I love you cric". We are nothing alike: I am Latina, and you are, well, not Latina! But I truly admire you, and you were for sure one of the best things that this PhD gave me. You pushed me to be a better person and taught me so much. I hope we can cherish our friendship forever and that you come to visit me a lot of times but, even if won't, you will be always in my heart, next to our laughs, talks, adventures and bitching sessions. Thank you for everything, cric and for being my family in Maastricht.

Bárbara, como já te disse foste o meu anjinho da guarda em Göttingen, obrigada por me acolheres e me aturares quando eu era chata e tinha medo do COVID. Adorei todos os momentos que passámos juntas e espero que esta amizade dure muito tempo.

Larina, the DIVA, you were the first person I met in Maastricht; you have been there for the best and the worst; you were my "mama". Thank you for always taking care of me, I will never forget when " I farted you", when we sang in the office "Say something I am giving up on you", your weird arms' flexibility, your "puurr". I miss you a lot and don't forget you are worth millions Larina.

Lorena, the amazing singer, we would put on a show on Ariana Grande, Cardi B, Britney B, and so on; thank you for all the beers, movies, talks, and bullying sessions to Larina. Above all, thank you for showing me the room and Sharknado. I hope you can come to visit me.

Janica, or should I say the Schnitzel Police?, thank you for always being up for anything, from mogee tea, painting walls, geocaching, trips, and baking unappropriated shapes of Christmas cookies (they were super good). I could always talk with you, saying anything I wanted, and you would not judge me.

Marilina, thank you for sharing abbracci, cappuccino, advice, talks, laughs, trips, hotel rooms, and German complaints.

Vasco and Cri, my portugues-ish cousins, thank you for all the advice and bike rides till home.

Robin, the Catman, diriridum, you are one of the most given people that I know. You give without asking anything back. You are always willing to help no matter the subject, time, or place. I wish you all of the best with your work and life.

Jordy, Jordano, you were my pulmonary guy, the only Dutch in the group; thank you for showing me support and being my buddy on Phaedra meetings.

Indira, my unofficial doctor, thank you for diagnosing me in the weirdest places and the weirdest times. I miss our trips, cappuccinos, and dancing at the Pina parties.

Joana, Giulia, Deepak, the consortium guys, I think of you as generous people always willing to help and always with a smile on your faces. Good luck with your PhD. I am sure you are going to do great!

To Nicolo, Fede, Ricardo, Andreia, and all group members, I wish you all the best, both on a professional and personal level.

To my Pharma office mattes: Artem, Pierre de Luc, my Kikinho, Alisa, and Kea thank you for all our conversations that could go on and on for hours… I could not have asked for better colleagues! I already miss you and good luck with your PhD!

Lu, you make my heart feel at home, obrigada por teres sempre tempo para me ouvir, por me ajudares a encontrar soluções para todos os problemas que arranjo, por me fazeres rir mesmo quando me acordas durante a noite ou entornas tudo à nossa volta. Mal posso esperar para saber o que a vida nos reserva. Gosto mu(u)ito de ti.

À minha familia, em especial à minha mãe e ao meu irmão que são as pessoas a quem eu mais desejo bem neste mundo, como alguém costuma dizer os amigos não existem, mas a minha familia

esteve sempre a apoiar me e a torcer por mim. Obrigada por acreditarem em mim sem vocês não teria conseguido! Por norma os agradecimentos começam por isso mesmo a agradecer, neste caso eu quero começar por pedir desculpa à minha querida Tia Tété, por não ter tempo de me despedir de ti. Estava na Holanda quando partiste e ficará para sempre a culpa de viver num país diferente que não me permite estar presente quando as pessoas mais precisam de nós.